A study on the deactivation and reactivation of supported nickel hydrogenation catalysts

by

SINQOBILE VUYISILE L MAHLABA

Submitted in fulfilment of the academic requirements of

Master of Science,

in Chemistry

School of Chemistry and Physics

College of Agriculture, Engineering and Science

University of KwaZulu-Natal

Durban

South Africa

As the candidate's supervisors, we have approved this dissertation for submission.

Signed: _____ Name: Holger B. Friedrich Date: _____

Signed: _____ Name: Abdul S. Mahomed Date: _____

May 2017

PREFACE

The research contained in this dissertation was completed by the candidate while based in the Discipline of Chemistry, School of Chemistry and Physics of the College of Agriculture, Engineering and Science, University of KwaZulu-Natal, Westville Campus, South Africa. The research was financially supported by the National Research Foundation.

The contents of this work have not been submitted in any form to another university and, except where the work of others is acknowledged in the text, the results reported are due to investigations by the candidate.

_____

Signed: Sinqobile Vuyisile Lusanda Mahlaba

Date: May 2017

DECLARATION 1: PLAGIARISM

I, Sinqobile Vuyisile Lusanda Mahlaba, declare that:

(i) the research reported in this dissertation, except where otherwise indicated or acknowledged, is my original work;

(ii) this dissertation has not been submitted in full or in part for any degree or examination to any other university;

(iii) this dissertation does not contain other persons' data, pictures, graphs or other information, unless specifically acknowledged as being sourced from other persons;

(iv) this dissertation does not contain other persons' writing, unless specifically acknowledged as being sourced from other researchers. Where other written sources have been quoted, then:

a) their words have been re-written but the general information attributed to them has been referenced;

b) where their exact words have been used, their writing has been placed inside quotation marks, and referenced;

(v) where I have used material for which publications followed, I have indicated in detail my role in the work;

(vi) this dissertation is primarily a collection of material, prepared by myself, published as journal articles or presented as a poster and oral presentations at conferences. In some cases, additional material has been included;

(vii) this dissertation does not contain text, graphics or tables copied and pasted from the Internet, unless specifically acknowledged, and the source being detailed in the dissertation and in the References sections.

_____

Signed: Sinqobile Vuyisile Lusanda Mahlaba

Date: May 2017

DECLARATION 2: CONFERENCE CONTRIBUTIONS

My role in each oral and poster presentation is indicated. The * indicates presenting author.

Oral presentations

1. Friedrich HB, Mahomed AS, Valand J, Mahlaba SVL* 2015. Octanal hydrogenation over supported nickel catalysts: Influence of support (Al_2O_3, SiO_2) on the catalytic behaviour of nickel. Oral presentation at the College of Science and Agriculture Postgraduate Research Day, UKZN, Pietermaritzburg, South Africa, 22 September 2015. Presented by SVL Mahlaba.

2. Friedrich HB, Mahomed AS, Valand J, Mahlaba SVL* 2016. Deactivation and reactivation of a 15 Ni/Al_2O_3 hydrogenation catalyst: effects of the poison and regeneration treatments on catalyst properties. Oral presentation at the 27th Annual conference of the Catalysis Society of South Africa 2016, Catalysis Society of South Africa, 6th to 9th November 2016, Drakensberg, South Africa. Presented by SVL Mahlaba.

Poster presentations

3. Friedrich HB, Mahomed AS, Valand J, Mahlaba SVL* 2015. Octanal hydrogenation over nickel catalysts on different supports. Poster presentation to the South African Chemical Institute Convention 2015, 29 November - 4 December 2015, Durban, South Africa. Presented by SVL Mahlaba.

4. Friedrich HB, Mahomed AS, Valand J, Mahlaba SVL* 2016. Effects of different regeneration methods on the activity and properties of a poisoned Nickel hydrogenation catalyst. Poster presentation at the Second EFCATS-CNRS European Summer School on Catalyst Preparation, Vogüé (Ardèche), France, 12th to 15th June 2016. Presented by SVL Mahlaba.

_____

Signed: Sinqobile Vuyisile Lusanda Mahlaba

Date: May 2017

ABSTRACT

The aim of this body of work was to establish a feasible technique for the regeneration of a phosphorus poisoned, nickel hydrogenation catalyst. Two catalysts were synthesised using the wet impregnation method, namely a nickel catalyst supported on γ-alumina (15 NiA), and one supported on silica (15 NiSi). The nickel weight loading was close to 15 wt.% for both catalysts (14.6 for 15 NiA and 14.7 for 15 NiSi), as determined by inductively coupled plasma – optical emission spectroscopy. Characterisation of the catalysts with hydrogen chemisorption, X-ray diffraction, temperature programmed reduction, scanning electron microscopy and transmission electron microscopy showed nickel to be better dispersed on the alumina support, compared to the silica support. Hence, the alumina supported catalyst had a higher metallic surface area.

Catalytic tests for the hydrogenation of octanal to octanol showed that the conversion and selectivity of both catalysts towards octanol was similar. Deactivation experiments for both catalysts were performed by conducting accelerated deactivation experiments during time-on-stream hydrogenation reactions. Deactivation was induced by hydrogenating feed contaminated with an exaggerated triphenylphosphine concentration of 500 ppm, in a continuous flow, high pressure, fixed bed reactor. The reactions were conducted at a temperature of 140 °C, 50 bars of hydrogen pressure, a liquid hourly space velocity of 18 h^{-1}, and a gas hourly space velocity of 540 h^{-1}. After deactivation had occurred, the catalysts were regenerated using three separate experiments, namely **(a)** a hydrogen treatment which involved passing hydrogen gas over the catalyst bed, **(b)** washing the catalyst bed with octanol, and **(c)** conducting a regeneration experiment that involved carrying out the octanol wash and hydrogen treatment regeneration experiments in tandem, and this experiment was termed the combined regeneration.

The recovered catalytic activity and octanol selectivity was in the sequence of hydrogen treatment < Octanol wash < Combined regeneration for both catalytic systems. Furthermore, higher catalytic activity and octanol selectivity was recovered for 15 NiSi compared to 15 NiA, although the catalyst took longer to deactivate than 15 NiA. Regeneration did not lead to the removal of phosphorus, but resulted in the formation of nickel phosphides, which were confirmed through characterisation by X-ray diffraction, high resolution transmission electron microscopy, and magnetic measurements.

From the results found in this study, the silica supported catalyst performed better compared to the alumina supported catalyst, since 15 NiSi had a comparable intrinsic activity to 15 NiA, was more resilient against deactivation, thereby taking longer than 15 NiA to deactivate. In addition, the catalyst was regenerated to a larger extent compared to 15 NiA.

ACKNOWLEDGMENTS

The expression “it takes a village” does not even begin to illustrate the collaborative effort it took to produce this body of work. Firstly, this study would not have been possible without the financial assistance from the National Research Foundation (NRF). I would like to sincerely acknowledge my supervisors Prof Holger Friedrich and Dr Abdul Mahomed for their patience and guidance throughout my Masters study. I would also like to thank my mentors, Dr Nico Prinsloo from Sasol for his valuable input, and Dr Jignesh Valand for his advice and help with maintenance of the reactor. A special mention goes to Dr Pheladi Mohlala, Ms Alisa Govender and Dr Willem Erasmus from Sasol. Words cannot begin to express my gratitude for your help.

Other members of the group have also contributed significantly to the success of my studies. I would like to thank Miss Letisha Deeplal for long discussions, and her help in getting my thoughts in order. I would also like to thank Drushan and Majid for their help with the reactor maintenance.

Many thanks to Phillip and Subashen from the Microscopy and Microanalysis unit from UKZN for their help with transmission electron microscopy imaging. I would also like to thank Dr Ruggero Vigliaturo for his assistance and input in the understanding of microscopy images.

To the friends who have been with me throughout, Khwezi, Maria, Mandy, Vuyo, Jenelle, Letisha, Shivania, Revana and Thabiso, thank you for providing an escape when the work got too real. Your friendship is truly appreciated.

Finally, I would like to acknowledge my family, Daya and Sya.

TABLE OF CONTENTS

Contents **Page**

LIST OF TABLES

LIST OF FIGURES

LIST OF SCHEMES

ABBREVIATIONS

%	: Percent
γ-Al_2O_3	: Gamma Alumina
15 NiA	: 15 % Nickel on alumina
15 NiSi	: 15 % Nickel on silica
ATR	: Attenuated total reflectance
BET	: Braunauer-Emmet-Teller
cm	: centimetre
°C	: Degrees Celsius
DSC	: Differential scanning calorimetry
EDX	: Energy dispersive X-ray spectroscopy
FID	: Flame ionization detector
GC	: Gas Chromatography
GHSV	: Gas hourly space velocity
h	: Hour
HAADF	: High angular annular dark field
HRTEM	: High resolution transmission electron microscopy
ICP-OES	: Inductively coupled plasma optical emission spectroscopy
IR	: Infrared spectroscopy
JCPDS	: Joint committee on powder diffraction
LHSV	: Liquid hourly space velocity
$m^2 g^{-1}$	: square meter per gram
mg	: milligram

ml : millilitre

ml min-1 : millilitres per minute

mmol : millimoles

MS : Mass spectrometry

MSI : Metal-support interaction

NiO : Nickel oxide

Ni : Nickel

NiP : Nickel phosphide

NMR : Nuclear magnetic resonance

ppm : parts per million

PSD : Pore size distribution

SEM : Scanning electron microscope

SiO_2 : Silica

STEM : Scanning transmission

TCD : Thermal conductivity detector

TEM : Transmission electron microscopy

TGA : Thermogravimetric analysis

TOS : Time on stream

TPP : Triphenylphosphine

TPR : Temperature programmed reduction

Wt. : Weight

XRD : X-ray diffraction

PXRD : Powder X-ray diffraction

EQUATIONS

Catalytic data processing

The following equations were used to quantify catalytic data.

The yield of a reaction is defined as the amount of product that was produced in a reaction divided by the amount of starting material. It is calculated using equation1.

$$Yield = \frac{amount\ of\ reactant\ converted\ to\ product}{amount\ of\ reactant\ introduced\ in\ the\ reactor} \quad \text{…equation 1}$$

The conversion is defined as the amount of reactant that was converted to product divided by the amount of starting material. It is calculated using the following equation:

$$Conversion = \frac{amount\ of\ reactant\ reacted}{amount\ of\ reactant\ introduced} \quad \text{…equation 2}$$

The selectivity is defined as the yield of the desired product divided by the overall amount of starting material converted to products and is calculated using the following equation 3.

$$Selectivity = \frac{yield}{conversion} \quad \text{…equation 3}$$

Space velocities

$$Liquid\ hourly\ space\ velocity\ (h^{-1}) = \frac{Reactant\ liquid\ flow\ rate\ (mL\ min^{-1})}{Catalyst\ volume\ (mL)}\ x\ \frac{60\ min}{1\ h}$$

...equation 4

$$Gas\ hourly\ space\ velocity\ (h^{-1}) = \frac{Reactant\ gas\ flow\ rate\ (mL\ min^{-1})}{Catalyst\ volume\ (mL)}\ x\ \frac{60\ min}{1\ h}$$

…equation 5

Chapter 1: Introduction

1.1 Background to this research

The chemicals industry is a cornerstone of modern civilization, with the global chemicals output estimated to be worth billions in US dollars per annum [1-3]. The transformation of bulk and commodity chemicals requires catalysts, and it has been reported that 85% of all industrial processes use a catalyst in some stage of their production process [4-6]. Catalysis has been estimated to constitute about 15 % of economic activities of industrialised countries, with the goods produced via catalysis having an estimated value of 900 billion US dollars [7]. Although the large scale industrial use of catalysis started around 300 years ago, ancient human civilizations reportedly exploited catalysis by using yeast in the fermentation of sugar to produce alcoholic beverages. However, it was not until the 19th century that the phenomenon was termed "catalysis" by J. J. Berzelius [1, 8, 9].

The basic definition of a catalyst is a substance that speeds up the rate of a reaction without being consumed, nor forming part of the products. A chemical reaction involves the cleavage of existing bonds, atomic rearrangements, and formation of new bonds, which results in the formation of the product. The initial cleavage of bonds requires a high energy of activation to break the existing bonds. The compensation of the high energy requirements could be achieved either through increasing the temperature at which the reaction takes place, or by lowering the required energy of activation through the use of a catalyst [10].

The catalyst achieves this by providing an alternative reaction pathway, requiring a lower activation energy compared to the uncatalyzed reaction. The reactants form intermediate compounds with the catalyst. The transient bonds between the catalyst and reactants have lower activation barriers than the bonds of the starting reactants, and hence require less energy to break. This accelerates the rate of the reaction, since the initial cleavage of bonds is most often the limiting step of the reaction. The formation of products at the end of the reaction results in the regeneration of the catalyst [10, 11]. Catalytic reactions always proceed via cycles of reaction steps, with the catalyst undergoing conversion from one form to another during the course of the reaction [12].

Many catalysts exist for various processes, and are therefore classified according to physical states or area of application. There are three main classes, namely homogeneous, heterogeneous

and biocatalysts. A homogeneous catalyst is in the same phase as the reactants and product, and usually involves the catalyst, reactants and products in the liquid phase. Heterogeneous catalysts are solid state materials, while the products and reactants exist in different phases to the catalyst. Biocatalysis refers to the catalytic application of enzymes, most notably in the fermentation of sugar products to produce alcohol [13]. Homogeneous and heterogeneous catalytic processes are largely exploited in industry. Of a total of 85 % of catalysed industrial processes, the use of heterogeneous catalysts is predominant, whereas homogeneous and biocatalysis are not as extensively applied [4, 14, 15]. Figure 1.1 provides a summary of the role of catalysis in the chemical industry.

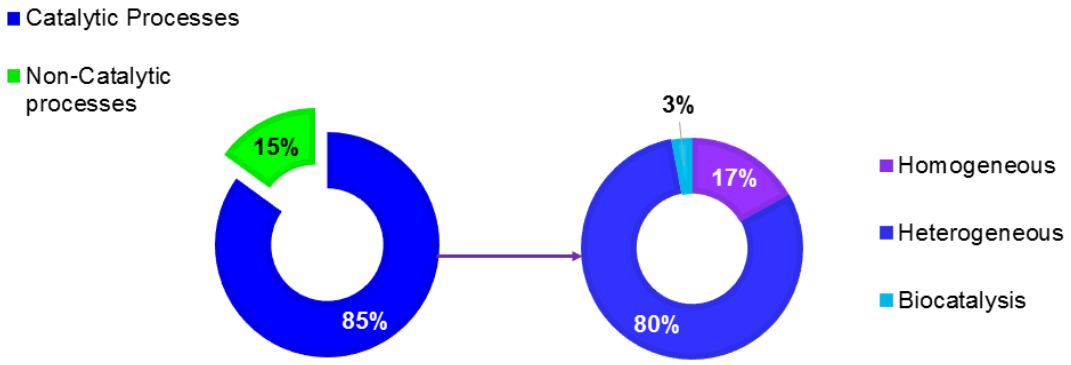

Figure 1.1: A summary of the important role of catalysis in industry [4]

1.1.1 Heterogeneous Catalysis

Heterogeneous catalysis usually involves the reaction of either gas or liquid reactants on the surface of porous, high surface area solids which are usually composite materials that are further classified as either bulk or supported metal catalysts [16, 17]. Bulk catalysts refer to catalytic solids such as zeolites and clays that are composed of different active components in an intimate mixture, while supported catalysts are usually composed of metallic species dispersed on the surface of a support [18, 19].

The use of heterogeneous catalysis is at the heart of the modern chemical industry, with the first commercial application of a heterogeneous catalyst going as far back as 1746, when the production of sulphuric acid by the Lead Chamber process was discovered by John Roebuck [1]. This led to a number of notable discoveries, one of which was the development of the ammonia catalytic process by Fritz Haber [20], that revolutionised the fertilizer industry and warfare by allowing the conversion of inactive atmospheric nitrogen to a reactive form that can be used for the production of fertilizers and explosives. The resulting increase in fertilizer

production dramatically increased global agricultural productivity and provided food security, thereby boosting the growth of the world population [21, 22].

South Africa itself has immensely benefited from the application of a heterogeneous catalytic process, namely the Fischer-Tropsch process, for the conversion of carbon monoxide and hydrogen gas to hydrocarbons [23]. This process was discovered in 1922 by Franz Fischer and Hans Tropsch, but was adopted by Sasol during an embargo on the import of petroleum sanctioned against the Apartheid government [24, 25]. The process enabled the synthesis of fuels and value added chemicals from coal and natural gas, which is relatively cheap compared to crude oil [26].

The applicability of heterogeneous catalysis has since evolved, and is not only confined to the production of chemicals, but other major drivers include transportation, polymers, agrochemicals, environmental protection, and sustainable energy [24, 27]. Catalysis is now at the forefront of environmental sustainability and 'green' processes, with the introduction of catalytic converters in the 1970's leading to a significant decrease in the environmental emission of harmful exhaust gases [24, 28, 29]. A lot of current research is directed towards the development of highly active catalysts for the valorisation and upgrading of bio-based feedstocks in a move towards greener, more sustainable sources of platform chemicals [30-33]. A more inclusive list of notable heterogeneous catalytic processes and discoveries is presented in Table 1.1.

Table 1.1: Summary of a few notable discoveries in heterogeneous catalysis [1, 24]

Process	**Catalyst**	**Main Inventor**	**Year**
Sulphuric acid	Lead chamber	Roebuck	1746
Sulphuric acid production via the Contact process	Pt, later V_2O_5	Phillips	1831
Nitric acid production via the Ostwald process	Pt gauze	Ostwald	1904
Ammonia synthesis	Fe	Haber	1909
Hydrogenation	Ni	Sabatier	1912
Methanol synthesis	ZnO-Chromia	BASF	1923
CO/H_2 to hydrocarbons	Fe, Co	Fischer and Tropsch	1923
Fluid catalytic cracking	Clays, zeolites	Houdry	1936

The extent to which heterogeneous catalysis is used in the industrial production of chemicals has been cited to comprise 85% of all industrial catalytic processes [4, 7]. From the value quoted, it is evident that heterogeneous catalysis is favoured over homogeneous catalysis. This is attributed to the numerous advantages afforded by a catalyst in a separate phase, such as ease of separation of catalyst from products, recyclability, and plausible application in continuous processes [34].

1.1.1.1 Supported metal catalysts

Most commercially applied heterogeneous catalysts consist of transition metals dispersed onto high surface area, porous carriers in the form of small, well divided particles. The high surface to volume ratio that results from the dispersion of the active phase into small particles results in a large number of active sites relative to metal mass. This reduces costs due to the rarity of some transition metals, such as those belonging to the platinum group metals [35-37].

Furthermore, the dispersion of metals into small particles imparts them with properties that differ from those of the metals in bulk and equilibrium states. Firstly, the dispersion of metals onto the support results in the formation of small particles that can be within the nanometre size range. In some cases, this can lead to a change in the behaviour of the metal nanoparticles, compared to the unsupported metal catalyst [38, 39]. According to Che and Bennet [40], the reduction in size of a metal particle to the nanoparticle size range results in the loss of its metallic properties due to the separation of electronic levels (valence bands), preventing the passage of electrons from one band to another. This leaves smaller metallic particles with high electron densities, imparting them with unique catalytic properties [37, 38]. The division of metals into small nanoparticles leaves them thermodynamically unstable due to an increase in the chemical potential, thus leaving them susceptible to sintering [38, 41].

The main function of the support is to stabilise the small metal nanoparticles against sintering and mechanical damage [35, 42, 43]. The support stabilises metal nanoparticles through electron transfer between the metal and support, resulting in a decrease in the electron density of the supported metal catalyst. A strong metal-support interaction results in the formation of smaller, well dispersed particles on the support after hydrogen reduction [44, 45]. In addition to providing stability and dispersion, the support also has a significant influence on the properties of the resultant catalyst and may contribute significantly to the activity and selectivity under operating conditions [46]. The most commonly used supports are single

oxides with high melting points such as titania, silica, alumina, and zirconia [37, 47]. Figure 1.2 is a schematic representation of a supported metal particle.

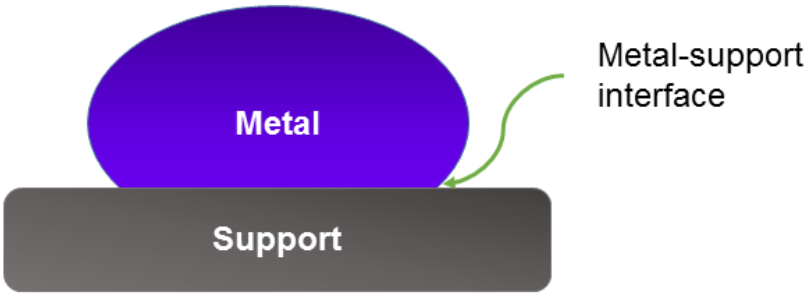

Figure 1.2: Schematic representation of a metal particle deposited on a support material

1.1.1.2 Catalyst preparation

The preparation of supported metal catalysts has been well documented, and a number of studies aimed towards improving methods used for the preparation of highly active supported metal catalysts have been conducted [17, 18, 48]. A recent review by Munnik *et al.* [49] was dedicated towards recent developments in catalyst synthesis and focused mainly on the deposition of active phases onto the support, hence concentrating on deposition-precipitation and impregnation, while the preparation of bulk oxide materials by co-precipitation was briefly mentioned [49].

Deposition-precipitation involves the mixing of a pre-formed support with a solution of the metal ion precursor. The support functions as a site of nucleation where the precursor metal ions will adsorb from solution. Precipitation onto the support is facilitated by the adjustment of pH in order to favour the formation of insoluble metal species, brought about by the addition of a basic solution to the support/precursor solution mixture [49]. Deposition-precipitation is the preferred method for the preparation of catalysts with metal weight loadings that are greater than 20% [17] and results in a catalyst with a highly uniform metal dispersion [50, 51].

Impregnation is frequently used due to its simple execution, low waste streams, low cost, and versatility across a wide range of metals, precursors and supports. This technique is usually performed for metal weight loadings that are less than 20 % due to metal precursor solubility limitations. Wet impregnation involves the use of excess precursor solution (to the pore volume of the support being impregnated), while pore volume impregnation uses a volume of solution

that is equivalent to the pore volume of the support. Impregnation typically involves three steps, starting with contacting the precursor solution with the support, followed by removal of excess solution by drying, then calcination of the solid to produce an oxide form of the catalyst, which could undergo further treatment such as reduction, depending on the application [17, 18]. The main disadvantage of using wet impregnation is the difficulty in controlling the resulting metal particle size and spatial distribution of metal on the support [49, 52].

Recently, there has been an increase in the use of sonication to improve the particle size distribution and metal dispersion of catalysts during wet impregnation, a process known as sonic assisted wet impregnation. This method involves treating the slurry obtained during the contacting stage with sonic waves for an amount of time, ranging from minutes to an hour [53]. This has been extensively used in the preparation of nanoparticles and photocatalysts, with good catalytic activity reported for catalysts prepared with the aid of sonication [54].

1.1.2 Catalytic hydrogenation

Catalytic hydrogenation is the addition of two hydrogen atoms to a double bond, usually promoted by a supported metal catalyst. Functional groups reduced using this method include, but are not limited to, alkenes, alkynes, carbonyl groups and amines [55, 56]. This is the most widely studied catalytic process as it finds application in the production of pharmaceuticals, fine chemicals, foodstuffs, and agrochemicals, which prompts the need for the development of cheaper and more effective catalysts. Hydrogenation is a surface reaction that proceeds via three principal steps, namely the adsorption of the substrates on the catalyst, catalytic reaction, and desorption of the products from the catalyst. However, the actual mechanism is much more complex [11]. The appropriate metal, as the active site, plays a crucial role since it functions to activate reactants through adsorption and dissociation of the reactants on the catalyst surface, which reduces the energy required for activation [7].

The metal serves to dissociate hydrogen gas on the surface, which is an important step during the reaction [57, 58]. Hence, the ability of a metal to dissociate hydrogen is a crucial requirement and an important factor in the choice of catalyst. In addition, the adsorption of the reactants on the metal surface must be strong enough for reactant dissociation, and weak enough to allow desorption of products from the catalyst surface [59]. Catalytic hydrogenation reactions on heterogeneous catalysts follow Langmuir-Hinshelwood kinetics, where both reactants adsorb onto the surface of the catalyst, to be activated. The reaction then proceeds

through five steps, which is better explained using the hydrogenation of ethylene as a model reaction in Figure 1.3.

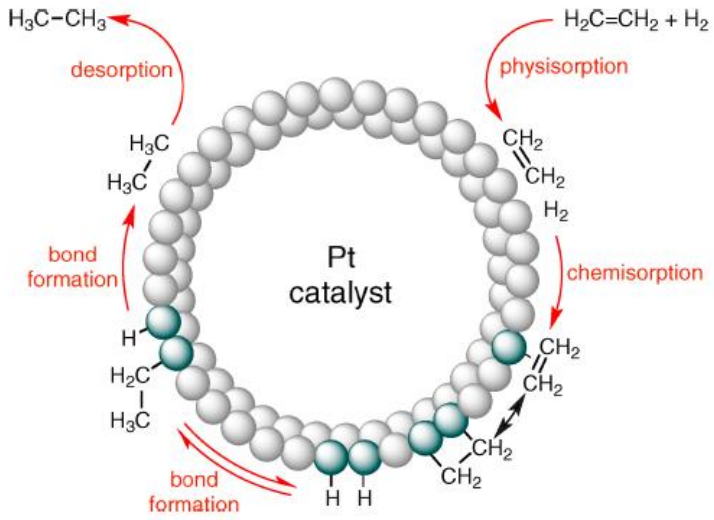

Figure 1.3: Schematic presentation of the surface processes occurring during the hydrogenation of ethylene (reused with permission from reference [7], Copyright © 2012, American Chemical Society)

The first step of the reaction is the diffusion of reactants from the bulk, and physisorption of the reactants on the surface of the catalyst, followed by the formation of chemicals bonds between the substrate and the catalyst surface (chemisorption). This is followed by the formation of a surface bound intermediate, which is the ethyl intermediate in this case. The intermediates migrate across the catalyst surface and react with surface bound hydrogen to form the C-H bonds, followed by desorption of the products. The actual addition of hydrogen to the substrate is assumed to follow the Horiuti-Polanyi mechanism, where the hydrogen molecule is first dissociated on the surface of the catalyst prior to the addition of atomic hydrogen to the substrate [60, 61]. The mechanism assumes a stepwise addition of the surface hydrogen to the adsorbed olefin [62].

1.1.3 Carbonyl hydrogenation

The hydrogenation of carbonyl groups to form alcohols is used for upgrading bulk chemicals into platform chemicals, and is especially useful during the synthesis of pharmaceuticals and upgrading of biomass derived feedstocks [63]. An example of this application is the hydrogenation of acetone for the production of isopropanol and other chemicals [64, 65], benzaldehyde for the production of benzyl alcohols [66-69], furfural [70, 71], aldehydes [72], carboxylic acids [31] and other bio-based feedstocks such as levulinic acid [73]. According to

Chen *et al*. [55], transition metals such as Pt, Pd, Rh, Ru, Ni, Cu and Co have been found to be effective in the hydrogenation of aldehydes, although Ni, Co and Cu are preferred for commercial applications due to their relatively low cost in relation to the more expensive platinum group metals.

The hydrogenation of carbonyls involves the addition of hydrogen gas to the C=O bond, resulting in its reduction into an alcohol. Several studies have been conducted to understand the mechanism of oxygenate hydrogenation on the surface of metal catalysts, which is still largely disputed. The reaction follows Langmuir-Hinshelwood kinetics, which involves the adsorption of both reactants on the catalyst surface [58]. The adsorption of carbonyls on the metal surface can proceed via two configurations; either adsorption of the aldehyde on the metal surface with a single metal atom via the two lone pair electrons on the oxygen [η^1(O) mode], or via adsorption whereby both carbon and oxygen of the carbonyl group adsorb on the surface metal atoms, forming a di-sigma complex [η^2(-C,O) mode], as represented in Figure 1.4 [72, 74]. Sinha and Neurock [75] report the preference of aldehydes to adsorb via the η^2(-C,O) mode, regardless of chain length.

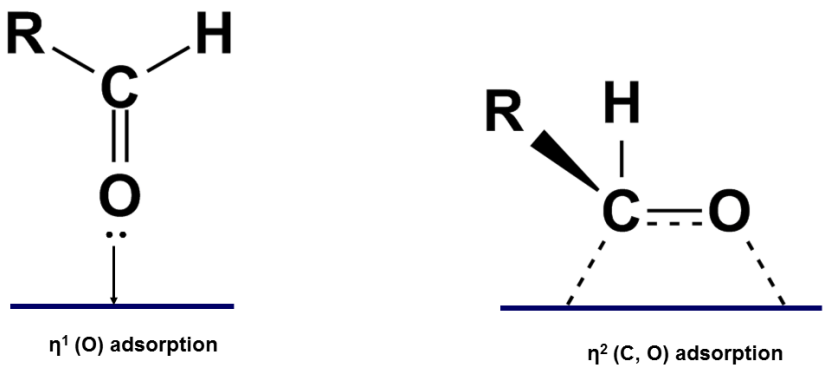

Figure 1.4: Possible C=O group adsorption modes onto a metallic active site [72, 74, 75]

The Horiuti-Polanyi mechanism is the universally accepted mechanism through which hydrogenation takes place [60, 61, 76]. However, the main dispute arises when it comes to the addition of the first hydrogen atom to the carbonyl group. The addition of hydrogen to the adsorbed carbonyl group occurs via either one of two pathways. The schematic representation shown in Figure 1.5 of the hydrogen addition to the C=O bond was adapted from Sitthisa *et al*. [74], proposed for the hydrogenation of furfural to furfuryl alcohol on the surface of a copper catalyst [74].

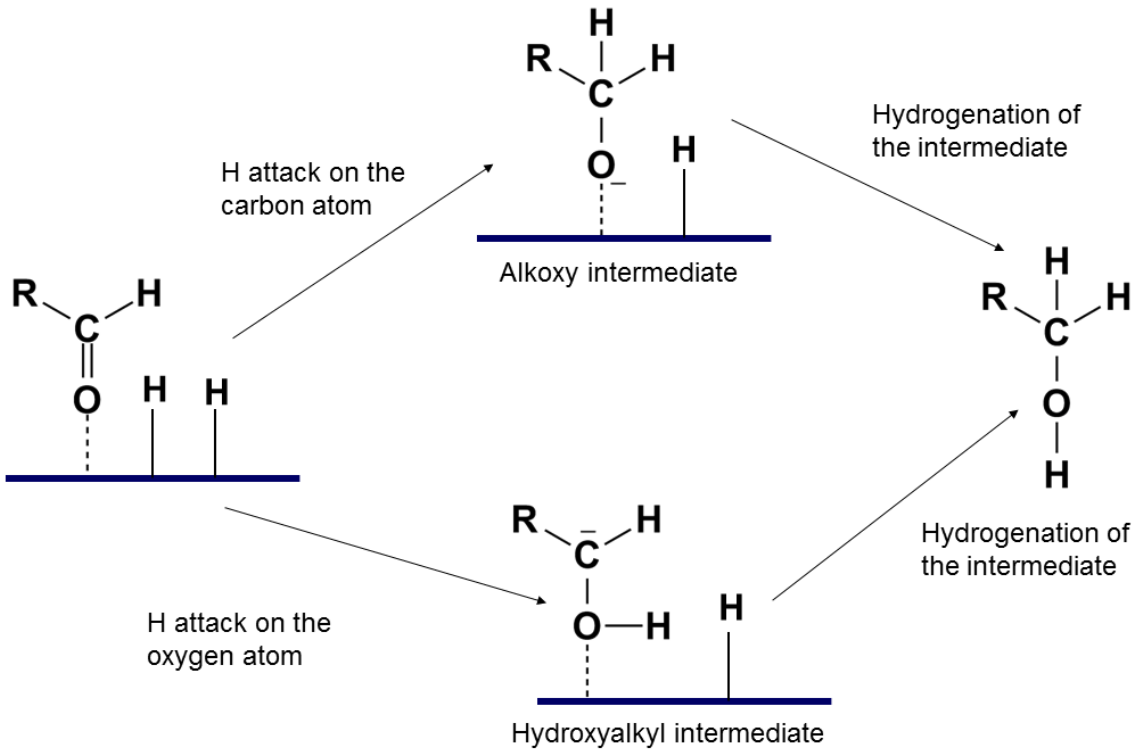

Figure 1.5: Possible intermediates during the hydrogenation of aldehydes [74]

The first pathway is referred to as the hydroxyl mechanism, and involves the addition of a surface bound hydrogen atom to the adsorbed carbonyl oxygen atom, forming a hydroxyalkyl intermediate. The second route is the alkoxy mechanism, which involves addition of the surface bound hydrogen atom to the adsorbed carbonyl carbon atom, forming an alkoxy intermediate [75]. The addition of a second hydrogen to both these intermediates results in the formation of an alcohol [74, 75].

1.1.3.1 Current research in aldehyde hydrogenation

The hydrogenation of α, β- unsaturated aldehydes to unsaturated alcohols is extensively studied and well documented in literature. The hydrogenation of aliphatic aldehydes to long chain alcohols has received correspondingly less attention [77-80]. The hydrogenation of unsaturated aldehydes is reviewed to gain further understanding of the properties of the catalyst systems used, in addition to the influence of various parameters on the activity and selectivity of the catalysts towards the activation of the C=O bond. According to a review article by Maeki-Arvela *et al.* [37], metals selective for the reduction of the C=O bond belong to groups 8, 9 and 10 of the periodic table, but their activity is greatly dependent on the supports used.

The selectivity for the reduction of the C=O bond is reportedly influenced by the size of metal particles; whereby bigger particles are reportedly more selective towards the reduction of the

C=O bond. This is attributed to bigger particles having a higher electron density compared to their smaller counterparts, although this claim is still disputed by some [37]. Smaller particles, on the other hand, are selective towards the C=C bond reduction [81, 82].

The metal dispersion and particle size is influenced by the preparation method and the nature of the support. Supports that are traditionally used during hydrogenation of α, β-unsaturated aldehydes include alumina, silica, titania and carbon [37]. Titania is a reducible support and is not widely used due to its tendency to interact strongly with the supported metal, leading to the formation of small, irreducible metal particles on the support. On the other hand, conventional, irreducible supports such as alumina and silica are preferred due to their intermediate to low metal support interaction (MSI), which is sufficient for the formation of well dispersed reducible metal particles on the surface of the support. According to published studies on conventional supports, the metal-support interaction strength for a specific metal decreases in the order of $TiO_2 > Al_2O_3 > SiO_2$ [38, 69].

Alternative supports have been investigated and include carbons [83], clays [84], and zeolites [85]. Thus, Kun *et al.* [84] conducted a study on the hydrogenation of crotonaldehyde over a clay supported Pt catalyst which was found to enhance the hydrogenation of the C=O functional group over C=C, resulting in an increase in the formation of the unsaturated alcohol. The presence of Lewis acid sites on the clay catalyst was reported to have enhanced the unsaturated alcohol selectivity. Proto *et al.* [86] have also investigated the use of Mayenite as a support for Pd in the hydrogenation of benzaldehyde, which performed better than a carbon supported Pd catalyst, and was more selective towards benzyl alcohol formation.

1.1.3.2 Hydrogenation of saturated aldehydes to alcohols

The industrial hydrogenation of aldehydes to primary alcohols for the production of detergents has been commercialised by Sasol, BASF, Shell and Evonik industries to name a few, where aldehydes are first obtained from the hydroformylation of olefins [87-89]. Oxo-alcohols are used as surfactants, polymer plasticisers, solvents in the manufacture of fine chemicals, and as ester components. These alcohols are commercially produced through a two-step hydroformylation-hydrogenation process, with each process taking place in separate reactors, under different reaction conditions [90]. Hydroformylation makes use of homogeneous cobalt-based catalysts, and produces the aldehyde. The resulting aldehyde leaves the product stream from the hydroformylation plant, and after distillation, is passed on to a hydrogenation reactor

with a heterogeneous catalyst typically based on coinage metals such as Cu or Ni, used as either single component or multi-metallic catalysts [90].

Aldehyde hydrogenation is usually carried out in the liquid phase, which allows for better temperature control through improved heat transfer, and enables the operations of the reactor under milder conditions compared to gas phase hydrogenation [64, 91-93]. The reactions are conducted at relatively low temperatures, between 90 °C and 180 °C, and high hydrogen pressures when catalysts based on Ni, Co, and Cu are used. A number of studies in the hydrogenation of long-chain aldehydes to alcohols exist, one of which includes a study by Valand *et al.* [94] that focused on the effects of using acidic Montmorillonite Clay K-10 as a support during the nickel catalysed hydrogenation of octanal to octanol, while Jeon *et al*. [95] have investigated the use of keiselghur supported nickel in the hydrogenation of a C_9 aldehyde into a C_9 alcohol.

Most of these studies show the possibility of the successful hydrogenation of aldehydes using single component nickel catalysts, whereas catalysts used in industry have multiple metallic components and are traditionally dispersed on alumina or silica supports. Examples include a $Cu/ZnO/Al_2O_3$ catalyst used for the manufacture of butanol and 2-ethyl hexanol, while other formulations include $Cu\text{-}Ni\text{-}Co\text{-}Mg/Al_2O_3$, and sulphided Ni-Mo and Co-Mo on Al_2O_3 [95, 96].

Silica and alumina have different surface acidic properties and their interaction with the metal is variable, leading to different catalytic properties and activities. A study by Saadi *et al*. [69] compared the hydrogenation activity of nickel catalysts dispersed on silica and alumina for the gas phase hydrogenation of benzaldehyde. High catalytic activity was reported for the silica supported catalyst, which was attributed to more available nickel due to the formation of larger nickel particles on the support, compared to the alumina catalyst [69, 97].

The surface acid/base functionalities of the support also influence the selectivity of the catalyst. Wang *et al.* [96] conducted a study on the reaction network of aldehydes on sulphided $Ni\text{-}Mo/Al_2O_3$ catalysts. The primary products from aldehyde hydrogenation are the alcohol, which is catalysed by the metal, and heavy products formed over support Brønsted acid/base sites. The choice of solvent also affects the activity and selectivity during hydrogenation. Hydrogenation rates are typically higher in polar solvents such as alcohols, compared to non-polar solvents [92, 93]. However, the reason has not been sufficiently established, as it does not have to do with hydrogen solubility in the solvent [98].

From the studies reviewed, the performance of a catalyst during aldehyde hydrogenation is dependent on the choice of metal, support, reaction conditions and solvent used, as well as the preparation method of the catalyst. The evaluation of the prepared catalyst is an integral part of catalyst design in order to gauge the activity and selectivity, as well as to establish optimal operating conditions. Catalytic evaluations are typically performed as either batch or continuous processes, which usually presents the need for a catalytic reactor.

1.1.3.3 Catalytic reactor systems in hydrogenation

The production of fine and bulk chemicals involves the use of either batch or continuous reactor systems, depending on the scale of production. Catalytic reactors are suitable for both gas and liquid phase processes, whereas the liquid phase hydrogenation of aldehydes is usually carried out in a continuous mode of operation using fixed bed reactors. This is preferred for large scale chemical production due to the ease of handling of large volumes of reactants, greater automation, and fewer required start-ups and shut downs, which improves process efficiency [99]. Continuous reactors can be operated with a fluidised bed, where the catalyst particles are in motion in the reaction solution, or a fixed bed, where the catalyst is immobilised in place [100].

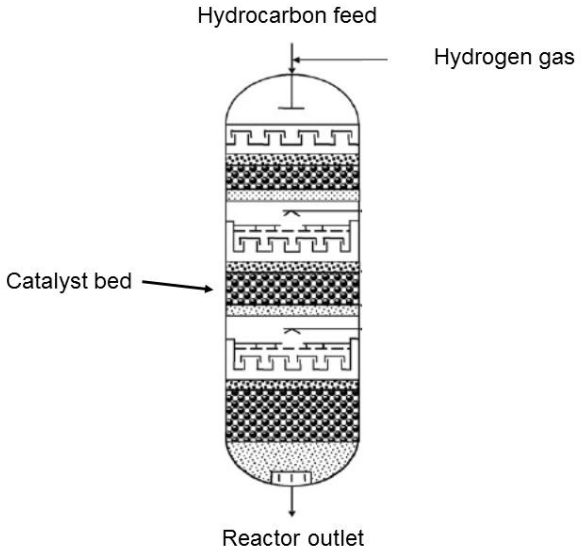

Figure 1.6: Schematic representation of a commercial fixed bed reactor [101]

Fixed bed reactors are preferred for hydrogenation processes due to low physical loss of expensive catalyst, and the possibilities of operation under high temperatures and pressures [101]. The hydrogenation reactions for this present study are carried out in a continuous flow,

fixed bed down flow reactor, whereby the liquid feed and hydrogen gas are fed concurrently. The full schematic of the reactor set up used for this study is presented in Chapter 3.

1.1.4 Catalyst deactivation

Heterogeneous catalysis remains a powerful tool for chemical transformations and in the race towards sustainable energy sources. Hence, a lot of research efforts have been directed towards the fundamental principles of catalyst synthesis and improvement of existing catalysts through the formulation of more active, selective and robust systems [102]. However, heterogeneous catalysts do not maintain their activity and selectivity indefinitely, as they tend to lose their activity with time, a process termed deactivation.

Formally, catalyst deactivation refers to the loss of catalytic activity and selectivity over time [103-105]. Although inevitable, the rate and extent of deactivation varies with different processes, ranging from seconds, in the case of fluid catalytic cracking reactions, up to several years for hydrogenation and ammonia synthesis catalysts [106-108]. The loss of activity results in a decrease in the productivity of a chemical process, adversely affecting the efficiency in utilization of chemical feedstocks, as the yield of the desired product is greatly reduced [108]. The decrease in product selectivity results in increased environmental costs for the disposal of larger volumes of by-product wastes [109]. In addition, the loss of activity leads to process shut downs to enable discharge of the inactive catalyst from the reactor, and subsequent loading of the new catalyst [109]. According to Bartholomew, the costs incurred by process shutdowns and catalyst replacement can amount to billions of dollars annually [104], notwithstanding costs associated with loss of production.

After discharge, two choices exist for the deactivated catalyst, either regeneration or disposal. Disposal of the spent catalyst presents a number of challenges; one being the stringent environmental laws governing the handling and proper containment of industrial wastes, and the public perception of chemical industries. In addition, prior to disposal, spent catalysts require specific treatments to comply with environmental legislations that are in place. This makes disposal expensive, since it also involves the loss of valuable metal components, leading to renewed interest in the study of catalyst deactivation [110].

The adverse economic and environmental effects of catalyst deactivation warrant an in-depth study into deactivation, as well as regeneration of supported metal catalysts. According to Argyle and Bartholomew [111], the topic has experienced a resurgence during the past three decades. Considerable effort has been directed towards the development of more stable

catalytic systems, with the view towards developing catalysts that are resistant to deactivation. An understanding of the catalyst and the process is first required to address the issue of deactivation, and investigate the possible avenues for regeneration.

This is especially relevant in the hydrogenation of aldehydes to alcohols, since process upsets resulting in the poor separation of the aldehyde product from the hydroformylation product stream potentially lead to contamination of the aldehyde feed with phosphine ligand. This would lead to the deactivation of the supported hydrogenation catalyst by phosphorus, which is a known catalyst poison. As such, this study aims to contribute to the existing body of knowledge by developing a feasible technique for the regeneration of a phosphorus poisoned hydrogenation catalyst. The deactivation of supported metal catalysts is discussed in depth in Chapter two, as shown in the outline, Section 1.2.

1.2 Outline

In **Chapter two**, the modes of catalyst deactivation are reviewed, such as poisoning, sintering, fouling and leaching while the possible regeneration techniques are also outlined. In **Chapter three**, the synthesis and characterisation methods for the present study are outlined, while **Chapter four** provides an in-depth discussion of the characteristics of the prepared catalysts. In **Chapter five**, the time on stream activity results of the prepared catalysts are presented and discussed for the hydrogenation of octanal in the presence and absence of poison in the feed. The results for both the alumina and silica supported catalytic systems are compared. The results obtained from the characterisation of the used catalysts are also presented and discussed. Finally, a summary and conclusion are provided in **Chapter six.**

1.3 References

[1] J.N. Armor, Catalysis Today 163 (2011) 3-9.

[2] C. Marcilly, Journal of Catalysis 216 (2003) 47-62.

[3] T.F. Degnan, Journal of Catalysis 216 (2003) 32-46.

[4] J.M. Thomas, K.D.M. Harris, Energy & Environmental Science 9 (2016) 687-708.

[5] J.G. de Vries, S.D. Jackson, Catalysis Science & Technology 2 (2012) 2009-2009.

[6] I.L.C. Buurmans, B.M. Weckhuysen, Nature Chemistry 4 (2012) 873-886.

[7] J. Heveling, Journal of Chemical Education 89 (2012) 1530-1536.

[8] B. Lindstroem, L.J. Pettersson, CATTECH 7 (2003) 130-138.

[9] A.J.B. Robertson, Platinum Metals Reviews 19 (1975) 64-69.

[10] G. Ertl, Angewandte Chemie International Edition 47 (2008) 3524-3535.

[11] E. Roduner, Chemical Society Reviews 43 (2014) 8226-8239.

[12] S.J. Meek, C.L. Pitman, A.J.M. Miller, Journal of Chemical Education 93 (2016) 275-286.

[13] S. Friedrich, F. Hahn, Tetrahedron 71 (2015) 1473-1508.

[14] B. Cornils, W.A. Herrmann, Journal of Catalysis 216 (2003) 23-31.

[15] I. Vural Gursel, T. Noel, Q. Wang, V. Hessel, Green Chemistry 17 (2015) 2012-2026.

[16] N. Pal, A. Bhaumik, RSC Advances 5 (2015) 24363-24391.

[17] M. Campanati, G. Fornasari, A. Vaccari, Catalysis Today 77 (2003) 299-314.

[18] C. Perego, P. Villa, Catalysis Today 34 (1997) 281-305.

[19] X. Carrier, E. Marceau, M. Che, Pure and Applied Chemistry 78 (2006) 1039-1055.

[20] D.E. Brown, T. Edmonds, R.W. Joyner, J.J. McCarroll, S.R. Tennison, Catalysis Letters 144 (2014) 545-552.

[21] M.J. Krische, Tetrahedron 61 (2005) 6169-6170.

[22] J.W. Erisman, M.A. Sutton, J. Galloway, Z. Klimont, W. Winiwarter, Nature Geosciences 1 (2008) 636-639.

[23] H. Schulz, Applied Catalysis A: General 186 (1999) 3-12.

[24] I. Fechete, Y. Wang, J.C. Védrine, Catalysis Today 189 (2012) 2-27.

[25] I. Mochida, O. Okuma, S.-H. Yoon, Chemical Reviews 114 (2014) 1637-1672.

[26] M.E. Dry, Catalysis Today 71 (2002) 227-241.

[27] G. Martino, Studies in Surface Science and Catalysis 130A (2000) 83-103.

[28] G. Centi, P. Ciambelli, S. Perathoner, P. Russo, Catalysis Today 75 (2002) 3-15.

[29] G. Centi, S. Perathoner, Catalysis Today 138 (2008) 69-76.

[30] M. Besson, P. Gallezot, C. Pinel, Chemical Reviews (Washington, DC, U. S.) 114 (2014) 1827-1870.

[31] J. Pritchard, G.A. Filonenko, R. van Putten, E.J.M. Hensen, E.A. Pidko, Chemical Society Reviews 44 (2015) 3808-3833.

[32] S. Dutta, S. De, B. Saha, M.I. Alam, Catalysis Science & Technology 2 (2012) 2025-2036.

[33] A.F. Lee, K. Wilson, Catalysis Today 242, Part A (2015) 3-18.

[34] S.G. Newman, K.F. Jensen, Green Chemistry 15 (2013) 1456-1472.

[35] F. Cavani, F. Trifiro, Catalysis Today 34 (1997) 269-279.

[36] C.-J. Jia, F. Schuth, Physical Chemistry Chemical Physics 13 (2011) 2457-2487.

[37] P. Maeki-Arvela, J. Hajek, T. Salmi, D.Y. Murzin, Applied Catalysis A: General 292 (2005) 1-49.

[38] A. Douidah, P. Marecot, S. Szabo, J. Barbier, Applied Catalysis A: General 225 (2002) 21-31.

[39] Q. Fu, W.-X. Li, Y. Yao, H. Liu, H.-Y. Su, D. Ma, X.-K. Gu, L. Chen, Z. Wang, H. Zhang, B. Wang, X. Bao, Science (Washington, DC, U. S.) 328 (2010) 1141-1144.

[40] M. Che, C.O. Bennett, in: H.P. D.D. Eley, B.W. Paul (Eds.), Advances in Catalysis, Academic Press, 1989, pp. 55-172.

[41] X.-F. Yang, A. Wang, B. Qiao, J. Li, J. Liu, T. Zhang, Accounts of Chemical Research 46 (2013) 1740-1748.

[42] H.M. Torres Galvis, J.H. Bitter, C.B. Khare, M. Ruitenbeek, A.I. Dugulan, K.P. de Jong, Science (Washington, DC, U. S.) 335 (2012) 835-838.

[43] G.C. Bond, Chemical Society Reviews 20 (1991) 441-475.

[44] S. Liang, C. Hao, Y. Shi, ChemCatChem 7 (2015) 2559-2567.

[45] T.Q. Nguyen, M.C.S. Escaño, H. Nakanishi, H. Kasai, H. Maekawa, K. Osumi, K. Sato, Applied Surface Science 288 (2014) 244-250.

[46] J.R.H. Ross, Heterogeneous Catalysis, Elsevier, Amsterdam, 2012, pp. 47-64.

[47] J.R.H. Ross, Heterogeneous Catalysis, Elsevier, Amsterdam, 2012, pp. 65-96.

[48] A. Gil, A. Diaz, L.M. Gandia, M. Montes, Applied Catalysis A: General 109 (1994) 167-179.

[49] P. Munnik, P.E. de Jongh, K.P. de Jong, Chemical Reviews (Washington, DC, U. S.) 115 (2015) 6687-6718.

[50] K.Y. Koo, U.H. Jung, W.L. Yoon, International Journal of Hydrogen Energy 39 (2014) 5696-5703.

[51] K.P. de Jong, in: P.A.J.P.G. G. Poncelet, B. Delmon (Editors), Studies in Surface Science and Catalysis, Elsevier, Amsterdam, 1991, pp. 19-36.

[52] T.M. Eggenhuisen, H. Friedrich, F. Nudelman, J. Zečević, N.A.J.M. Sommerdijk, P.E. de Jongh, K.P. de Jong, Chemistry of Materials 25 (2013) 890-896.

[53] J.C. Colmenares, W. Ouyang, M. Ojeda, E. Kuna, O. Chernyayeva, D. Lisovytskiy, S. De, R. Luque, A.M. Balu, Applied Catalysis B: Environmental 183 (2016) 107-112.

[54] G. Zhang, Y. Du, Y. Xu, Y. Zhang, Journal of Industrial and Engineering Chemistry 20 (2014) 1677-1683.

[55] B. Chen, U. Dingerdissen, J.G.E. Krauter, H.G.J. Lansink Rotgerink, K. Moebus, D.J. Ostgard, P. Panster, T.H. Riermeier, S. Seebald, T. Tacke, H. Trauthwein, Applied Catalysis A: General 280 (2005) 17-46.

[56] F. Nerozzi, Platinum Metals Reviews 56 (2012) 236-241.

[57] G.M. Psofogiannakis, G.E. Froudakis, Chemical Communications (Cambridge, U. K.) 47 (2011) 7933-7943.

[58] F. Zaera, Physical Chemistry Chemical Physics 15 (2013) 11988-12003.

[59] A.J. Medford, A. Vojvodic, J.S. Hummelshøj, J. Voss, F. Abild-Pedersen, F. Studt, T. Bligaard, A. Nilsson, J.K. Nørskov, Journal of Catalysis 328 (2015) 36-42.

[60] B. Yang, X.-Q. Gong, H.-F. Wang, X.-M. Cao, J.J. Rooney, P. Hu, Journal of the American Chemical Society 135 (2013) 15244-15250.

[61] B. Mattson, W. Foster, J. Greimann, T. Hoette, N. Le, A. Mirich, S. Wankum, A. Cabri, C. Reichenbacher, E. Schwanke, Journal of Chemical Education 90 (2013) 613-619.

[62] K. Tanaka, in: L. Cerveny (Ed.), Studies in Surface Science and Catalysis, Elsevier, Amsterdam, 1986, pp. 79-104.

[63] H. Liu, Q. Hu, G. Fan, L. Yang, F. Li, Catalysis Science and Technology 5 (2015) 3960-3969.

[64] M.T. Shah, A. Balouch, K. Rajar, Sirajuddin, I.A. Brohi, A.A. Umar, ACS Applied Materials & Interfaces 7 (2015) 6480-6489.

[65] O.V. Shutkina, O.A. Ponomareva, P.A. Kots, I.I. Ivanova, Catalysis Today 218–219 (2013) 30-34.

[66] F. Pinna, F. Menegazzo, M. Signoretto, P. Canton, G. Fagherazzi, N. Pernicone, Applied Catalysis A: General 219 (2001) 195-200.

[67] X. Kong, L. Chen, Catalysis Communications 57 (2014) 45-49.

[68] M.A. Vannice, D. Poondi, Journal of Catalysis 169 (1997) 166-175.

[69] A. Saadi, R. Merabti, Z. Rassoul, M.M. Bettahar, Journal of Molecular Catalysis A: Chemical 253 (2006) 79-85.

[70] G.W. Huber, S. Iborra, A. Corma, Chemical Reviews (Washington, DC, U. S.) 106 (2006) 4044-4098.

[71] M. Manikandan, A.K. Venugopal, K. Prabu, R.K. Jha, R. Thirumalaiswamy, Journal of Molecular Catalysis A: Chemical 417 (2016) 153-162.

[72] M. Mavrikakis, M.A. Barteau, Journal of Molecular Catalysis A: Chemical 131 (1998) 135-147.

[73] M.J. Climent, A. Corma, S. Iborra, Green Chemistry 16 (2014) 516-547.

[74] S. Sitthisa, T. Sooknoi, Y. Ma, P.B. Balbuena, D.E. Resasco, Journal of Catalysis 277 (2011) 1-13.

[75] N.K. Sinha, M. Neurock, Journal of Catalysis 295 (2012) 31-44.

[76] C.J. Heard, C. Hu, M. Skoglundh, D. Creaser, H. Groenbeck, ACS Catalysis 6 (2016) 3277-3286.

[77] A. Stolle, T. Gallert, C. Schmoger, B. Ondruschka, RSC Advances 3 (2013) 2112-2153.

[78] G.F. Santori, M.L. Casella, O.A. Ferretti, Journal of Molecular Catalysis A: Chemical 186 (2002) 223-239.

[79] G.M.R. van Druten, V. Ponec, Applied Catalysis A: General 191 (2000) 153-162.

[80] E.V. Ramos-Fernández, J. Ruiz-Martínez, J.C. Serrano-Ruiz, J. Silvestre-Albero, A. Sepúlveda-Escribano, F. Rodríguez-Reinoso, Applied Catalysis A: General 402 (2011) 50-58.

[81] P. Claus, S. Schimpf, R. Schodel, P. Kraak, W. Morke, D. Honicke, Applied Catalysis A: General 165 (1997) 429-441.

[82] W. Huo, C. Zhang, H. Yuan, M. Jia, C. Ning, Y. Tang, Y. Zhang, J. Luo, Z. Wang, W. Zhang, Journal of Industrial and Engineering Chemistry 20 (2014) 4140-4145.

[83] F. Zhao, Y. Ikushima, M. Chatterjee, M. Shirai, M. Arai, Green Chemistry 5 (2003) 76-79.

[84] I. Kun, G. Szollosi, M. Bartok, Journal of Molecular Catalysis A: Chemical 169 (2001) 235-246.

[85] M. Lashdaf, V.-V. Nieminen, M. Tiitta, T. Venäläinen, H. Österholm, O. Krause, Microporous and Mesoporous Materials 75 (2004) 149-158.

[86] A. Proto, R. Cucciniello, A. Genga, C. Capacchione, Catalysis Communications 68 (2015) 41-45.

[87] Focus on Surfactants 2008 (2008) 2-3.

[88] E. Van Driessche, J.-J.G. Muls, A. Van Vliet, C.R. Beck, C.M. Yarbrough, Plasticizer alcohol and production improvement, ExxonMobil Chemical Patents Inc., USA . 2010, p. 13pp.

[89] J. Rudolph, A. Ulonska, R. Papp, R. Paciello, B. Breitscheidel, K. Faller, Preparation of C17 alcohol mixtures by oligomerization and hydroformylation of olefins, BASF SE, Germany . 2009, p. 32pp.

[90] G.M. Torres, R. Frauenlob, R. Franke, A. Boerner, Catalysis Science and Technology 5 (2015) 34-54.

[91] S. Mukherjee, M.A. Vannice, Journal of Catalysis 243 (2006) 108-130.

[92] N.M. Bertero, A.F. Trasarti, C.R. Apesteguía, A.J. Marchi, Applied Catalysis A: General 394 (2011) 228-238.

[93] B.S. Akpa, C. D'Agostino, L.F. Gladden, K. Hindle, H. Manyar, J. McGregor, R. Li, M. Neurock, N. Sinha, E.H. Stitt, D. Weber, J.A. Zeitler, D.W. Rooney, Journal of Catalysis 289 (2012) 30-41.

[94] J. Valand, A.S. Mahomed, S. Singh, H.B. Friedrich,Journal of Porous Materials 23 (2016) 175-183.

[95] J.-K. Jeon, J.-H. Yim, Y.-K. Park, Chemical Engineering Journal 140 (2008) 555-561.

[96] X. Wang, R.Y. Saleh, U.S. Ozkan, Journal of Catalysis 231 (2005) 20-32.

[97] S. Soled, Science 350 (2015) 1171-1172.

[98] I. McManus, H. Daly, J.M. Thompson, E. Connor, C. Hardacre, S.K. Wilkinson, N. Sedaie Bonab, J. ten Dam, M.J.H. Simmons, E.H. Stitt, C. D'Agostino, J. McGregor, L.F. Gladden, J.J. Delgado, Journal of Catalysis 330 (2015) 344-353.

[99] K.R. Westerterp, E.J. Molga, K.B. van Gelder, Chemical Engineering and Processing: Process Intensification 36 (1997) 17-27.

[100] J.R.H. Ross, Heterogeneous Catalysis, Elsevier, Amsterdam, 2012, pp. 97-121.

[101] F.S. Mederos, J. Ancheyta, J. Chen, Applied Catalysis A: General 355 (2009) 1-19.

[102] O.A. Abdelrahman, H.Y. Luo, A. Heyden, Y. Román-Leshkov, J.Q. Bond, Journal of Catalysis 329 (2015) 10-21.

[103] S. David Jackson, Chemical Engineering Journal 120 (2006) 119-125.

[104] C.H. Bartholomew, Applied Catalysis A: General 212 (2001) 17-60.

[105] J.J. Birtill, Focus on Catalysts 2004 (2004) 1-2.

[106] J.A. Moulijn, A.E. van Diepen, F. Kapteijn, Applied Catalysis A: General 212 (2001) 3-16.

[107] S.T. Sie, Applied Catalysis A: General 212 (2001) 129-151.

[108] J. Hagen, Industrial catalysis : a practical approach, Wiley-VCH Verlag, Weinheim, Germany, 2005, pp 195-203

[109] J.J. Birtill, Catalysis Today 81 (2003) 531-545.

[110] D.L. Trimm, Applied Catalysis A: General 212 (2001) 153-160.

[111] M.D. Argyle, C.H. Bartholomew, Catalysts 5 (2015) 145-269.

Chapter 2: Review of catalyst deactivation

2.1 Catalyst deactivation

Catalyst deactivation mainly occurs via chemical, physical and thermal processes, which are further classified into several mechanisms that vary amongst gas or liquid phase processes. Most reviews that have been published cover the deactivation of catalysts applied for high temperature gas phase catalytic processes [1-3]. The current literature available is limited as it does not provide much information on liquid phase systems [4, 5].

2.2 Deactivation mechanisms

Modes of catalyst deactivation are subdivided into several mechanisms, which are presented in Table 2.1 [1, 2, 4, 6, 7]. Understanding the different deactivation mechanisms is of pivotal importance for the prevention and reversal of the deactivation process. Since catalysis is a kinetic phenomenon, the deactivation of catalysts leads to lower rates of reaction and, hence, reduced process efficiency.

Table 2.1: Mechanisms and types of catalyst deactivation [1, 2, 4, 6, 7]

Mechanism	Type	Description
Poisoning	Chemical	Strong chemisorption of contaminant species on catalytically active sites, prevent reactant adsorption
Fouling	Physical	Deposition of species from reaction medium onto catalyst pores, results in pore blockage
Thermal Degradation	Thermal	Thermally induced loss of catalytically active sites through a decrease in metal dispersion, formation of larger metal crystallites, or solid transformations
Leaching	Chemical	Dissolution of active phase into the reaction medium
Attrition/Crushing	Physical	Loss of internal surface area due to collapse of the support

To address problems caused by the deactivation of catalysts and to attempt to either prevent or remedy the issue of deactivation, an understanding of how this phenomenon occurs is imperative. A review by Bartholomew [1] addressed the mechanistic aspects of catalyst

deactivation as presented in Table 2.1, while Forzatti and Lietti [7] attempted to give a mathematical description of the effects of deactivation on the kinetics of the catalytic process. Abdelrahman *et al.* [5] and Sadaba *et al.* [4] have also made contributions through studies based on the leaching of solid catalysts in liquid phase reactions [4, 5]. In addition, these reviews aimed to provide methods to delay catalyst deactivation and improve efficiency in an attempt at prolonging the lifetime of the catalysts.

This chapter focuses on mechanisms that occur in liquid phase processes, which include poisoning, leaching, sintering and fouling. Vapour-solid/solid-solid transformations are applicable to high temperature processes, and so will not be discussed further, as the present study concerns low temperature, liquid phase hydrogenation reactions.

2.2.1 Poisoning

The "poisoning" of a catalyst results from the strong adsorption of a catalyst poison onto the catalytically active site, causing a loss of activity by decreasing the catalytically active surface area. The loss of catalytically active sites usually leads to a gradual deactivation of the catalyst. The extent of deactivation of a catalyst by poisoning is determined by the nature of the interaction of the poison with the catalytic surface, consequently affecting both activity and selectivity of the catalyst [8]. Catalyst poisons are usually present as feed contaminants at very low concentrations [9]. Poisons tend to interact very strongly with metals, whereas a separate term applies for reactants that are too slow to diffuse from the catalyst surface. These species are reversibly adsorbed and thus have temporary effects on the overall activity of the catalysts. They are therefore referred to as inhibitors [4, 7, 10].

The property that lends supported transition metal catalysts their activity is the availability of the metal's d-orbitals for reactant adsorption. During hydrogenation reactions, the reactant molecules adsorb onto the catalytically active site and subsequently dissociate. The dissociated reactants undergo surface migration to react with other dissociated molecules and form products, which then desorb from the active site and diffuse away from the catalyst surface to the bulk reactant phase. Poisons, however, form stable bonds with the active sites, a process that is irreversible as they do not desorb. Instead, they form strong coordinative bonds with the active metal [11].

Hagen [11] classifies catalyst poisons into three groups, consisting of non-metallic ions, metal ions, and unsaturated molecules. Forzatti and Lietti [7] further expand on this classification by specifying groups 15 and 16 elements of the periodic table as the most potent poisons for metal-

based catalysts incorporating Fe, Ni, Co, Pt, etc. The poisons reportedly chemisorb onto the surface atoms of these metals, which are catalytically active for chemical transformations. Chemisorption takes place via the lone pairs residing on the p-orbitals of these poisons. For a chemical species to be classified as a potential poison, it must have either one of the following properties, i.e. the molecule/atom must have unoccupied orbitals/unshared electrons or multiple bonds (such as olefins). Common catalyst poisons are listed in Table 2.2 [2, 11].

Table 2.2: Common poison species for supported metal catalysts

Chemical type	**Poison example**	**Mode of action**	**Metals affected**	**Process**
Groups 15 and 16	N, P, As, Sb, O, S, Se, Te	Strong chemisorption through *s* and *p* orbitals	Ni, Fe, Pt, Pd, Cu, Pt/Rh	Hydrogenation, ammonia synthesis, ammonia oxidation, automotive catalytic converters
Group 17 (halogens)	F, Cl, Br, I	Strong chemisorption through *s* and *p* orbitals and formation of volatile metal halides	Ni, Fe, Pt, Pd, Cu	Hydrogenation, ammonia synthesis
Toxic heavy metals and ions	As, Pb, Hg, Bi, Sn, Cd, Fe	Occupation of *d*-orbital and alloy formation	Ni, Pt, Pd, Cu, SiO_2-Al_2O_3, zeolites	Hydrogenation, catalytic cracking, ammonia oxidation
Unsaturated molecules	CO, NO, HCN, Benzene, ethyne, unsaturated hydrocarbons	Chemisorption through multiple bonds and back bonding	Ag	Ethylene oxidation to ethylene oxide

The extent of catalyst poisoning is dependent on the nature of the poisoning species, while the sensitivity of the catalyst to the poison mainly depends on the number of catalytically active

sites, the strength of chemisorption of the poison, and how effective the poison is towards the inhibition of the catalytic activity [12].

The effects of a poison species may be reversible or irreversible. In other words, the poison may be either transient, semi-transient, or permanent. A transient poison can be displaced, which enables catalyst recovery. A semi-transient poison has irreversible effects at reaction conditions, but can be reversed by changing the reaction conditions. This enables catalyst regeneration. A permanently poisoned catalyst cannot be regenerated [13]. An example of semi-transient poisoning applies in the deactivation of steam reforming catalysts by adsorbed sulphur that can be removed at high temperatures by hydrogenation with steam, making the regeneration of the catalyst possible [11].

Poisons may also tend to be selective or non-selective. Selective poisons preferentially deactivate the most active site [14], while non-selective poisons interact with all active sites, regardless of their nature. For non-selective poisons, the activity of the catalyst declines linearly with the amount of adsorbed poison [8]. An example of selective poisoning is the modification of Pt-Re/Al_2O_3 reforming catalysts through sulphur poisoning in order to limit the catalysts high hydrocracking activity [7]. Sulphur selectively deactivates catalytic sites that are highly active for hydrocracking, thus limiting activity [1, 2].

Due to their strong chemisorption onto active sites, poisons tend to accumulate on the catalyst surface, and are therefore highly effective even at very low concentrations [7]. The poisoning of a catalyst proceeds via three stages, initiated by the adsorption of the poison onto the catalyst surface. Poisonous species compete with reactants for adsorption onto the active site, diminishing the number of sites available for catalytic reactions to occur. The second stage is the surface reconstruction of the catalyst induced by the poison, and the third stage is the reaction of the catalyst with the poison to form ”metal-poison compounds” [8]. Bartholomew further expanded on this model by proposing a five-fold poisoning mechanism based on the action of the sulphur atom as it poisons an active site of a nickel ethylene hydrogenation catalyst [15]. This model pertains to poisoning of the catalytic surface, but does not address poisoning at the pellet scale and the effects of poisoning on the larger scale.

2.2.1.1 The sulphur poisoning model

Sulphur is the most widely reviewed catalyst poisoning agent because it deactivates catalysts across a wide range of applications, such as catalytic reforming, hydrogenation, catalytic cracking, methanol synthesis, etc., as most feed stocks contain traces of sulphur impurities [13, 16]. In fact, almost all catalyst deactivation reviews that include poisoning address deactivation by sulphur poisoning, hence, the choice of using sulphur to explain the action of a poison, and its overall effects on the catalyst that lead to deactivation.

Initially, the poison (in this case, sulphur) competes with the reactants for adsorption onto the active site. The poison induces both geometric (physical) and electronic changes on the active site [17, 18]. For instance, the poison physically blocks the site, preventing any reactants from adsorbing onto the occupied site. A further assumption is that the poison only blocks a certain number of active sites. However, it has been noted in practice that the chemical interaction between the poison and metal induces electronic effects on adjacent active sites, resulting in the effects of the poison having a wider radius than the expected geometric proportions of the poison itself. The electronic effects, also referred to as ligand effects, are induced by the long-range depletion of surface electrons by the poison, which depletes the number of electrons available for bonding with a reactant [19-21].

In short, a poison physically blocks an active site in three dimensions, and electronically modifies neighbouring atoms such that their ability to adsorb and dissociate oncoming reactants is diminished [2, 8, 22]. Additionally, the poison may inhibit the surface mobility of dissociated reactants, preventing surface reactions that follow the Langmuir-Hinshelwood type surface reaction mechanism and, hence, the formation of reaction products [2].

2.2.1.2 Poisoning at the catalyst pellet and catalyst bed

The catalyst pellet undergoes poisoning via two possible mechanisms, either through a uniform mode or by a shell progressive mode. During uniform poisoning, all active sites are deactivated uniformly throughout the pellet, whilst for shell progressive poisoning, the active sites are deactivated from the outside of the pellet to the inside. The shell progressive model, also referred to as pore mouth poisoning, was proposed based on the assumption that strongly adsorbed poisons accumulate at the exterior of the porous catalyst pellet, with the amount of adsorbed poison diminishing further into the catalyst pores. This supposedly results in the pore having two zones; a zone that is saturated with poison and is effectively deactivated, whilst the

second zone remains un-poisoned [7], although the poison front moves towards the pore interior with time [23].

During uniform catalyst poisoning, the poison is evenly distributed throughout the catalyst pellet [7, 9]. This is usually ascribed to non-selective poisons with low affinities for active sites [7, 9]. In practice, deactivation by poisoning is an average of these two models. For a shell-progressive model, the rate of reaction declines rapidly for internal mass transfer controlled processes, while the decline in activity of a uniformly poisoned catalyst is not as rapid under mass transfer control [7, 9]. On the reactor scale, the adsorption of the poison on the catalyst bed is non-uniform. The poison concentration decreases as the poison travels down the catalyst bed, meaning that deactivation is more pronounced at the top of the catalyst bed and least pronounced at the bottom [2, 6].

2.2.1.3 Phosphorous poisoning

Reduced phosphorous species are known to be site-blocking catalyst poisons that are highly effective even at low concentrations, usually encountered in methanol synthesis reactions, natural gas oxidation catalysts, hydrodesulphurization catalysts and automotive catalysts [24-28]. Phosphorous is a non-selective poison that indiscriminately targets both the support as well as the metallic active sites by forming coordinative bonds with the metal via its lone pair of electrons, and bonds to the Brønsted and Lewis sites on the support [29]. This has been observed in the case of automotive catalysts, where phosphates from engine oil additives form bonds with the metal, occlude catalyst pores, and further react with the alumina support to form $AlPO_4$, which is acidic [24].

Phosphorus is an electronegative element with a lone pair of electrons, and uses these electrons to coordinate to a vacant d-orbital of a metal. The accompanying pi back-donation of electrons from the metal to the phosphorus results in a bond that is highly covalent in nature [30, 31]. According to Chandrasekaran *et al.* [32], the metal-phosphorus bond is predominantly metallic, and therefore fairly strong. Phosphorus induces both electronic and geometric effects on the catalyst, which affect the adsorption and dissociation of reactants [33]. According to Kiskinova and Goodman [34], the adsorption of phosphorus on a nickel catalyst decreases the hydrogen uptake of the catalyst. The hydrogen may also instead adsorb on phosphorus, hindering the surface activation of hydrogen by the catalyst [34]. A conceptual model of the adsorption of phosphorus on nickel is presented in Figure 2.1, showing the association of phosphorus with the Ni atoms.

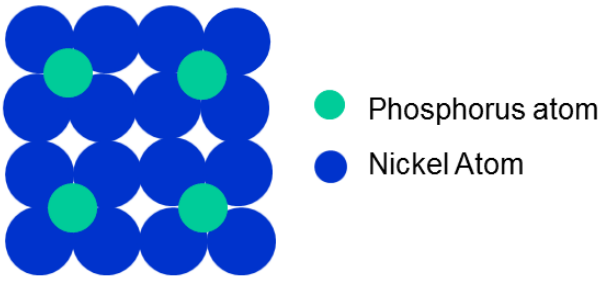

Figure 2.1: Conceptual model of the adsorption of phosphorus onto nickel [35].

The model agrees with the report made by Goodman [36], which states that the number of nickel atoms that can be affected by a single phosphorus atom, is four. Due to its lower electronegativity, the effect of phosphorus has a smaller radius compared to sulphur, since the long range electronic effects of sulphur extend to a much wider atomic radius of up to ten neighbouring nickel atoms [36].

The effects of phosphorus on a catalyst are not only electronic, but also physical and chemical. Quinn *et al.* [37] evaluated phosphine (PH_3) as one of the contaminants affecting the performance of a commercially available $Cu/Zn/Al_2O_3$ catalyst for methanol synthesis. Phosphine was found to be a potent catalyst poison that resulted in a drop in the reaction rate constant, and was found to have accumulated on the catalyst surface, which was attributed to phosphine having reacted with metallic copper to form a Cu_3P species under reducing conditions [37]. The formation of metal-phosphorus compounds has been observed in an unrelated study, where a Ni/YSZ (yttria stabilised zirconia) based solid oxide fuel cell electrode was exposed to phosphine gas. The authors reported the formation of a nickel phosphide phase, in addition to phosphorus induced migration of nickel, resulting in the formation of nickel-phosphide agglomerates [38]. Phosphorus also reacts with catalyst support materials such as alumina, forming an acidic $AlPO_4$, or ceria, forming cerium phosphate [24, 39-41].

2.2.1.4 Poisoning of hydrogenation catalysts

The poisoning of liquid phase hydrogenation catalysts by strongly adsorbed heteroatom containing molecules has been cited as one of the contributing factors in the deactivation of liquid phase catalysts. According to Besson and Gallezot [42], the leading cause through which these molecules deactivate liquid phase catalysts is through their accumulation on the catalyst surface, in addition to their effectiveness at low concentrations. The adsorption of these poisoning species is irreversible under liquid phase hydrogenation conditions, since the

processes occur at temperatures not sufficiently high to facilitate desorption of these species. The accumulation of the catalyst poison results in a steady increase in deactivation with time and, hence, a decrease in the catalytic activity.

Sulphur is the most extensively studied poison for hydrogenation catalysts, and has been covered in several reviews [1, 7, 25, 42], as well as in significant volumes of published studies [43-45]. Some studies have involved the comparison of different supports to gauge their effects in the stability of a catalyst towards sulphur poisoning. Thus, a study by Pinna *et al.* [45] compared the stability of 5 wt.% palladium catalysts on alumina, silica and carbon against sulphur poisoning during the hydrogenation of benzaldehyde. An overall decrease in the hydrogenation activity was reported across all supports, with the carbon supported catalyst being most significantly deactivated. The poisoning of the Pd/C catalyst also led to an improvement in the selectivity towards benzyl alcohol, the desired product.

The effects of phosphorus poisoning have been discussed in studies on the deactivation of catalysts used for the hydrogenation of natural fats and oils to fatty alcohols. A study by Huang *et al.* [46] details the deactivation of a Cu/Zn catalyst used for the hydrogenation of dodecyl methyl ester to dodecanol. The main aim of the study was to observe the effects of an increase in trimethyl phosphate concentration from zero to 1.0 mmol per gram of catalyst on the hydrogenation activity and selectivity of a Cu/Zn catalyst prepared by co-precipitation. An increase in the contaminant concentration resulted in an overall decrease of the activity and selectivity. The addition of 1.0 mmol of trimethyl phosphate per gram of catalyst resulted in complete deactivation, with no observable conversion of the feed. The used and deactivated catalyst samples were extensively characterised to observe the effects of the poison on the physicochemical properties of the catalyst itself, and the impact of increasing the contaminant concentration. The results obtained from XPS confirmed the presence of phosphorous on the surface of the deactivated catalysts. Furthermore, the BET surface area of the catalysts was found to decrease with increasing trimethyl phosphate concentration. From BET results, the authors argued that the increase in adsorbed trimethyl phosphate resulted in the blockage of smaller pores, thereby leading to a decrease in the BET surface area. From the concluding remarks, it can be assumed that the authors attributed the deactivation of the Cu/Zn catalyst on the physical adsorption of trimethyl phosphate [46].

Aldehyde hydrogenation catalysts are known to deactivate through phosphorus poisoning, although not a lot of reports exist in the open literature addressing this problem. Instead,

representative studies involving liquid phase hydrogenation and catalyst deactivation through poisoning by phosphorous and sulphur have been reviewed, to gain insight into the effects of phosphorous on the overall activity and physicochemical properties of the catalysts used in these studies. A study by Maeki-Arvela *et al*. [47] details the deactivation of Pd/C catalysts in the hydrogenation of β – sitosterol to β-sitostanol. The catalysts underwent deactivation by phosphorous and sulphur poisons contained in the feed, resulting in a decrease in the conversion of β-sitosterol.

McCue *et al.* [13] studied the interaction between phosphorus and a palladium catalyst for the selective hydrogenation of acetylene. CO chemisorption results confirmed the adsorption of triphenylphosphine (PPh_3) onto metal crystallites on the catalyst surface, since the metallic surface area was lowered for PPh_3 modified catalysts, compared to the blank Pd/TiO_2 sample. In addition, the metallic surface area decreased with an increasing molar ratio of the ligand. The decrease in metallic surface area was attributed to the direct adsorption of a fraction of the added ligand onto the metal surface, while some of the ligand was suspected to have adsorbed onto the support.

The FTIR results indicated an increase in CO adsorbed in the bridge mode in comparison to species adsorbed in the linear mode, with the addition of PPh_3. The authors attributed this to a loss of 3-fold hollow active sites, leading to a suggestion that the ligand blocks sites associated with CO adsorption due to the bulky nature of PPh_3. The susceptibility of the ligand towards decomposition was monitored by thermogravimetric analysis coupled with mass spectrometry. The ligand was found to remain intact even at temperatures as high as 600 Kelvins (327 °C), since no fragments attributed to its decomposition were detected by mass spectrometry [13].

2.2.2. Leaching

Leaching is the loss of active sites through dissolution of the catalytically active phase into the reaction medium, and can be encountered in reactions performed in the liquid and gas phase [48]. This is cited as the main cause of deactivation for reactions in the liquid phase [5, 42, 49]. It is defined as the formation of a new phase that is soluble in the reaction medium from an insoluble solid phase, and is influenced by pH [4, 16, 50]. Sadabà *et al*. [4] reported two main mechanisms through which leaching occurs. The first mechanism involves the direct solubilisation of metal oxides, hydroxides and carbonates into the reaction medium due to a slight solubility in the solvent used for the reaction, e.g. water.

According to the second mechanism, leaching occurs as a form of extraction, where the solvent reacts with the components of the solid catalyst, forming soluble species that dissolve within the reaction medium. This is mainly observed in reactions occurring in the presence of acidic or basic solutions. This model is modified in the case of organic solvents. Polar solvents and organic compounds containing oxygen, nitrogen or sulphur functionalities act as chelating agents that form complexes with supported metals, resulting in soluble complexes that are dissolved in the liquid medium [51]. These compounds reportedly have effective extraction capabilities [4, 51]. Leaching by extraction occurs via the mechanism illustrated in Figure 2.2 [16].

Leaching has been widely encountered in the conversion of biomass to value added products [4, 52, 53]. Hengne and Rode [53] conducted a study on the hydrogenation of levulinic acid and its esters into γ-valerolactone using Cu-ZrO_2 and Cu-Al_2O_3 composite catalysts in water and methanol. Leaching was observed for the Cu-Al_2O_3 catalysts in both water and methanol, with more leaching observed in water. The Cu-ZrO_2 catalyst fared better in water, whilst no leaching was observed in methanol. Leaching was attributed to the complexation of copper with levulinic acid to form a soluble metal carboxylate that resulted in a blue solution.

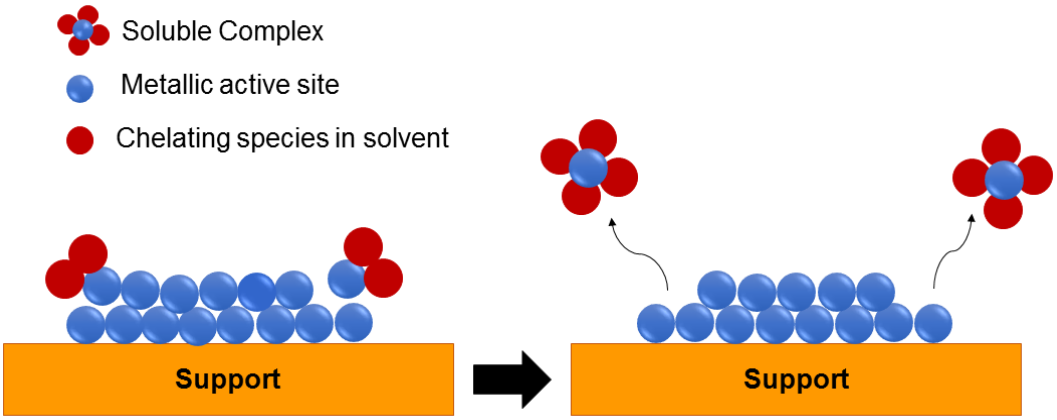

Figure 2.2: Leaching of metal active site through chelation by solvent molecules (redrawn with permission from reference [16], Copyright © 2001 Elsevier)

The leaching of metal catalysts has been observed during liquid phase hydrogenation of hydrocarbons [54]. Panpranot *et al.* [55-58] have extensively studied the leaching of Pd supported catalysts used in liquid phase hydrogenation reactions. From one of their studies, the leaching of silica supported palladium was established to be one of the contributing factors in the deactivation of the catalyst during a liquid phase hydrogenation of hexene in ethanol [58].

2.2.3 Fouling (coking and carbon deposition)

Fouling is defined as the physical deposition of species from the fluid phase onto the catalyst surface, resulting in the decline of catalytic activity through the physical blockage of the catalyst's active sites or pores. This may also lead to the disintegration of catalyst particles, and effectively reduces the surface area of the catalyst. According to Argyle and Bartholomew [2], fouling refers to both carbon deposition and coking, which originate from different sources. Carbon is defined as originating from the disproportionation of CO, whilst coke is produced from the decomposition or condensation of hydrocarbons on the catalyst surface [1, 7].

Coke has different forms that vary from polymeric species to graphitic form, forming from side reactions occurring during the catalytic processing of hydrocarbons. These side reactions mainly take place on acidic sites of the catalysts, and involve polymerization or condensation of hydrocarbons into heavy, unsaturated by-products that remain deposited on the catalyst surface as carbonaceous residues [59-61]. At high temperatures, the heavy, polymeric by-product species may be dehydrogenated to carbon, resulting in the formation of what is referred to as coke. Aromatic and unsaturated hydrocarbons are commonly reported coke precursors, and may either form as by-products or are introduced in the reaction feed [7]. In essence, the polymeric residues act as coke precursors, and may chemisorb onto the active sites of the catalyst [1].

A review by Bartholomew [1] states two kinds of reactions, namely coke sensitive and coke insensitive. For coke sensitive reactions, coke is deposited onto the catalytically active sites, resulting in activity decline over time, whilst for coke insensitive reactions, coke precursors deposited on the catalyst are removed by hydrogen or other gasifying agents such as H_2O and O_2 [1]. As such, reactions that are coke sensitive are those that utilize acidic catalysts and operate in a hydrogen deficient environment [1, 16]. According to various sources, catalytic cracking, hydro-desulphurization, and steam reforming catalytic processes are most prone to coking, although the most coke sensitive process is petroleum reforming through catalytic cracking.

Bartholomew [1] provided an illustration, adapted in Figure 2.3, that shows the effects of fouling on supported metal catalysts. It was reported that the carbon may block access of reactants to active sites by either forming physical multi-layers on the catalyst, or by strongly chemisorbing onto the surface. Alternatively, the carbonaceous deposits may encapsulate the metal particles, resulting in complete deactivation of the active site, or physically plug

micropores and mesopores, which prevents the diffusion of reactants to pore active sites [1]. The deposition of coke in catalyst pores results in a decrease in the catalyst's surface area, which significantly affects mass transfer controlled reactions. The accumulation of coke within catalyst pores decreases their effective diameter, resulting in increased diffusion resistance of reactants and products in and out of the catalyst pores [7].

Liquid phase reactions usually occur at lower temperatures compared to gas phase reactions, but are also affected by fouling, especially over acidic catalysts, through the formation of by-products [59, 62, 63]. Hence, it is to be expected that fouling would be listed as one of the contributing factors towards the deactivation of liquid phase hydrogenation catalysts. A review by Besson and Gallezot [42] focuses on deactivation by leaching, poisoning and metal oxidation. However, the deposition of oligomeric species on supported metal catalysts was briefly mentioned in relation to the oxidation of 3-hydroxypropanal. Fouling of hydrogenation catalysts is only mentioned in the case of deposition of inactive metals brought about by corrosion of reactor components.

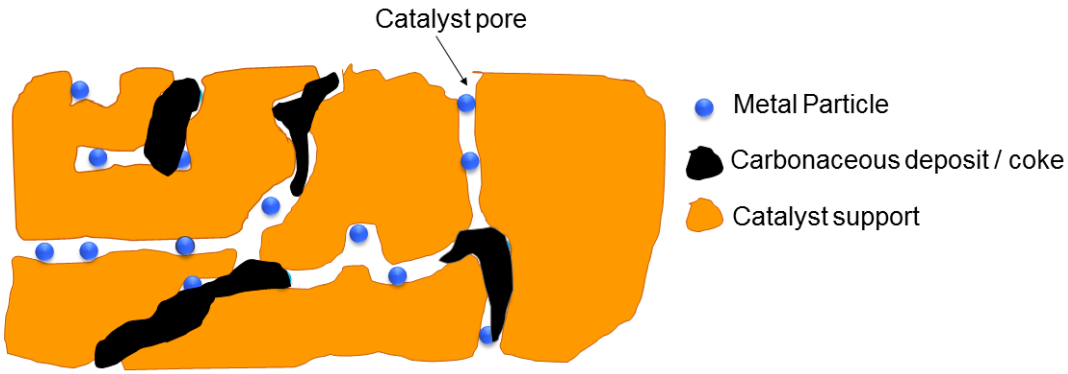

Figure 2.3: Conceptual model depicting the crystal encapsulation and pore plugging of a supported metal catalyst by carbonaceous deposits [1, 16] (redrawn with permission from reference [16], Copyright © 2001 Elsevier)

Despite a lack of reports addressing fouling of liquid phase hydrogenation catalysts, a study by Maeki-Arvela *et al*. [47] found that it may play a minor role in the deactivation of liquid phase hydrogenation catalysts. The study entailed the deactivation of palladium catalysts supported on mesoporous and microporous carbon, during the hydrogenation of β – sitosterol to β - sitostanol. Catalyst deactivation was attributed to both fouling and poisoning of the catalyst by sulphur and phosphorous contaminants. However, there was a significant decrease in the surface area of the microporous catalyst due to fouling.

2.2.4 Sintering

Sintering is defined as the growth of metal crystallites, and occurs for both supported and unsupported catalysts [15]. Catalysts are supported to achieve a high degree of dispersion, which is proportional to the number of catalytically active sites. High metal dispersion results in a higher metallic surface area and, hence, a greater number of exposed active sites on the catalyst carrier. Sintering causes the aggregation of small crystallites into bigger particles [64]. This results in an overall decrease of the metal dispersion and metallic surface area [7, 65].

Reviews by Argyle and Bartholomew [2] and Bartholomew [1] attribute crystallite growth by sintering to three mechanisms, namely (a) crystallite migration, (b) atomic migration and (c) vapour transport, which is reported to occur at high temperatures and applies to vapour phase catalytic reactions. Reviews by Moulijn *et al.* [16], Forzatti and Lietti [7] only mention crystallite migration and atomic migration. The crystallite migration model depicts sintering as occurring through the diffusion of metal crystallites along the support surface. The migrating crystallites collide and coalesce into a larger crystallite.

Atomic migration, also referred to as Ostwald ripening, attributes sintering through the escape of atoms from a metal crystallite. Atoms escape from small crystallites, and diffuse across the surface of the support. The atoms collide with, and are captured by, larger crystallites, which leads to the formation of larger particles [1, 66, 67]. Since the formation of larger crystallites is favoured due to their stability in comparison to smaller ones, the larger crystallites are formed at the expense of the smaller ones. The actual process may involve all the mechanisms occurring in conjunction with each other [1]. Figure 2.4 depicts the growth of a metal particle due to sintering, taken from [1].

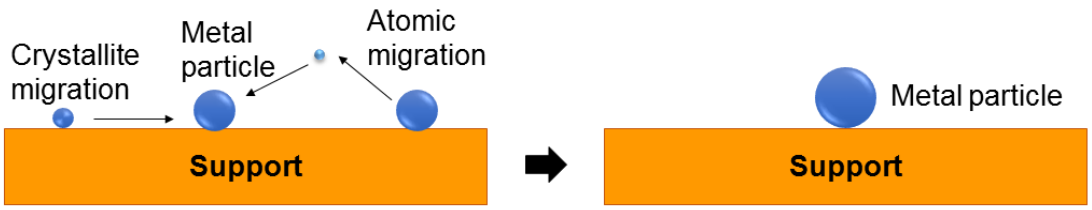

Figure 2.4: Sintering of a metal particle by both atomic migration and crystallite migration [1] (redrawn with permission from reference [1], Copyright © 2001 Elsevier)

The relationship between sintering and temperature can be understood in relation to the melting point of the metal. For instance, the mobility of atoms increases closer to the melting point,

which leads to faster solid state diffusion [16]. In order to approximate the temperature at which sintering occurs, Tamman and Hüttig temperatures are used, and these are directly related to the melting temperature of the metal according to a fractional approximation represented by the following semi-empirical expressions [16];

$T_{Hüttig} = 0.3T_{melting}$

$T_{Tamman} = 0.5T_{melting}$

When the Hüttig temperature is reached, atoms located at crystal defect sites become increasingly mobile and diffuse on the surface, while bulk atoms become mobile when the Tamman temperature is reached [68]. At the melting temperature, the mobility is sufficiently high, such that the atoms start exhibiting liquid-phase behaviour. As such, sintering rates for metals and metal oxides start being significant above the Hüttig temperature, and are very high near the Tamman temperature [2]. Another factor to take into consideration when estimating the temperature at which solids become mobile is the size and morphology of the metal crystallites. For small particles, the temperature at which mobility occurs may be lower than that indicated by the Tamman and Hüttig temperatures [16].

Sintering is also dependent on the environment in which the catalyst is being operated. For instance, it is more prevalent under oxidizing conditions, compared to reducing conditions [1]. The physicochemical properties of a metal also influence how susceptible the metal crystallites are to sinter. The stability of a metal crystallite against sintering decreases with a decreasing melting point, in the order; Ru > Ir >Rh > Pt > Pd > Ni > Cu > Ag [1]. The relationship between the metal and support may also play a role, with a stronger metal-support interaction resulting in an added stability towards sintering [69]. However, if the metal-support interaction is too great, it decreases the availability of active sites through the formation of a metal-support compound via solid state transformation [7].

Solid state transformation is an extreme form of sintering which involves the change of a crystalline phase into an inactive phase [7]. An example of phase transformation is the incorporation of nickel supported on γ-Al_2O_3 into the support. This is induced at high temperatures and results in the formation of a nickel-aluminate spinel, and is brought about by a strong interaction between the small, finely divided nickel particles and the support. This decreases the number of catalytically active sites, as the amount of active nickel is lowered [7].

Sintering is also observed for liquid phase hydrogenation reactions at lower temperatures, which is driven by atomic migration rather than temperature induced migration, as reported in high temperature gas phase systems [7]. The migration of atoms during liquid phase reactions is facilitated through the extraction of atoms from metal crystallites by chelating molecules which contain heteroatoms such as compounds with oxygen, sulphur, or nitrogen functionalities and organic acids which transport these atoms to bigger crystallites [42, 64, 70]. Triphenylphosphine has also been observed to induce sintering through Ostwald ripening [38, 71-73].

Smejkal *et al.* [74] have shown the occurrence of sintering at lower temperatures, although sintering has been previously reported for high temperature processes [67, 74]. During the study, extensive sintering was observed for a Pd-Au/SiO_2 catalyst used in the production of the vinyl acetate monomer. Although the reaction was carried out in the gas phase, it was done at relatively low temperatures, in the range of 150 to 190 °C. The most surprising outcome of this study was that sintering was more severe at lower temperatures (155 °C) compared to higher temperatures, as particle agglomeration was more pronounced [74].

A study by Panpranot *et al.* [56] showed, during the hydrogenation of 1-hexene in ethanol over 0.5 wt.% palladium catalysts supported on amorphous silica and MCM-41, that there was significant sintering of the catalysts despite the mild reaction conditions. This was shown by results obtained from chemisorption, transmission electron microscopy and X-ray diffraction analyses.

2.3 Post reaction Characterisation

The deactivation of catalysts not only affect their activity and selectivity, but also leads to the modification of physical characteristics and surface compositions. Fouling specifically affects the porosity of the catalyst and support, leaching results in a change in the catalyst composition, poisoning diminishes the number of catalytically active sites, whilst sintering affects metal dispersion. Therefore, the characterisation of deactivated catalysts is an important component in deactivation studies, leading to further understanding of the deactivation mechanisms. This helps in determining whether deactivation is due to a singular event, or is a result of a combined effect of the different mechanisms [12].

Catalyst deactivation is usually diagnosed through the changes in the activity of the catalyst during time on line reactions, such as a reduction in the conversion and changes or loss of

product selectivity. Despite this, further characterisation of the physicochemical properties of the discharged catalysts is important, as the observed properties can then be correlated to the behaviour of the catalyst as it loses its efficiency [75].

Surface area analysis is one of the most useful techniques for the identification of fouling, since the deposition of polymeric condensation products leads to the blockage of catalyst pores, resulting in an overall decrease in the material's surface area. Thermogravimetric analysis and differential scanning calorimetric analysis (TGA-DSC) is another effective method of determining the extent of deposition of carbonaceous species on the catalyst [76]. Additionally, Raman spectroscopy and infrared spectroscopy are useful techniques in the determination of adsorbed organics [77].

Electron microscopy techniques are useful in the characterisation of the surface characteristics, including the surface composition of different species that might be adsorbed onto the spent catalysts. The use of scanning electron microscopy, coupled with energy-dispersive X-ray spectroscopy, is particularly helpful in the observation of poison distribution, giving information on the location of the poison, whereas transmission electron microscopy is useful in determining the extent of sintering [78, 79].

Additionally, the characterisation of the surface chemical properties is crucial, as these can be correlated to the selectivity changes experienced during operation. Deactivation may affect or influence the acidity of the catalyst, leading to a change in the selectivity of by-products. This could be related to a change in the strengths of the catalysts' acid sites, which could be characterised by the adsorption of an appropriate acidity probe molecule, such as by ammonia temperature programmed desorption, or by pyridine adsorption infrared spectroscopy [76].

2.4 Regeneration

Following the deactivation of a catalyst, the choice could be either disposal or regeneration. Disposal is undesirable from an economic standpoint, as it results in the loss of expensive metals. In addition, it is not advisable from an environmental perspective, due to more stringent laws put in place that regulate the disposal of materials that are potentially harmful to the environment [80]. Hence, disposal is at most considered the last resort, while other alternatives are considered. A more feasible alternative is regeneration, which is the recovery and restoration of lost catalytic activity [2].

Regeneration hinges upon several factors that include, but are not limited to, the deactivation mechanism and the reversibility of the process, the economic viability and necessity of regeneration, and the catalytic process mode (batch or continuous). The regeneration of catalysts deactivated by carbon deposition is much easier than the regeneration of sintered catalysts. Some poisons can be removed through changing reaction conditions, whilst others are irreversible [2]. Prior to deciding on the regeneration method, the deactivation mechanism must be well established, as must the effects that the regeneration treatment will have on the properties of the catalyst after regeneration.

Different regeneration treatments have been reported, and these vary across processes, and modes of deactivation [2, 44, 81]. As most industrial processes are performed in a continuous mode of operation similar to this study, the ensuing discussion focuses on regeneration during continuous processes. Jackson lists three possible methods of regeneration, namely thermal, reductive and oxidative [6].

Thermal regenerations involve treatment of the spent catalyst at high temperatures, and may be coupled with either reductive or oxidative regeneration. Carbonaceous species adsorbed onto catalysts are removed through gasification in air, water, carbon dioxide, or hydrogen gas at moderate to high temperatures to remove polymeric species, whilst temperatures are much higher for the removal of graphitic carbon [2, 81-83]. This treatment has its own drawbacks, since the treatment of catalysts at high temperatures under oxidizing condition causes sintering and other changes in the properties of the catalyst, resulting in the recovered activity being less than the intrinsic activity [2, 6, 82].

Sintering is reported to be mainly irreversible, yet re-dispersion has been shown to be possible [79, 84]. Re-dispersion is usually achieved through treatment at high temperatures with chlorine and oxygen, a process termed oxychlorination [79]. Other re-dispersion methods include either treatment with a mixture of gases containing hydrochloric acid, water vapour, oxygen and nitrogen under high temperatures or treatment at high temperature with static oxygen, followed by reduction [82, 85]. Re-dispersion has mainly been reported for catalysts based on noble metals such as platinum, rhenium and rhodium, whose applications range from naphtha reforming to automobile exhaust catalysts [82, 85].

Studies documented in literature only address the regeneration of methane combustion and methanation catalysts poisoned by sulphur species using hydrogen [86-88], while not a lot exist on the regeneration of phosphorus poisoned catalysts. A study by Hoyos *et al.* [89] details the

regeneration of alumina supported platinum and palladium catalysts used for the dehydrogenation of cyclohexane. The sulphur poisoned catalysts were regenerated by treating the catalysts under a flow of hydrogen, at varying temperatures. The activity of palladium was sufficiently recovered with hydrogen treatment at higher temperatures, while the regeneration of the platinum catalyst proved less effective. The regeneration of a sulphur poisoned Pt [90], Pd [91] and Ni [92] hydrogenation catalysts has also been documented.

A method for the regeneration of an aldehyde hydrogenation catalyst poisoned by phosphorus was reported in a recent patent by Kim *et al.* [93]. The method involved the deactivation of a supported metal (Ni or Pt) hydrogenation catalyst with phosphorus (triphenylphosphine), followed by regeneration, which was carried out *in situ* without removal of the catalyst from the reactor system. This is advantageous as it eliminates the need for additional catalyst treatments, such as re-reduction of the catalyst after reintroduction into the reactor. According to the authors, the catalytic activity was sufficiently recovered. However, it is not explicitly stated to what extent. The effects of poisoning and regeneration on the selectivity of the products were also not discussed.

Another study by L'Argentière and Fígoli [92] on the poisoning effects of thiophene in the hydrogenation of styrene, showed a decrease in activity for the Ni/SiO_2 catalyst with exposure to thiophene. The activity was reportedly recovered by treatment with hydrogen and 2-butyne. However, the recovered activity was lower than the initial activity. Hydrogen treatment was also found to be effective in regeneration of an arsenic poisoned CeO_2-WO_3 / TiO_2 catalyst used for the selective catalytic reduction of NO_x [94].

From the mentioned studies, hydrogen treatment appears to be an effective regeneration technique for poisoned metallic catalysts, hence the motivation behind its use for regeneration of the poisoned hydrogenation catalysts in the present study. Although the study focuses on catalyst deactivation by poisoning, other mechanisms are also considered as they could simultaneously contribute to the overall deactivation of the catalysts.

2.5 Aims and Objectives

The main aim of this study was to establish a feasible method for the regeneration of phosphorus poisoned nickel hydrogenation catalysts supported on γ-alumina and commercial silica during the time on stream hydrogenation of octanal to octanol. The catalysts were dispersed on two different supports to observe the influence of the support on the extent of

deactivation, and ease of regeneration of the poisoned catalysts through several regeneration procedures. The regeneration treatments included the use of hydrogen, octanol, and a combination of the two. In addition, the relationship between phosphorus and the active metal was probed to understand the nature of the nickel-phosphorus interaction and to establish whether the poison selectively deactivates the metal or if it also affects the support. The effects of deactivation and regeneration on the catalyst properties were also probed through characterisation to determine the changes in metal dispersion, catalyst surface acidity, surface area, and the site of phosphorus adsorption.

2.6 References

[1] C.H. Bartholomew, Applied Catalysis A: General 212 (2001) 17-60.

[2] M.D. Argyle, C.H. Bartholomew, Catalysts 5 (2015) 145-269.

[3] S.T. Sie, Applied Catalysis A: General 212 (2001) 129-151.

[4] I. Sadaba, M. Lopez Granados, A. Riisager, E. Taarning, Green Chemistry 17 (2015) 4133-4145.

[5] O.A. Abdelrahman, H.Y. Luo, A. Heyden, Y. Román-Leshkov, J.Q. Bond, Journal of Catalysis 329 (2015) 10-21.

[6] S. David Jackson, Chemical Engineering Journal 120 (2006) 119-125.

[7] P. Forzatti, L. Lietti, Catalysis Today 52 (1999) 165-181.

[8] L.L. Hegedus, R.W. McCabe, in: B. Delmon, G.F. Froment (Eds.), Studies in Surface Science and Catalysis, Elsevier, Amsterdam, 1980, pp. 471-505.

[9] L.M. Madeira, A.E. Rodrigues, The Canadian Journal of Chemical Engineering 91 (2013) 203-211.

[10] J.P. Boitiaux, J. Cosyns, F. Verna, in: B. Delmon, G.F. Froment (Eds.), Studies in Surface Science and Catalysis, Elsevier, Amsterdam, 1987, pp. 105-123.

[11] J. Hagen, Industrial catalysis : a practical approach, 2nd Edition, Wiley-VCH Verlag, Weinheim, Germany, 2005, pp 195-203.

[12] J. Haber, J.H. Block, B. Delmon, Pure and Applied Chemistry 67 (1995) 1257-1306.

[13] A.J. McCue, F.-M. McKenna, J.A. Anderson, Catalysis Science & Technology 5 (2015) 2449-2459.

[14] G.C. Bond, M.R. Gelsthorpe, R.R. Rajaram, R. Yahya, in: A.Z. Claudio Morterra, C. Giacomo (Eds.), Studies in Surface Science and Catalysis, Elsevier, Amsterdam, 1989, pp. 167-177.

[15] C.H. Bartholomew, in: B. Delmon, G.F. Froment (Eds.), Studies in Surface Science and Catalysis, Elsevier, Amsterdam, 1987, pp. 81-104.

[16] J.A. Moulijn, A.E. van Diepen, F. Kapteijn, Applied Catalysis A: General 212 (2001) 3-16.

[17] J.A. Rodriguez, J. Hrbek, Accounts of Chemical Research 32 (1999) 719-728.

[18] L.S. Escandón, S. Ordóñez, A. Vega, F.V. Díez, Journal of Hazardous Materials 153 (2008) 742-750.

[19] J.M. MacLaren, J.B. Pendry, D.D. Vvedensky, R.W. Joyner, Surface Science 162 (1985) 322-328.

[20] L.-Y. Gan, R.-Y. Tian, X.-B. Yang, S.-L. Peng, Y.-J. Zhao, Physical Chemistry Chemical Physics 13 (2011) 14466-14475.

[21] K. Habermehl-Ćwirzeń, J. Lahtinen, Surface Science 573 (2004) 183-190.

[22] C.H. Rochester, R.J. Terrell, Journal of the Chemical Society, Faraday Transactions 1: Physical Chemistry in Condensed Phases 73 (1977) 609-621.

[23] J. Markos, A. Brunovska, J. Ilavsky, Chemical Papers 41 (1987) 375-393.

[24] H.P. Buwono, S. Minami, K. Uemura, M. Machida, Industrial & Engineering Chemistry Research 54 (2015) 7233-7240.

[25] M.V. Twigg, M.S. Spencer, Applied Catalysis A: General 212 (2001) 161-174.

[26] M. Kärkkäinen, T. Kolli, M. Honkanen, O. Heikkinen, A. Väliheikki, M. Huuhtanen, K. Kallinen, J. Lahtinen, M. Vippola, R.L. Keiski, Topics in Catalysis 59 (2016) 1044-1048.

[27] S.M.A.M. Bouwens, J.P.R. Vissers, V.H.J. De Beer, R. Prins, Journal of Catalysis 112 (1988) 401-410.

[28] S. Eijsbouts, J.N.M. Vangestel, E.M. Vanoers, R. Prins, J.A.R. Vanveen, V.H.J. Debeer, Applied Catalysis A: General 119 (1994) 293-303.

[29] L. Baltusis, J.S. Frye, G.E. Maciel, Journal of the American Chemical Society 109 (1987) 40-46.

[30] G. Westermark, I. Persson, Colloids and Surfaces A: Physicochemical and Engineering Aspects 144 (1998) 149-166.

[31] M. Saidy, M.Y. Zhou, K.A.R. Mitchell, Surface and Interface Analysis 28 (1999) 84-91.

[32] L. Chandrasekaran, N. Saunders, A.P. Miodownik, Calphad 11 (1987) 163-164.

[33] J. Yu, J.B. Spencer, Chemical Communications (Cambridge) (1998) 1103-1104.

[34] M. Kiskinova, D.W. Goodman, Surface Science 108 (1981) 64-76.

[35] K. Asakura, H. Ishii, S. Konishi, Y. Kitajima, T. Ohta, H. Kuroda, Physica B (Amsterdam) 208 & 209 (1995) 465-466.

[36] D.W. Goodman, Accounts of Chemical Research 17 (1984) 194-200.

[37] R. Quinn, T.A. Dahl, B.A. Toseland, Applied Catalysis A: General 272 (2004) 61-68.

[38] H. Sezer, I.B. Celik, Electrochimica Acta 155 (2015) 421-430.

[39] S.J. Sawhill, K.A. Layman, D.R. Van Wyk, M.H. Engelhard, C. Wang, M.E. Bussell, Journal of Catalysis 231 (2005) 300-313.

[40] X. Li, H. Cheng, G. Liang, L. He, W. Lin, Y. Yu, F. Zhao, Catalysts 5 (2015) 759-773.

[41] M.J. Rokosz, A.E. Chen, C.K. Lowe-Ma, A.V. Kucherov, D. Benson, M.C. Paputa Peck, R.W. McCabe, Applied Catalysis B: Environmental 33 (2001) 205-215.

[42] M. Besson, P. Gallezot, Catalysis Today 81 (2003) 547-559.

[43] J.R. Chang, S.L. Chang, Journal of Catalysis 176 (1998) 42-51.

[44] J.H. Pazmino, C. Bai, J.T. Miller, F.H. Ribeiro, W.N. Delgass, Catalysis Letters 143 (2013) 1098-1107.

[45] F. Pinna, F. Menegazzo, M. Signoretto, P. Canton, G. Fagherazzi, N. Pernicone, Applied Catalysis A: General 219 (2001) 195-200.

[46] H. Huang, G. Cao, S. Wang, Korean Journal of Chemical Engineering 30 (2013) 1710-1715.

[47] P. Maeki-Arvela, G. Martin, I. Simakova, A. Tokarev, J. Warna, J. Hemming, B. Holmbom, T. Salmi, D.Y. Murzin, Chemical Engineering Journal (Amsterdam, Netherlands) 154 (2009) 45-51.

[48] C.-R. Chang, Z.-J. Zhao, K. Kohler, A. Genest, J. Li, N. Rosch, Catalysis Science & Technology 2 (2012) 2238-2248.

[49] B.J. O'Neill, D.H.K. Jackson, A.J. Crisci, C.A. Farberow, F. Shi, A.C. Alba-Rubio, J. Lu, P.J. Dietrich, X. Gu, C.L. Marshall, P.C. Stair, J.W. Elam, J.T. Miller, F.H. Ribeiro, P.M. Voyles, J. Greeley, M. Mavrikakis, S.L. Scott, T.F. Kuech, J.A. Dumesic, Angewandte Chemie-International Edition 52 (2013) 13808-13812.

[50] A.I. Abdulagatov, Y. Yan, J.R. Cooper, Y. Zhang, Z.M. Gibbs, A.S. Cavanagh, R.G. Yang, Y.C. Lee, S.M. George, ACS Applied Materials & Interfaces 3 (2011) 4593-4601.

[51] I.W.C.E. Arends, R.A. Sheldon, Applied Catalysis A: General 212 (2001) 175-187.

[52] Z.-p. Yan, L. Lin, S. Liu, Energy & Fuels 23 (2009) 3853-3858.

[53] A.M. Hengne, C.V. Rode, Green Chemistry 14 (2012) 1064-1072.

[54] D.Y. Murzin, E. Toukoniitty, J. Hajek, Reaction Kinetics and Catalysis Letters 83 (2004) 205-212.

[55] J. Panpranot, O. Tangjitwattakorn, P. Praserthdam, J.G. Goodwin, Applied Catalysis A: General 292 (2005) 322-327.

[56] J. Panpranot, K. Phandinthong, P. Praserthdam, M. Hasegawa, S.-i. Fujita, M. Arai, Journal of Molecular Catalysis A: Chemical 253 (2006) 20-24.

[57] J. Panpranot, K. Pattamakomsan, J.G. Goodwin, P. Praserthdam, Catalysis Communications 5 (2004) 583-590.

[58] J. Panpranot, K. Pattamakomsan, P. Praserthdam, Reaction Kinetics and Catalysis Letters 86 (2005) 141-147.

[59] C. Flego, S. Peratello, C. Perego, L.M.F. Sabatino, G. Bellussi, U. Romano, Journal of Molecular Catalysis A: Chemical 204-205 (2003) 581-589.

[60] C.H. Collett, J. McGregor, Catalysis Science & Technology 6 (2016) 363-378.

[61] D.E. Boldrini, G.M. Tonetto, D.E. Damiani, Chemical Engineering Journal 270 (2015) 378-384.

[62] M. Kuhn, M. Lucas, P. Claus, Catalysis Communications 72 (2015) 170-173.

[63] P.A. Sermon, M.S.W. Vong, M.A. Martin-Luengo, Studies in Surface Science and Catalysis 88 (1994) 319-326.

[64] F. Behafarid, B. Roldan Cuenya, Surface Science 606 (2012) 908-918.

[65] S.R. Challa, A.T. Delariva, T.W. Hansen, S. Helveg, J. Sehested, P.L. Hansen, F. Garzon, A.K. Datye, Journal of the American Chemical Society 133 (2011) 20672-20675.

[66] A. Cao, R. Lu, G. Veser, Physical Chemistry Chemical Physics 12 (2010) 13499-13510.

[67] A.K. Datye, Q. Xu, K.C. Kharas, J.M. McCarty, Catalysis Today 111 (2006) 59-67.

[68] T.W. Hansen, A.T. De La Riva, S.R. Challa, A.K. Datye, Accounts of Chemical Research 46 (2013) 1720-1730.

[69] K. An, Q. Zhang, S. Alayoglu, N. Musselwhite, J.-Y. Shin, G.A. Somorjai, Nano Letters 14 (2014) 4907-4912.

[70] P. Munnik, M.E.Z. Velthoen, P.E. de Jongh, K.P. de Jong, C.J. Gommes, Angewandte Chemie-International Edition 53 (2014) 9493-9497.

[71] O. Demircan, W. Zhang, C. Xu, J. Zondlo, H.O. Finklea, Journal of Power Sources 195 (2010) 3091-3096.

[72] R.-K. Chiang, R.-T. Chiang, Inorganic Chemistry 46 (2007) 369-371.

[73] C. Xu, J.W. Zondlo, M. Gong, X. Liu, Journal of Power Sources 196 (2011) 116-125.

[74] Q. Smejkal, D. Linke, U. Bentrup, M.M. Pohl, H. Berndt, M. Baerns, A. Brückner, Applied Catalysis A: General 268 (2004) 67-76.

[75] J.J. Birtill, Catalysis Today 81 (2003) 531-545.

[76] Y. Wang, G. Luo, X. Xu, J. Xia, Catalysis Communications 57 (2014) 83-88.

[77] M. Burgener, R. Wirz, T. Mallat, A. Baiker, Journal of Catalysis 228 (2004) 152-161.

[78] P.G. Menon, Chemical Reveiws (Washington, D. C.) 94 (1994) 1021-1046.

[79] F.C. Galisteo, R. Mariscal, M.L. Granados, J.L.G. Fierro, R.A. Daley, J.A. Anderson, Applied Catalysis B: Environmental 59 (2005) 227-233.

[80] D.L. Trimm, Applied Catalysis A: General 212 (2001) 153-160.

[81] C.I. Meyer, A.J. Marchi, A. Monzon, T.F. Garetto, Applied Catalysis A: General 367 (2009) 122-129.

[82] A. Monzon, T.F. Garetto, A. Borgna, Applied Catalysis A: General 248 (2003) 279-289.

[83] A.M. Amin, E. Croiset, C. Constantinou, W. Epling, International Journal of Hydrogen Energy 37 (2012) 9038-9048.

[84] X. Chen, Y. Cheng, C.Y. Seo, J.W. Schwank, R.W. McCabe, Applied Catalysis B: Environmental 163 (2015) 499-509.

[85] J. Okal, L. Kepinski, L. Krajczyk, W. Tylus, Journal of Catalysis 219 (2003) 362-371.

[86] D.J. Fullerton, A.V.K. Westwood, R. Brydson, M.V. Twigg, J.M. Jones, Catalysis Today 81 (2003) 659-671.

[87] J.M. Jones, V.A. Dupont, R. Brydson, D.J. Fullerton, N.S. Nasri, A.B. Ross, A.V.K. Westwood, Catalysis Today 81 (2003) 589-601.

[88] C.F.J. König, P. Schuh, T. Huthwelker, G. Smolentsev, T.J. Schildhauer, M. Nachtegaal, Catalysis Today 229 (2014) 56-63.

[89] L.J. Hoyos, M. Primet, H. Praliaud, Journal of the Chemical Society, Faraday Transactions 88 (1992) 3367-3373.

[90] M.-V. Mathieu, M. Primet, Applied Catalysis 9 (1984) 361-370.

[91] P.C. L'Argentiere, N.S. Fígoli, Applied Catalysis 61 (1990) 275-282.

[92] P.C. L'Argentiere, N.S. Fígoli, Journal of Chemical Technology and Biotechnology 69 (1997) 261-265.

[93] D.C. Kim, S.S. Eom, D.H. Ko, M.H. Hong, O.H. Kwon, Method for regenerating hydrogenation catalyst poisoned during hydrogenation of hydroformylation product, LG Chem, Ltd., South Korea 2013, p. 18pp.; Chemical Indexing Equivalent to 160:67398 (KR).

[94] X. Li, J. Li, Y. Peng, H. Chang, T. Zhang, S. Zhao, W. Si, J. Hao, Applied Catalysis B: Environmental 184 (2016) 246-257.

Chapter 3: Experimental procedures

3 Introduction

The two catalysts under study were synthesised using wet impregnation, a method which has been reviewed and explained in the first chapter. The synthesised catalysts underwent characterisation using a range of techniques to determine their properties. These techniques included microscopic, thermal and spectroscopic techniques discussed in more detail further on. These were also employed for the characterisation of the used, deactivated and regenerated catalysts to observe changes in the catalyst properties due to the different regeneration treatments. The observed properties of the used catalysts were then correlated to the *in situ* catalytic behaviour of the catalyst before deactivation, during the actual deactivation experiments, and after regeneration. All characterisation experiments, except for scanning electron microscopy imaging and temperature programmed reduction, were carried out at the University of KwaZulu-Natal. Scanning electron microscopy and back scattered electron imaging, as well as temperature programmed reduction, were carried out at the Sasol Infrachem Laboratory in Sasolburg.

3.1 Catalyst synthesis

Nickel catalysts used for this study were supported on gamma alumina and silica using the wet impregnation technique [1-3]. An appropriate mass of nickel nitrate hexahydrate ($Ni(NO_3)_2 \cdot 6\,H_2O$, Sigma Aldrich) was dissolved in a minimum amount of deionized water, and introduced slowly to a slurry of the support with the aid of a separating funnel. The resulting mixture was stirred for three hours at room temperature. Thereafter, the mixture was sonicated for half an hour at room temperature, and stirred further for an hour on a magnetic stirrer hot plate. Excess solvent was subsequently evaporated by slow heating on the hotplate until a paste formed, which was dried overnight in an oven set at a temperature of 110 °C. The precursor solid was ground and calcined for five hours under a stream of air at 550 °C. Prior to hydrogenation reactions, the calcined precursor was converted to pellets, then crushed and sieved to a size between 300-600 microns. One batch (15 g) for each catalyst was prepared, and all subsequent catalytic testing and time on stream experiments were performed using catalyst samples from these batches.

3.2 Catalyst characterisation

A range of characterisation techniques were employed to gain understanding of the physicochemical characteristics of the prepared catalysts, and to correlate these to the observed behaviour of the catalyst during catalytic activity evaluations. The characterisation techniques outlined in this chapter were also used to characterise the catalysts after deactivation and regeneration.

3.2.1 Inductively coupled plasma-optical emission spectroscopy (ICP-OES)

The accurate nickel loading of the prepared catalysts, as well as the phosphorus content of the used/regenerated catalysts were quantified using inductively coupled plasma-optical emission spectroscopy on a Perkin Elmer Precisely Optima DV 5300 Optical Emission Spectrometer. Prior to analysis, the samples were digested using aqua regia (1:3 nitric acid to hydrochloric acid ratio) in a CEM Mars 6 OneTouch Technology microwave digestion unit, using easy prep sample vessels, at a maximum temperature of 200 °C and a pressure of 328 psi. The aqua regia was prepared using 55 % nitric acid (chemically pure, Promark Chemicals) and 32 % hydrochloric acid (Analytical Reagent, Promark Chemicals). The samples were pre-digested overnight at room temperature in the EasyPrep microwave vessels prior to the microwave digestion. In addition, a set of multi-element standards of nickel and phosphorus were prepared and used for the calibration of the instrument and, hence, to obtain accurate nickel and phosphorus concentrations of the samples. The spectral line used for nickel was 231 nm, while for phosphorus quantitation was 177 nm.

3.2.2 Powder X-ray and *in situ* X-ray diffraction (PXRD)

The crystallinity of the prepared catalysts was determined by powder X-ray diffraction using a Bruker Advance D8 diffractometer equipped with an Anton Paar XRK 900 reaction chamber and TCU 750 temperature control unit. The instrument employed a Cu K_α radiation source with wavelength of 0.15406 nm. The behaviour of the catalysts under reducing conditions were also observed with the aid of *in situ* XRD. The analysis was carried out using 5 % H_2 in N_2. The temperature was ramped from 100 °C to 600 °C at a rate of 50 °C/min to investigate the phase change and formation of metal from the metal oxide.

3.2.3 Surface area analysis

The surface areas and porosity of the prepared and used catalyst samples were measured using nitrogen physisorption at -196°C. The analyses were performed on a three port Micromeritics Tristar 3020 surface area and porosity analyser. Prior to analysis, the samples were degassed

under a flow of nitrogen at 90 °C for an hour. The temperature was raised to 200 °C and the samples were degassed at this temperature for twelve hours. The samples were then cooled, weighed, and analysed. The surface area of the samples was determined using the Brunauer-Emmet-Teller (BET) equation, whilst the cumulative pore volume, average pore diameter and pore size distribution (PSD) of the samples were determined by applying the Barrett-Joyner-Halenda (BJH) theory to the desorption branch of the nitrogen sorption isotherm.

3.2.4 Temperature programmed reduction (TPR)

Temperature programmed reduction experiments were carried out to study the reducibility of the catalyst, and the analyses were performed on a Micromeritics Autochem 2920 coupled with a MKS Instruments Cirrus Mass Spectrometer. The sample (approximately 50 mg) was placed between two layers of quartz wool in a quartz U-tube. The tube was fitted with a thermocouple for continuous temperature measurements. Prior to analysis, the sample was dried under helium at a flow of 50 ml min^{-1} by heating the sample from room temperature, at a rate of 5 °C min^{-1}, to 120 °C and held there for ten minutes to remove any adsorbed moisture. The sample was thereafter cooled to room temperature. The actual analysis was performed by heating the sample from room temperature to 950 °C, at a rate of 10 °C min^{-1} under a flow of pure hydrogen at 50 ml min^{-1}. The sample was subsequently held at 950 °C for ten minutes, while mass spectrometry was used to detect the evolved gases. The amount of hydrogen consumed by the sample during reduction was measured using a thermal conductivity detector (TCD).

3.2.5 Hydrogen chemisorption and oxygen titration

The metal dispersion of nickel on the alumina support was measured by hydrogen chemisorption on a Micromeritics ASAP 2020 Chemisorption analyser at 50 °C. The catalyst was reduced at 550 °C for 240 minutes. Oxygen titration was performed at 550 °C to determine the degree of reduction. The samples (50 mg) were placed between two layers of quartz wool in a quartz U-tube and degassed at 200 °C overnight under vacuum on the instrument prior to analysis. The metal dispersion on the silica supported catalyst was measured under similar conditions to the alumina supported catalyst; however, reduction and oxygen titration were performed at 400 °C.

3.2.6 Scanning electron microscopy (SEM)

Cross sectional scanning electron microscopy imaging was performed on the fresh and used catalyst samples. The samples were mixed with Akasel epoxy resin and Akasel cure in plastic moulds, then cured for 24 hours to form resin blocks. The blocks were then polished using

diamond paste with progressively smaller particles on the surfaces where the catalyst powders were located to obtain a smooth surface. After polishing, the samples were coated with carbon to prevent charging. The back scattered electron imaging and electron dispersive X-ray spectroscopy analysis were carried out on a Zeiss EVO 40 instrument with a tungsten filament, at an accelerating voltage of 20 kV and a probe current of 1.5 nA. The filament current was kept at 2.403 A. EDS analyses were performed using a Bruker XFlash SDD detector, controlled by Bruker Esprit software. For the analysis of each sample, an acquisition time of 300 seconds was used to generate sufficient information for the element maps.

3.2.7 Transmission electron microscopy (TEM)

Transmission electron microscopy images were obtained using a Jeol JEM-1010 electron microscope. The images were captured and analysed using iTEM software. The samples were suspended in ethanol and sonicated for ten minutes prior to analysis, while the used catalysts were first ground to a fine powder, suspended in ethanol, then sonicated. The samples were mounted on copper grids and analysed using the Megaview III soft imaging system at an operating voltage of 100 kV.

High resolution transmission electron microscopy imaging was performed on a Jeol JEM 2100 using the iTEM software for imaging. The microscope used a LaB_6 gun and was equipped with a Gatan ultrascan camera for imaging. This was used to obtain high resolution images, as well as electron diffraction patterns, dark field images and to carry out STEM-EDX analysis. The sample preparation was similar to that used for low-resolution transmission electron microscopy imaging.

3.2.8 Thermogravimetric analysis (TGA)

Normal thermogravimetric and differential scanning calorimetry analyses were performed on a TA SDQT600 instrument. The sample was heated from room temperature to 900 °C under a flow of air set at a flow rate of 15 °C/min, and a flow rate of 50 mL/min. Mass spectra were obtained with a MKS Instruments Cirrus Mass Spectrometer.

3.2.9 Vibrating sample magnetometer measurements (VSM)

The magnetic properties of the reduced, poisoned and regenerated catalysts were measured on a Lakeshore Model 735 vibrating sample magnetometer at room temperature. A mass of 20 mg of sample was loaded onto the sample holder, attached to the sample rod and placed inside a Janis model helium cryostat. Measurements were conducted in an applied external magnetic field range of -14 to 14 kOe.

3.2.10 Attenuated Transmission Reflectance – Infrared Spectroscopy (ATR-IR)

Infrared spectra were obtained using a Perkin Elmer spectrometer, equipped with a Universal Sampling Accessory and diamond crystal that was used to apply force to the sample for analysis. The obtained spectra were analysed and processed with Spectrum 100 software. For analysis, approximately 20 mg of sample was placed on the diamond crystal, and subjected to a force of 120 gauge, and the spectra were subsequently collected. The samples did not require any treatment prior to analysis.

3.2.11 Fourier transform infrared spectroscopy (FTIR)

Infrared spectra of the fresh and used catalyst samples were obtained using a Perkin Elmer FTIR Spectrometer RX using a KBr disc. A small mass of sample, approximately 3 mg was ground in a mortar and pestle with approximately 300 mg of KBr, then compressed into a disc which was then analysed by the FTIR spectrometer.

3.3 Catalytic testing

The liquid phase hydrogenation of octanal was carried out in a high pressure, continuous flow fixed bed reactor. The deactivation and regeneration studies were performed *in situ* using the same reactor system.

3.3.1 Reactor set-up

The reactor system was constructed of stainless steel ¼ inch tubing and fittings from Swagelok. Gases to the system were delivered from connected nitrogen and hydrogen cylinders, whose lines were maintained at a pressure of 50 bars by pressure regulators. The gas flow rates entering the system were set and maintained by Bronkhorst mass flow meters (MFCs). Shut off valves were placed before and after the MFCs to control the flow of gases into and out of the system, and one-way valves were placed after the MFCs and shut off valves to prevent the backflow of gases and liquid feed. The gases entered the reactor concurrently with the liquid feed. The feed was fed from a feed reservoir at the T-piece where the gas and feed lines intersected, as schematically represented in Figure 3.1.

The feed was delivered from a reservoir placed on a balance via a LabAlliance isocratic HPLC pump which maintained the liquid flow rate. The pump was connected to a Teflon tube fitted with a filter, placed inside the feed reservoir. The feed travelled through a one-way valve prior to entering a T-piece, then passed onto the stainless-steel reactor tube with a diameter of 2 cm and a length of 26 cm. The tube was fitted into a steel heating block affixed to the wall for

support, and secured with steel bolts fitted with copper seal rings that were affixed to the heating block with a torque wrench. A 30 cm heating band connected to a temperature control unit was placed around the block and covered with an insulating jacket to provide heat and to maintain the set temperature. The temperature of the catalyst bed was monitored with a sliding thermocouple placed in a thermowell and connected to a temperature control unit.

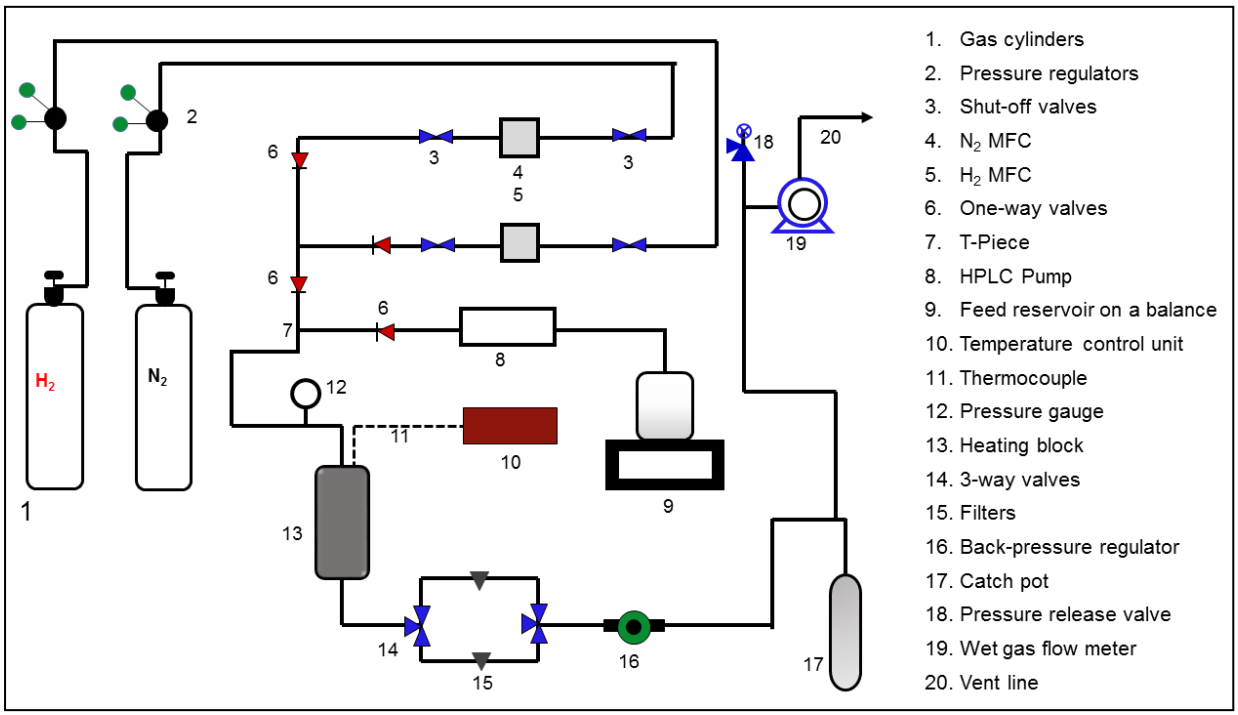

Figure 3.1: A schematic set-up of the reactor lines and components

The product stream consisting of liquid products and unreacted hydrogen exited the reactor and passed through a three-way valve, then through one of two parallel 2 µm filters before entering the backpressure regulator, which was used to set and maintain the pressure at which the catalytic tests were performed. The product stream was separated into the gas and liquid components in the catch pot, after which point the gas travelled to the Ritter wet gas flow meter which monitored the amount of hydrogen and other evolved gases during the catalytic tests. The excess gas was vented while the product was collected in the catch pot.

3.3.2 Catalytic tests and product quantification

The catalysts were mixed with 2 mL of carborundum, then packed into the reactor tube and sandwiched between glass wool plugs and carborundum to maintain the structure of the bed and ensure even mixing and temperature distribution along the tube. The catalysts were activated by first drying under a flow of nitrogen for two hours at 200 °C, prior to a gradual

increase in the temperature and hydrogen flow. The catalysts were then reduced under a flow of hydrogen for a period of 24 hours. Following this, the temperature was reduced to the reaction temperature (140 °C) and the system was pressurised using hydrogen to 50 bars. The alumina supported catalyst was reduced at 450 °C while the silica-supported catalyst was reduced at 350 °C; temperatures which were determined with the use of *in situ* X-ray diffraction and temperature programmed reduction.

Catalytic testing conditions were optimized during previous studies [4] and the testing was performed at a hydrogen pressure of 50 bars. The temperature for all catalytic testing performed was set at 140 °C, while the liquid hourly space velocity was 18 h^{-1}. The substrate to hydrogen ratio was 1:2, and a volume of 2 mL of catalyst was used throughout the study. The products were quantified using a Perkin Elmer Autosystems XL Gas Chromatograph equipped with a Flame Ionization Detector and a Petro-Elite column. The products were injected into the column with a 1 µL syringe set to deliver a volume of 0.5 µL.

3.3.2.1 Time on stream catalytic tests

Time on stream testing of the catalyst was performed in five steps. The first step was the hydrogenation of feed consisting of 10 wt.% octanal in octanol to evaluate the intrinsic activity of the catalysts towards the hydrogenation of octanal. This feed was termed "clean feed". The second step involved the introduction of poisoned feed which was spiked with a concentration of 500 ppm of triphenylphosphine to induce deactivation by poisoning. After deactivation, the clean feed was re-introduced to establish whether there was a need for regeneration (step 3). The fourth step was the regeneration experiment, while the fifth step involved the reintroduction of clean feed to evaluate the effectiveness of each regeneration experiment. During testing with 15 NiA, the catalytic activity tests were performed as outlined in Figure 3.2, in order to track the changes in the properties of the catalyst after each step of the reaction. At the end of the experiment, the catalyst was removed from the reactor after each step for characterisation purposes. For 15 NiSi, the catalytic activity tests involved carrying out steps 1, 2 and 5.

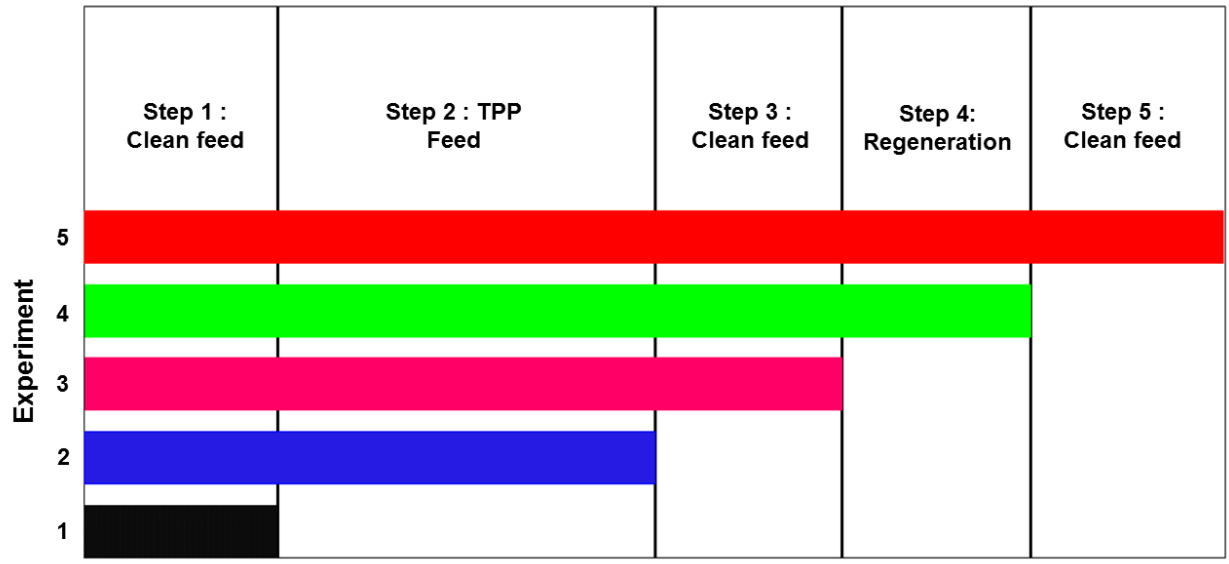

Figure 3.2: Schematic representation of catalytic testing experiments

3.3.2.2 Catalyst regeneration

Regeneration experiments were conducted as follows; after step 3, the liquid feed flow into the reactor was stopped, and the pressure was slowly released to atmospheric pressure. The temperature was increased to 200 °C. Three separate regeneration experiments were performed, which were; regeneration with hydrogen, regeneration by washing with octanol, and a regeneration experiment that involved washing the catalyst bed with octanol prior to commencing the regeneration using the hydrogen treatment. The hydrogen treatment and solvent wash regeneration experiments were each conducted for 20 hours, while the combined regeneration was conducted for 24 hours (12 hours octanol wash, followed by 12 hours of hydrogen treatment). After regeneration, the reactor was cooled to 140 °C, re-pressurised to 50 bars, and the reaction was restarted by introducing clean feed (step 5, Fig. 3.2). To determine any removal of phosphorus during regeneration, the product streams were analysed using inductively coupled optical emission spectroscopy to test for leaching of any nickel, as well as the presence of phosphorus species in octanol washings from the solvent wash regeneration.

3.4 References

[1] J.-X. Guo, Y.-F. Qu, S. Shu, X.-J. Wang, H.-Q. Yin, Y.-H. Chu, New Journal of Chemistry 39 (2015) 5997-6015.

[2] M. Campanati, G. Fornasari, A. Vaccari, Catalysis Today 77 (2003) 299-314.

[3] P. Munnik, P.E. de Jongh, K.P. de Jong, Chemical Reveiws (Washington, DC, U. S.) 115 (2015) 6687-6718.

[4] J. Valand, A.S. Mahomed, S. Singh, H.B. Friedrich, Journal of Porous Materials 23 (2016) 175-183.

Chapter 4: Characterisation of fresh catalysts

4.1 Introduction

The prepared catalysts were characterised to establish their morphological and physicochemical characteristics, in order to correlate these to the behaviour of the catalysts under operating conditions. This was achieved by focusing on techniques that would give insight into these properties, such as physisorption and elemental analysis, electron microscopy, temperature programmed techniques and diffraction analyses. The discussion in this chapter concerns the properties of the fresh, calcined catalysts prior to any hydrogenation reactions. The discussion of the characteristics of the used catalysts takes place in Chapter 5.

4.1.1 Inductively Coupled Plasma-Optical Emission Spectroscopy

The accurate nickel loading of the alumina and silica supported catalysts was determined to be 14.5 and 14.7 wt.% respectively (Table 4.1), which was close to the desired loading of 15 wt.%. The alumina supported catalyst is henceforth referred to as 15 NiA, while the silica supported catalyst is referred to as 15 NiSi.

Table 4.1: Elemental composition and porosity characteristics of the bare supports and calcined catalysts

Sample	Ni loading (wt.%)	BET surface area (m^2 g^{-1})	Pore volume (cm^3 g^{-1})	Pore size (nm)
γ-Al_2O_3	-	232	0.8	13.7
15 NiA	14.5	176	0.5	8.8
SiO_2	-	140	0.6	15.6
15 NiSi	14.7	99	0.3	4.0

4.1.2 Physisorption analysis

The porous structure of the supports and calcined catalysts was probed with the aid of surface area measurements. The BET surface area of the supports was determined to be 232 m^2 g^{-1} for γ-Al_2O_3 and 140 m^2 g^{-1} for SiO_2. The surface area of calcined 15 NiA was measured to be 176 m^2 g^{-1}, whilst that of calcined 15 NiSi was 99 m^2 g^{-1}. The BET surface area, pore volumes and pore sizes of the bare supports, and corresponding catalysts are given in Table 4.1. The

supported catalysts have a lower surface area compared to the bare supports, which is attributed to the deposition of nickel oxide in the pores of the silica and alumina supports [1].

The diameters of both the gamma alumina and silica supports are 14 and 16 nm respectively, which puts them within the mesoporous pore size range [2]. The mesoporosity of the supports was maintained for the impregnated and calcined catalysts, which suggests maintenance of the support integrity with calcination. The decrease in the pore size of the supported catalysts indicates the occupation of the pores by NiO particles, which is more pronounced for the silica supported catalyst. This suggests the formation of large NiO clusters that block the larger pores, resulting in a smaller average pore size measurement for the 15 NiSi catalyst when compared to the silica support by itself [1]. The change in the porosity of the supports with Ni loading was monitored with the aid of BET isotherms, presented in Figure 4.1. The isotherms of both catalysts and supports exhibit type IV behaviour and type H1 hysteresis loops, based on the IUPAC classification, which is typical of mesoporous materials [2].

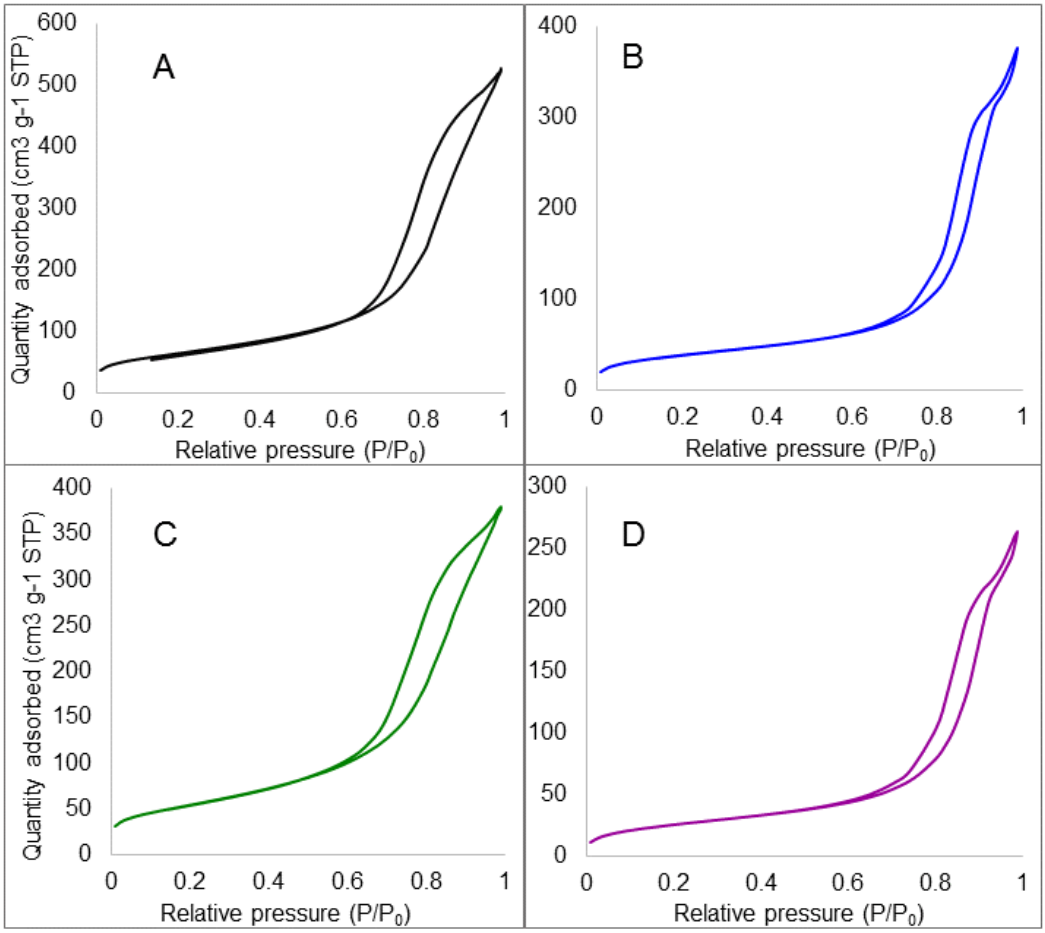

Figure 4.1: N_2 adsorption-desorption isotherms for A) γ-Al_2O_3, B) SiO_2, C) 15 NiA and D) 15 NiSi

The shape of the hysteresis loops suggests both alumina and silica have pores with uniform size and shape [2, 3]. The volume of nitrogen adsorbed was lower for the impregnated catalysts, compared to the supports, which corresponds to the lower surface area of the impregnated catalysts.

4.1.3 Powder X-ray diffraction

The bulk phase composition and crystallinity of the bare supports and the catalysts were determined by powder X-ray diffraction. The XRD diffractograms of the supported 15 NiA and bare alumina are shown in Figure 4.2. The diffractogram of the bare γ-alumina is included to distinguish between the alumina and NiO peaks, and consists of peaks corresponding to the JCPDS card number 75-0921 [4].

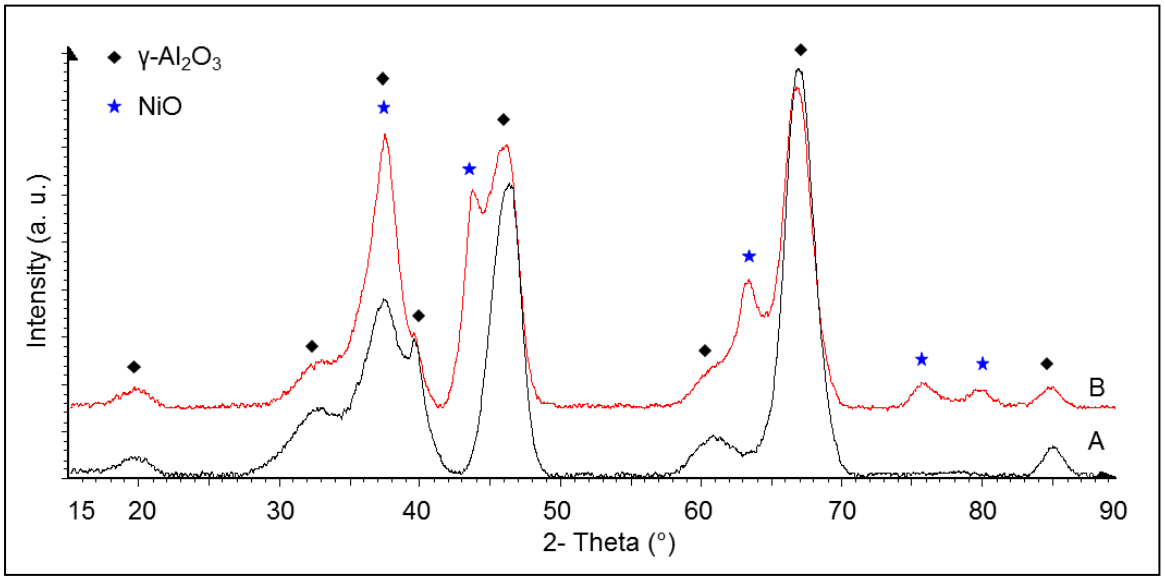

Figure 4.2: Powder X-ray diffractogram of A) alumina and B) the calcined 15 NiA catalyst precursor

The diffractogram of the 15 NiA catalyst retains the characteristic alumina peaks, whilst also displaying peaks corresponding to nickel oxide (NiO) at 37°, 44°, 63°, 76° and 79° 2θ angles (JCPDS card number 78-0643) [5]. The nickel oxide peaks are largely broad and in places overlap with the alumina peaks, indicating the presence of NiO in the form of small particles, which would suggest a good dispersion of nickel oxide on the alumina support [6]. The peak broadening may also be as a result of the overlap between NiO and the alumina peaks [7]. This has been reported in literature, where NiO peaks were indistinguishable from those of the alumina support, and was attributed to either a high degree of metal dispersion on the support, or the amount of metal oxide being below the detection limit for XRD [8, 9].

In contrast to the alumina supported catalyst, the diffractogram of the silica supported catalyst, presented in Figure 4.3, displays sharp peaks of a relatively high intensity, and a broad peak at the 2θ angle of 20°, attributed to silica [10]. The sharpness of the peaks indicates highly crystalline, bulk nickel oxide particles on the silica support. According to Yenumala *et al*. [6], the high crystallinity of nickel oxide on silica is due to a weak interaction between the metal oxide and silica. This leads to the poor dispersion of metal on silica, and, hence, results in the formation of large nickel oxide clusters [6].

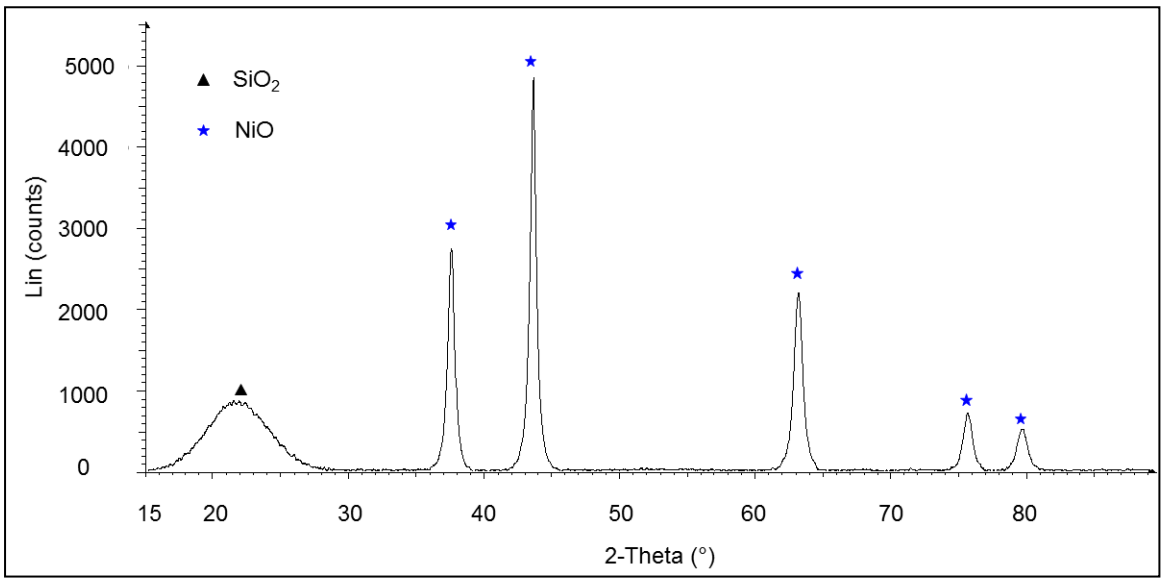

Figure 4.3: Powder XRD pattern of the calcined 15 NiSi catalyst precursor

Hydrogenation reactions are catalysed by metals in their reduced form. Hence, NiO in this case is considered a catalyst precursor, and requires pre-treatment at high temperatures under a stream of hydrogen gas to obtain the active form of the catalyst. As such, the phase transformation undergone by the catalyst precursors under a reducing atmosphere were studied with *in situ* XRD. The XRD diffractograms showing the transformation of NiO to Ni^0 on 15 NiA under the influence of changing temperature are presented in Figure 4.4. From Figure 4.4, the reduction of NiO to nickel occurs at a temperature of 550 °C, as noted by the appearance of peaks representing metallic Ni (JCPDS card number 04-0850) [11, 12]. The relatively high reduction temperature is attributed to the strong interaction between nickel oxide and alumina [13].

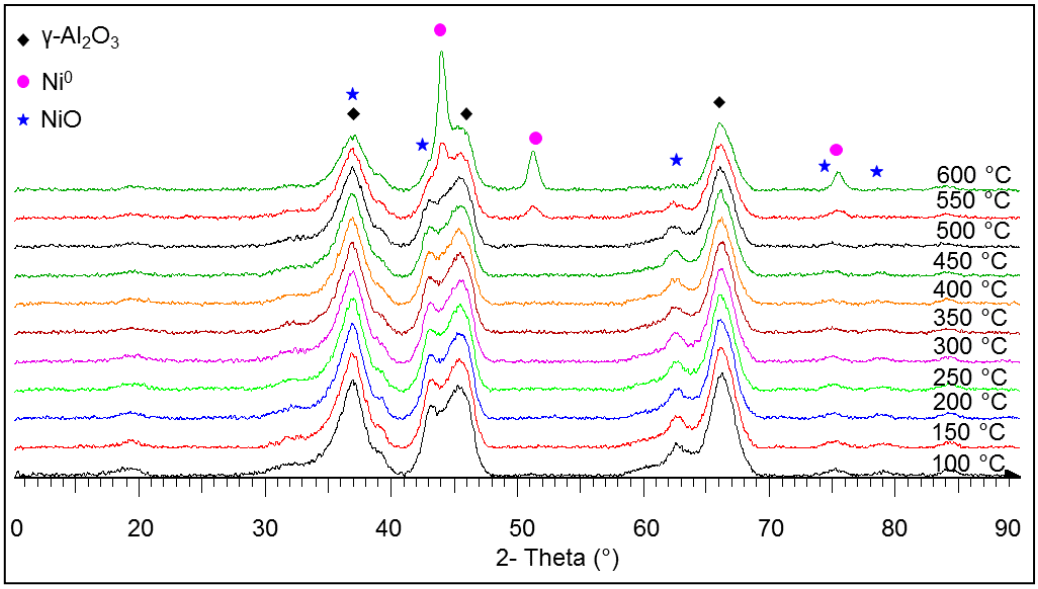

Figure 4.4: Phase changes undergone by NiO on the 15 NiA catalyst precursor under a reducing environment

The phase transformation of the 15 NiSi catalyst precursor under a hydrogen atmosphere was also monitored by *in situ* XRD, with the XRD patterns of the phase transformations presented in Figure 4.5. In contrast to the 15 NiA catalyst precursor, reduction in this case occurred at a lower temperature, 350 °C, indicated by the appearance of Ni^0 peaks (JCPDS card number 04-0850) [11, 12].

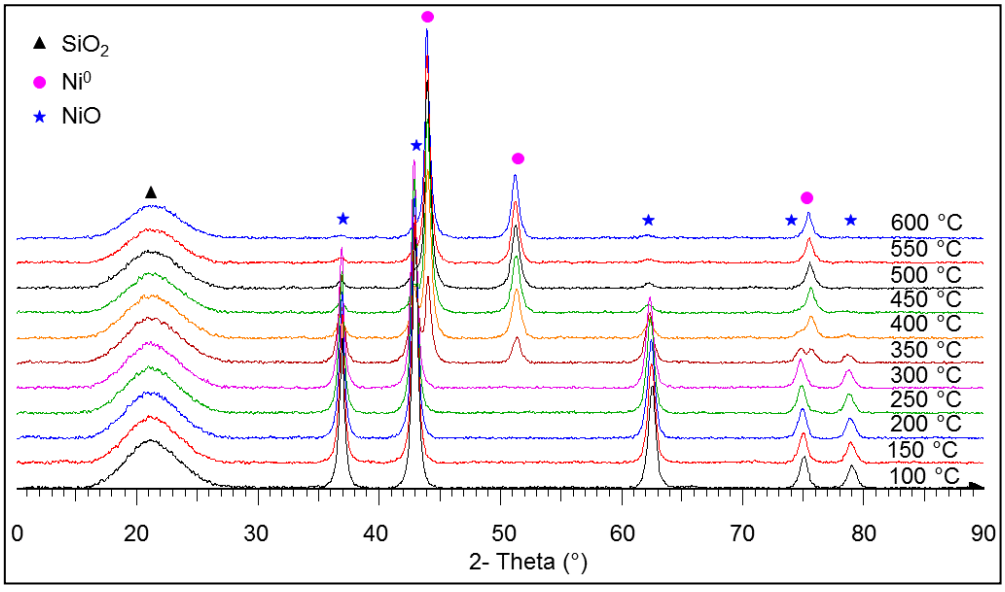

Figure 4.5: Phase changes undergone by NiO on the 15 NiSi catalyst precursor under a reducing environment

The low reduction temperature is attributed to the weak interaction between nickel oxide and silica [14]. It was also noted that the peaks representing Ni^0 for the 15 NiSi catalyst were sharper and narrower than the Ni^0 peaks for the alumina supported catalyst, indicating that the alumina support is better able to stabilize the metal particles against sintering, as opposed to the silica support.

4.1.4 Hydrogen chemisorption

Hydrogen chemisorption is one of the techniques used for the determination of the surface area of the supported metal that is available for catalysis [15-17]. The adsorption of hydrogen is used as a form of titration, based on the assumption of a 1:1 ratio between a hydrogen atom and an exposed metal atom [18]. This method was used to determine the amount of available nickel, and, hence, the degree of dispersion and crystallite sizes of Ni^0 on the gamma alumina and silica support. The results are presented in Table 4.2. The extent of metal dispersion is mainly affected by the preparation method, type of support used, and catalyst pre-treatment methods [19, 20].

Table 4.2: Summary of results obtained from hydrogen chemisorption of 15 NiA and 15 NiSi

Catalyst	Metal dispersion (%)	Metallic surface area ($m^2\ g^{-1}$ of sample)	Crystallite size (nm)	Degree of reduction (%)
15 NiA	12.2	9.9	7.9	84.0
15 NiSi	4.6	4.1	20.8	90.3

Nickel catalysts are typically calcined to form oxide precursors, then reduced under a flow of hydrogen to form metallic nickel. The main aim of supporting metal catalysts is to disperse the metal into small, finely divided particles with a greater exposed metal surface area, which often correlates to the activity of the catalyst. Simply put, higher metal dispersion, smaller metal crystallites and greater metallic surface area all result in a greater number of active sites, and hence, higher catalytic activity [21].

Prior to chemisorption analysis, 15 NiA was reduced at 550 °C, whilst 15 NiSi was reduced at 400 °C. From the chemisorption data in Table 4.2, 15 NiA has a higher metal dispersion when compared to 15 NiSi, with the crystallites for 15 NiA having an average size of 7.9 nm. The metallic surface area was 9.9 $m^2\ g^{-1}$, while the dispersion itself was 12.2 %. In contrast, for the

15 NiSi catalyst, the metallic surface area was 4.1 m^2 g^{-1}, the Ni crystallite size was 20.8 nm, while the metal dispersion was 4.6 %. The results obtained from chemisorption support the results obtained from XRD analysis, which indicated that NiO was dispersed as small particles on the alumina support, while NiO supported on silica was suggested to exist in a highly crystalline but poorly dispersed form.

The comparatively lower metal dispersion of nickel on silica arises from the poor interaction between nickel and silica, resulting in the formation of larger metal crystallites. The degree of reduction for both 15 NiA and 15 NiSi was determined by oxygen titration, which showed a 90 % reduction of nickel oxide to metallic nickel for the catalyst supported on silica, whereas the degree of reduction for the alumina supported catalyst was 84 %. The slightly lower degree of reduction observed for 15 NiA, despite the much higher reduction temperature, is largely attributed to the existence of nickel species that interact strongly with the alumina support. This results in less nickel being available for catalysis, since some of it remains in the oxide form [22]. The reducibility of the catalyst precursors was then determined using temperature programmed reduction to observe the ease of reduction of the catalysts.

4.1.5 Temperature programmed reduction

Temperature programmed techniques are used for the determination of different properties of supported catalysts, such as oxidation, reduction, and sorption of a probe molecule. In the present case, temperature programmed reduction was used to probe the reducibility of NiO on the two different supports, which gives further insight into the strength of the interaction between metal and support. The reduction profile of the 15 NiA catalyst precursor is presented in Figure 4.6.

The trace of the temperature programmed reduction of 15 NiA showed three reduction maxima and a shoulder peak around 700 °C. Deconvolution showed five reduction peaks. The first peak shows reduction occurring around 170 °C, which is relatively low, while the second peak shows a reduction at 232 °C. This has been observed in the reduction of supported nickel nanoparticles, and was attributed to the reduction of a nickel oxide nanoparticle layer present on nickel nanoparticles, but may also indicate the reduction of free NiO on the 15 NiA precursor [23-25]. The next peak was at 400 °C, which indicates the reduction of bulk NiO having a weak interaction with the alumina support [9, 25]. The largest reduction peak was at 546 °C, which is attributed to the reduction of highly dispersed NiO having a strong interaction

with the support, or the reduction of larger NiO particles [14, 25]. The reduction peak at 755 °C is attributed to the reduction of nickel aluminate surface spinel species [9, 25].

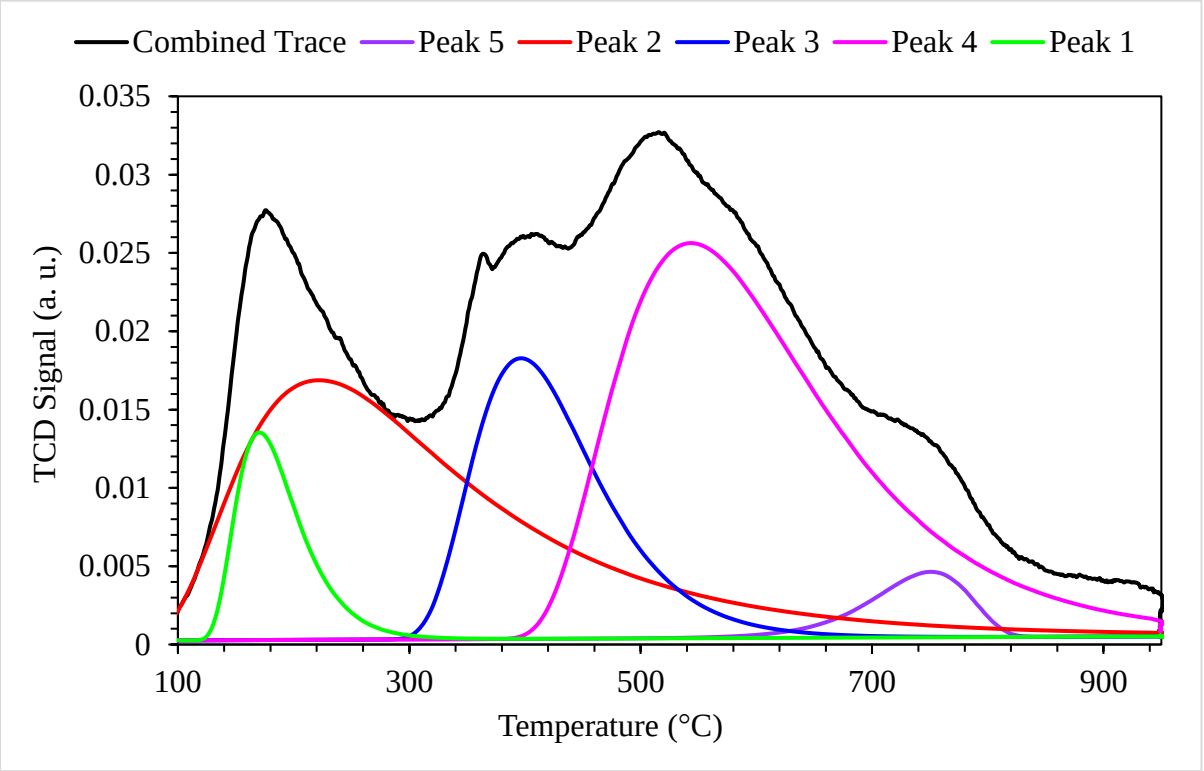

Figure 4.6: Hydrogen temperature programmed reduction profile of 15 NiA, also showing the peak deconvolution (peaks 1-5)

The reduction profile of the 15 NiSi catalyst precursor is presented in Figure 4.7. The combined trace showed three reduction maxima, which were deconvoluted to reveal three reduction peaks attributed to the reduction of NiO species in different environments. The first reduction peak at 274 °C is attributed to the reduction of free nickel oxide. The major reduction peak at 320 °C corresponds to the reduction of bulk NiO that weakly interacts with the support, while the peak around 400 °C corresponds to the reduction of NiO that has a stronger interaction with the support [26]. The reduction of the catalyst was complete at approximately 430 °C.

Overall, the 15 NiSi catalyst precursor was easier to reduce compared to 15 NiA, due to the weaker interaction between nickel and silica, than with alumina.

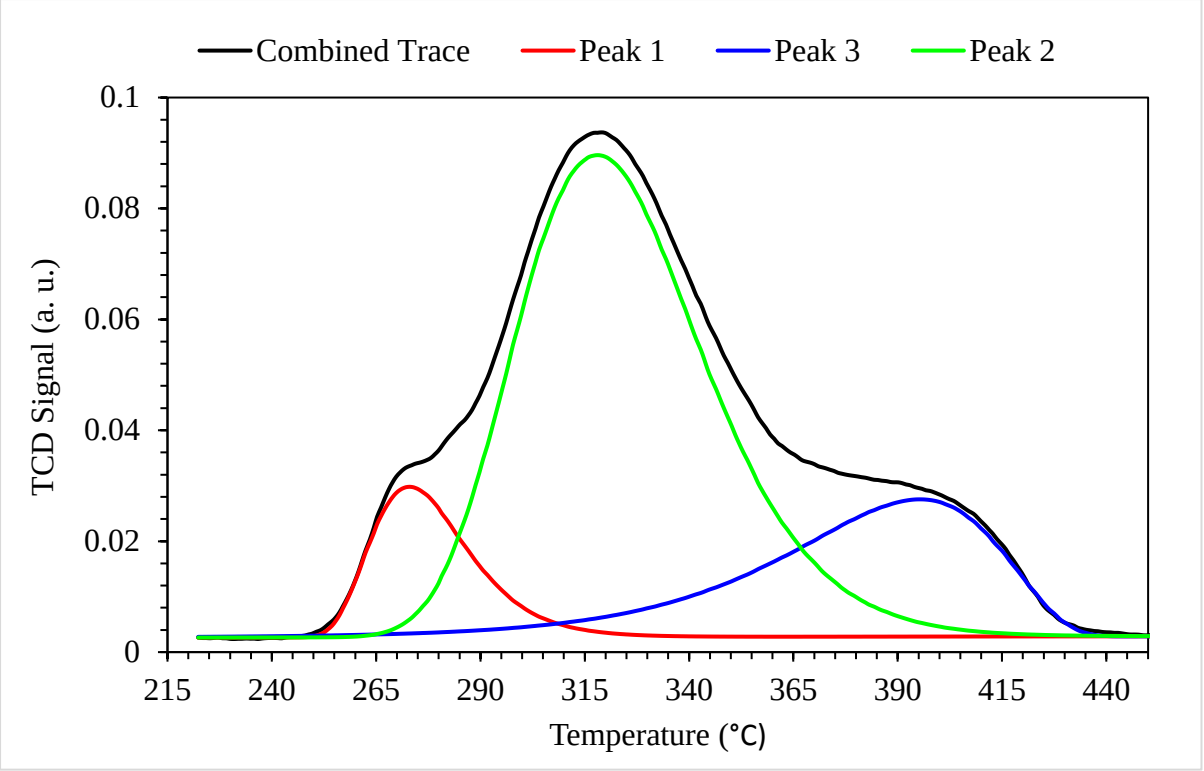

Figure 4.7: Hydrogen temperature programmed reduction profile of 15 NiSi, also showing the peak deconvolution (peaks1-3)

4.1.6 Scanning electron microscopy

The SEM images of the fresh, calcined 15 NiA and 15 NiSi catalysts are presented in Figure 4.8. The image of the 15 NiA precursor shows a rough morphology composed of stacked particles in the shape of thin, irregular plates. The nickel oxide particles are not distinguishable from the support, indicating a good dispersion of nickel oxide on the alumina surface. In contrast, the image obtained for the 15 NiSi catalyst precursor shows the presence of distinct NiO particles on the surface of the silica support, which suggests a poor metal dispersion. This indicates a lower metallic surface area available for catalysis, and correlates to the information obtained from the hydrogen chemisorption analysis.

Backscattered electron microscopy imaging and electron dispersive X-ray spectroscopy (EDX) element maps were obtained for both catalyst precursors. The images and accompanying element maps are presented in Figure 4.9. The 15 NiA image and accompanying element map shows NiO to be well dispersed on the catalyst surface, while the 15 NiSi element map shows large green clusters, confirming the poor NiO dispersion on the silica support (Figure 4.9, C and D).

In addition, the distribution of NiO on alumina is somewhat uniform throughout the particles shown in Figure 4.9 (A and B). However, there are some areas of the support that are unoccupied by the metal oxide.

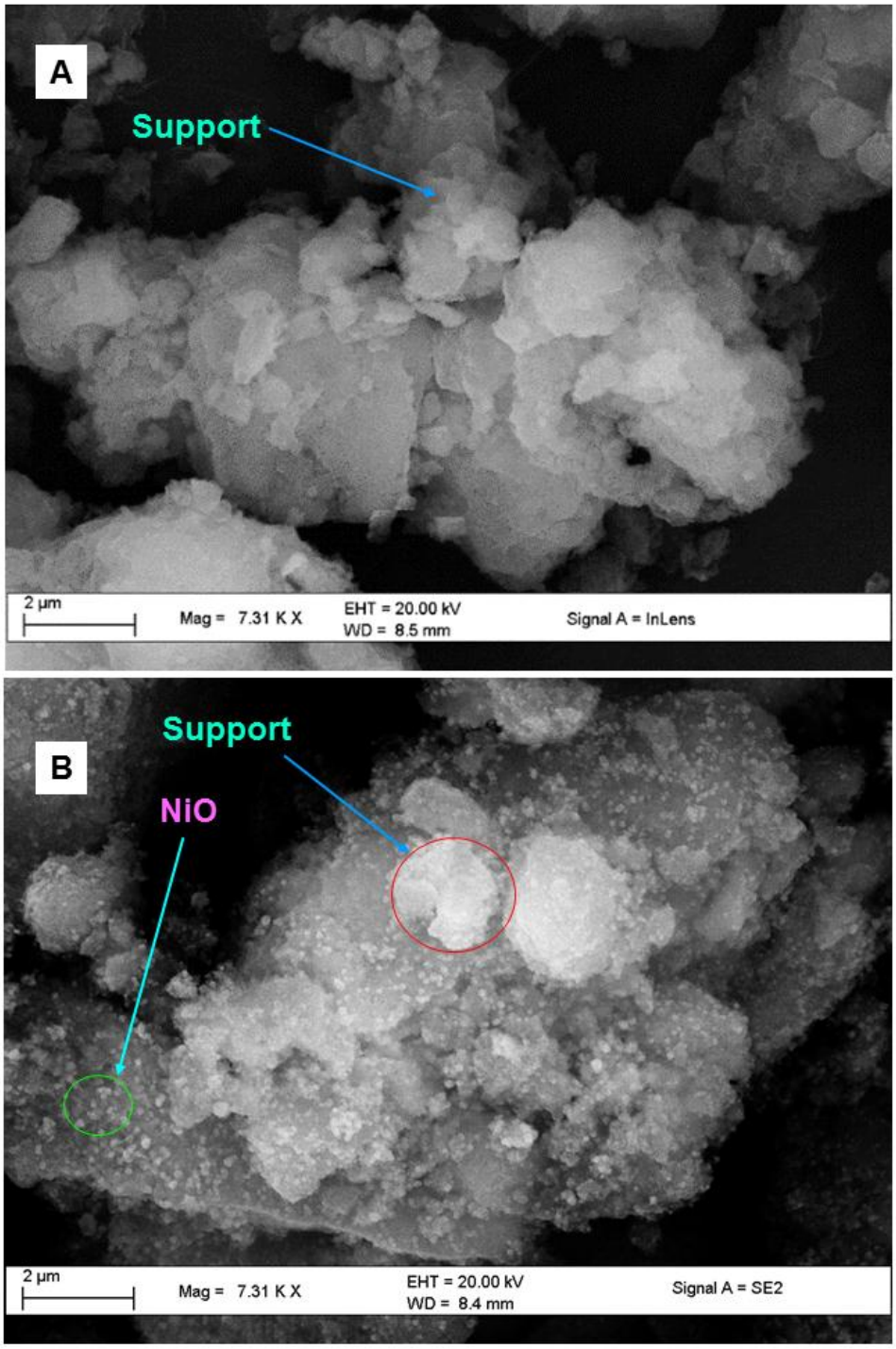

Figure 4.8: SEM images of A) 15 NiA and B) 15 NiSi catalyst precursors, with the NiO particles and support morphology highlighted with circles

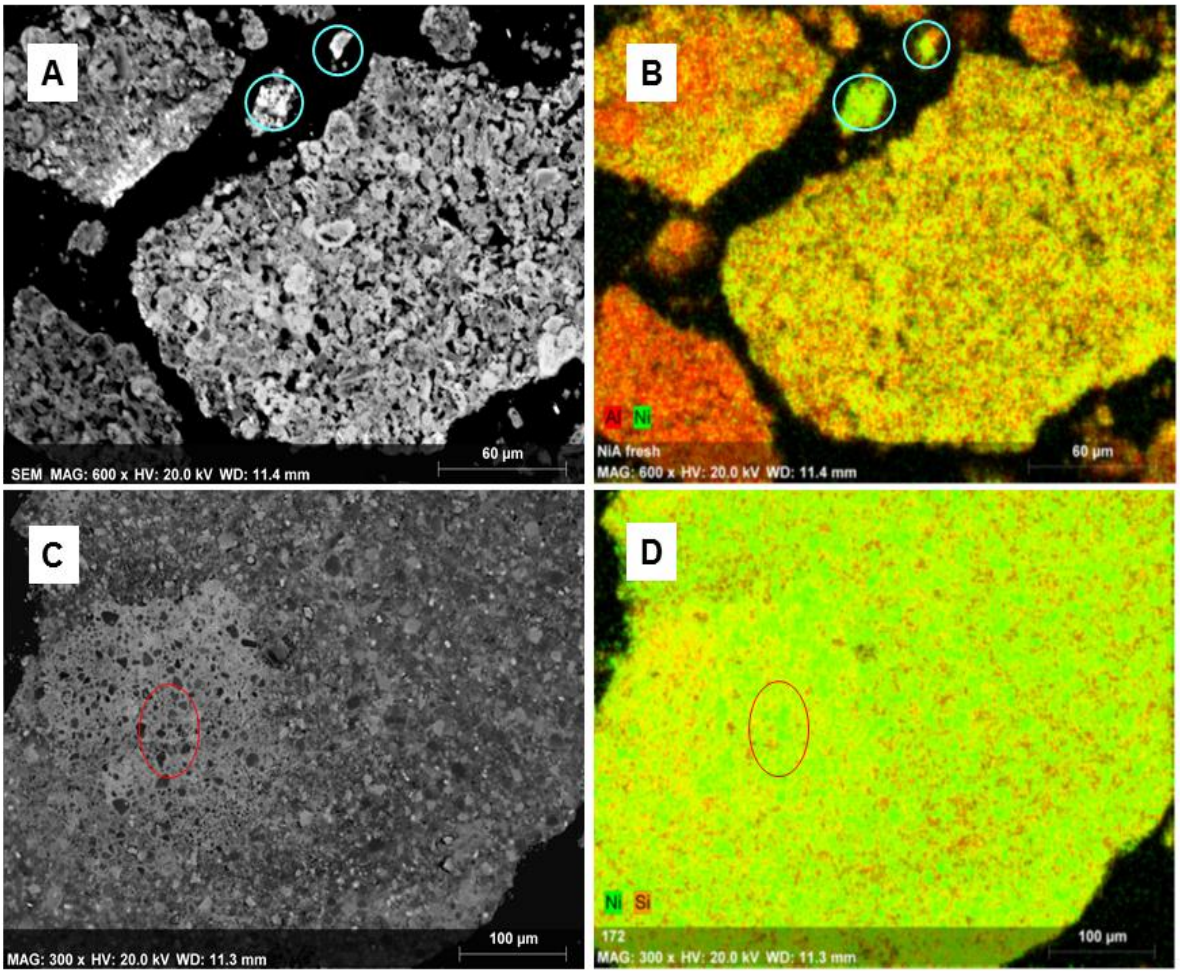

Figure 4.9: Backscattered scanning electron microscopy images and corresponding EDX maps of the 15 NiA (A and B) and 15 NiS (C and D) catalyst precursors, with circles highlighting NiO on the support

4.1.7 Transmission electron microscopy

The particle shape, size, surface morphology and metal particle distribution of the prepared catalysts were obtained using transmission electron microscopy. This analysis was performed to obtain a visualisation of the morphology of the 15 NiA and 15 NiSi catalysts, and to correlate the metal particle sizes obtained from TEM measurements to those obtained from hydrogen chemisorption. The TEM micrographs are presented in Figure 4.10, with the corresponding particle size distribution (histograms). For 15 NiA, the average NiO particle size, which was determined to be 7 nm, corresponds to the Ni crystallite size obtained with hydrogen chemisorption in Table 4.2. The micrograph also shows NiO to be well dispersed on the catalyst surface.

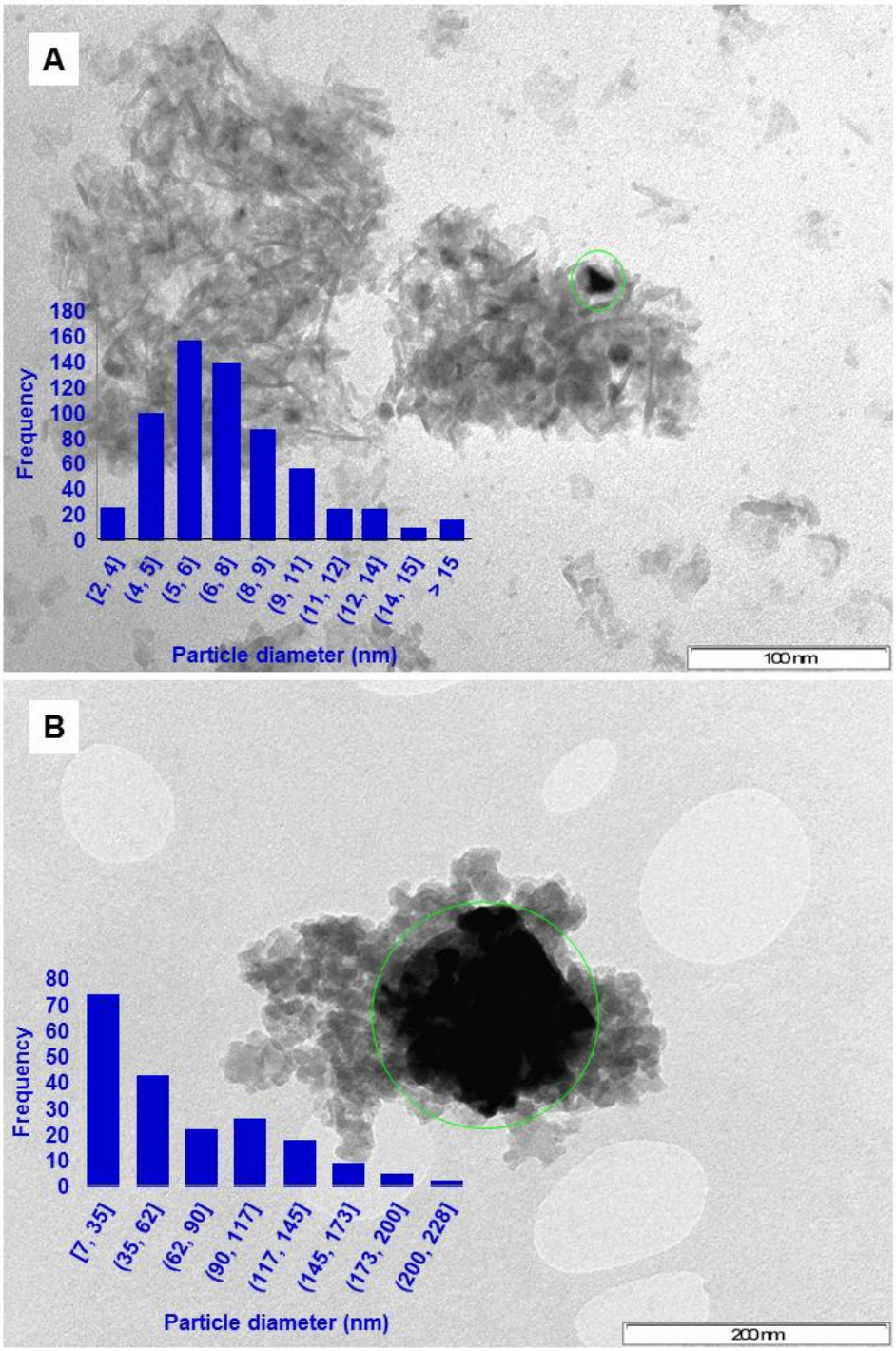

Figure 4.10: TEM micrographs and accompanying histograms showing the NiO particle size distribution on 15 NiA (A) and 15 NiSi (B). The NiO particles are circled in green

However, for the 15 NiSi catalyst, the dispersion of NiO is relatively poor, with the average NiO particle size determined to be 65 nm, which is much larger than the 21 nm determined for the Ni crystallite size from hydrogen chemisorption. The NiO particles on both supports are highlighted in green to provide a visual distinction of the particle sizes.

For 15 NiA, the majority of the nickel oxide particles are within the 4 to 15 nm range. The nickel oxide particles on 15 NiSi have a more heterogenized particle size distribution, with most particles falling within 17 to 47 nm, while others are as large as 150 nm in diameter. The large NiO particles on the silica support suggest that the support merely acted as a binder, since from the temperature programmed reduction and chemisorption, it appears the support has very little interaction with the active phase. The results from hydrogen chemisorption and transmission electron microscopy analyses were not unexpected, since the difficulty of achieving high dispersion of the active phase on the silica support has been reported [27].

4.2 Summary

The characterisation techniques employed for probing the properties of the prepared catalysts helped to establish the major differences between the effects of alumina and silica as supports for a nickel hydrogenation catalyst. The accurate metal loading was determined with inductively coupled plasma optical emission spectroscopy, which showed the nickel loading on both catalysts to be similar and close to the theoretical values. Bulk analysis with powder X-ray diffraction indicated the difference in the nickel oxide dispersion on both supports. The 15 NiSi catalyst had larger nickel clusters with a poor metal dispersion and lower metallic surface area. The nickel phase on the 15 NiA catalyst was well dispersed, and had a higher metallic surface area compared to 15 NiSi.

Furthermore, all the characterisation techniques proved, collaboratively, the poor dispersion of nickel on silica and high dispersion of nickel on alumina. This was indicated by information obtained from X-ray diffraction, which was also corroborated by hydrogen chemisorption, temperature programmed reduction, scanning electron microscopy and transmission electron microscopy. The 15 NiSi catalyst was easier to reduce, since a higher degree of reduction was achieved at a lower temperature. On the other hand, the 15 NiA catalyst is comparably more difficult to reduce, since it required a higher reduction temperature, which could be attributed to the stronger interaction of NiO with the support.

4.3 References

[1] M.A. Goula, N.D. Charisiou, K.N. Papageridis, A. Delimitis, E. Pachatouridou, E.F. Iliopoulou, International Journal of Hydrogen Energy 40 (2015) 9183-9200.

[2] M. Thommes, K. Kaneko, A.V. Neimark, J.P. Olivier, F. Rodriguez-Reinoso, J. Rouquerol, K.S.W. Sing, Pure and Applied Chemistry 87 (2015) 1051-1069.

[3] G. Leofanti, M. Padovan, G. Tozzola, B. Venturelli, Catalysis Today 41 (1998) 207-219.

[4] H. Wu, G. Pantaleo, V. La Parola, A.M. Venezia, X. Collard, C. Aprile, L.F. Liotta, Applied Catalysis B: Environmental 156–157 (2014) 350-361.

[5] G. Zhu, C. Xi, H. Xu, D. Zheng, Y. Liu, X. Xu, X. Shen, RSC Advances 2 (2012) 4236-4241.

[6] S.R. Yenumala, S.K. Maity, D. Shee, Catalysis Science & Technology 6 (2016) 3156-3165.

[7] R. Fréty, M.R. Santos, R.F. Sales, A.O.S. Silva, C.B.M. Barbosa, J.G.A. Pacheco, Journal of the Brazilian Chemical Society 25 (2014) 2433-2443.

[8] P. Kumar, S.R. Yenumala, S.K. Maity, D. Shee, Applied Catalysis A: General 471 (2014) 28-38.

[9] L. Smolakova, M. Kout, E. Koudelkova, L. Capek, Industrial & Engineering Chemistry Research 54 (2015) 12730-12740.

[10] L. Liu, X. Ma, J. Li, International Journal of Energy Research 38 (2014) 860-874.

[11] D. Dutta, D.K. Dutta, Applied Catalysis A: General 487 (2014) 158-164.

[12] A. Wang, H. Yin, H. Lu, J. Xue, M. Ren, T. Jiang, Langmuir 25 (2009) 12736-12741.

[13] C.H. Bartholomew, R.J. Farrauto, Journal of Catalysis 45 (1976) 41-53.

[14] A. Saadi, R. Merabti, Z. Rassoul, M.M. Bettahar, Journal of Molecular Catalysis A: Chemical 253 (2006) 79-85.

[15] S. Smeds, T. Salmi, L.P. Lindfors, O. Krause, Applied Catalysis A: General 144 (1996) 177-194.

[16] C.H. Bartholomew, R.B. Pannell, J.L. Butler, Journal of Catalysis 65 (1980) 335-347.

[17] D.G. Mustard, C.H. Bartholomew, Journal of Catalysis 67 (1981) 186-206.

[18] M.R. Gogate, Applied Catalysis A: General 514 (2016) 203-213.

[19] P. Maeki-Arvela, J. Hajek, T. Salmi, D.Y. Murzin, Applied Catalysis A: General 292 (2005) 1-49.

[20] P. Munnik, P.E. de Jongh, K.P. de Jong, Chemical Reviews (Washington, DC, U. S.) 115 (2015) 6687-6718.

[21] A. Borodzinski, M. Bonarowska, Langmuir 13 (1997) 5613-5620.

[22] J.C. Rodriguez, A.J. Marchi, A. Borgna, A. Monzon, Journal of Catalysis 171 (1997) 268-278.

[23] S. Ali, M.J. Al-Marri, A.G. Abdelmoneim, A. Kumar, M.M. Khader, International Journal of Hydrogen Energy 41 (2016) 22876-22885.

[24] D.R. Abd El-Hafiz, M.A. Ebiad, R.A. El-salamony, Materials for Renewable and Sustainable Energy 3 (2014) 1-13.

[25] R. Molina, G. Poncelet, Journal of Catalysis 173 (1998) 257-267.

[26] S. He, X. Zheng, L. Mo, W. Yu, H. Wang, Y. Luo, Materials Research Bulletin 49 (2014) 108-113.

[27] S. Soled, Science 350 (2015) 1171-1172.

Chapter 5: Catalytic results and discussion

Catalytic activity tests were performed in a stainless steel, continuous flow fixed bed reactor. The reactor configuration was presented in Chapter 3. The nickel weight loading (15 %) and catalytic conditions were optimised by Valand *et al.* [1]. The chosen weight loading has an added advantage since it is sufficient to provide high catalytic activity, whilst being low enough to allow sufficient interaction between the support and the poison. This approach was also used to establish the role of the supports in the deactivation of the catalysts, and to ascertain if the poison alters the surface acid/base functionality of the supports. Therefore, the weight loading of nickel used in this study was significantly less than is normally used for commercial applications [2, 3].

Catalytic tests were performed at a liquid hourly space velocity of 18 h^{-1}, a hydrogen to substrate ratio of 2:1, 50 bar hydrogen pressure, and a temperature of 140 °C. Prior to deactivation, the baseline activity was established using feed that consisted of 10 wt.% octanal diluted with octanol, which is referred to as clean feed (CF). The contaminated feed had a composition of 10 wt.% octanal with 500 ppm of triphenylphosphine in octanol, and is designated as TPP feed.

5.1 Catalytic activity

The intrinsic activities of the prepared catalysts, 15 NiA and 15 NiSi, towards octanal hydrogenation under optimised conditions are presented in Figure 5.1. Both catalysts display a similar, high octanal conversion, with a correspondingly high octanol selectivity. The by-product selectivity varies slightly for each catalyst because of their different acid-base properties.

Gamma alumina is a bifunctional support that possesses Brønsted acid and basic sites, whereas silica has Brønsted acid sites [4-6]. The main by-products are the C_{24} acetal and C_{16} diol, while octyl ether and 2-hexyl decanol form in smaller quantities, and are hence referred to as other products. By-product formation is catalysed by the support, whereas the hydrogenation of octanal is catalysed by the metal particles [7]. The mechanism through which the carbonyl group of an aldehyde adsorbs and undergoes hydrogenation on a metal surface has already been reviewed in the first chapter. The slightly higher by-product selectivity of the 15 NiSi catalyst is attributed to its relatively poor metal dispersion as determined by hydrogen chemisorption,

which possibly resulted in a greater number of exposed acid sites that catalyse by-product formation.

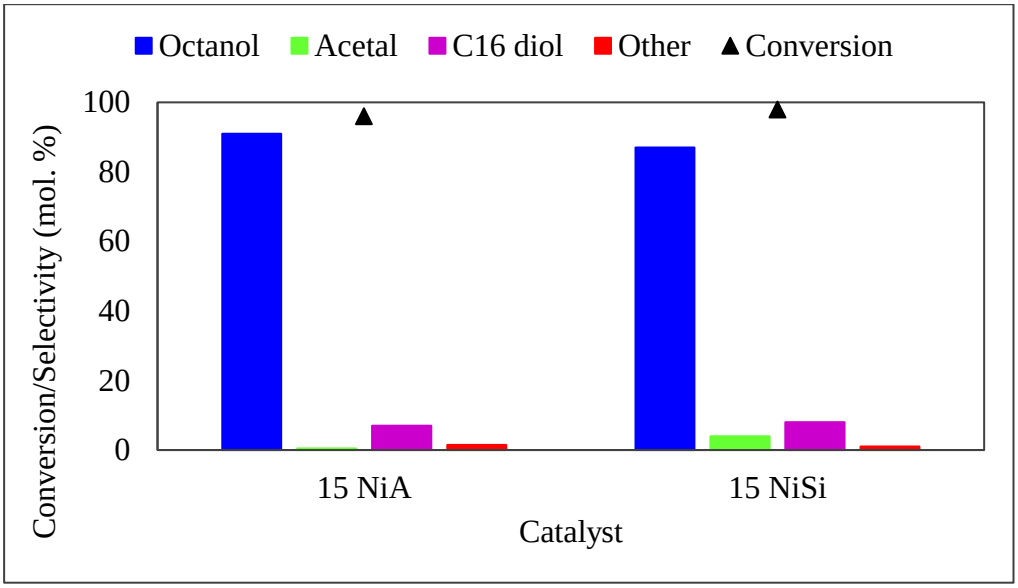

Figure 5.1: Conversion and selectivity of the 15 NiA and 15 NiSi catalysts

The formation of the C_{24} acetal is catalysed by Brønsted acid sites on the support, and is a product of the reaction of an octanal molecule with two octanol molecules [7, 8]. The octanal carbonyl oxygen is first protonated over the Brønsted acidic site of the support, followed by a reaction with the first octanol molecule to form a hemiacetal intermediate [7, 9]. The intermediate dehydrates to an oxonium ion, which reacts with the second octanol molecule to form the C_{24} acetal, as depicted in reaction Scheme 5.1 [7].

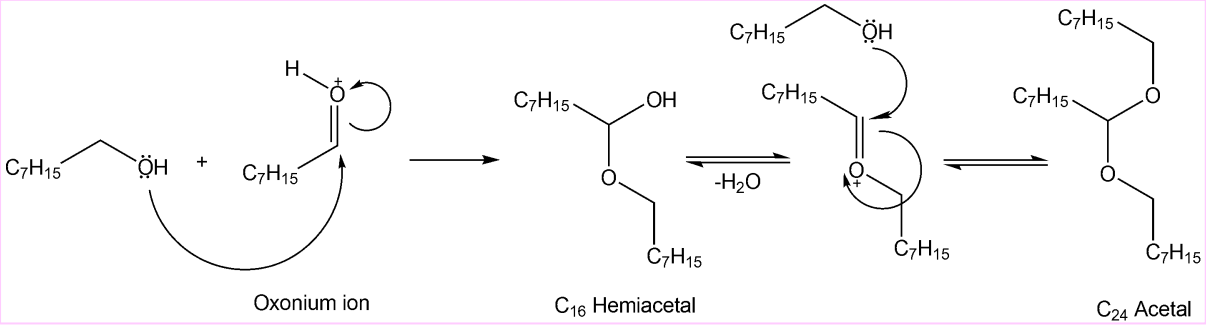

Scheme 5.1: Formation of the C_{24} acetal over Brønsted acid sites [7]

The dioctyl ether forms from the acid catalysed reaction of two octanol molecules via a dehydration process, which also produces water, as per Scheme 5.2. The dioctyl ether may also form from the hydrocracking of the C_{24} acetal, yielding the dioctyl ether, and octanol [7].

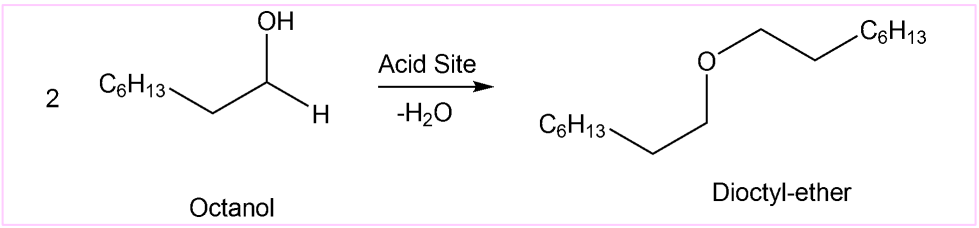

Scheme 5.2: Formation of dioctyl ether from two octanol molecules [7]

The formation of C_{16} diol, on the other hand, is a base catalysed reaction, but can also be catalysed by Brønsted acid sites [10, 11]. The C_{16} diol forms from a reaction between two octanal molecules. One aldehyde molecule undergoes hydrogen abstraction from an α-carbon by a weak basic site of the support, forming a nucleophilic carbanion. The second aldehyde molecule is protonated on the carbonyl oxygen by a weak acid site, making the carbonyl carbon electrophilic. The nucleophilic carbanion subsequently attacks the electrophilic carbonyl carbon, forming an aldol intermediate that is hydrogenated into the corresponding C_{16} diol, as shown in Scheme 5.3.

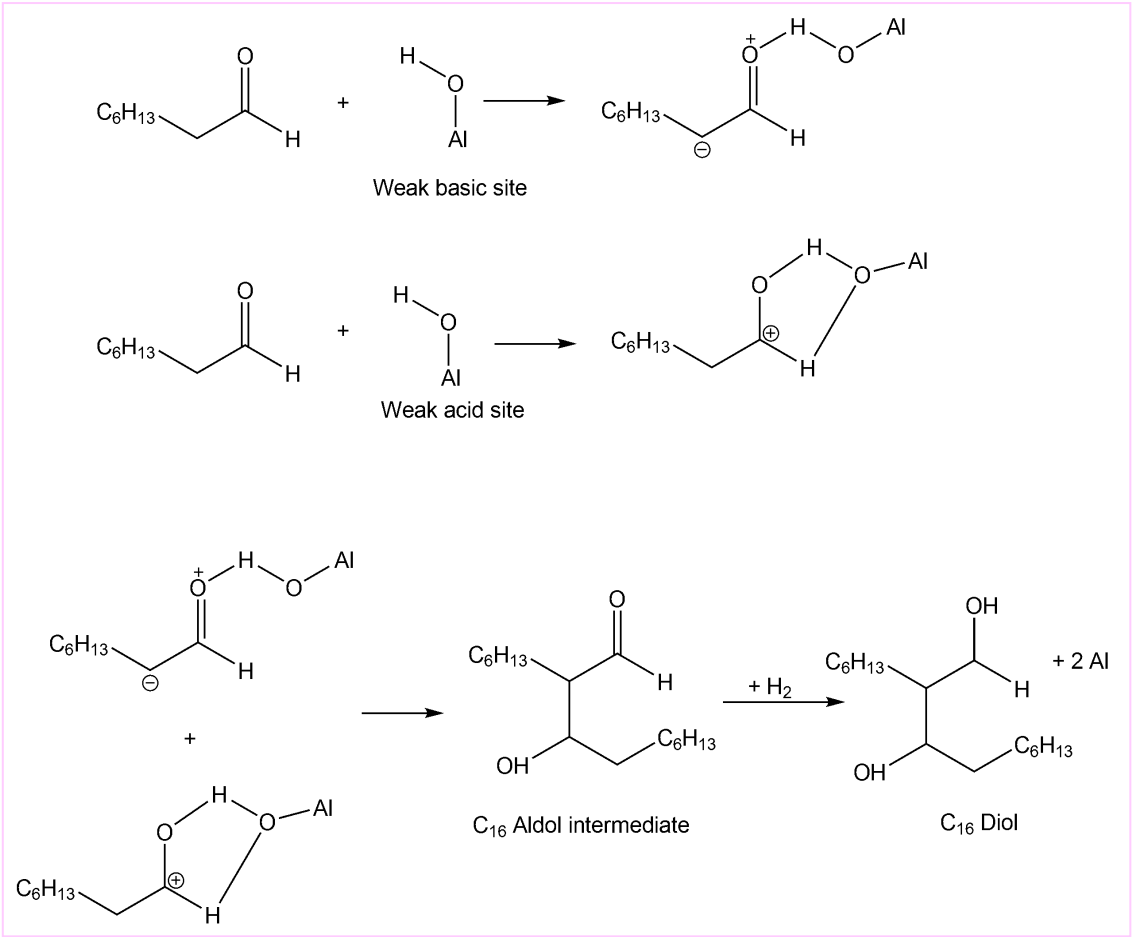

Scheme 5.3: Acid/Base catalysed formation of the C_{16} diol [7]

The C_{16} diol molecule can further undergo dehydration and hydrogenation, resulting in the formation of 2-hexyl decanol, as depicted in reaction Scheme A1 (Appendix), which includes the complete reaction network.

5.2 Deactivation and regeneration of 15 NiA

The accelerated deactivation of 15 NiA was performed by introducing feed contaminated with triphenylphosphine having a concentration of 500 ppm. Time on stream deactivation and regeneration experiments were conducted in the sequence of CF-TPP-CF-Regeneration-CF. The initial experiment (CF) was conducted until the catalyst reached stable conversion and selectivity. The poisoned feed was subsequently introduced. After a significant decline in the conversion had occurred, the flow of poisoned feed into the reactor was ceased, and the non-contaminated feed was re-introduced to determine if deactivation was reversed with removal of the poisoned feed.

5.2.1 Influence of TPP as poison on the activity of 15 NiA

Figure 5.2 gives the catalytic activity profile before, during and after the introduction of poisoned feed. The graph is divided into three zones, namely **Zone A** (clean feed), **Zone B** (poisoned feed) and **Zone C** (clean feed). The initial conversion and octanol selectivity were 96 and 87 % respectively. After steady state was reached (9 hours), the conversion was 98 %, while the octanol selectivity was 88 %. After the introduction of the poisoned feed, the catalytic conversion gradually declined over a period of about 38 hours to a value of 30 %, caused by the adsorption of triphenylphosphine onto the catalytically active sites.

The overall product selectivity profile remained largely unchanged for the entire duration of the TPP feed run, with the only change being the inversion in the C_{24} acetal and C_{16} diol selectivity observed after 27 hours on stream (**Zone B**). Initially, the C_{24} acetal selectivity was 1 %, but increased to 6 % at the end of the poisoning experiment, while the selectivity of the C_{16} diol, which was the predominant by-product, decreased from 9 % to 1 %. This suggests a change in the acid-base properties of the catalyst, since the C_{24} acetal formation is catalysed by Brønsted acid sites [1, 7, 12].

The preservation of the overall selectivity profile in **Zone B** indicates non-selective poisoning of the catalyst by triphenylphosphine. According to Forzatti and Lietti [13], a non-selective poison decreases the overall activity without affecting the product selectivity, as observed in the present case [13].

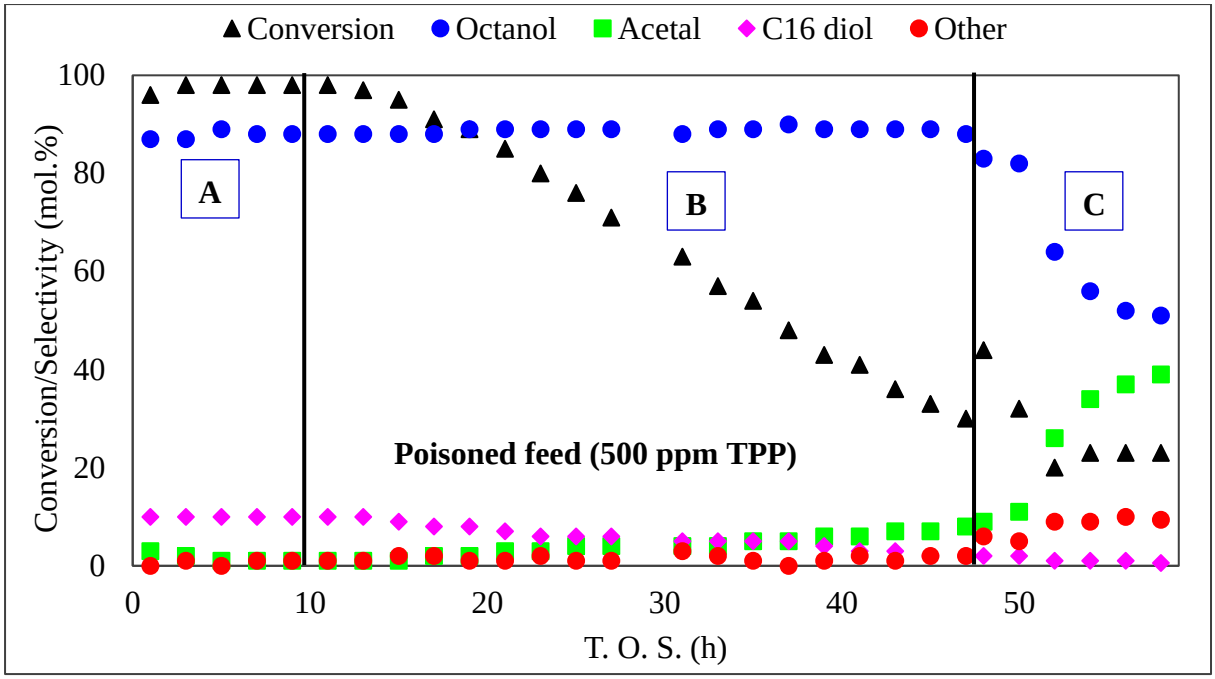

Figure 5.2: Activity profile before (**Zone A**), during (**Zone B**) and after exposure of the 15 NiA catalyst to poisoned feed (**Zone C**)

Poisons also tend to target the most coordinatively unsaturated active sites, leaving residual metal active sites. In addition, the deactivation of a catalyst bed is non-uniform, since the poison front propagates from the entrance of the catalyst bed and moves progressively downward, leaving the topmost layer saturated with poison, while the bottom remains moderately poisoned, as presented in Figure A1 (Appendix). The residual catalytic activity at the end of the poisoning experiment is due to the combination of the non-poisoned region of the catalyst bed and residual nickel active sites [14]. Some nickel sites may remain unaffected by the poison due to the steric bulk of the triphenylphosphine molecule, which has a cone angle of 145°, and large phenyl groups that would physically block the approach and adsorption of reactants onto small metal particles [15, 16]. Subsequent decomposition of triphenylphosphine under the hydrogen atmosphere [17] would then result in the sterically blocked particles being exposed, which adds to the number of residual catalytically active sites.

The reintroduction of clean feed in **Zone C** led to a further decline in the catalytic activity. The conversion momentarily increased from 30 % to 44 %, but subsequently decreased to a steady state conversion of 23 %. The octanol selectivity decreased from 88 % to 51 %. This was accompanied by a subsequent increase in the by-product selectivity. The C_{24} acetal selectivity underwent a significant increase from 6 % to 39 %, whilst that of the other products increased from 2 % to 10 %. In contrast, the selectivity towards the C_{16} diol decreased to less than 1 %.

The decline in catalytic activity and lower steady state conversion in **Zone C** suggests a distribution of adsorbed triphenylphosphine onto residual nickel sites by the re-introduction of clean feed, further deactivating the catalyst [13, 14]. The increase in the C_{24} acetal indicates the *in situ* formation of additional support acid sites from the reaction of phosphorus, alumina, and water. Water is formed *in situ* from the support catalysed reactions, such as the formation of the C_{16} diol by aldol condensation, C_{24} acetal and dioctyl ether [18]. The water creates an oxidising environment, thereby enabling the oxidation of reduced phosphorus species [19, 20], allowing them to react with the alumina to form acidic $AlPO_4$, or other acidic phosphorus-alumina species [21].

The decrease in octanol selectivity was an indication of irreversible deactivation under the process conditions, since discontinuation of the poisoned feed did not recover lost activity, but instead resulted in a further decline in octanol selectivity. This justified a need for regeneration, which was attempted by performing three separate experiments aimed at developing a viable technique for the recovery of both catalytic activity and selectivity.

5.2.2 Regeneration of 15 NiA

Regeneration experiments were conducted by either introducing hydrogen at a GHSV of 600 h^{-1}, or passing octanol at a liquid hourly space velocity (LHSV) of 18 h^{-1}, at a temperature of 200 °C. The regeneration temperature was chosen based on reports from literature [22]. The third type of regeneration process, which was a combined regeneration method, involved passing octanol through the catalyst bed for twelve hours, followed by the introduction of hydrogen for a further 12 hours. Where the regeneration data is presented, **Zones A** and **B** are omitted as they are a repetition of what was observed in Figure 5.2. **Zone C** is included to illustrate the extent to which the activity was recovered. The regeneration procedure is indicated after **Zone C** for each of the methods.

5.2.2.1 Regeneration with hydrogen

Regeneration was carried out by stopping the clean feed, slowly releasing the hydrogen pressure, and increasing the temperature and the flow rate of hydrogen gas. The clean feed was reintroduced after regeneration to determine the extent to which the catalytic activity was recovered. The activity profile after hydrogen regeneration is presented in Figure 5.3. After regeneration, the conversion and selectivity were momentarily recovered.

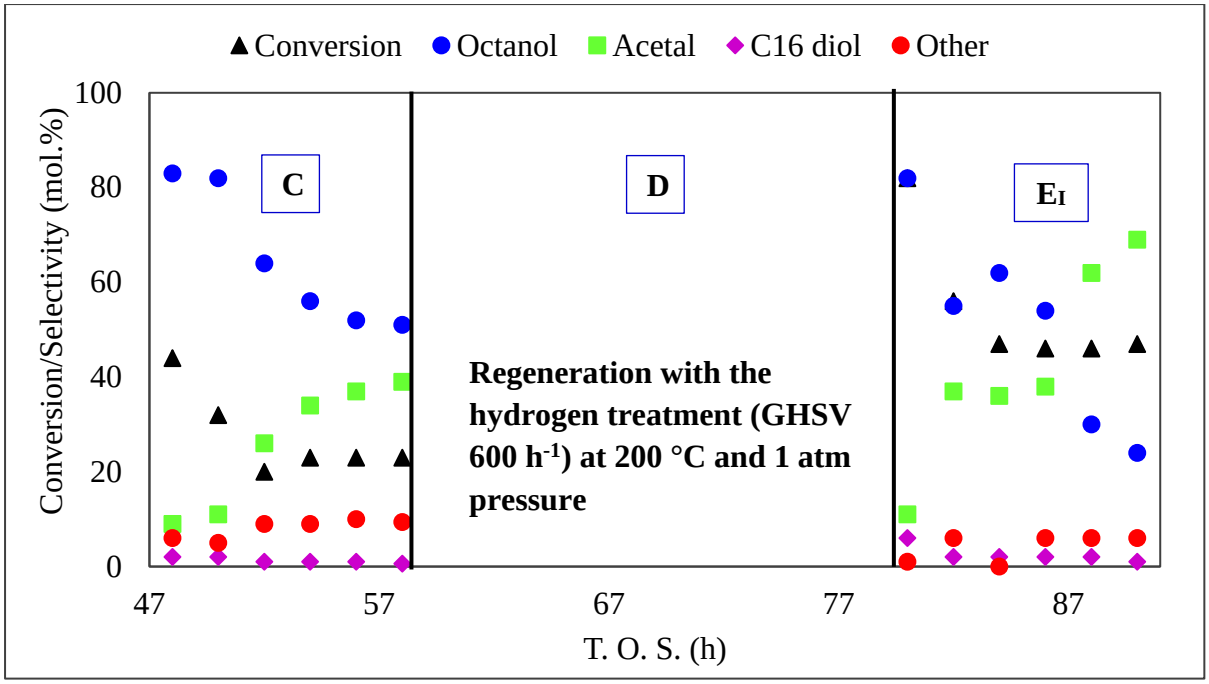

Figure 5.3: Activity profile of 15 NiA before and after regeneration with hydrogen: (**C**) clean feed before regeneration, (**D**) regeneration step, (**EI**) clean feed after regeneration

Both the conversion and selectivity increased to about 82 %. The conversion then decreased to 46 % after a few hours, while at the same time the octanol selectivity progressively declined, accompanied by an increase in the acetal selectivity. The momentary recovery of octanol selectivity suggests the regeneration of nickel active sites, and its subsequent decline suggests a continuous depletion in the number of recovered nickel active sites. The higher C_{24} acetal selectivity indicates a significant increase in Brønsted acidic sites.

The low catalytic activity after regeneration, and declining octanol selectivity, suggest the continued deactivation of nickel active sites, possibly due to phosphorus species initially residing on the support migrating back onto cleaned nickel sites, resulting in secondary deactivation of the catalyst. This possibly suggests hydrogen only cleans nickel, and fails to remove the poison adsorbed on the support. To test this hypothesis, solvent regeneration was attempted.

5.2.2.2 Regeneration with octanol

The solvent wash regeneration method was performed under the same conditions as the hydrogen treatment, except no hydrogen gas was flowed through. Octanol was passed through the catalyst bed at a liquid hourly space velocity of 18 h^{-1} for twelve hours after steps indicated in **Zones A** to **C** in Figure 5.2. The octanol washings were drained, and the reactor was then

re-pressurised to 50 bars with hydrogen. Figure 5.4 presents the activity profile of 15 NiA after the octanol wash regeneration.

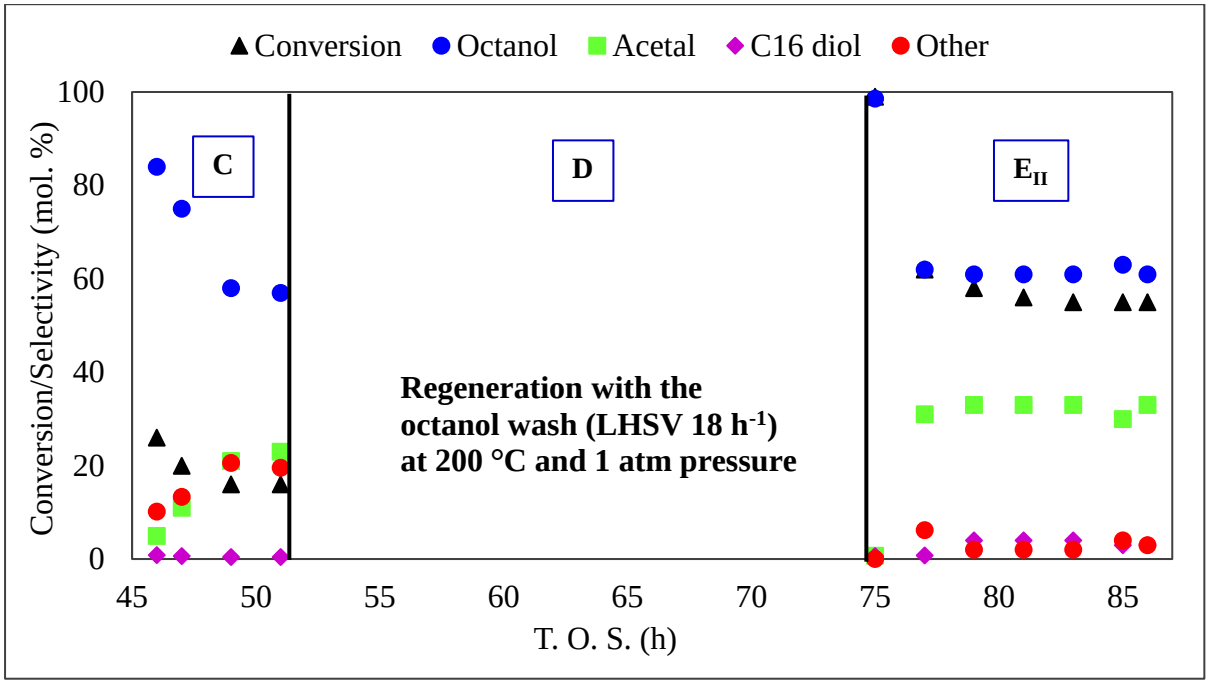

Figure 5.4: Activity profile of 15 NiA before and after regeneration with octanol: (**C**) clean feed before regeneration, (**D**) regeneration step, (**E_{II}**) clean feed after regeneration

Compared to the hydrogen treatment (Figure 5.3), the octanol wash regeneration improved the recovered octanol selectivity, suggesting a better recovery of nickel active sites. However, the C_{24} acetal selectivity was still much higher than that observed before the regeneration. In fact, it increased from 21 % to a steady state selectivity of 31 %. The conversion was slightly higher in this case, at 55 %, compared to 47 % obtained with the hydrogen treatment regeneration experiment.

The slight recovery of the catalytic activity and selectivity suggests a recovery of some nickel active sites, possibly though the removal of phosphorus from the catalyst. Furthermore, the stable octanol selectivity indicates removal of mobile phosphorus species, which prevented the secondary deactivation of nickel active sites. Despite the improvement in the conversion and octanol selectivity, the C_{24} acetal selectivity remained high, suggesting the poison induced formation of acid sites was not reversed by regeneration. Thereafter, the combined regeneration experiment was carried out.

5.2.2.3 Combination of solvent washing and hydrogen treatment

This regeneration experiment was carried out by first performing the solvent wash regeneration for twelve hours, followed by the hydrogen regeneration for another twelve hours. The reactor was cooled for a further four hours under a flow of hydrogen at atmospheric pressure, then re-pressurised to 50 bars once the temperature had cooled to the reaction temperature (140 °C). Thereafter, the hydrogenation reaction was restarted. In Figure 5.5, we can observe the extent of recovery of the activity and selectivity achieved with the combined regeneration.

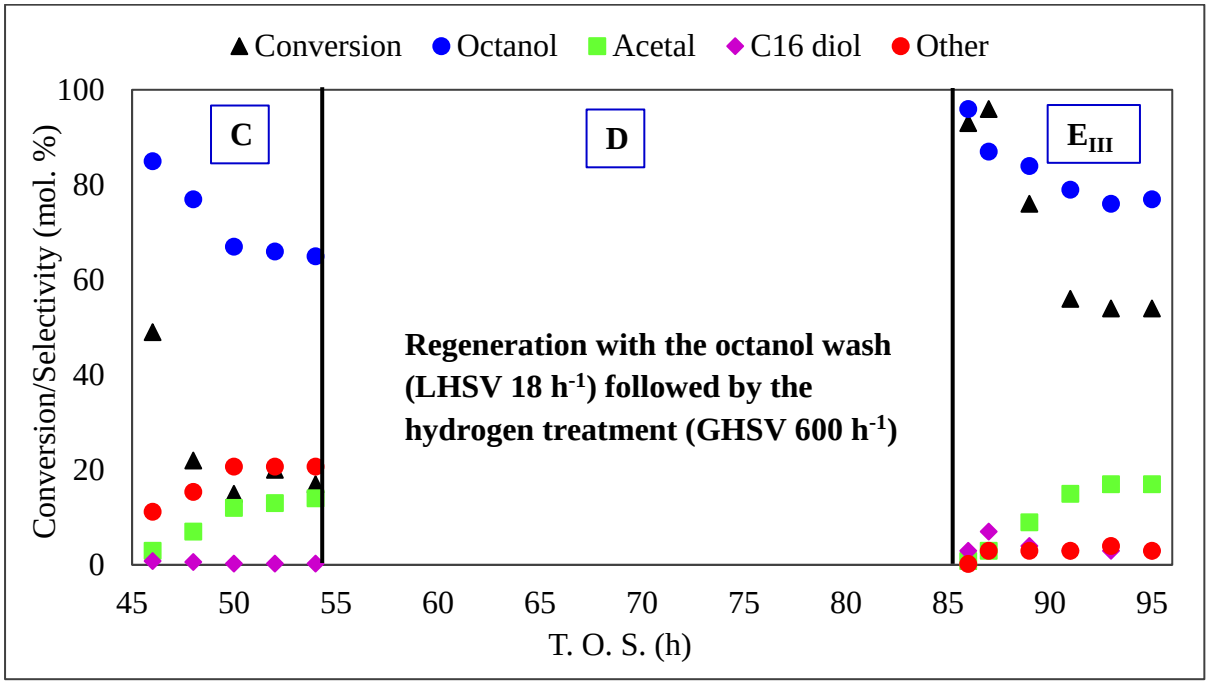

Figure 5.5: Activity profile of 15 NiA before and after regeneration with octanol and hydrogen: (**C**) clean feed before regeneration, (**D**) regeneration step, (**E**$_{III}$) clean feed after regeneration

The combined regeneration had a significantly more positive effect on the octanol selectivity, which increased from the 54 % achieved with the octanol wash regeneration, to 77 % after the combined regeneration, while the acetal selectivity remained below 20 % (**Zone E**$_{III}$, Figure 5.5). This indicates that the combination of both solvent washing and hydrogen treatment was effective in the regeneration of the catalyst, by cleaning nickel sites for octanal hydrogenation.

From the results obtained from all the regeneration methods, a major observation was the change in the by-product selectivity after regeneration of the catalyst (cf. **Zone E**$_{I-III}$). The catalyst becomes more acidic after exposure to triphenylphosphine, which is indicated by the higher C_{24} acetal selectivity exhibited by the regenerated catalysts. The C_{24} acetal selectivity is not as pronounced after the combined regeneration, which suggests that the acidity of the

catalyst regenerated by the combined regeneration method is not as high, when compared to the individual hydrogen and octanol wash regeneration experiments.

For all three regeneration experiments, there was no experimental evidence attesting to the removal of the poison from the catalyst bed and out of the reactor, since no phosphorus species were detected by GC-FID and NMR analysis in the exit product streams and octanol washings obtained during the solvent wash regeneration. Hence, the used catalysts were analysed to determine if phosphorus was retained after regeneration, and to establish the location of phosphorus.

5.2.3 Characterisation of the poisoned and regenerated 15 NiA catalyst

The poisoned and regenerated catalysts were characterised to determine the chemical and structural effects of phosphorus poisoning and regeneration on the catalysts. This was achieved by performing elemental analysis to quantify the amount of phosphorus retained on the catalysts, X-ray diffraction and magnetic measurements, transmission electron microscopy imaging and surface area analysis to observe changes in the physicochemical properties of the catalysts, and thermal analysis to determine if fouling contributed to catalyst deactivation. The relationship between nickel and phosphorus was also probed with scanning electron microscopy and electron dispersive measurements, while the surface composition of phosphorus and nickel was quantified with the aid of scanning transmission electron microscopy, coupled with electron dispersive X-ray analysis.

5.2.3.1 Physicochemical properties

Elemental analysis of phosphorus and nickel conducted by inductively coupled plasma-optical emission spectroscopy was undertaken to quantify the total amount of Ni and P present on the fresh, used and deactivated catalysts in order to compare the relative amount of phosphorus deposited on each catalyst. This was to confirm the findings from GC-FID and NMR analyses of exit product streams and octanol washings, which showed no evidence of phosphorus exiting the reactor, suggesting the retention of phosphorus by the catalysts despite regeneration. Table 5.1 presents results obtained from the elemental analysis of 15 NiA, which confirmed the presence of phosphorus on the poisoned and regenerated catalysts. The minor variations in the phosphorus compositions is an effect of different batches of poisoned feed used during the poisoning study, which might have had slight variations in the TPP concentrations. The description of the catalyst at different stages in the process is also given in Table 5.1.

Table 5.1: Textural properties and elemental compositions on the fresh, used and poisoned 15 NiA catalyst samples

Sample	**Description**	**Ni (wt.%)**	**P (wt.%)**	**BET Surface area (m^2 g^{-1})**	**Average Ni particle size[a]**
15 NiA	Fresh	14.5	-	176	7
15 NiA-U	Used, non-poisoned	14.5	-	138	8
15 NiA-P	Poisoned	14.6	1.6	143	17
15 NiA-H	Hydrogen treatment regeneration	14.2	1.5	126	19
15 NiA-S	Octanol wash regeneration	14.6	1.8	133	22
15 NiA-SH	Combined regeneration	14.7	1.9	130	13

[a]determined from TEM

The similarities in the phosphorus weight loadings for 15 NiA-P, 15 NiA-H, 15 NiA-S and 15 NiA-SH confirm that phosphorus was not removed from the catalyst by regeneration and was retained, despite the recovery of the catalytic activity, suggesting either the redistribution of phosphorus on the catalyst bed, or that regeneration may have induced the diffusion of phosphorus into the nickel bulk. This phenomenon has been observed previously during the synthesis of nickel phosphide nanoparticles using phosphine ligands as reported by Henkes *et al.* [23, 24].

In addition to the ICP data, the data for BET analysis also showed changes in the physical properties of the catalyst. The BET surface area analysis results showed a decrease in the surface areas of the used, poisoned and regenerated catalysts, indicating the deposition of carbonaceous species [25]. The decrease in the surface areas also suggests sintering of the active phase, which would result in the blockage of pores, and, hence, a lower surface area. This was confirmed by particle size analysis using TEM, which showed notable agglomeration of the Ni active phase.

Thermal analysis was carried out under an oxygen atmosphere, and the results (Figure A3, Appendix) showed that all used catalysts had a mass loss of 3 % in the temperature range of 100 °C, due to the desorption of physisorbed water. The major mass loss for all catalysts occurred at 200 °C, which was shown by mass spectrometry to be due to the combustion of carbonaceous species deposited on the catalyst. The 15 NiA-U (non-poisoned) catalyst gives a relatively large CO_2 peak, at mass 44, compared to both 15 NiA-H (hydrogen treatment regeneration) and 15 NiA-SH (combined regeneration). The non-poisoned catalyst (15 NiA-U) underwent the largest weight loss compared to the other catalysts, suggesting the deposition of more carbonaceous species compared to the other used catalysts.

The changes in the acidity of the catalysts could not be quantified with the temperature programmed desorption of *n*-propylamine (Figure A2), suggesting the changes occur *in situ*. However, the disappearance of the peaks at 310 °C and 435 °C for 15 NiA and the appearance of sharper peaks at approximately 270 °C for both 15 NiA-H and 15 NiA-SH indicates a change in the acid-base properties, induced by the exposure of the catalyst to triphenylphosphine. It was hypothesized that triphenylphosphine interacts with the alumina support to form an aluminium phosphate phase, which resulted in the changes in the acid/base properties of the catalyst after deactivation.

To confirm the presence of $AlPO_4$, the catalyst samples were characterised using Fourier transform infrared spectroscopy. From the results in Figures A5-A9 (Appendix), the spectra of the poisoned and regenerated catalyst samples (Figure A7-A9) differ from the spectra of the non-poisoned 15 NiA sample (Figure A5-A6) by the presence of a broad band at approximately 1100 cm^{-1}. This band is attributed to the P-O stretching vibrations that are characteristic of $AlPO_4$ [18, 26].

Further characterisation was then carried out to observe structural changes induced by the exposure of the catalyst to phosphorus, and to confirm agglomeration of the active nickel phase.

5.2.3.2 Structural analysis of the poisoned and regenerated catalysts

Structural analysis was performed using XRD, TEM and HRTEM to determine the morphological and bulk changes induced by the interaction of phosphorus with nickel. The nature of the interaction between nickel and phosphorus was also probed by conducting magnetic measurements.

5.2.3.2.1 Powder X-ray diffraction and Magnetic measurements

The bulk phase analysis of the poisoned/regenerated catalysts was performed using powder X-ray diffraction to observe any phase changes induced by poisoning of the catalyst with phosphorus. As shown in Figure 5.6, there are no distinguishable peaks that can be attributed to the formation of a distinct nickel phosphide phase. This suggests that if the reaction between nickel and phosphorus resulted in the formation of a nickel phosphide phase, it was largely amorphous or in a concentration that is below the detection limit of this technique [27].

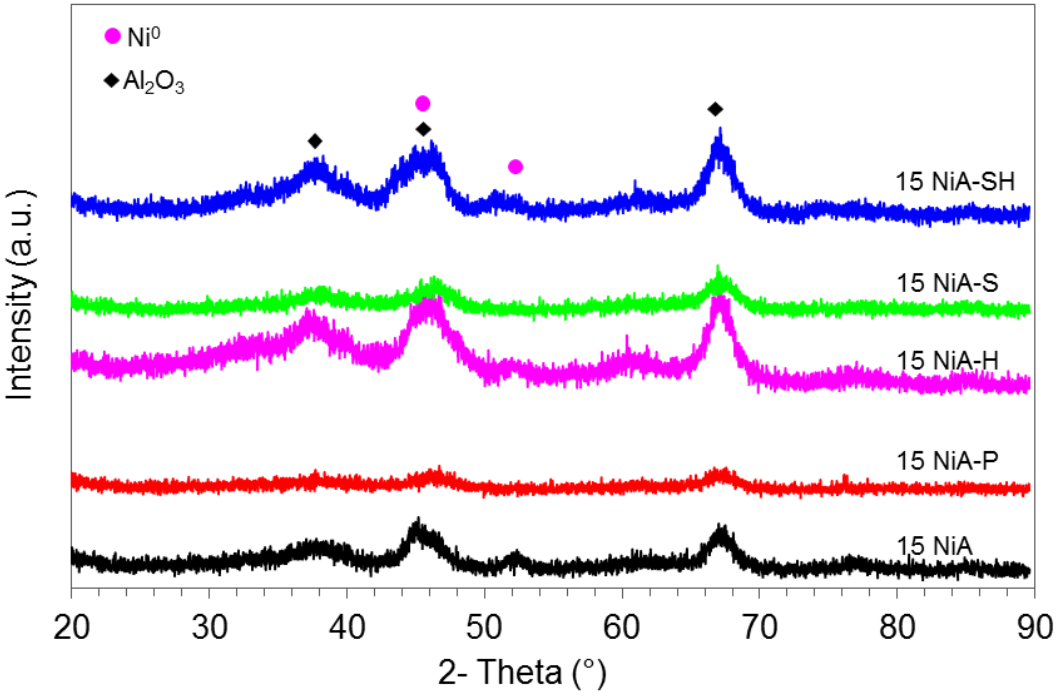

Figure 5.6: Powder X-ray diffraction patterns of the reduced, poisoned, and regenerated 15 NiA catalysts

Magnetic measurements were performed on the reduced, poisoned, and regenerated catalysts to gain further insight into the interaction between Ni and P. Metallic nickel is ferromagnetic, whereas doping nickel with phosphorus has been shown to decrease its magnetism, depending on the amount of phosphorus. As indicated by the magnetic hysteresis loops in Figure 5.7, the (reduced) 15 NiA catalyst gave a saturation magnetization of 4.0 emu/g, while 15 NiA-P, 15 NiA-H and 15 NiA-SH samples gave magnetizations of 0.9, 1.3, 0.9 and 1.3 emu/g respectively.

The lower saturation magnetization of the poisoned and regenerated catalysts indicates an interaction between Ni and P. This means the catalyst loses its ferromagnetism and becomes

paramagnetic, a quality that has been observed during the synthesis of nickel phosphide nanoparticles from a reaction of nickel nanoparticles with trioctylphosphine as a phosphorus source [17, 28, 29]. The catalyst does not lose its ferromagnetism entirely, suggesting that not all the nickel reacts with phosphorus, and some may remain in a metallic state. A study by Chen *et al.* [17] found that the degree of interaction between Ni and P was dependent on the temperature at which phosphorised Ni/SiO_2 samples that were exposed to a solution of triphenylphosphine were treated with hydrogen. For instance, the higher the temperature, the more Ni interacted with P, leading to a lower saturation magnetization.

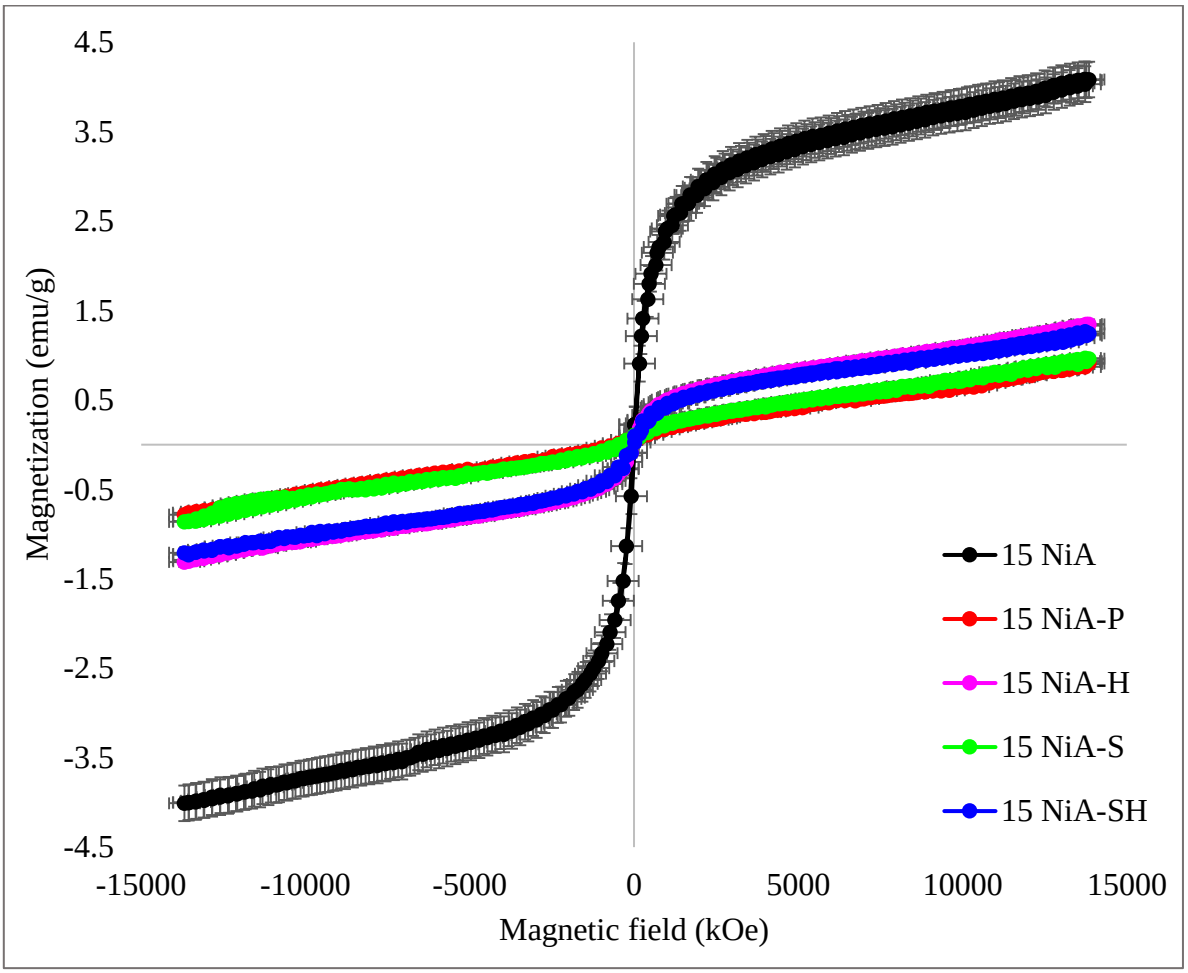

Figure 5.7: Magnetic hysteresis loops on 15 NiA, 15 NiA-P, 15 NiA-H, 15 NiA-S and 15 NiA-SH at room temperature

5.2.3.2.2 Transmission electron microscopy

The distribution of nickel on the support was studied with transmission electron microscopy to observe any changes in the morphology of the active phase. From Figure 5.8, notable agglomeration was observed for catalysts that were exposed to the triphenylphosphine

contaminated feed. The observed agglomeration significantly affected the average particle diameters of the active phase throughout the catalyst samples, as they were larger than the particle sizes of NiO on 15 NiA and the nickel particle sizes on 15 NiA-U. This suggests that phosphorus induced sintering of the active nickel phase, an observation also reported by Sezer and Celik [30], and Demircan *et al*. [31].

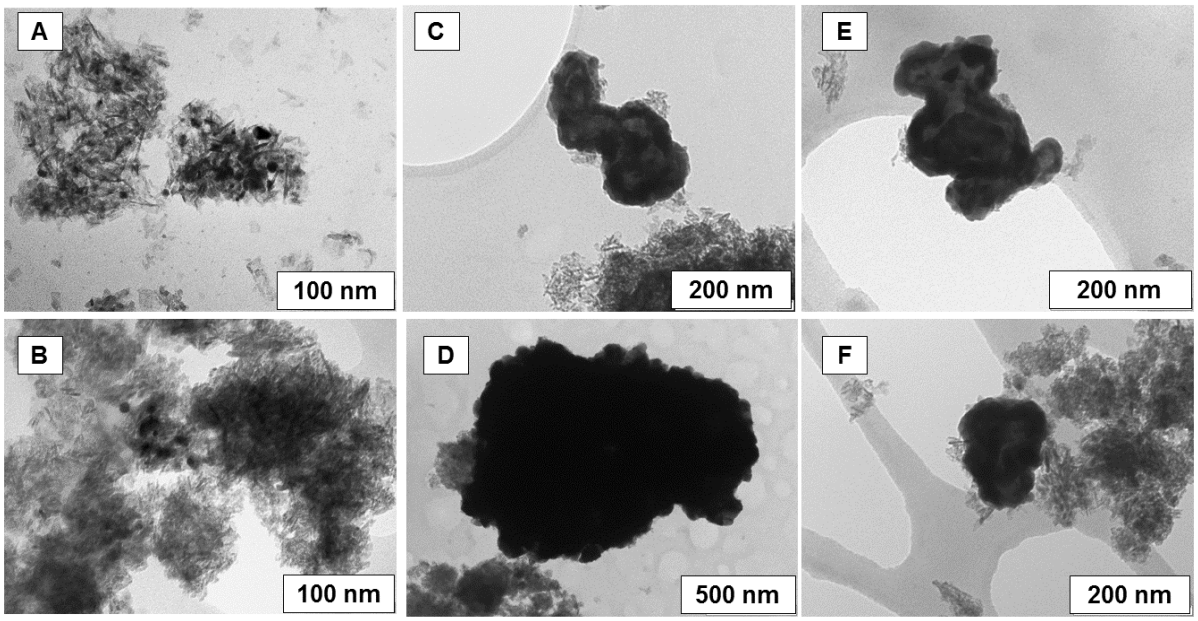

Figure 5.8: TEM images showing agglomeration of Ni on A) 15 NiA, B) 15 NiA-U, C) 15 NiA-P, D) 15 NiA-H, E) 15 NiA-S and F) 15 NiA-SH

Although the mechanism is not entirely understood, sintering possibly occurs via Ostwald ripening, induced by the formation of soluble nickel-phosphorous species, through etching of the Ni active phase by the high concentration of triphenylphosphine in the feed [32]. The dissolved nickel-phosphorous species are then deposited on Ni particles that serve as nucleation sites for the aggregation of the active phase [33]. Despite the larger cluster size observed for the 15 NiA-H sample in Figure 5.8, the 15 NiA-S underwent sintering to a greater extent, since the average particle size diameter was determined to be 22 nm, as presented in Table 5.1. Thus sintering, in addition to poisoning, may have also contributed towards the deactivation of 15 NiA, and the lower catalytic activity recovered after regeneration may be due, in part, to the loss of active metal surface area that was caused by the observed sintering.

5.2.3.2.3 High resolution transmission electron microscopy

The high-resolution transmission electron microscopy images were obtained for the poisoned and regenerated catalysts, and are presented in Figure 5.9. The insets show the images obtained

at a lower magnification, to show the morphology of the active phase on the poisoned and regenerated catalyst. The images showed the presence of crystallised nickel phosphide particles.

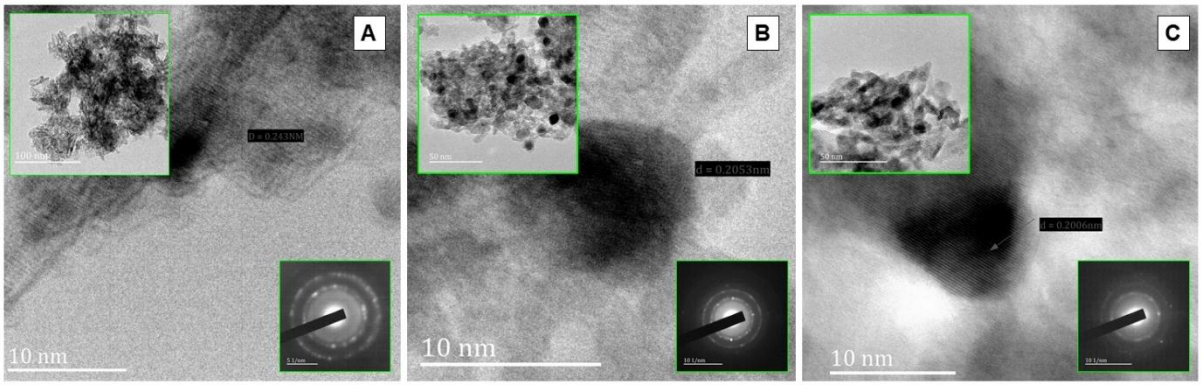

Figure 5.9: HRTEM images and corresponding selected area electron diffraction patterns obtained for A) 15 NiA-P, B) 15 NiA-H and C)15 NiA-SH

The 15 NiA-P catalyst had a lattice spacing of 0.243 nm, which corresponds to the (2 1 0) plane of a phosphorus rich NiP_2 phase [34]. The d-spacing value of 0.2053 nm on the 15 NiA-H catalyst corresponds to the (2 0 1) plane of Ni_2P, while the lattice spacing (0.2006 nm) on 15 NiA-SH corresponds to the (2 1 0) plane of Ni_2P [17, 35, 36]. The selected area electron diffraction patterns have spotty ring structures, which may indicate that the nickel phosphide phase is crystalline [37].

5.2.3.3 Relationship between Ni and P in the poisoned and regenerated catalysts

The selectivity profiles observed during the poisoning of the catalyst (**Zone B**, Figure 5.2) suggests non-selective deposition of phosphorus over both the metallic and support active sites, whereas the phosphorus seemed to migrate to residual nickel sites when the clean feed was reintroduced, resulting in further catalyst deactivation. This suggests a change in the phosphorus distribution on the catalyst surface. Furthermore, elemental analysis showed the retention of phosphorus on the catalyst bed even after regeneration, despite the restoration of activity and octanol selectivity by the octanol wash and the combined regeneration.

To that effect, HAADF STEM-EDX analyses of the regenerated catalysts were conducted to obtain a semi quantitative measure of the phosphorus surface content for the different catalyst samples, with the poisoned catalyst serving as a reference. The line scans and corresponding ratios of the nickel and phosphorus surface concentrations were obtained for 15 NiA-P, 15 NiA-H, 15 NiA-S and 15 NiA-SH and are presented in Figure 5.10. The semi-quantitative

analysis showed a variation in the surface atomic ratios of phosphorus and nickel. The typical P:Ni ratio was found to be 1:2 for 15 NiA-P, whilst it varied for the regenerated catalysts.

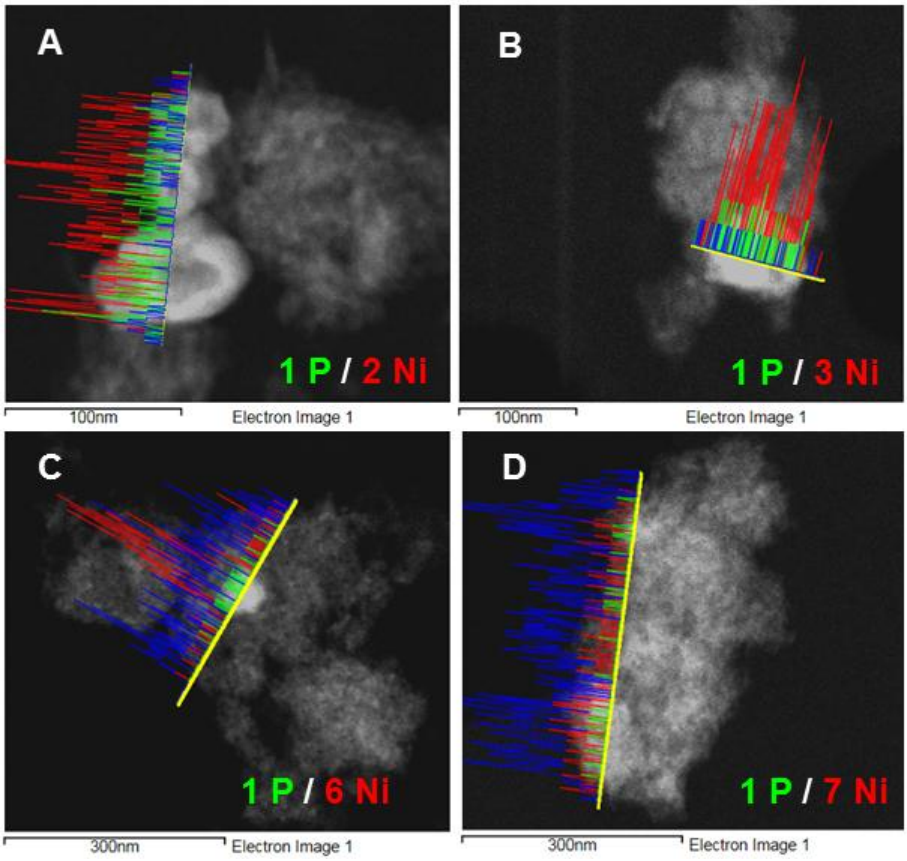

Figure 5.10: Variations in the P/Ni surface ratio of A) 15 NiA-P, B) 15 NiA-H, C)15 NiA-S and D) 15 NiA-SH

The hydrogen regenerated catalyst on average had the highest phosphorus concentration in relation to nickel, whereas the combined regeneration had the lowest. This may explain the observed catalytic activity and octanol selectivity obtained after each regeneration method. After hydrogen regeneration, it was observed that the catalytic activity and octanol selectivity were momentarily recovered, but both the activity and selectivity declined, accompanied by a corresponding increase in the C_{24} acetal selectivity. This was attributed to the secondary poisoning of the catalyst by adsorbed phosphine species on the support, but could also suggest the diffusion of phosphorus from the nickel bulk due to solubility limitations of phosphorus in nickel [27, 32], leading to further poisoning of the catalyst. The higher surface concentration of phosphorus on 15 NiA-H could likely be due to the occurrence of both these mechanisms.

5.3 Deactivation and regeneration of 15 NiSi

In a comparative study, the nickel on silica catalyst (15 NiSi) was poisoned during time on stream hydrogenation of octanal to octanol under the same reaction conditions as those used for the 15 NiA catalyst, and regenerated by hydrogen treatment, octanol washing, and a combined regeneration experiment. The aim was to understand the effects of metal particle size and the interaction between metal and support during poisoning, and the ease of catalyst regeneration.

5.3.1 Influence of TPP as poison on the catalytic activity of 15 NiSi

The activity profile of the 15 NiSi catalyst before, during and after poisoning is presented in Figure 5.11. The catalyst stability was first evaluated for the hydrogenation of clean feed, where the conversion prior to poisoning was 96 % and the octanol selectivity was 87 %, as shown in **Zone A**. The predominant by-product was the C_{16} diol. The introduction of poisoned feed led to a gradual decline in the conversion. Over time, the octanol selectivity increased, and the by-product selectivity decreased slightly. This behaviour of increasing octanol selectivity with decreasing conversion suggests non-selective adsorption of the poison on the catalyst surface. The decrease in by-product selectivity indicates deactivation of the support active sites, in addition to the deactivation of the nickel sites. The conversion stabilises at 20 % since some Ni sites remain active, possibly due to the steric hindrance of the TPP molecule.

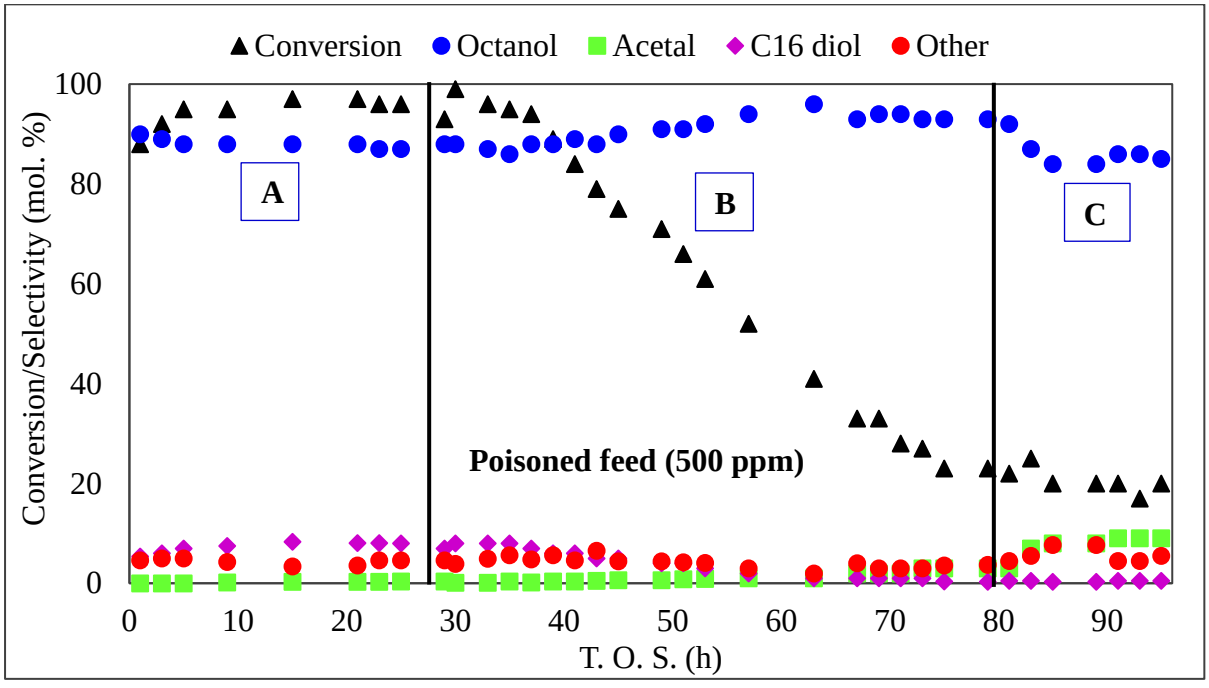

Figure 5.11: Activity profile before (**Zone A**), during (**Zone B**) and after exposure of the 15 NiSi catalyst to poisoned feed (**Zone C**)

The reintroduction of clean feed (**Zone C**), after the poisoning experiment, did not reverse the loss of activity. There was a slight increase in the by-product selectivity, accompanied by a corresponding decline in the selectivity towards octanol, suggesting the cleaning of active sites on the support and transport of adsorbed phosphorus species from the support onto nickel sites. The conversion did not decline further after the reintroduction of clean feed, and the decrease in octanol selectivity was not as pronounced as that observed for the alumina supported catalyst (cf. Figure 5.2, **Zone C**).

5.3.2 Regeneration of 15 NiSi

Regeneration experiments were performed similarly to the 15 NiA experiments. The regeneration of the 15 NiSi catalyst was performed in order to observe the differences in the catalytic activity recovery in comparison to 15 NiA, as well as to relate how the characteristics of each of the supports, such as acidity and the strength of the metal support interaction, influenced the extent of the recovery of the catalytic activity.

5.3.2.1 Regeneration with hydrogen

From Figure 5.12, the percentage recovery achieved after hydrogen regeneration was low. Furthermore, the octanol selectivity gradually declined from 86 % to 73 % over a period of ten hours, while the C_{24} acetal selectivity slightly increased to 17 %.

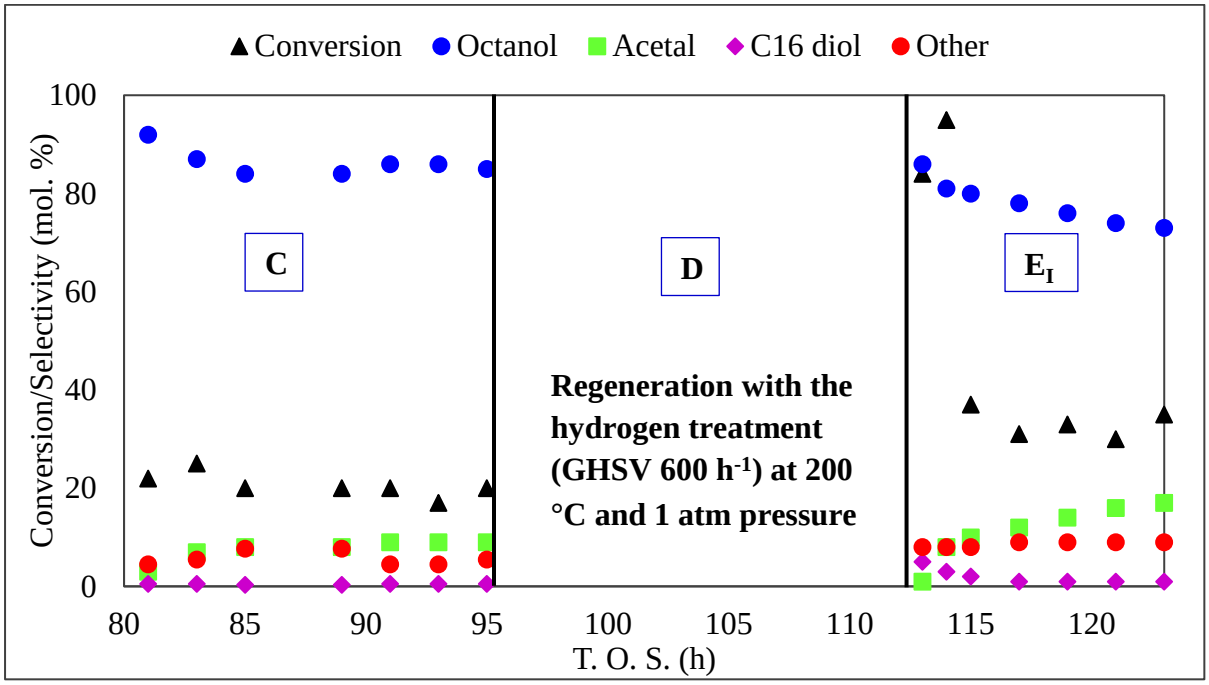

Figure 5.12: Activity profile of 15 NiSi before and after regeneration with hydrogen: (**C**) clean feed before regeneration, (**D**) regeneration step, (**E**$_{\mathbf{I}}$) clean feed after regeneration

The octanol selectivity, after regeneration with the hydrogen treatment, was slightly lower than the selectivity that was displayed by the catalyst before regeneration, suggesting loss of nickel sites after regeneration. The loss is possibly due to the transport of phosphorus from the support onto cleaned nickel sites, which indicates that the hydrogen regeneration was not very effective in removing phosphorus species from the support.

5.3.2.2 Regeneration with octanol

The results for the activity and selectivity over 15 NiSi, after solvent regeneration, are presented in Figure 5.13. The recovered activity using the octanol wash was much higher compared to the results obtained with the hydrogen regeneration. The octanol selectivity did not decrease after regeneration, and was similar to that observed prior to deactivation. The conversion was recovered to a significant extent, from 19 % to a value of 63 %.

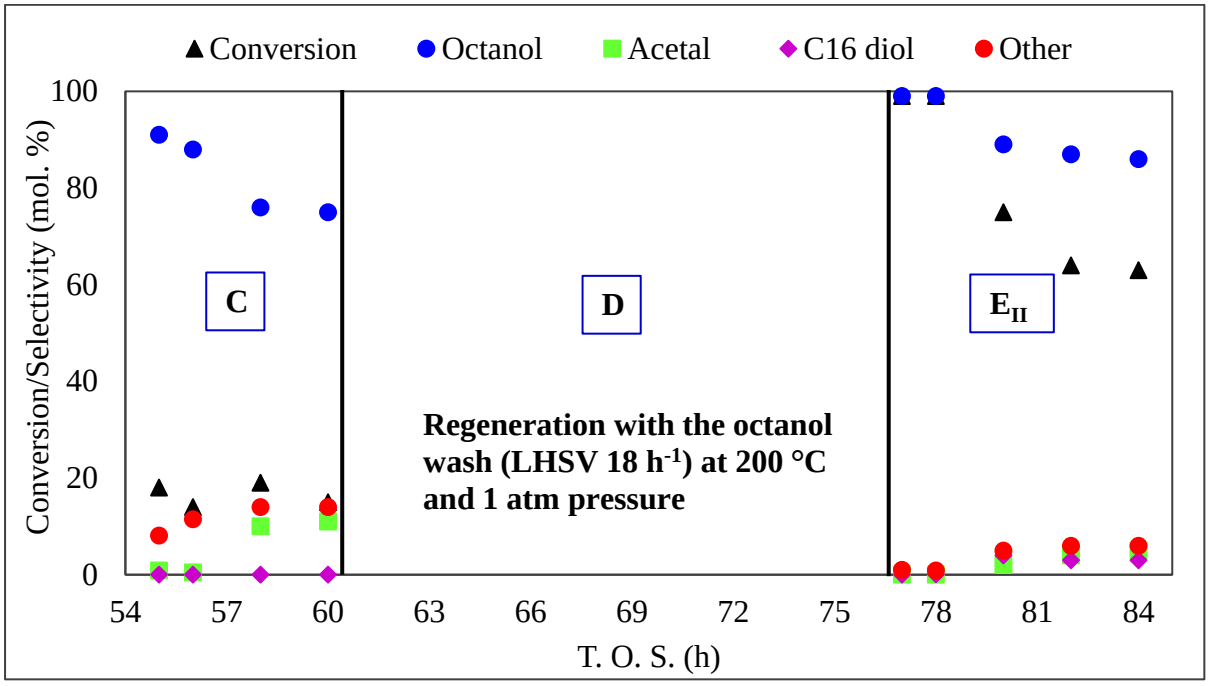

Figure 5.13: Activity profile of 15 NiSi before and after regeneration with octanol: (**C**) clean feed before regeneration, (**D**) regeneration step, (**E**$_{II}$) clean feed after regeneration

The combined regeneration was attempted to establish if the conversion could be further improved when compared to the solvent only washing procedure, as well as to determine whether the solvent and hydrogen regeneration have a synergistic effect when performed sequentially for the regeneration of 15 NiSi.

5.3.2.3 Combination of solvent washing and hydrogen treatment

The combined regeneration experiment resulted in an improved recovery of the catalytic activity. This can be observed in **Zone E_{III}**, Figure 5.14. The octanol selectivity of the regenerated catalyst was similar to that of the non-poisoned catalyst (cf. Figure 5.11, **Zone A**). Although the conversion of the regenerated catalyst was still lower than the conversion of the non-poisoned catalyst, it was higher than when just the solvent washing was used. Thus, by using the combined regeneration method, the octanol selectivity was almost fully recovered. The correspondingly low C_{24} acetal selectivity suggests that the support does not react with the phosphorus to form more, or stronger acidic sites, while the stable octanol selectivity indicates that the catalyst does not undergo secondary poisoning.

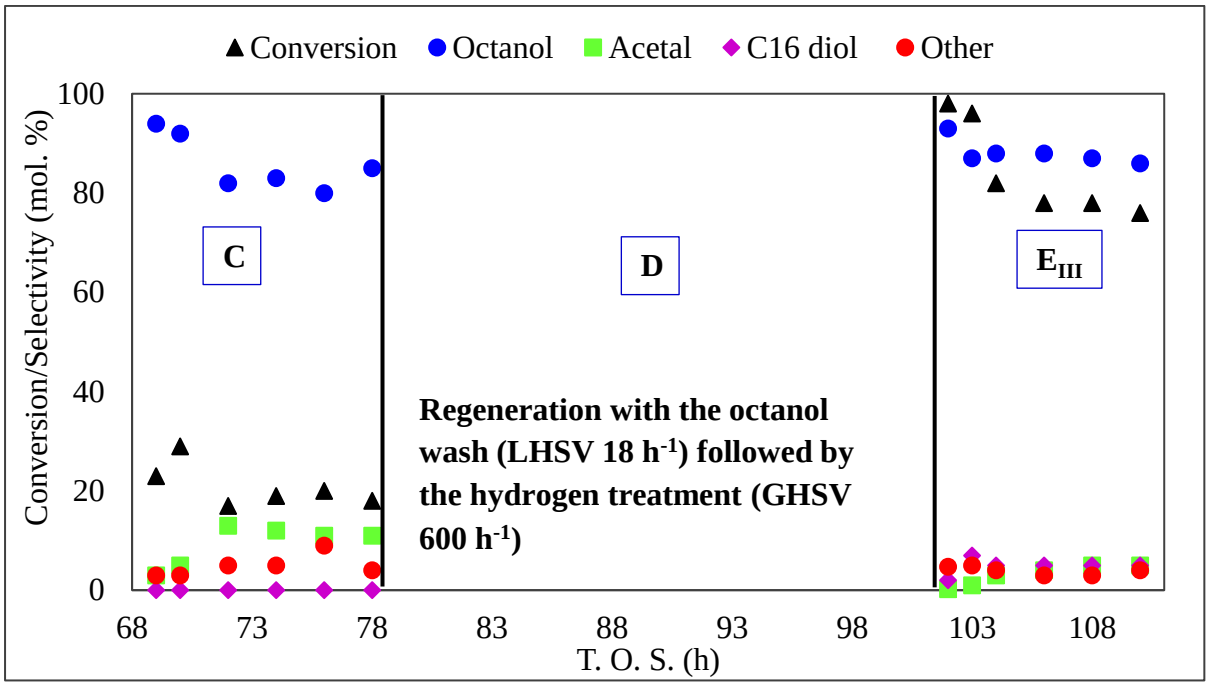

Figure 5.14: Activity profile of 15 NiSi before and after regeneration with octanol and hydrogen: (**C**) clean feed before regeneration, (**D**) regeneration step, (**E_{III}**) clean feed after regeneration

5.3.3 Characterisation of the poisoned and regenerated 15 NiSi catalyst

The effects of phosphorus on the structural properties of the catalysts were investigated by employing various characterisation techniques. The properties of the used catalysts (poisoned and regenerated) are discussed further.

5.3.3.1 Physicochemical properties

Phosphorus and nickel on the used catalysts were quantified using ICP-OES to establish if any loss of the active phase occurred, via leaching, as well as to investigate the effectiveness of each regeneration experiment in the removal of phosphorus. From the amounts of nickel and phosphorus shown in Table 5.2, it was concluded that no loss of nickel occurred via leaching. Additionally, the phosphorus content of the regenerated catalyst samples similar to that of the poisoned catalyst. This suggests that regeneration was not effective in removing phosphorus from the catalysts. Analysis of the octanol washings from the regeneration experiment by ICP-OES also did not show any traces of phosphorus, which suggests the retention of phosphorus despite regeneration.

Table 5.2: Ni and P compositions and physicochemical properties of the fresh, used and poisoned 15 NiSi catalyst samples

Sample	**Description**	**Ni (wt.%)**	**P (wt.%)**	**BET Surface area (m^2 g^{-1})**	**Average Ni particle size[a]**
15 NiSi	Fresh	14.7	-	99	65
15 NiSi-U	Used, non-poisoned	14.8	-	77	40
15 NiSi-P	Poisoned	14.8	2.7	77	71
15 NiSi-H	Hydrogen treatment regeneration	14.9	2.8	79	64
15 NiSi-S	Octanol wash regeneration	14.8	2.5	88	72
15 NiSi-SH	Combined regeneration	14.9	2.5	87	65

[a]determined from TEM

In addition, results from surface area analyses showed that the BET surface areas of the used catalysts did not decline to a significant extent, suggesting a minimum adsorption of carbonaceous species on the catalyst surface. Thermal analysis of the used catalysts showed that the catalysts experienced two major weight losses, and the results are presented in Figure A4 (Appendix). The first weight loss of about 2 % occurred around 100 °C, and was attributed

to the desorption of physisorbed water. The second weight loss occurs around 300 °C, and was attributed to the combustion of adsorbed carbonaceous species. The catalysts also underwent a weight gain around 350 °C, attributed to the possible oxidation of the metallic nickel and/or the Ni_xP_y phase.

5.3.3.2 Structural analysis of 15 NiSi

The influence of the poison on the catalyst properties was investigated further by characterisation to probe the effects of the poison on the structural and bulk phase composition of the catalyst. The 15 NiSi catalyst samples underwent similar characterisation to the 15 NiA catalyst.

5.3.3.2.1 Powder X-ray diffraction and magnetic measurements

The powder X-ray diffraction analyses of the reduced 15 NiSi catalyst, the poisoned, and regenerated catalysts were performed to observe phase changes induced by the exposure of the catalyst to the phosphorus poison. From the results presented in Figure 5.15, there is a distinct difference between the XRD pattern of the reduced 15 NiSi catalyst and the poisoned catalyst. The XRD pattern of the reduced 15 NiSi catalyst shows peaks at 2θ values of 45°, 52° and 77° that correspond to Ni crystalline phases with (1 1 1), (2 0 0) and (2 2 0) planes (JCPDS file 04-0850) [38, 39], while there is also a peak at 36° that corresponds to the presence of NiO (1 1 1) plane (JCPDS file 78-0429) due to passivation [39].

The peaks corresponding to the (2 0 0) and (2 2 0) Ni^0 planes are significantly diminished for the poisoned and regenerated catalysts, while the overall peak intensity has decreased, indicating a reduction in the amount of Ni^0. Furthermore, XRD patterns corresponding to the Ni_2P phase (JCPDS file 65-1989) are seen [28, 29, 40]. The Ni_2P planes present for the poisoned and regenerated catalysts correspond to the (1 1 1), (2 0 1), (2 1 0) and (3 0 0) crystal phases at 2θ values of 43°, 45°, 48°, and 56.5° respectively. The presence of the peaks corresponding to the Ni^0 phase on the regenerated catalyst XRD diffractograms indicates the existence of some metallic Ni, albeit in small amounts [17, 36]. This suggests that there is a reaction of the supported nickel particles with phosphorus, forming a nickel phosphide phase. However, not all of nickel reacts with phosphorus. According to Wang *et al.* [41], larger Ni particles do not completely react with phosphorus. Hence, the presence of metallic Ni is attributed to the incomplete reaction of large Ni particles with phosphorus.

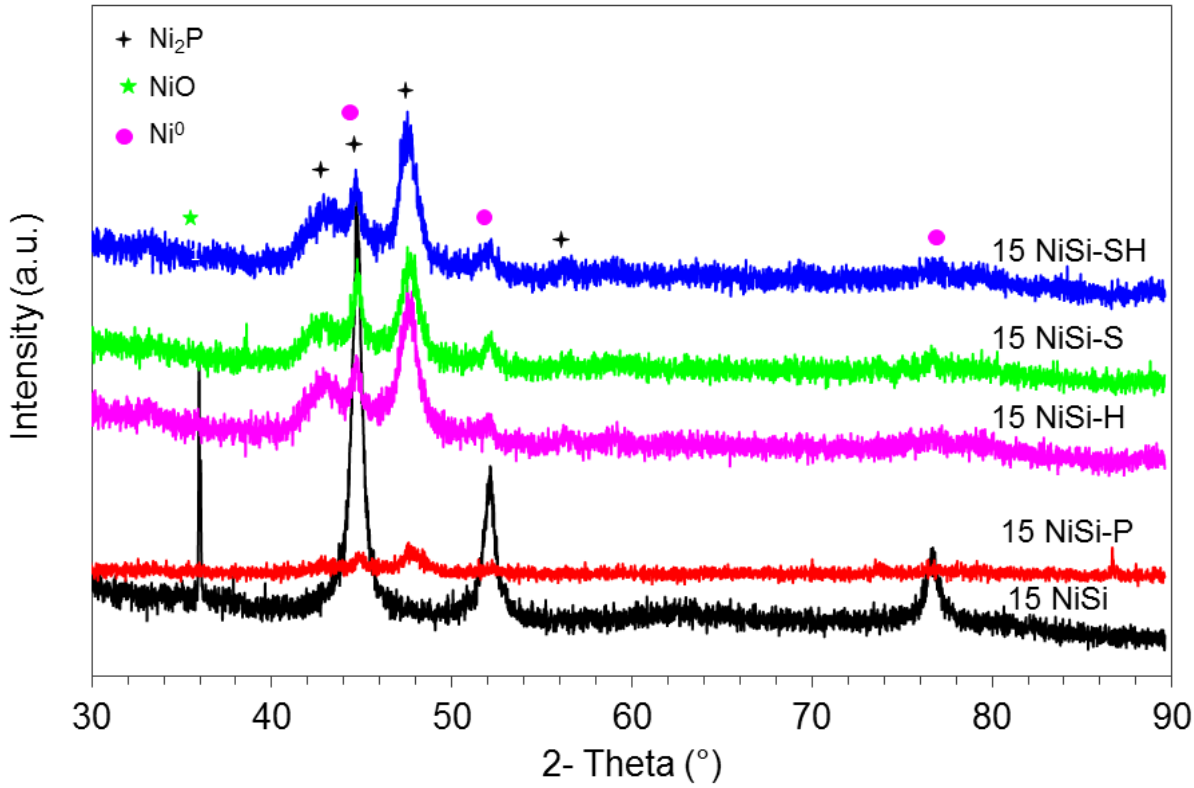

Figure 5.15: XRD patterns of the reduced 15 NiSi catalyst, 15 NiSi-P, and the 15 NiSi catalysts after undergoing regeneration experiments [28, 29, 42]

Magnetic properties of the reduced 15 NiSi and poisoned catalysts were obtained using a Vibrating Sample Magnetometer. The saturation magnetization decreased for the poisoned and regenerated catalysts, similar to the behaviour observed for the 15 NiA catalysts, indicating an interaction between Ni and P. The saturation magnetization of the non-poisoned catalyst was 2.3 emu/g, while it was 1.8 emu/g, 1.2 emu/g, 1.6 emu/g and 1.5 emu/g for 15 NiSi-P, 15 NiSi-H, 15 NiSi-S and 15 NiSi-SH respectively. The catalysts did not lose their ferromagnetic character, which suggests that not all nickel reacts with phosphorus. This is in agreement with data from XRD as shown in Figure 5.15.

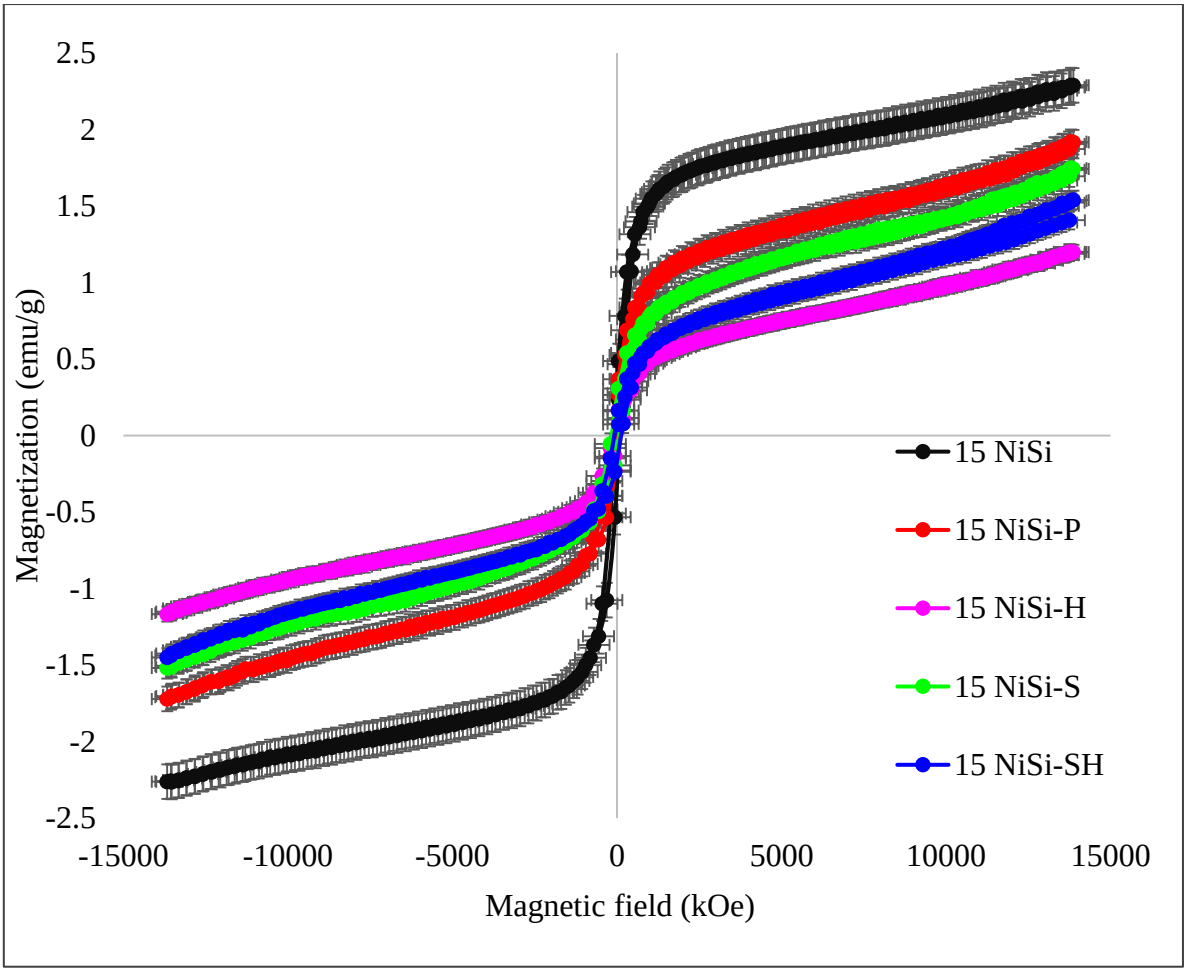

Figure 5.16: Magnetic hysteresis loops on 15 NiSi, 15 NiSi-P, 15 NiSi-H, 15 NiSi-S and 15 NiSi-SH at room temperature

5.3.3.2.2 Transmission electron microscopy

Transmission electron microscope images are presented in Figure 5.17. The average Ni particle size was determined to be around 40 nm for 15 NiSi-U, 65 nm for 15 NiSi, 15 NiSi-H and 15 NiSi-SH, 71 nm for 15 NiSi-P and 72 nm for 15 NiSi-S. The particle sizes of 15 NiSi were larger than the 15 NiSi-U sample, likely because the latter was reduced. The Ni particles for 15 NiSi-P and 15 NiSi-S have an amorphous appearance, and the morphology of the particles is not clearly defined. The sintering of the active phase is also more apparent on the 15 NiSi-S sample, as observed from the larger average particle size observed for this sample in Figure 5.17 E, and Table 5.2.

The lower conversion observed for 15 NiSi-S after regeneration is attributed to the loss of active nickel surface due to the agglomeration of the active phase. This results in a lower number of catalytically active sites that are available for the conversion of octanal to octanol.

The agglomeration is possibly induced by the solvent, via Ostwald ripening. On the other hand, agglomeration was not observed for the 15 NiSi-SH catalyst due to the second stage regeneration being performed under the flow of hydrogen gas. Heating the catalyst under a flow of hydrogen may have induced an annealing process that resulted in the crystallization of the Ni_2P phase [17, 27]. This has also been observed by Chen *et al*. [17], who reported the crystallization of nickel phosphide nanoparticles by heating at 300 °C under a flow of hydrogen.

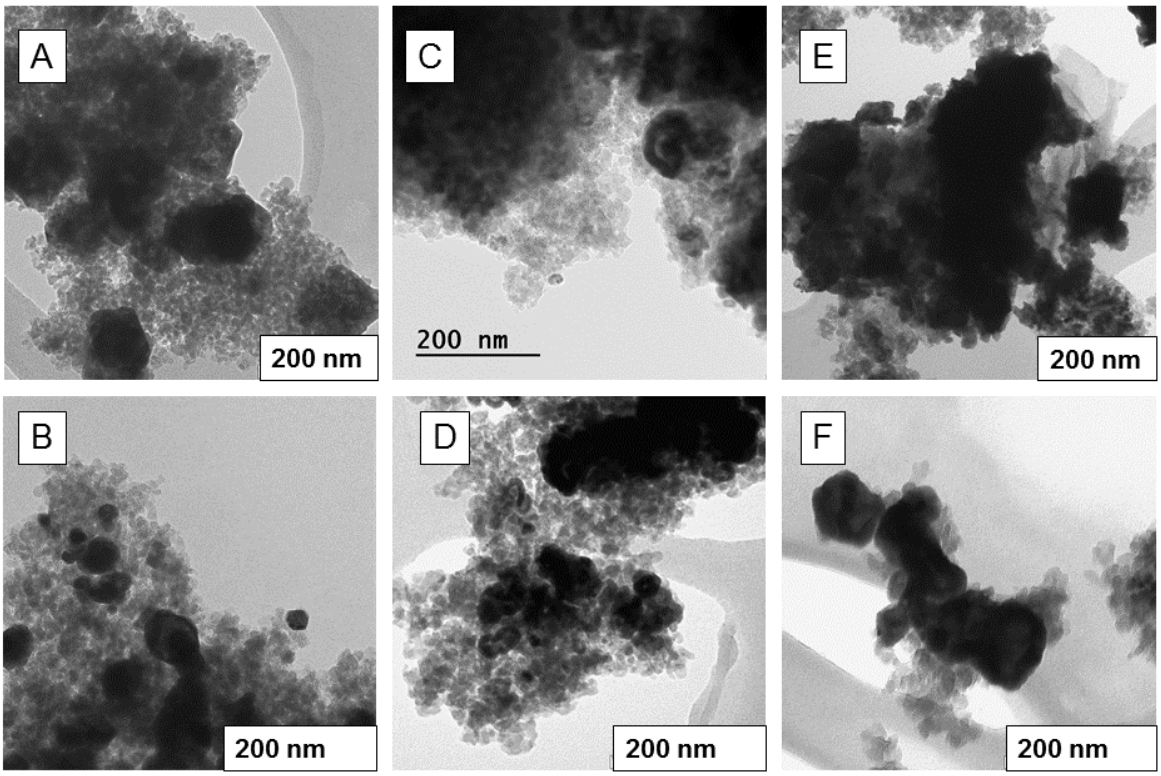

Figure 5.17: TEM images obtained for A) 15 NiSi, B) 15 NiSi-U, C) 15 NiSi-P, D) 15 NiSi-H, E) 15 NiSi-S and F) 15 NiSi-SH

The crystallization of Ni_2P is favoured by the hydrogen atmosphere, which enables the reduction of triphenylphosphine via hydrogenolysis to a more reactive form such as phosphine, that reacts easier with the nickel to form the Ni_2P crystalline phase [23]. According to Chen *et al.* [17], the use of nitrogen gas was not as effective in the formation of crystalline Ni_2P, but it is possible [17, 23, 43].

5.3.3.2.3 High resolution transmission electron microscopy

High resolution transmission electron microscopy images, presented in Figure 5.18 A-C, were obtained for 15 NiSi-H, 15 NiSi-S and 15 NiSi-SH catalysts. The insets show the morphology

of the catalyst particles at lower magnifications. Selected area electron diffraction patterns were also obtained to determine the crystallinity of the Ni_2P phase present in the catalysts. Measurements of the lattice fringes observed corresponded to the *d*-spacing values of nickel phosphide phases.

The *d*-spacing value on the 15 NiSi-H catalyst (Figure 5.18 A) was determined to be 0.25 nm, corresponding to the (0 0 2) crystallographic plane of $Ni_{12}P_5$ [44]. The $Ni_{12}P_5$ phase sometimes co-exists with Ni_2P, and is sometimes a precursor for Ni_2P, which forms with heating at higher temperatures [45]. The 15 NiSi-S (Figure 5.18 B) and 15 NiSi-SH (Figure 5.18 C) catalysts have *d*-spacing values of 0.19 nm each, corresponding to the (2 1 0) crystallographic plane of the Ni_2P phase [17, 29, 46]. The selected area electron diffraction pattern of 15 NiSi-H and 15 NiSi-S indicate that these two samples are mostly amorphous, although the spots on the 15 NiSi-S suggest that the catalyst may also possess some isolated crystalline phases. The pattern for15 NiSi-SH has a spotty ring structure, indicating that the Ni_2P phase is crystalline [37, 47].

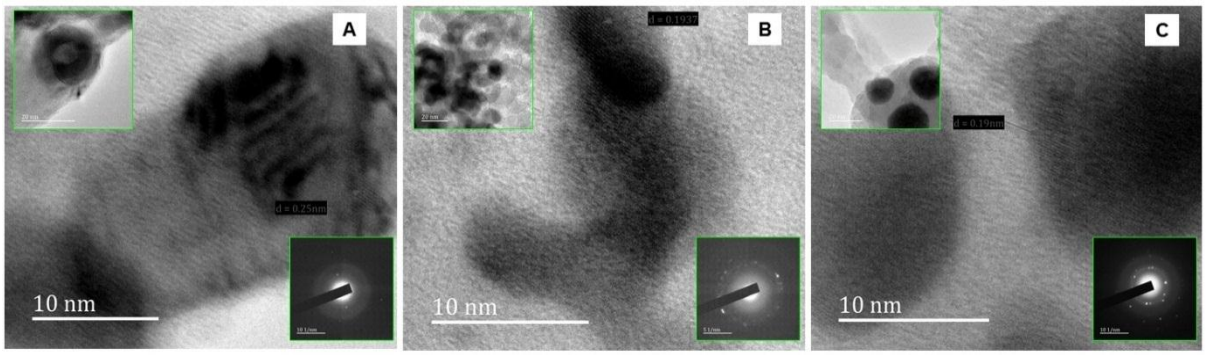

Figure 5.18: HRTEM images and selected area diffraction patters obtained for A)15 NiSi-H, B)15 NiSi-S and C) 15 NiSi-SH

Both the 15 NiSi-H and 15 NiSi-SH catalysts have more defined Ni_2P particles compared to the 15 NiSi-S catalyst. This is due to the hydrogen treatment at high temperatures inducing an annealing effect on the amorphous Ni_2P phase, resulting in well-formed crystalline particles [17, 27, 48, 49]. From Figure 5.18 A, the 15 NiSi-H catalyst appears to have regularly shaped nickel phosphide particles, while in Figure 5.18 B (and inset image), the Ni_2P particles for the 15 NiSi-S catalyst seem to be amorphous and appear clustered together. However, some of the particles are crystalline, since lattice fringes were observed in some regions of the samples [28]. The Ni_2P particles for the 15 NiSi-SH catalyst (Figure 5.18 C) also appear to have a regular, spherical shape.

5.3.3.4 Relationship between Ni and P in the poisoned and regenerated catalysts

From the regeneration experiments, it was established that the hydrogen treatment was not effective in recovering the catalytic activity and octanol selectivity, and displayed a higher C_{24} acetal selectivity, suggesting an increase in the catalyst's Brønsted acidity. On the other hand, the solvent wash regeneration and the combined regeneration were more effective in recovering activity and the octanol selectivity. The increase in acidity brought about by the exposure of the catalyst to phosphorus was reversed by these two regeneration experiments. To that effect, the relationship between nickel and phosphorus in the poisoned and regenerated catalysts was established using SEM-EDX and STEM-EDX to observe any differences in the surface distribution of Ni and P on the surface of the regenerated catalysts.

5.3.3.4.1 Scanning electron microscopy-electron dispersive X-ray spectroscopy

The SEM BSE-EDX maps, presented in Figure 5.19, show phosphorus to be mostly associated with nickel for both the poisoned and regenerated catalysts.

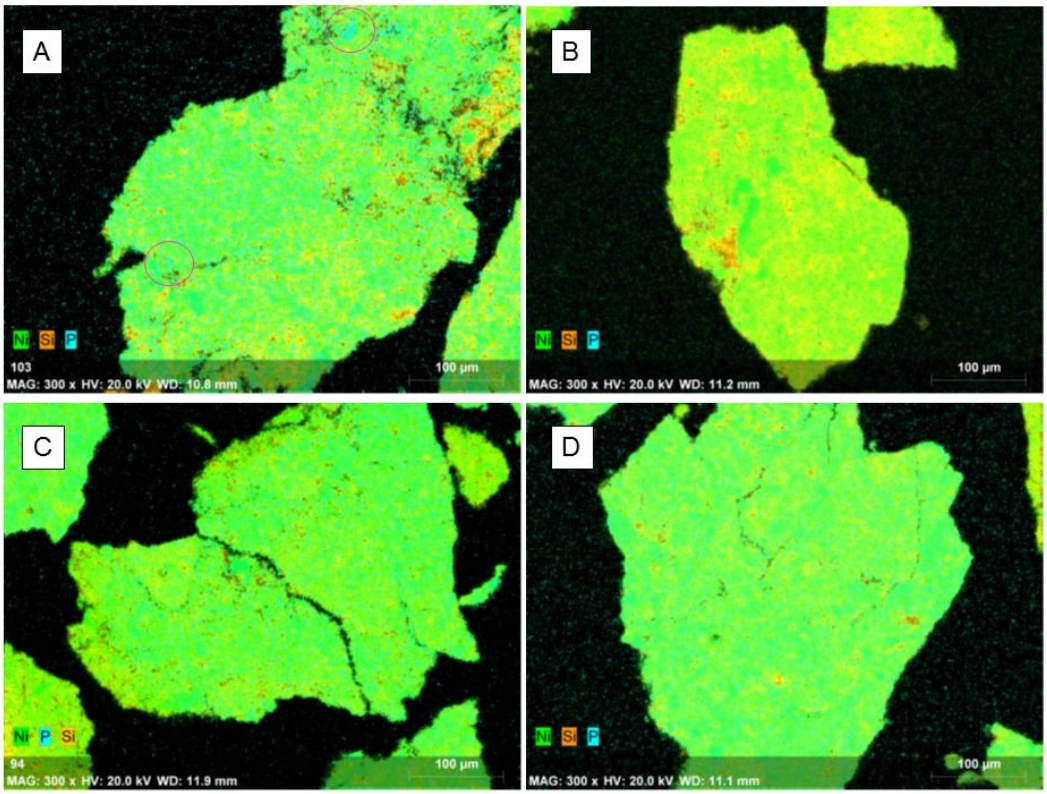

Figure 5.19: SEM-EDX element maps showing the relationship between Ni and P on A) 15 NiSi-P, B) 15 NiSi-H, C) 15 NiSi-S and D) 15 NiSi-SH

For the poisoned catalyst, the blue colour, which represents the phosphorus map, is quite distinctive in certain areas of the 15 NiSi-P element map, while for the regenerated catalysts,

the colour is homogenised with green, which is the colour indicating nickel on the element map. From the maps, there is no indication of an interaction between phosphorus and the silica support, since there are distinct unoccupied areas of silica. The individual element maps are shown in Figure A15-A18 (Appendix).

5.3.3.4.2 Scanning transmission electron microscopy

STEM-EDX analysis show a variable P:Ni surface ratio of the poisoned and regenerated catalysts, as presented in Figure 5.20. The poisoned catalyst has a higher surface composition of phosphorus, and the Ni: P ratio was determined to be 2:1. The hydrogen regenerated catalyst had a variable nickel-phosphorus composition, whose average ratio of P:Ni was 1:3. The 15 NiSi-S and 15 NiSi-SH had similar average phosphorus surface compositions, with P:Ni surface ratios of 1:4.

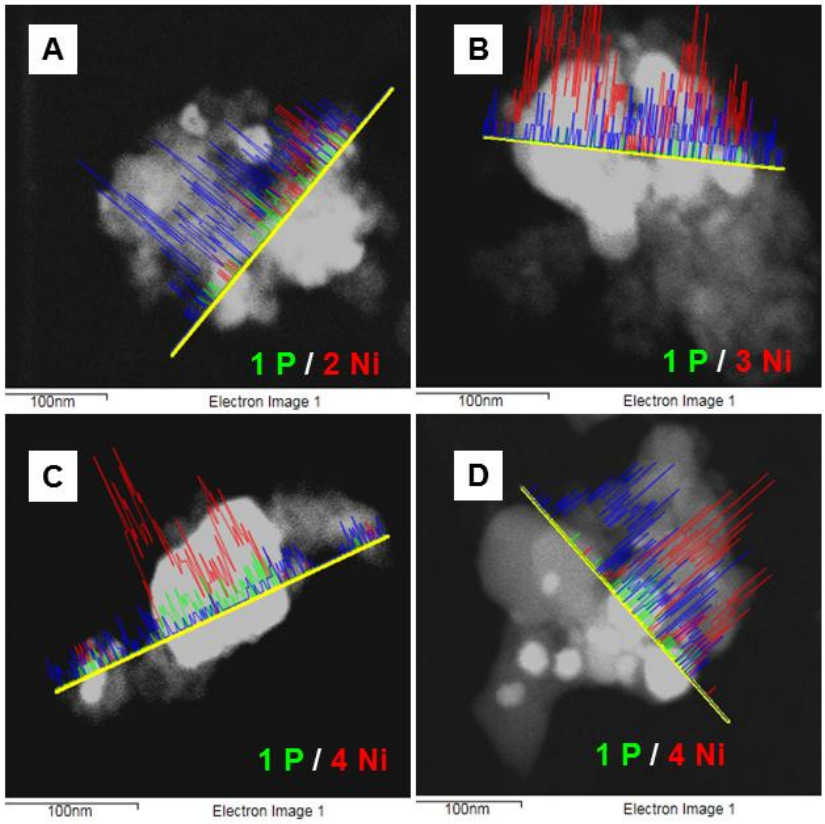

Figure 5.20: Variations in the P/Ni surface ratio of A) 15 NiSi-P, B)15 NiA-H and C) 15 NiSi-S and D) 15 NiSi-SH

5.4 Comparison between 15 NiA and 15 NiSi

Characterisation showed that the dispersion of nickel was higher on the alumina support compared to the silica support, which was attributed to the stronger interaction between the

alumina support and nickel, while the weaker MSI of nickel on silica resulted in a poor metal dispersion, and, hence, larger nickel clusters on the silica support. The silica supported catalyst was found to have a higher degree of reduction compared to the alumina supported catalyst, as shown by chemisorption analysis results in Table 4.2. The catalytic data and characterisation results indicated a difference in the interaction of triphenylphosphine with each of the two catalysts.

5.4.1 Relationship between the catalysts and triphenylphosphine

The adsorption of triphenylphosphine on both catalysts was found to be non-selective, since poisoning only affected the catalytic conversion, while the octanol selectivity remained unaffected [13]. Phosphorus has been observed to adsorb on both the active metal and support by McCue *et al.* [50], while Baltusis *et al.* report the weak adsorption of phosphorus species such as trimethylphosphine and phosphates on the Lewis and Brønsted acidic sites of alumina [51]. Sawhill *et al.* [52] have reported the weak adsorption of phosphorus species on silica which, however, only pertained to interaction between silica and phosphate species, and does not mention triphenylphosphine. Catalytic results indicated that the adsorption of triphenylphosphine occurred on both the Ni sites, responsible for hydrogenation, and the active sites of the support which were responsible for the formation of by-products.

Triphenylphosphine adsorbs dissociatively on nickel at low coverages, but physisorbs non-dissociatively on both nickel and the support at higher coverages, leading to multilayer coverage over time [30, 53-55]. Dissociation of the phosphines proceeds via the Ni catalysed P-C bond cleavage, which could occur via hydrogenolysis in the presence of hydrogen [17]. The liberated phosphorus reacts with surface nickel atoms to form an amorphous nickel phosphide phase, which is reported to be catalytically inactive for the adsorption and dissociation of molecular hydrogen [17, 56, 57]. However, crystalline nickel phosphide has been shown to be catalytically active for hydrodesulphurization [52, 58, 59] and hydrodeoxygenation [60, 61] reactions.

The interaction between the catalyst and the poison differs for each support. For instance, alumina is reported to interact strongly with phosphorus, leading to the formation of acidic $AlPO_4$ on the surface of the support. This has been found by Li *et al.*, [62] who reported that doping of an alumina supported nickel catalyst resulted in an increase in the concentration of acid sites on the catalyst. The FTIR spectra obtained for the poisoned and regenerated 15 NiA catalyst also indicated the possible presence of $AlPO_4$ due to the appearance of broad bands in

the spectra of these catalysts, which are centred in the IR region that is attributed to the stretching vibrations of a P-O species [18]. The postulated interaction between the 15 NiA catalyst and triphenylphosphine is presented in Scheme 5.4. The reaction between alumina and phosphorus contributed to the high C_{24} acetal selectivity observed for the 15 NiA catalyst even after regeneration.

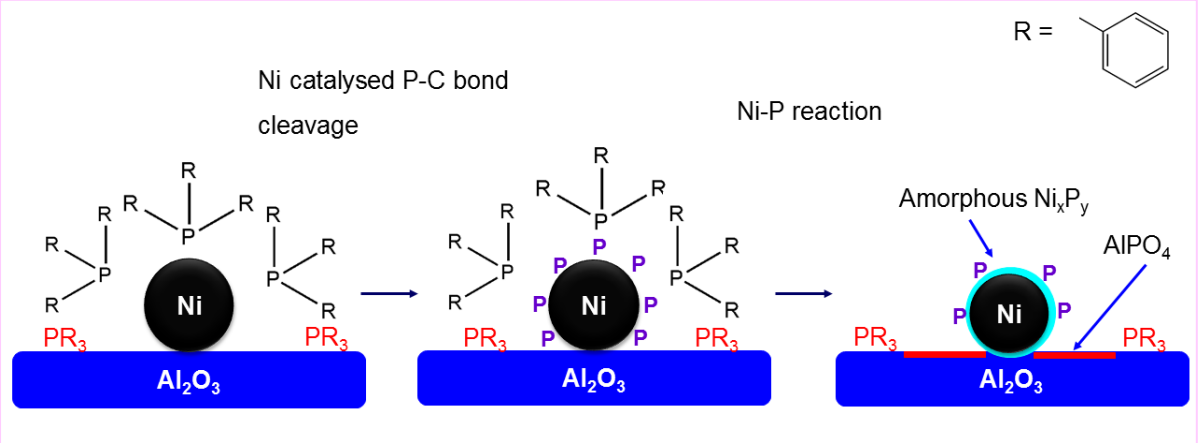

Scheme 5.4: Proposed interaction of triphenylphosphine with nickel particles and the 15 NiA catalyst

For the silica supported catalyst, phosphorus is weakly adsorbed on the support surface and does not react with the support. However, the phosphorus may undergo oxidation by water, resulting in the formation of oxidised species weakly adsorbed on the support [20, 63]. These oxidised species may be weakly acidic [63], contributing to the acetal formation observed in Figure 5.11, **Zone C**. The proposed interaction between the poison and the silica supported catalyst is presented in Scheme 5.5.

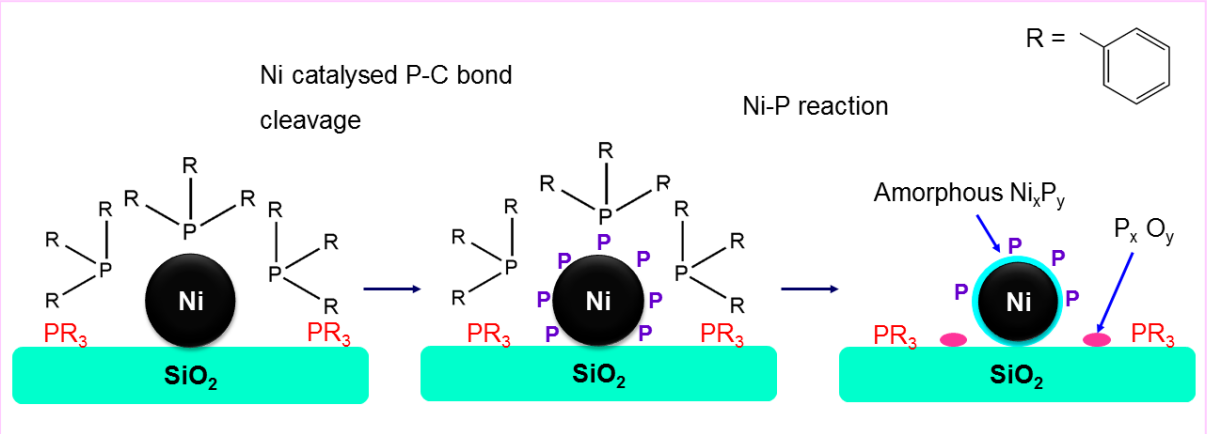

Scheme 5.5: Proposed interaction of triphenylphosphine with nickel particles and the 15 NiSi catalyst

An important observation is the change in the behaviour of triphenylphosphine during adsorption, and after interacting with nickel under reducing conditions. Initially, triphenylphosphine is a non-selective poison that uniformly deactivates the catalyst. However, on contact with the catalyst, triphenylphosphine is converted to reduced species that selectively deactivate nickel active sites, while increasing the selectivity of by-products [64]. This is more pronounced for the 15 NiA catalyst, as observed from Figure 5.2, **Zone C**. The conversion of triphenylphosphine was indicated by the presence of unidentified products in the GC chromatographs of the product streams and octanol washings (Figure A22-A26), which were possibly formed from the decomposition of TPP on contact with nickel.

5.4.2 Comparison of 15 NiA and 15 NiSi

Exposure of both catalysts to feed contaminated with triphenylphosphine led to a decline in their catalytic activity. The 15 NiA catalyst required 38 hours to deactivate on stream, while the 15 NiSi catalyst required 50 hours for its activity to decline to the same extent as the 15 NiA catalyst. The flow of the poisoned feed into the reactor was stopped when triphenylphosphine was detected by GC-FID in the product streams.

Both catalysts were regenerated under similar conditions. All regeneration experiments recovered catalytic activity to varying degrees. Figure 5.21 provides a comparison of the steady state activity and selectivity of 15 NiA and 15 NiSi after regeneration with the hydrogen treatment. The hydrogen treatment regeneration experiment recovered the least activity and octanol selectivity, while the combined regeneration was the most effective, since it resulted in the highest recovery of the catalytic activity and octanol selectivity. The effectiveness of each regeneration experiment also varied for each of the supports used. The regeneration of 15 NiA with the hydrogen treatment did not recover the octanol selectivity, which, instead, decreased to 24 %, while the C_{24} acetal selectivity increased to 69 %. Although the regeneration of 15 NiSi with the hydrogen treatment resulted in a conversion lower than that of 15 NiA, octanol still remained the primary product, with a selectivity of 73 %, whilst the C_{24} acetal selectivity was 17 %.

Figure 5.22 provides a comparison of the steady state activity and selectivity of 15 NiA and 15 NiSi after regeneration with the octanol wash. Regenerating the catalysts by washing with octanol led to an improvement in the recovered activity. For 15 NiA, the octanol selectivity achieved with this technique was an improvement, compared to that achieved with the hydrogen treatment. The octanol selectivity after regeneration was 61 %, while the acetal

selectivity was 33 %. The conversion was also slightly higher, with the steady state conversion being 55 %. The recovered conversion and selectivity were also improved by the octanol wash for 15 NiSi. The steady state conversion was 63 %, while the octanol selectivity was 86 %, which was similar to the octanol selectivity of the non-poisoned catalyst.

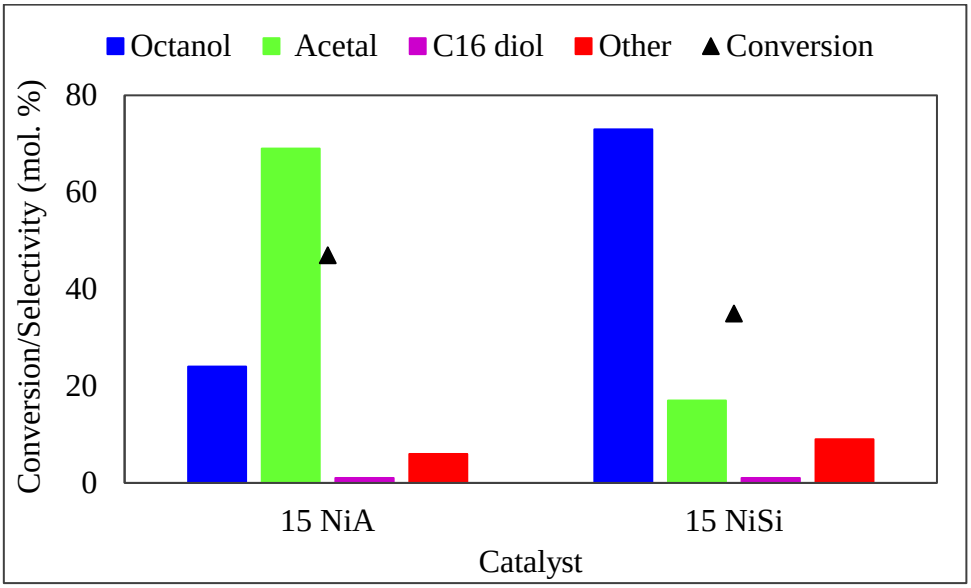

Figure 5.21: Comparison of the steady state conversion and selectivity recovered using the hydrogen treatment regeneration for the 15 NiA and 15 NiSi catalysts

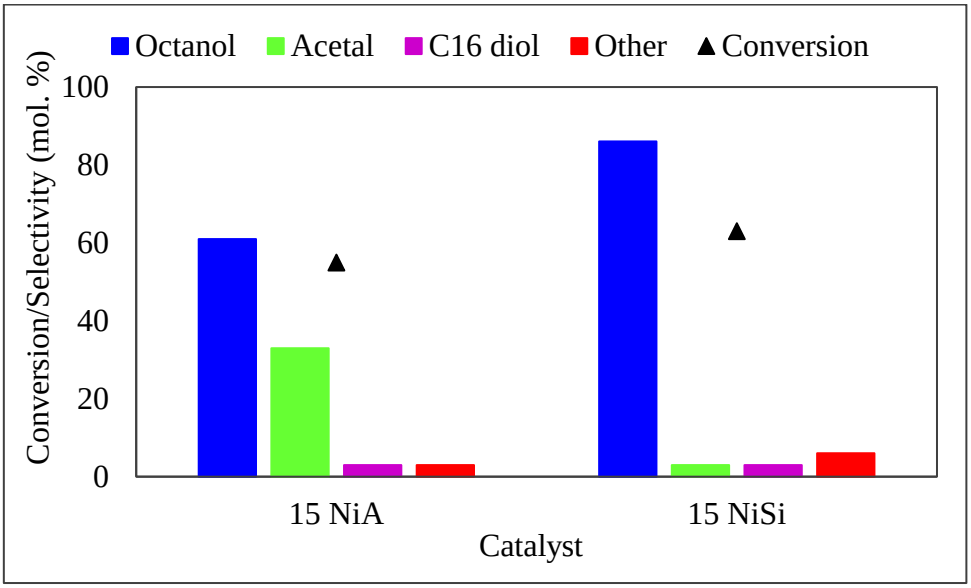

Figure 5.22: Comparison of the steady state conversion and selectivity recovered using the solvent wash regeneration for the 15 NiA and 15 NiSi catalysts

The combined regeneration was found to be the most effective for both catalyst systems, as shown in Figure 5.23. For 15 NiA, the conversion recovered was similar to that recovered with the octanol wash (54 %), while there was an improvement in the recovery of the octanol selectivity, which was 77 %. For 15 NiSi, the octanol selectivity was 86 %, which is similar to that obtained with the octanol wash, while there was an improvement in the conversion (76 %), compared to that obtained with the octanol wash, which was 63 %.

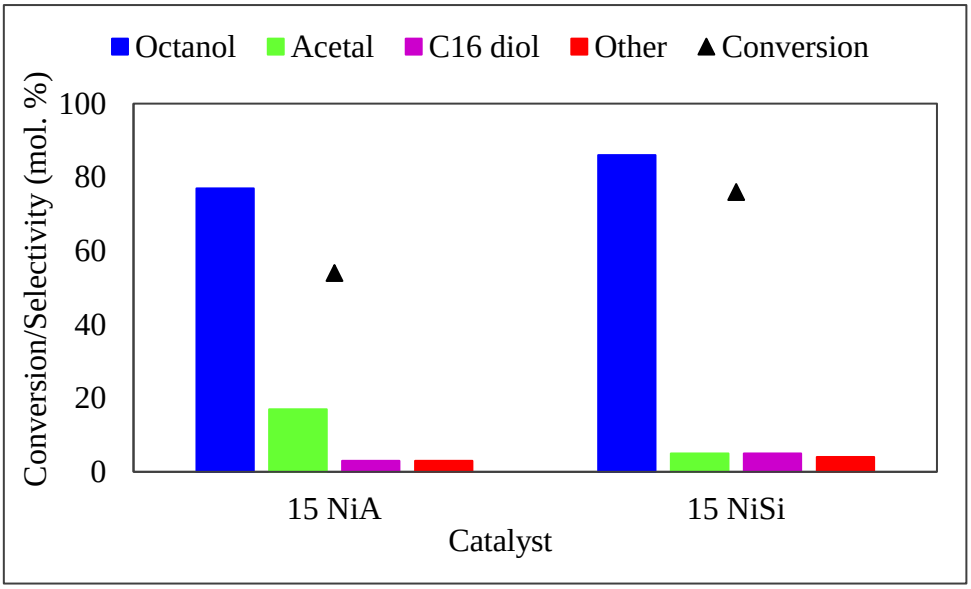

Figure 5.23: Comparison of the steady state conversion and selectivity recovered using the combined regeneration for the 15 NiA and 15 NiSi catalysts

The activity of the non-poisoned 15 NiA catalyst and the activity recovered with the different regeneration techniques for this catalyst are compared in Figure 5.24. When compared to fresh 15 NiA, the conversion and octanol selectivity recovered by the different regeneration techniques was still lower than the activity of the non-poisoned catalyst, although the combined regeneration improved the recovery of the octanol selectivity. However, the C_{24} acetal selectivity remained significantly high despite regeneration.

The silica supported catalyst was more successfully regenerated compared to the alumina catalyst as shown in Figure 5.25, since there was a significant improvement in the recovered activity. The octanol selectivity, recovered with the octanol wash and combined regeneration experiments, was similar to that of the non-poisoned catalyst. The catalytic conversion was also recovered to a significant extent. Furthermore, the C_{24} acetal selectivity was lower after the combined regeneration experiment, indicating that the acid/base properties of the 15 NiSi catalyst were not altered significantly by the poison.

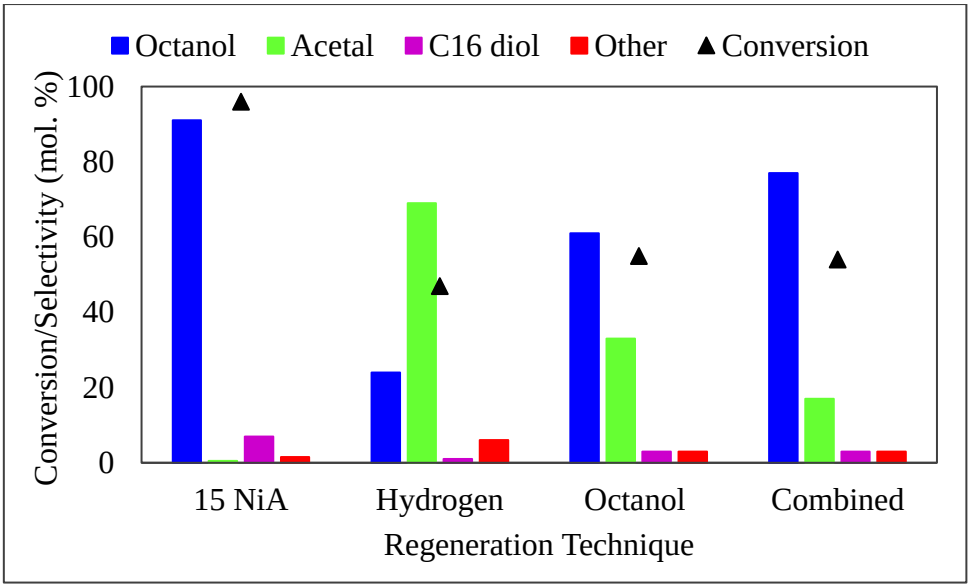

Figure 5.24: Comparison between the activity of the non-poisoned 15 NiA catalyst, and the activity that was recovered using the different regeneration techniques

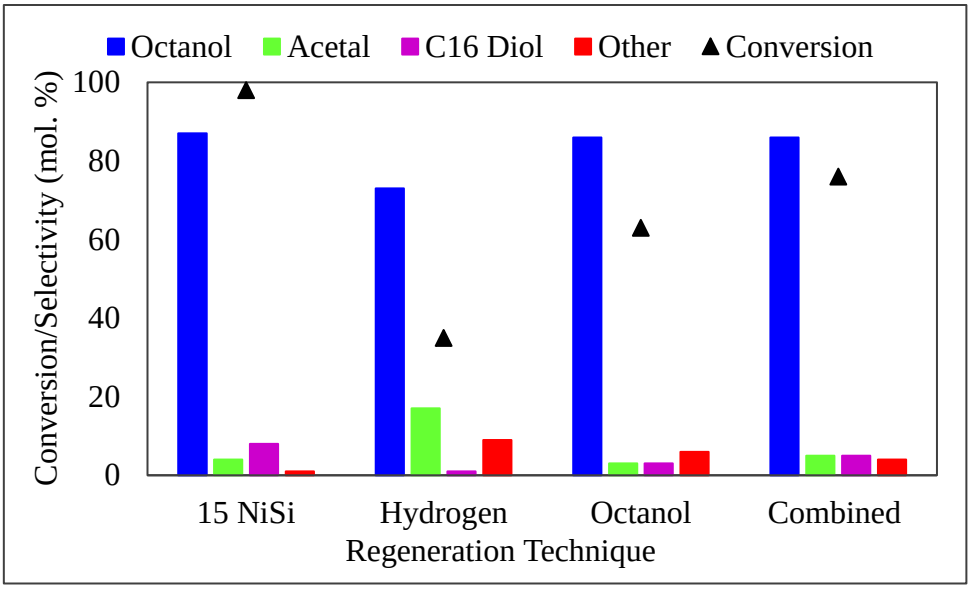

Figure 5.25: Comparison between the activity of the non-poisoned 15 NiSi catalyst, and the activity that was recovered using the different regeneration techniques

The results of the elemental analysis shown in Tables 5.1 and 5.2 showed that the catalysts retained phosphorus even after regeneration. The 15 NiSi catalyst was found to retain more phosphorus compared to 15 NiA. This is attributed to the longer time on stream it took for 15 NiSi to deactivate to the extent of 15 NiA, leading to 15 NiSi retaining a larger amount of phosphorus.

The phosphorus uptake was lower for the 15 NiA catalyst due to the shorter time that was required for the catalyst to deactivate, as opposed to 15 NiSi. This could be correlated to the metal support interaction. From the XRD and TPR results in Chapter four, it was concluded that the alumina interacts strongly with nickel. To that effect, the 15 NiA catalyst has a lower degree of reduction compared to the 15 NiSi catalyst, as shown by the oxygen titration results, presented in Table 4.2. A low uptake of phosphorus by a nickel catalyst supported on alumina has been reported by Wang *et al.* [65] during the synthesis of supported nickel phosphide catalysts using triphenylphosphine as a phosphorus source. The authors attributed the low phosphorus uptake by the alumina supported catalyst to the low reducibility of nickel on alumina, brought about by the strong interaction between the support and nickel. Hence, the catalyst was not completely reduced, meaning that some nickel species were not available to react with triphenylphosphine, leading to the low uptake of phosphorus. The effects of the incomplete reduction of a catalyst on the adsorption of poison has been reported previously [66].

The 15 NiA catalyst was expected to be more robust against poisoning since the catalyst had a higher metallic surface area and metal dispersion, and hence, more catalytically active sites. In addition, alumina is known to delay deactivation of a catalyst by adsorbing and reacting with poisons such as sulphur and phosphorus, which minimises the amount of poison that adsorbs on the active metal and increases the catalysts' tolerance of the poison [67-69]. Therefore, 15 NiSi was expected to deactivate faster, which was not the case. In fact, the 15 NiSi catalyst proved more resilient, since it took a longer time on stream to deactivate, and was found to have a higher amount of retained phosphorus (Table 5.2), compared to 15 NiA. The higher poison uptake by 15 NiSi is attributed to the poor interaction between nickel and silica. This led to the presence of large Ni clusters on the silica support that were easier to reduce than 15 NiA, resulting in the availability of more nickel to react with phosphorus, whereas some of the nickel on 15 NiA was unavailable for reaction with phosphorus, due to it being present in an unreduced, oxide form [70-72]. However, this does not correlate with data obtained from hydrogen chemisorption, which showed that the 15 NiA catalyst had a higher metallic surface area compared to 15 NiA. From chemisorption data, it was expected that the 15 NiSi catalyst would react with less phosphorus, which was not the case, as seen from Tables 5.1. and 5.2.

Geometric effects may have influenced the extent of poison uptake by both 15 NiA and 15 NiSi catalysts. Triphenylphosphine has bulky phenyl groups, that physically block the approach of reactants and other triphenylphosphine molecules towards the supported nickel particles [73-

75]. Since 15 NiA has smaller nickel particles, it requires less triphenylphosphine for the nickel particles to be saturated, since the approach of reactants to smaller particles would be more sterically hindered, whereas the larger Ni clusters on 15 NiSi may be able to accommodate a greater number of TPP molecules, whilst still maintaining catalytic activity. This would enable a greater uptake of the poison by 15 NiSi. In addition, the 15 NiSi catalyst has a wider pore size distribution compared to 15 NiA, as shown in Figures A19 (Appendix). The larger pores on 15 NiSi potentially contribute to the higher uptake of phosphorus by the catalyst.

The interaction between Ni particles on alumina and silica and triphenylphosphine is illustrated in Scheme 5.6, based on the assumption that the supported nickel particles are spherical. The adsorption of triphenylphosphine on the larger Ni particles on 15 NiSi may be at an angle that enables the adsorption of other triphenylphosphine molecules on the same particle, as well as the approach of octanal. This would then lend the 15 NiSi catalyst a measure of 'robustness' against poisoning, which could explain the longer time required for the 15 NiSi catalyst to be saturated with poison.

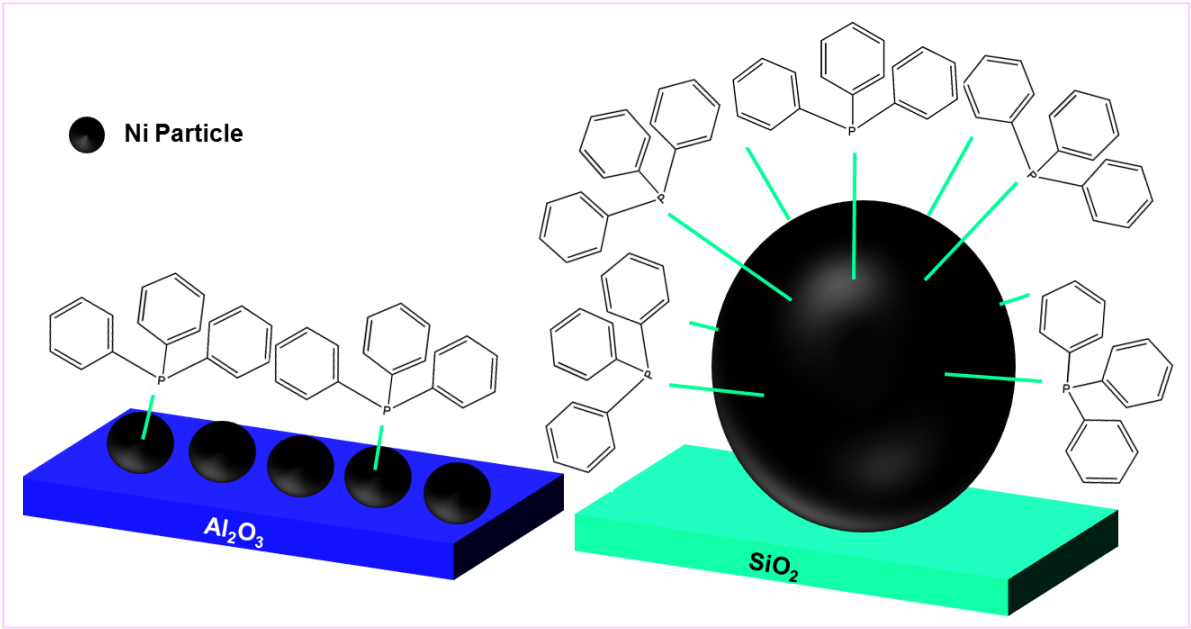

Scheme 5.6: Scheme illustrating the steric effects of triphenylphosphine on its adsorption on the smaller Ni particles of 15 NiA, and how larger particles on 15 NiSi are able to accommodate a larger number of ligands

Characterisation of the poisoned catalysts showed that phosphorus was largely associated with nickel, while there was a change in the phosphorus and nickel distribution on the catalysts

regenerated with hydrogen, both as a stand-alone, and as part of the combined regeneration experiments. Furthermore, characterisation of the poisoned and regenerated catalysts by XRD and, to a lesser extent, HRTEM, showed the presence of a nickel-phosphide phases on 15 NiSi. It was difficult to confirm which phosphide phase formed on 15 NiA, since the XRD diffractograms did not yield much information. However, HRTEM images suggested the presence of Ni_2P on the regenerated catalysts. Semi-quantitative analysis of the surface concentration of phosphorus on the catalyst surface by STEM -EDX analysis also showed that the phosphorus surface concentration decreased in the following order; poisoned catalysts > hydrogen regeneration > solvent wash regeneration > combined regeneration (15 NiA). For 15 NiSi, the order was as follows; poisoned catalyst > hydrogen regeneration > solvent wash = combined regeneration. Magnetic measurements also confirmed the incorporation of phosphorus into nickel, indicated by the lower magnetic properties of the poisoned and regenerated catalysts, compared to the reduced catalysts.

This, together with the results from the quantitative analysis of phosphorus and nickel, suggests that regeneration transformed metallic nickel into nickel phosphide species, instead of removing phosphorus. This has been previously reported for the synthesis of unsupported nickel phosphide nanoparticles, where nickel particles transformed into nickel phosphide through reaction with a solution consisting of trioctylphosphine or triphenylphosphine under a flow of inert gases, via a diffusion based mechanism [23, 24, 32, 44, 76].

From reported studies, the proposed regeneration mechanism infers that regeneration with hydrogen facilitates temperature assisted diffusion of phosphorus into the nickel bulk. For the 15 NiA catalyst, this would lead to the formation of a metastable Ni_xP_y phase due to solubility limitations of phosphorus in the small nickel particles on the support [32]. In addition, it is possible that regeneration with hydrogen leads to the displacement of phosphorus from nickel to the support [77], as depicted in Scheme 5.7. This would result in a number of nickel sites being cleaned, thereby enabling the hydrogenation of octanal to octanol. This inference is supported by the momentary recovery in the octanol selectivity and catalytic activity as observed in Figure 5.3, **Zone E_I**.

The subsequent decline in octanol selectivity and lower steady state conversion suggest a continued deactivation of the catalyst, which arises from the solvent (liquid feed) assisted redistribution of phosphorus from support onto previously cleaned nickel sites [77]. Furthermore, solubility limitations of phosphorus in nickel result in the diffusion of phosphorus

from the metastable nickel phosphide phase onto the nickel surface atoms under process conditions, which leads to re-poisoning of the regenerated nickel sites, as depicted in the simplified diagram in Scheme 5.7 [27, 32].

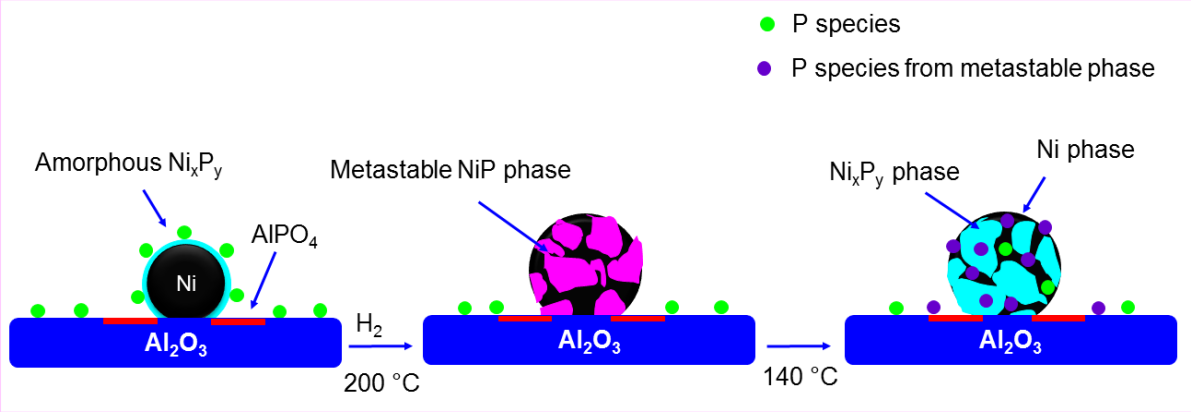

Scheme 5.7: The proposed formation of a metastable Ni_xP_y phase brought about by the hydrogen induced diffusion of phosphorus into nickel, accompanied by the subsequent diffusion of phosphorus from the metastable phase under process conditions, leading to the formation of a more stable Ni_xP_y phase (possibly Ni_2P), and secondary poisoning of the catalyst [27, 32].

The octanol selectivity over 15 NiSi-H did not decline to the same extent as over 15 NiA-H, which suggests that the diffusion of phosphorus out of the metastable Ni_xP_y phase was not as extensive as it was for 15 NiA due to the larger clusters of Ni on the silica support. The metastable Ni_xP_y species possibly only form on the smaller Ni particles. Even so, the reaction scheme presented in Scheme 5.7 is also applicable to the silica supported catalyst, apart from the reaction between phosphorus and the support. The corresponding increase in the C_{24} acetal selectivity over 15 NiSi is attributed to the oxidation of phosphorus on the surface Ni_xP_y phase by water [78, 79]. This generates additional Brønsted acidic P-OH groups on the catalyst that catalyses C_{24} acetal formation [63, 80, 81].

Washing with solvent resulted in a better recovery of the activity and octanol selectivity for both catalysts. It is believed that the solvent achieved this by a) cleaning the support and redistributing phosphorus onto unoccupied nickel sites, b) inducing the diffusion of phosphorus into nickel, [17, 49, 82] and c) dissolving soluble Ni-TPP complexes [83], which led to cleaning of nickel active sites, while also inducing the sintering of the active phase by Ostwald ripening, since the dissolved complexes do not necessarily leave the reactor, but are redeposited in the

catalyst bed. Cleaning of the support by the solvent prevents secondary poisoning of the catalyst by support adsorbed phosphorus.

The combined regeneration of 15 NiA led to a significant improvement in the octanol selectivity, despite the recovered conversion being almost similar to that obtained using the solvent wash regeneration. The better octanol selectivity, and, hence, recovery in nickel active sites arises from a synergistic effect between the combined action of the solvent wash regeneration and hydrogen treatment. The solvent possibly facilitated the redistribution of phosphorus throughout the catalyst bed and/or nickel sites, leading to a more effective diffusion of phosphorus into nickel during the hydrogen treatment, which possibly resulted in the formation of more stable Ni_xP_y species. This prevented poisoning of the catalyst, induced by phosphorus solubility limitations, leading to an improvement in the recovery of catalytic activity and octanol selectivity. Furthermore, washing the silica support with solvent removed support adsorbed phosphorus species, preventing their migration back onto cleaned nickel sites. The higher octanol selectivity could also be related to the efficient crystallization of Ni_2P, due to the longer regeneration time (greater than 24 hours) compared to the individual regeneration steps [33].

Although characterisation indicated the formation of nickel phosphide phases with regeneration, results from XRD showed that not all the nickel reacted with phosphorus, since some metallic nickel was detected by XRD in the case of 15 NiSi, and the P/Ni ratio was too low for the formation of pure Ni_2P. Additionally, magnetization measurements showed an overall decrease in the saturation magnetization of the poisoned and regenerated catalysts, which suggests only a decrease in the ferromagnetic character of the nickel catalysts, but not a complete loss altogether. This is taken as an indication of the presence of metallic nickel, suggesting the presence of mixed Ni_xP_y and metallic Ni phases.

The reaction of triphenylphosphine with metallic nickel particles can either result in the formation of core-shell nickel-phosphide particles (with a nickel phosphide core and a metallic nickel shell, or vice versa, depending on the author). These core shell particles have been reported in the synthesis of nickel phosphide nanoparticles by several authors. However, the expected shape is still in dispute. Carenco *et al.* [29] suggest the formation of a dense Ni_2P core and a lighter Ni shell, although Zheng *et al*. [46] suggest the formation of a dense Ni core and a lighter Ni_2P shell.

Alternatively, the nanoparticles could form a composite of metallic Ni and Ni_2P, which forms from the crystallization of the amorphous Ni_xP_y phase into Ni_2P and metallic Ni, resulting in Ni with nickel phosphide islands [27]. It is expected that regeneration induces the formation of these mixed phases, which explains the recovery of catalytic activity when the octanol wash and combined regeneration experiments were conducted. Images obtained from the HRTEM analysis did not provide sufficient proof to support the core shell hypothesis, whilst BSE-EDX analysis and STEM-EDX line scans showed varying nickel-phosphorus concentrations on different regions of the regenerated catalysts. This possibly indicates the presence of mixed Ni/Ni_2P phases which formed from the crystallization of the amorphous nickel phosphide phase into Ni_2P and Ni phases [27, 84].

The results obtained with the solvent wash regeneration and the combined regeneration show that incorporation of the solvent washing step has a beneficial effect on the activity recovery. This is possibly due to the distribution of the poison throughout the catalyst bed, in addition to the cleaning of the support by the octanol. This would result in less phosphorus diffusing into the nickel bulk, since most of the poison is evenly distributed, resulting in a more effective diffusion of P into Ni. This possibly forms a more stable Ni_2P phase, which does not lead to the re-poisoning of the catalyst.

Further characterisation with transmission electron microscopy showed that exposure of the catalysts to phosphorus contaminated feed resulted in sintering of the active phase, which was more pronounced for the 15 NiA catalysts. This was also observed for the solvent regenerated 15 NiSi catalyst. The lower activity after regeneration is an artefact of the sintering of active nickel, resulting in the loss of catalytically active surface that was not recovered with regeneration. However, the active phase on the silica supported catalyst did not sinter to a significant extent, as opposed to the alumina supported catalyst.

The conversion over 15 NiSi-SH was still lower than that over the non-poisoned 15 NiSi catalyst. This was attributed to the sintering of the active phase, since the poisoned and regenerated catalysts have larger metal particles compared to the non-poisoned 15 NiSi sample, as determined from transmission electron microscopy measurement results in Table 5.2.

From the results obtained in this study, the silica supported catalyst was more successfully regenerated. To that effect, the weak interaction between nickel and silica was beneficial as it resulted in the presence of Ni in large clusters on the silica support, which had a positive effect in the end as it led to a more phosphorus tolerant catalyst that was also effectively regenerated.

Furthermore, the weak interaction between silica and phosphorus was an added advantage, since the catalyst did not undergo secondary deactivation. This contributed towards the successful regeneration of the catalyst.

5.4.3 Conclusions

The results from this study showed that it was possible to recover the hydrogenation activity of nickel catalysts poisoned by phosphorus, during the hydrogenation of octanal. Triphenylphosphine was initially non-selective. However, dissociation and interaction of triphenylphosphine with the support and nickel resulted in the generation of new, more selective active sites, which was indicated by an increase in the selectivity of acid catalysed by-products. The extent of recovery of the activity depended on the type of support used, the interaction between metal and support, the regeneration experiment, the interaction between the poison and support, as well as the size of Ni clusters on the support. Furthermore, sintering was found to also contribute to the deactivation, and influenced the extent to which the catalysts could be regenerated. To that effect, the 15 Ni/SiO_2 catalyst was more effectively regenerated using the combined regeneration method.

5.5 References

[1] J. Valand, A.S. Mahomed, S. Singh, H.B. Friedrich, Journal of Porous Materials 23 (2016) 175-183.

[2] J.-K. Jeon, J.-H. Yim, Y.-K. Park, Chemical Engineering Journal 140 (2008) 555-561.

[3] M.A. Ermakova, D.Y. Ermakov, Applied Catalysis A: General 245 (2003) 277-288.

[4] X. Yang, Z. Sun, D. Wang, W. Forsling, Journal of Colloid and Interface Science 308 (2007) 395-404.

[5] A.A. Tsyganenko, E.N. Storozheva, O.V. Manoilova, T. Lesage, M. Daturi, J.-C. Lavalley, Catalysis Letters 70 (2000) 159-163.

[6] A. Saadi, R. Merabti, Z. Rassoul, M.M. Bettahar, Journal of Molecular Catalysis A: Chemical 253 (2006) 79-85.

[7] X. Wang, R.Y. Saleh, U.S. Ozkan, Journal of Catalysis 231 (2005) 20-32.

[8] N.B. Lorette, W.L. Howard, J.H. Brown, The Journal of Organic Chemistry 24 (1959) 1731-1733.

[9] J.M. Bell, D.G. Kubler, P. Sartwell, R.G. Zepp, The Journal of Organic Chemistry 30 (1965) 4284-4292.

[10] M.J. Climent, A. Corma, H. Garcia, R. Guil-Lopez, S. Iborra, V. Fornés, Journal of Catalysis 197 (2001) 385-393.

[11] M.J. Climent, A. Corma, R. Guil-López, S. Iborra, J. Primo, Journal of Catalysis 175 (1998) 70-79.

[12] T. Chetty, H.B. Friedrich, V.D.B.C. Dasireddy, A. Govender, P.J. Mohlala, W. Barnard, ChemCatChem 6 (2014) 2384-2393.

[13] P. Forzatti, L. Lietti, Catalysis Today 52 (1999) 165-181.

[14] M. Østberg, V.F. Andersen, Catalysis Today 272 (2016) 19-24.

[15] G. Westermark, H. Kariis, I. Persson, B. Liedberg, Colloids and Surfaces A: Physicochemical and Engineering Aspects 150 (1999) 31-43.

[16] G. Westermark, I. Persson, Colloids and Surfaces A: Physicochemical and Engineering Aspects 144 (1998) 149-166.

[17] J. Chen, M. Han, S. Zhao, Z. Pan, Z. Zhang, Catalysis Science & Technology 6 (2016) 3938-3949.

[18] H.P. Buwono, S. Minami, K. Uemura, M. Machida, Industrial & Engineering Chemistry Research 54 (2015) 7233-7240.

[19] H. Guo, G. Iqbal, B.S. Kang, International Journal of Applied Ceramic Technology 8 (2011) 68-73.

[20] H. Kishimoto, K. Yamaji, M.E. Brito, T. Horita, H. Yokokawa, Journal of Mining and Metallurgy Section B: Metallurgy 44 (2008) 39-48.

[21] A. Montesinos-Castellanos, T.A. Zepeda, B. Pawelec, J.L.G. Fierro, J.A. de los Reyes, Chemistry of Materials 19 (2007) 5627-5636.

[22] D.C. Kim, S.S. Eom, D.H. Ko, M.H. Hong, O.H. Kwon, Method for regenerating hydrogenation catalyst poisoned during hydrogenation of hydroformylation product, LG Chem, Ltd., South Korea . 2013, p. 18pp.; Chemical Indexing Equivalent to 160:67398 (KR).

[23] A.E. Henkes, Y. Vasquez, R.E. Schaak, Journal of the American Chemical Society 129 (2007) 1896-1897.

[24] A.E. Henkes, R.E. Schaak, Chemistry of Materials 19 (2007) 4234-4242.

[25] H. Wang, Y. Wang, Topics in Catalysis 59 (2016) 65-72.

[26] R.L. Frost, A. López, Y. Xi, N. Murta, R. Scholz, Journal of Molecular Structure 1048 (2013) 420-425.

[27] Y. Tan, D. Sun, H. Yu, B. Yang, Y. Gong, S. Yan, Z. Chen, Q. Cai, Z. Wu, CrystEngComm 16 (2014) 9657-9668.

[28] L.M. Moreau, D.-H. Ha, H. Zhang, R. Hovden, D.A. Muller, R.D. Robinson, Chemistry of Materials 25 (2013) 2394-2403.

[29] S. Carenco, X.F. Le Goff, J. Shi, L. Roiban, O. Ersen, C. Boissiere, C. Sanchez, N. Mezailles, Chemistry of Materials 23 (2011) 2270-2277.

[30] H. Sezer, I.B. Celik, Electrochimica Acta 155 (2015) 421-430.

[31] O. Demircan, W. Zhang, C. Xu, J. Zondlo, H.O. Finklea, Journal of Power Sources 195 (2010) 3091-3096.

[32] R.-K. Chiang, R.-T. Chiang, Inorganic Chemistry 46 (2007) 369-371.

[33] D. Li, K. Senevirathne, L. Aquilina, S.L. Brock, Inorganic Chemistry 54 (2015) 7968-7975.

[34] J. Li, J. Li, X. Zhou, Z. Xia, W. Gao, Y. Ma, Y. Qu, ACS Applied Materials & Interfaces 8 (2016) 10826-10834.

[35] J. Chen, D. Ci, Q. Yang, K. Li, Applied Surface Science 320 (2014) 643-652.

[36] D.P. Kumar, J. Choi, S. Hong, D.A. Reddy, S. Lee, T.K. Kim, ACS Sustainable Chemistry & Engineering 4 (2016) 7158-7166.

[37] Y. Pan, Y. Liu, J. Zhao, K. Yang, J. Liang, D. Liu, W. Hu, D. Liu, Y. Liu, C. Liu, Journal of Materials Chemistry A 3 (2015) 1656-1665.

[38] J. Pal, T. Pal, RSC Advances 6 (2016) 83738-83747.

[39] M. Varkolu, V. Velpula, S. Ganji, D.R. Burri, S.R. Rao Kamaraju, RSC Advances 5 (2015) 57201-57210.

[40] J. Chen, S. Zhou, D. Ci, J. Zhang, R. Wang, J. Zhang, Industrial & Engineering Chemistry Research 48 (2009) 3812-3819.

[41] J. Wang, H. Chen, Y. Fu, J. Shen, Applied Catalysis B: Environmental 160–161 (2014) 344-355.

[42] L.M. Moreau, D.-H. Ha, C.R. Bealing, H. Zhang, R.G. Hennig, R.D. Robinson, Nano Letters 12 (2012) 4530-4539.

[43] H. Song, M. Dai, H. Song, X. Wan, X. Xu, C. Zhang, H. Wang, Catalysis Communications 43 (2014) 151-154.

[44] T. Tian, L. Ai, J. Jiang, RSC Advances 5 (2015) 10290-10295.

[45] S.E. Habas, F.G. Baddour, D.A. Ruddy, C.P. Nash, J. Wang, M. Pan, J.E. Hensley, J.A. Schaidle, Chemistry of Materials 27 (2015) 7580-7592.

[46] X. Zheng, S. Yuan, Z. Tian, S. Yin, J. He, K. Liu, L. Liu, Chemistry of Materials 21 (2009) 4839-4845.

[47] A. Wang, H. Yin, H. Lu, J. Xue, M. Ren, T. Jiang, Langmuir 25 (2009) 12736-12741.

[48] N. Winkler, M. Peterlechner, G. Wilde, Journal of Materials Chemistry C 3 (2015) 7543-7551.

[49] J. Wang, A.C. Johnston-Peck, J.B. Tracy, Chemistry of Materials 21 (2009) 4462-4467.

[50] A.J. McCue, F.-M. McKenna, J.A. Anderson, Catalysis Science & Technology 5 (2015) 2449-2459.

[51] L. Baltusis, J.S. Frye, G.E. Maciel, Journal of the American Chemical Society 109 (1987) 40-46.

[52] S.J. Sawhill, K.A. Layman, D.R. Van Wyk, M.H. Engelhard, C. Wang, M.E. Bussell, Journal of Catalysis 231 (2005) 300-313.

[53] R.B. Wexler, J.M.P. Martirez, A.M. Rappe, Chemistry of Materials 28 (2016) 5365-5372.

[54] L.V. Goncharova, S.K. Clowes, R.R. Fogg, A.V. Ermakov, B.J. Hinch, Surface Science 515 (2002) 553-566.

[55] J. Chen, L. Sun, R. Wang, J. Zhang, Catalysis Letters 133 (2009) 346-353.

[56] M. Kiskinova, D.W. Goodman, Surface Science 108 (1981) 64-76.

[57] R. Prins, M.E. Bussell, Catalysis Letters 142 (2012) 1413-1436.

[58] R. Li, Q. Guan, R. Wei, S. Yang, Z. Shu, Y. Dong, J. Chen, W. Li, The Journal of Physical Chemistry C 119 (2015) 2557-2565.

[59] S.T. Oyama, Y.-K. Lee, Journal of Catalysis 258 (2008) 393-400.
[60] J.-S. Moon, E.-G. Kim, Y.-K. Lee, Journal of Catalysis 311 (2014) 144-152.
[61] H. Chen, J. Tan, Y. Zhu, Y. Li, Catalysis Communications 73 (2016) 46-49.
[62] X. Li, H. Cheng, G. Liang, L. He, W. Lin, Y. Yu, F. Zhao, Catalysts 5 (2015) 759-773.
[63] A. Infantes-Molina, E. Gralberg, J.A. Cecilia, E. Finocchio, E. Rodriguez-Castellon, Catalysis Science & Technology 5 (2015) 3403-3415.
[64] C.H. Bartholomew, in: B. Delmon, G.F. Froment (Eds.), Studies in Surface Science and Catalysis, Elsevier, Amsterdam, 1987, pp. 81-104.
[65] J. Wang, Y. Fu, H. Chen, J. Shen, Chemical Engineering Journal 275 (2015) 89-101.
[66] A. Aguinaga, M. Montes, J.M. Asua, Journal of Chemical Technology & Biotechnology 52 (1991) 369-381.
[67] L.S. Escandón, S. Ordóñez, A. Vega, F.V. Díez, Journal of Hazardous Materials 153 (2008) 742-750.
[68] L.J. Hoyos, H. Praliaud, M. Primet, Applied Catalysis A: General 98 (1993) 125-138.
[69] J.K. Lampert, M.S. Kazi, R.J. Farrauto, Applied Catalysis B: Environmental 14 (1997) 211-223.
[70] H.-S. Sheu, J.-F. Lee, S.-G. Shyu, W.-W. Chou, J.-R. Chang, Journal of Catalysis 266 (2009) 15-25.
[71] C. Xie, Y. Chen, M.H. Engelhard, C. Song, ACS Catalysis 2 (2012) 1127-1137.
[72] P. Maeki-Arvela, J. Hajek, T. Salmi, D.Y. Murzin, Applied Catalysis A: General 292 (2005) 1-49.
[73] F.M. McKenna, L. Mantarosie, R.P.K. Wells, C. Hardacre, J.A. Anderson, Catalysis Science & Technology 2 (2012) 632-638.
[74] F.-M. McKenna, J.A. Anderson, Journal of Catalysis 281 (2011) 231-240.
[75] F.-M. McKenna, R.P.K. Wells, J.A. Anderson, Chemical Communications 47 (2011) 2351-2353.
[76] S. Carenco, A. Leyva-Pérez, P. Concepción, C. Boissière, N. Mézailles, C. Sanchez, A. Corma, Nano Today 7 (2012) 21-28.
[77] I. Czekaj, R. Struis, J. Wambach, S. Biollaz, Catalysis Today 176 (2011) 429-432.
[78] P. Liu, J.A. Rodriguez, Y. Takahashi, K. Nakamura, Journal of Catalysis 262 (2009) 294-303.
[79] J.A. Cecilia, A. Infantes-Molina, E. Rodríguez-Castellón, A. Jiménez-López, S.T. Oyama, Applied Catalysis B: Environmental 136–137 (2013) 140-149.
[80] J. Chen, T. Guo, K. Li, L. Sun, Catalysis Science & Technology 5 (2015) 2670-2680.

[81] S.-K. Wu, P.-C. Lai, Y.-C. Lin, Catalysis Letters 144 (2014) 878-889.

[82] L. Li, C. Han, L. Yang, X. Wang, B. Zhang, Industrial & Engineering Chemistry Research 49 (2010) 1658-1662.

[83] S. Carenco, C. Boissiere, L. Nicole, C. Sanchez, P. Le Floch, N. Mezailles, Chemistry of Materials 22 (2010) 1340-1349.

[84] H. Li, W. Wang, H. Li, J.-F. Deng, Journal of Catalysis 194 (2000) 211-221.

Chapter 6: Conclusions and recommendations

The deactivation of supported metal catalysts with time has been cited as a prominent drawback in the application of heterogeneous catalysis for chemical transformations. Of all the deactivation mechanisms, poisoning is one of the more difficult processes to reverse. The deactivation of aldehyde hydrogenation catalysts by phosphorus poisoning has not been studied to a significant extent, which made it difficult to predict the effects of phosphorus on the behaviour and activity of the catalysts studied during the execution of this study. Previous studies into the deactivation of hydrogenation catalysts have extensively focused on the reversal of sulphur poisoning through regeneration, whereas phosphorus poisoning has only received attention in the study of solid oxide fuel cells and automotive catalysts.

To that effect, this study was aimed at developing a feasible method for the regeneration of nickel based aldehyde hydrogenation catalysts. The catalysts were dispersed on two different supports (gamma alumina and silica) in order to observe their effects on the interaction between the active phase and the poison. The two catalysts prepared were characterised to observe their physicochemical characteristics, which differed significantly. The gamma alumina supported catalyst (15 NiA) had a higher metal dispersion and, hence, smaller nickel particles on the support, compared to the silica supported catalyst (15 NiSi). The higher metal dispersion on the 15 NiA catalyst led to a strong interaction between the metal and support, which meant that the catalyst required a higher reduction temperature. However, the intrinsic activities of both 15 NiA and 15 NiSi were equivalent.

Time on stream deactivation studies were conducted in a continuous flow, high pressure fixed bed reactor operated at a temperature of 140 °C, under 50 bars of hydrogen pressure. The hydrogenation of the aldehyde feed poisoned with triphenylphosphine led to the deactivation of the catalysts. The poison was observed to initially behave non-selectively, adsorbing on both the active metal and support sites. However, at the reintroduction of clean feed, the poison appeared to become more selective, migrating from the support to active metallic sites. This was attributed to the loss of phenyl groups and reduction of triphenylphosphine into a more reactive species. The interaction between the poison and catalyst differed across the two supports. The strong interaction between alumina and phosphorus resulted in the formation of $AlPO_4$ which increased the acidity of the catalyst, and hence, the selectivity of the C_{24} acetal and other acid catalysed by-products, whilst lowering the octanol selectivity. In contrast, the

silica supported catalyst only interacted weakly with phosphorus, and thus did not have long term implications on the product selectivity.

Regeneration resulted in the recovery of lost catalytic activity; however, this was largely dependent on the regeneration experiment conducted. The hydrogen treatment regeneration was not successful for both catalysts, resulting in a gradual decline in the octanol selectivity, accompanied by increase in the C_{24} acetal selectivity when the clean feed was reintroduced. Regeneration experiments incorporating the octanol wash resulted in a better recovery of the octanol selectivity, and decreased the C_{24} acetal selectivity, which was notable for both 15 NiA and 15 NiSi. Of the three regeneration experiments conducted, the combined regeneration was found to be most effective.

Regeneration did not lead to the removal of phosphorus, but resulted in the conversion of nickel to nickel phosphide, as indicated by magnetism studies and XRD, especially in the case of the silica supported catalyst. Characterisation suggested that a nickel phosphide phase formed which corresponded to Ni_2P. The silica supported catalyst took a longer time to deactivate, likely due to larger Ni particles, which were able to accommodate a higher number of bulky triphenylphosphine molecules. The 15 NiSi catalyst also retained a larger amount of phosphorus compared to 15 NiA. The 15 NiSi catalyst was easier to regenerate, since the activity recovery was greater than that obtained for 15 NiA when the solvent wash and combined regeneration experiments were conducted. The recovered 15 NiSi activity was ascribed to the catalyst not sintering to a significant extent, as opposed to the 15 NiA catalyst.

The main challenges in the execution of this study lay in determining the nature of the interaction of phosphorus with nickel, and quantifying the change in acidity of the 15 NiA catalyst. From this study, the regeneration of a phosphorus poisoned catalyst was found to be influenced by a number of factors, such as the nature of the support, the interaction between the metal and support, as well as the regeneration treatment. The octanol wash step proved to be important, since incorporating it into the regeneration experiments resulted in an improvement in the recovery of the catalytic activity, and most notably, the octanol selectivity. The viability of the combined regeneration makes it potentially applicable in an industrial setting, since it was effective for a system that was severely deactivated by an exaggerated amount of poison. Under real conditions, the extent of deactivation is generally not experienced to this extreme, and the concentration of poison is much lower than that used in this study. The data also showed that the silica supported catalyst is a more poison resistant system compared

to 15 NiA, since the catalyst performed better overall, was more resilient against deactivation when it was exposed to contaminated feed (taking longer to deactivate than the alumina supported catalyst), and was easier to regenerate. This was indicated by the much higher activity recovery for 15 NiSi by the combined regeneration, compared to the recovered activity of 15 NiA by the same regeneration technique. To that effect, the 15 NiSi system is preferable due to its apparent robustness against deactivation by poisoning with phosphorus, and its ease of regeneration.

Appendix

Appendix index

Index 1: List of figures

Index 2: List of tables

Table **Page**

Index 3: List of schemes

Appendix 1: Reaction scheme

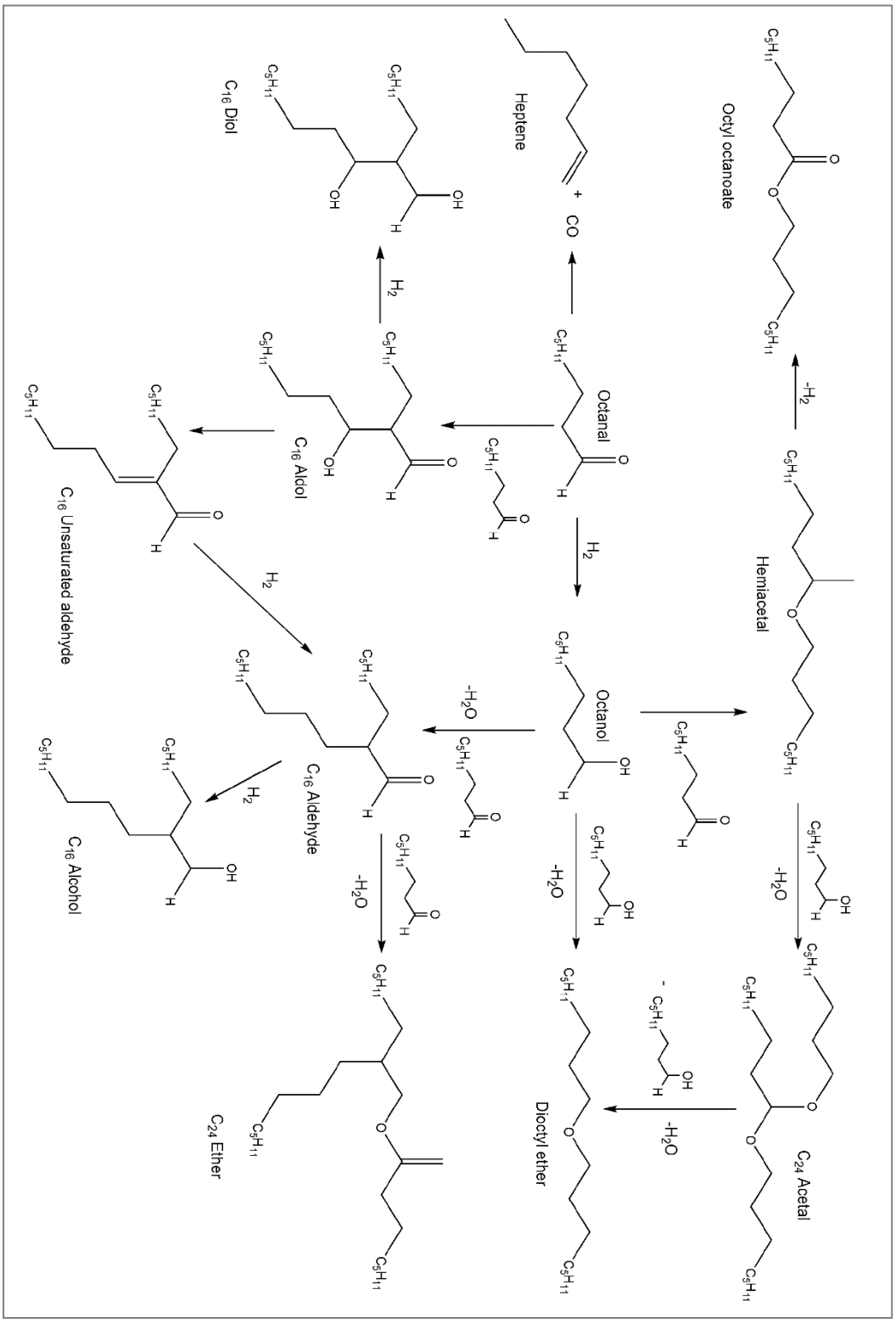

Scheme A1: Proposed octanal hydrogenation adapted from the propanal hydrogenation scheme adapted from Wang *et al* [Reference 7, Chapter 5]

Appendix 2: Figures

A2.1: Schematic representation of the interaction between the poison and the catalyst bed

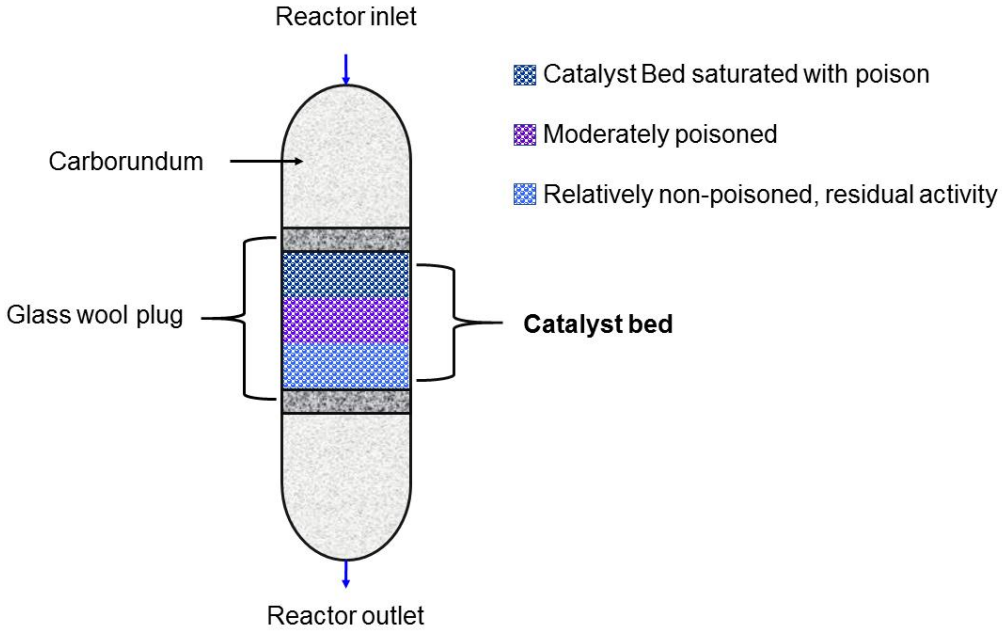

Figure A1: Proposed schematic presentation of the progression of poison down the catalyst bed

A2.2: Temperature programmed desorption for the characterisation of acidity changes

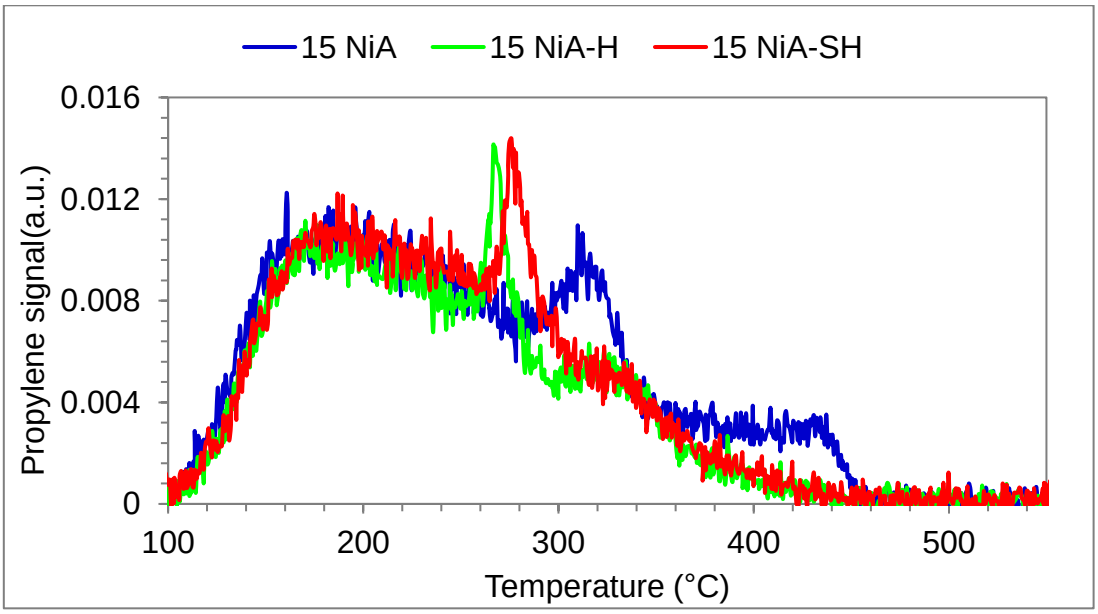

Figure A2: *n*-propylamine temperature programmed desorption from 15 NiA

A2.3: Thermogravimetric analysis

TGA-MS profiles were obtained for 15 NiA-U, 15 NiA-H and 15 NiA-SH, to determine if there is evolution of species associated with the desorption of phosphorus from the catalyst. From the results obtained, the weight loss was only due to the desorption of physisorbed water, and the combustion of carbonaceous species adsorbed on the catalyst.

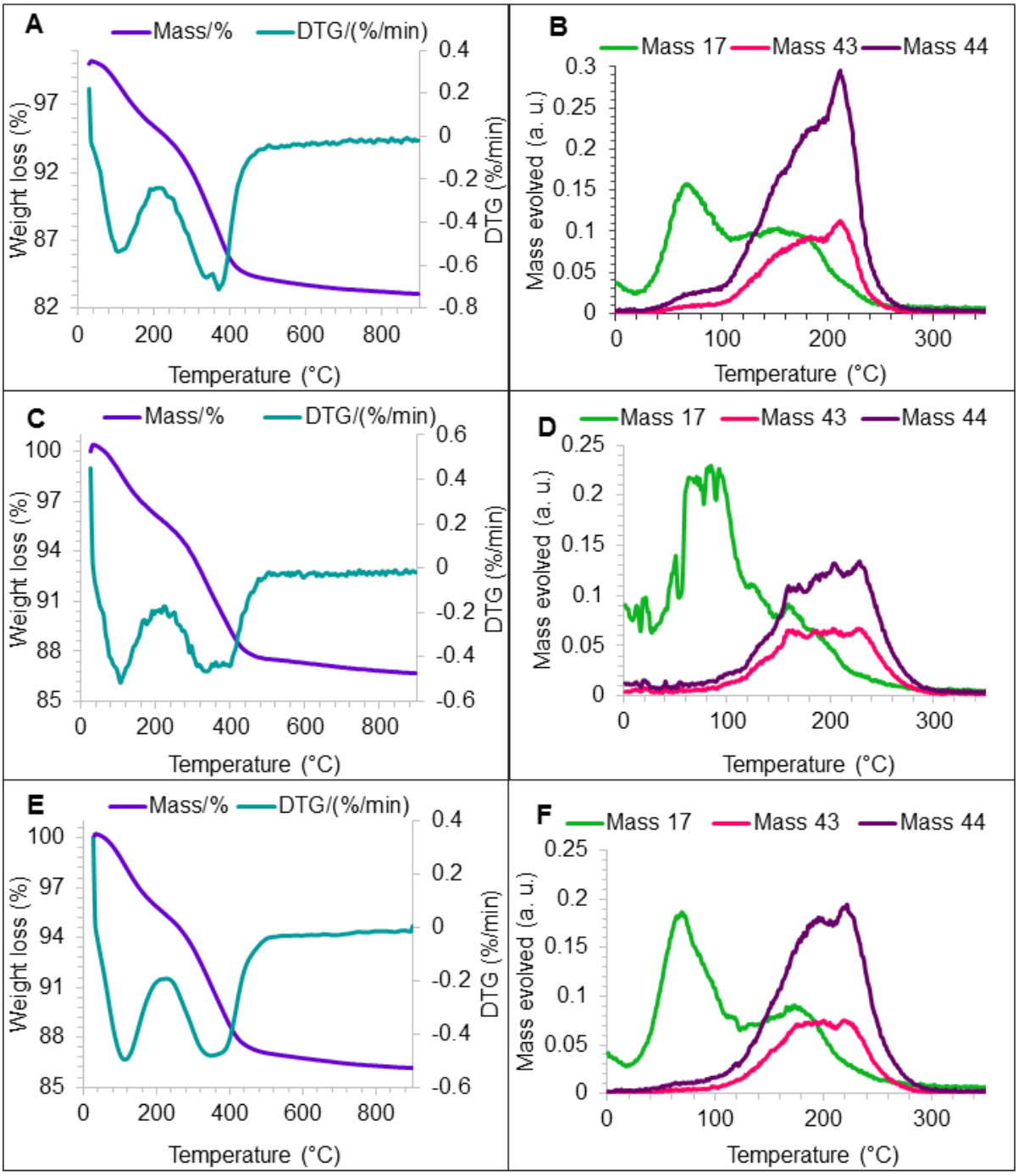

Figure A3: TGA-MS profiles for 15 NiA-U (A:TGA; B: MS), 15 NiA-H (C:TGA; D:MS) and 15 NiA-SH (D: TGA; F:MS)

Thermogravimetric analysis was also performed for the regenerated 15 NiSi catalyst samples, and are presented in Figure A4.

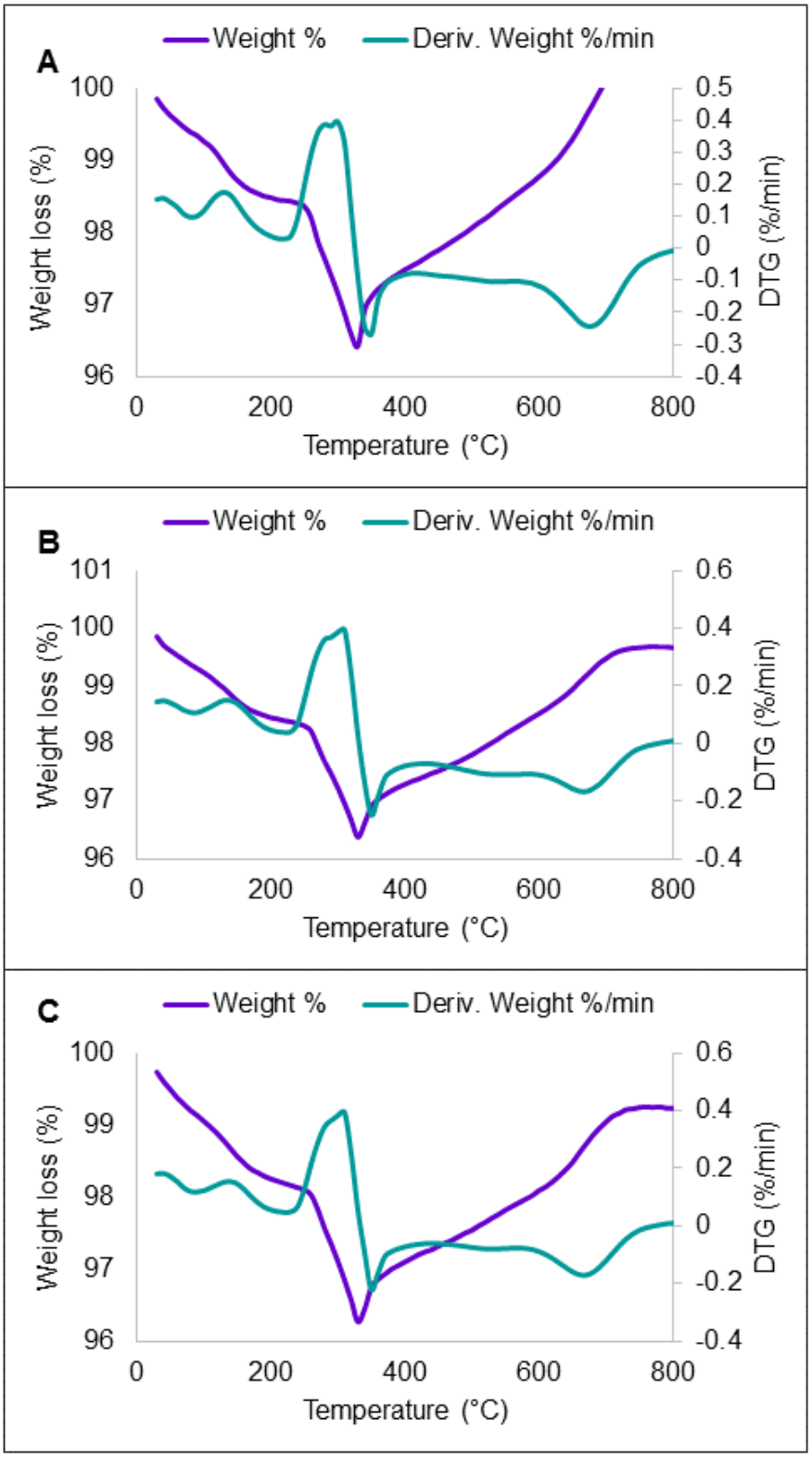

Figure A4: TGA weight loss profiles of A) 15 NiSi-H, B) 15 NiSi-S and C) 15 NiSi-SH

A2.4: Fourier transform infrared spectroscopic analysis of the 15 NiA series

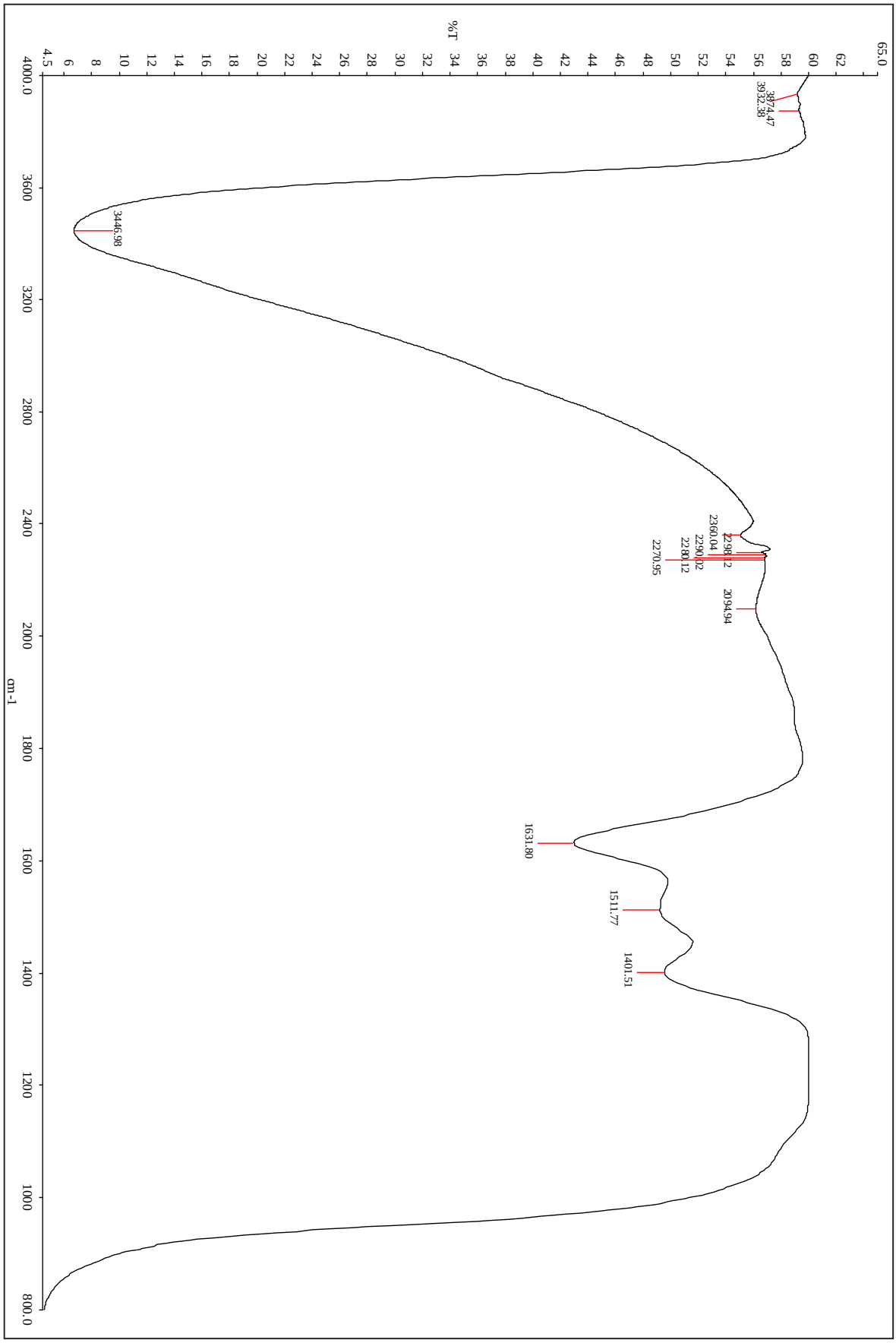

Figure A5: Infrared spectra of the fresh, non-reduced 15 NiA catalyst

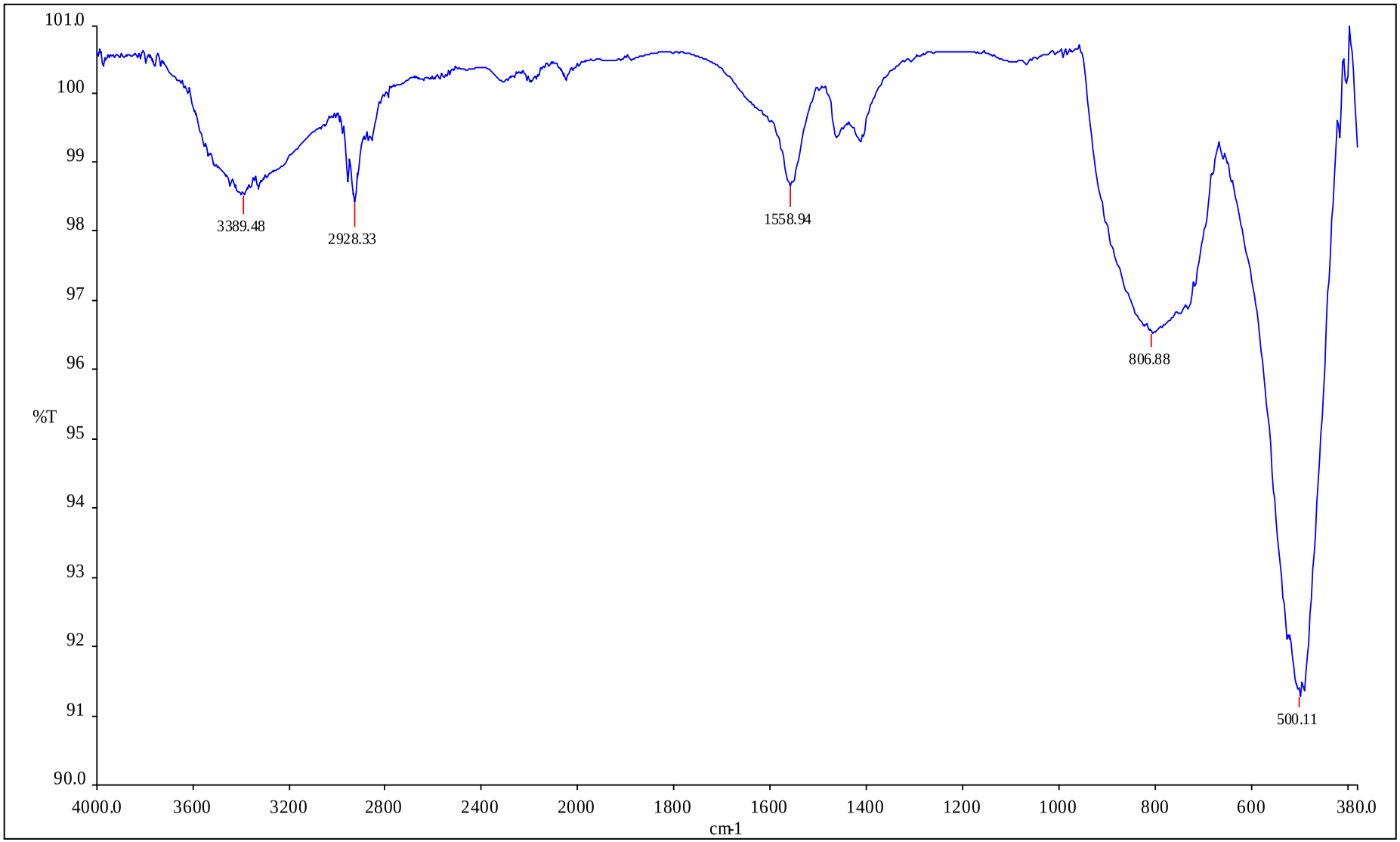

Figure A6: Infrared spectra of the reduced 15 NiA catalyst after hydrogenation of the clean, non-poisoned feed (15 NiA-U)

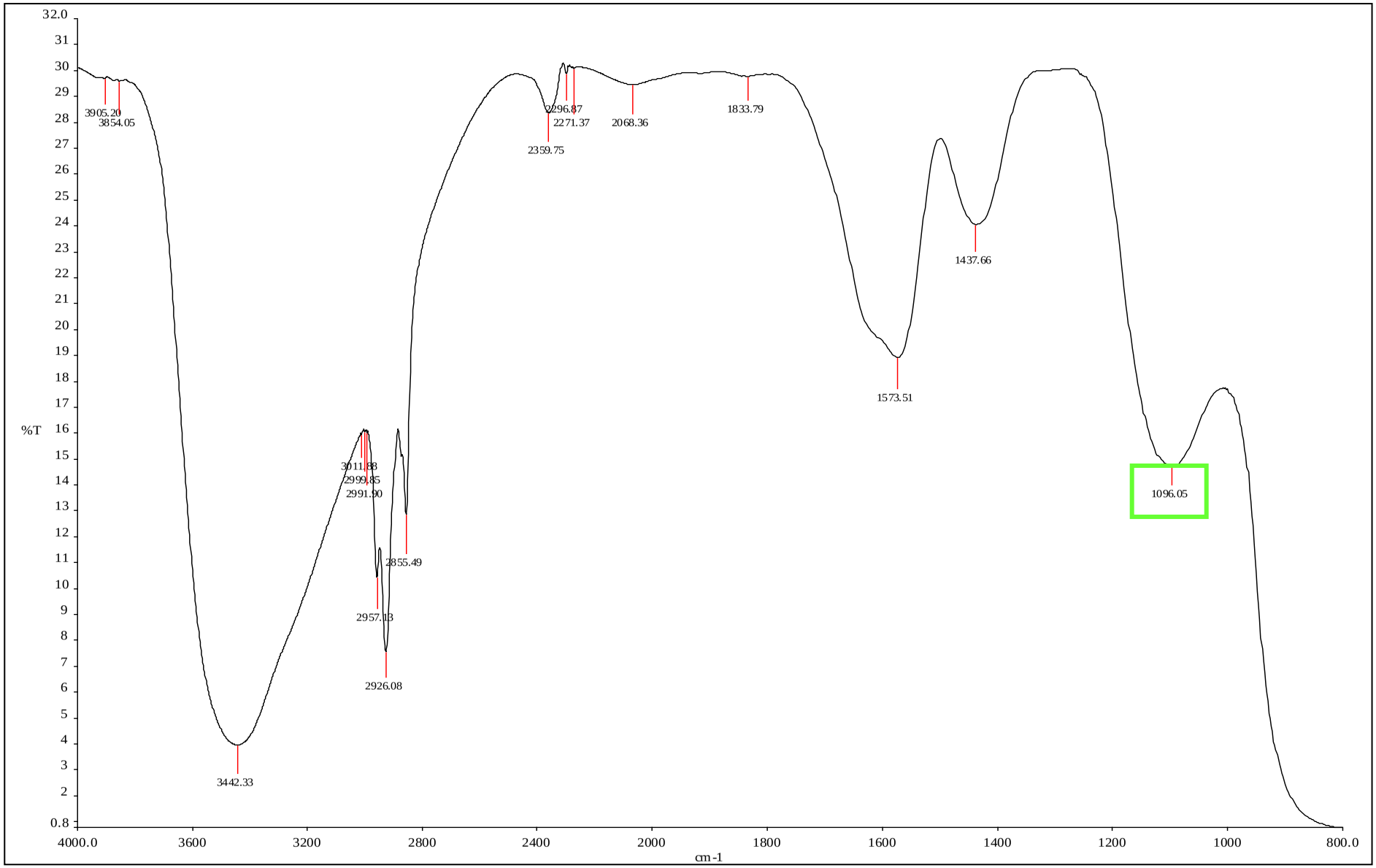

Figure A7: Infrared spectrum of the 15 NiA catalyst samples that was poisoned, but not regenerated (15 NiA-P). The green box highlights the $AlPO_4$ stretch

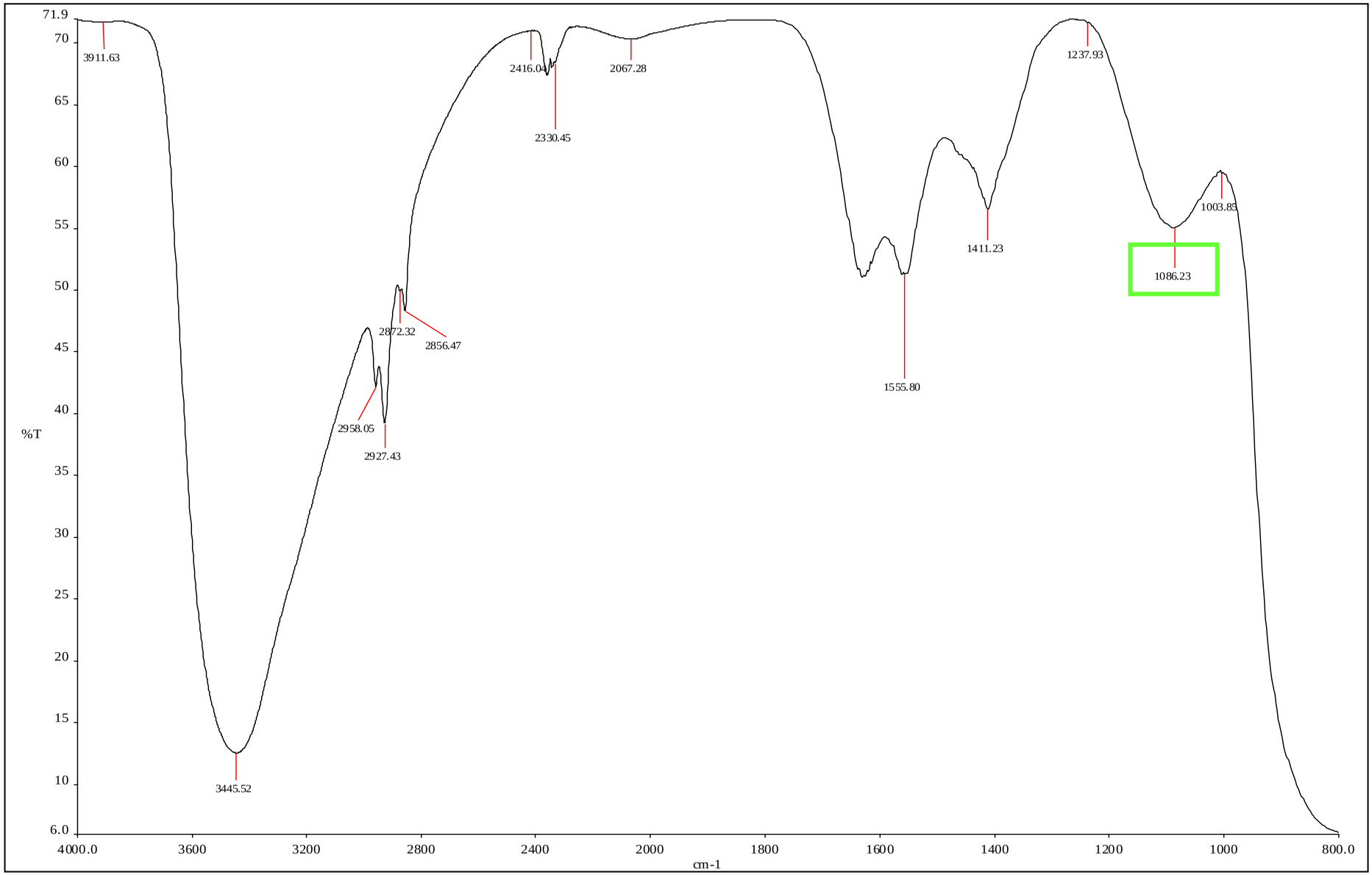

Figure A8: Infrared spectrum of the 15 NiA catalyst sample that was regenerated with the hydrogen treatment (15 NiA-H). The green box highlights the $AlPO_4$ stretch

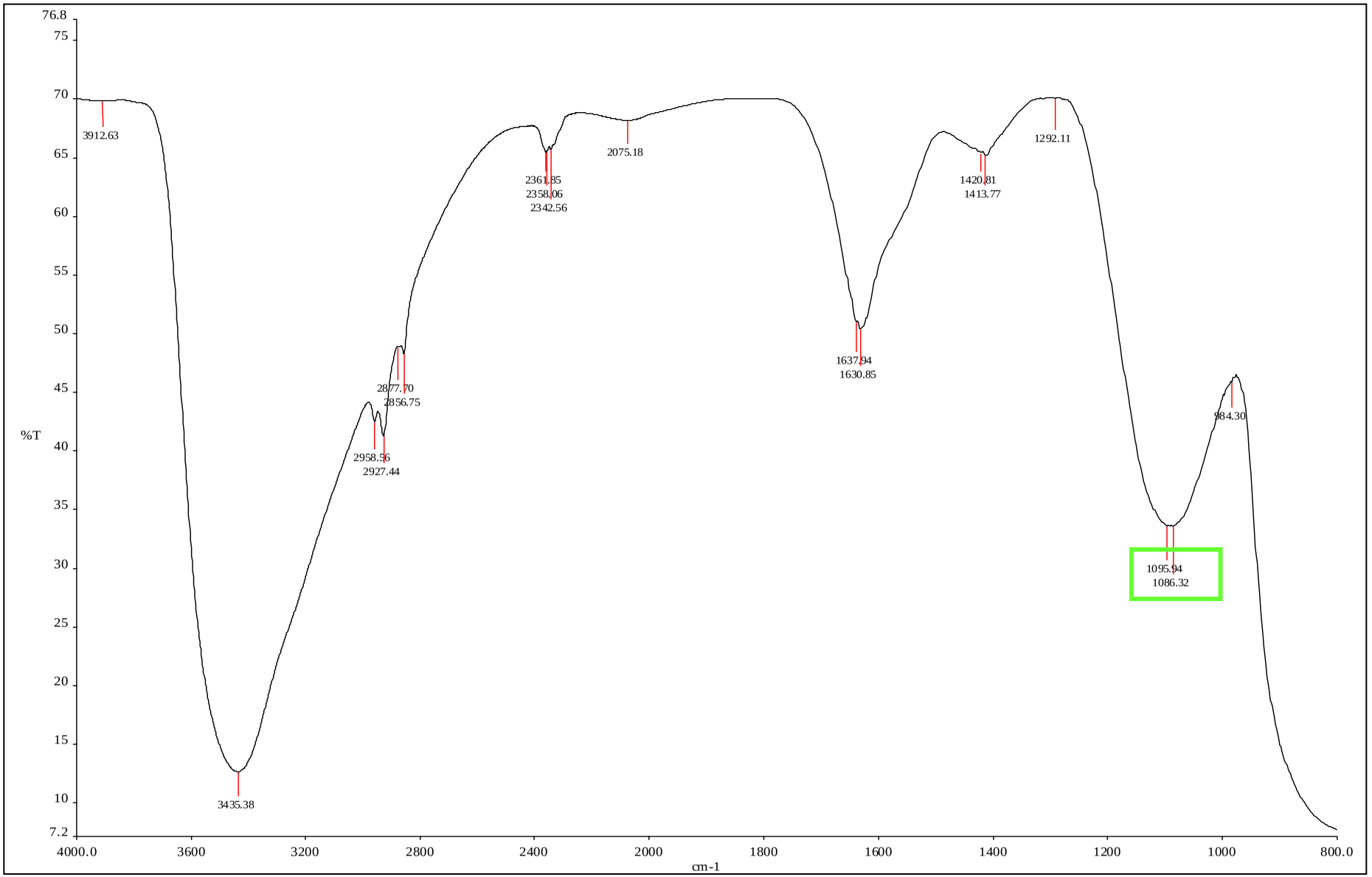

Figure A9: Infrared spectrum of the 15 NiA catalyst sample that was regenerated using the combined regeneration experiment (octanol wash followed by the hydrogen treatment, 15 NiA-SH). The green box highlights the $AlPO_4$ stretch

A2.5: Scanning electron microscopy (Backscattered electron imaging, and scanning electron microscopy-electron dispersive X-ray mapping and line scans)

Backscattered SEM-EDX line scans were obtained for the poisoned and regenerated catalyst samples.

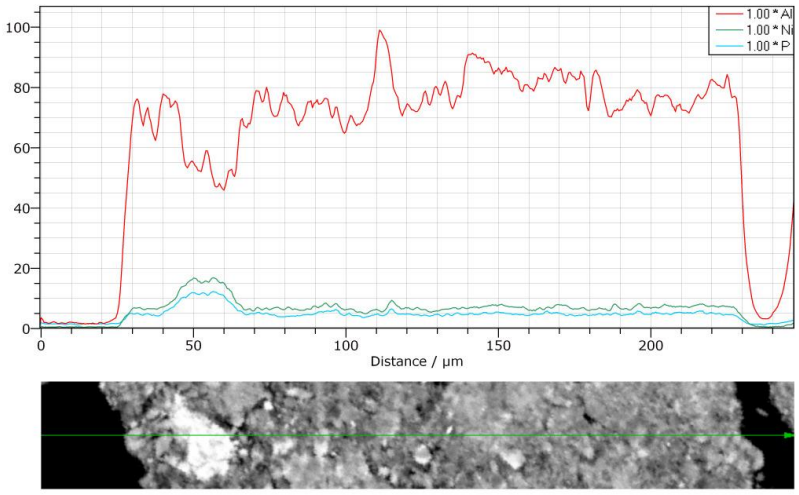

Figure A10: BSE-EDX line scan of the 15 NiA catalyst that was removed after poisoning, before regeneration (after step 3, Figure 3.2, Chapter 3)

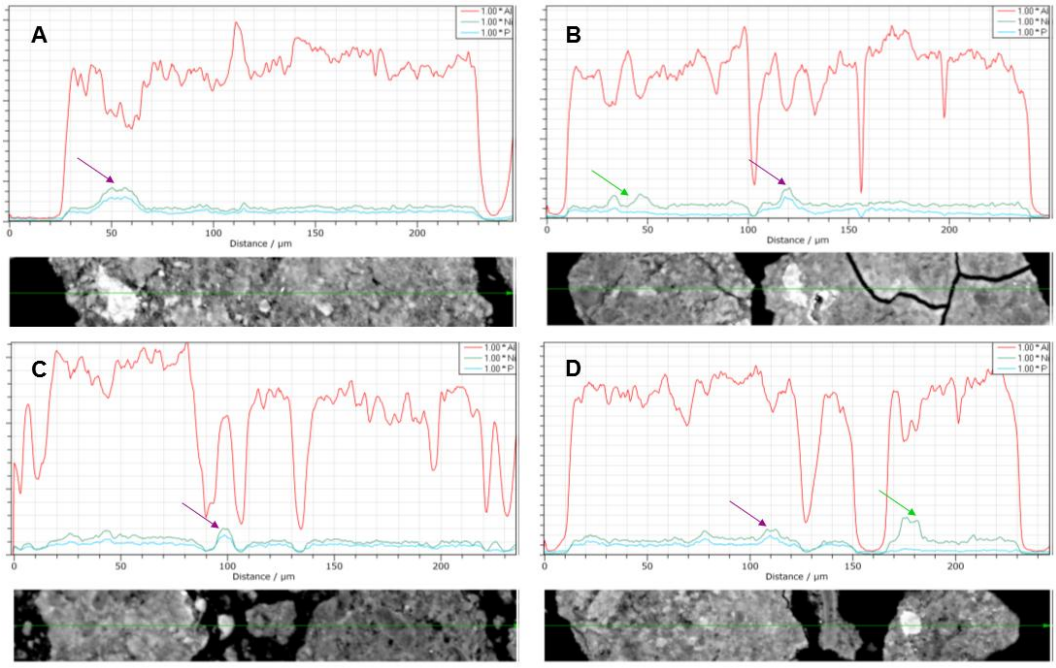

Figure A11: Nickel-phosphorus distribution on A) 15 NiA-P, B) 15 NiA-H, C) 15 NiA-S and D) 15 NiA-SH

A series of experiments were performed wherein the catalyst was removed from the reactor after the regeneration steps, before the reintroduction of clean feed. These reactions were run in the sequence of CF-TPP-CF-Regeneration, and were performed for characterisation purposes. This was to observe any changes in the distribution of phosphorus with the reintroduction of clean feed. BSE-EDX maps were obtained for the catalyst samples after removal from the reactor.

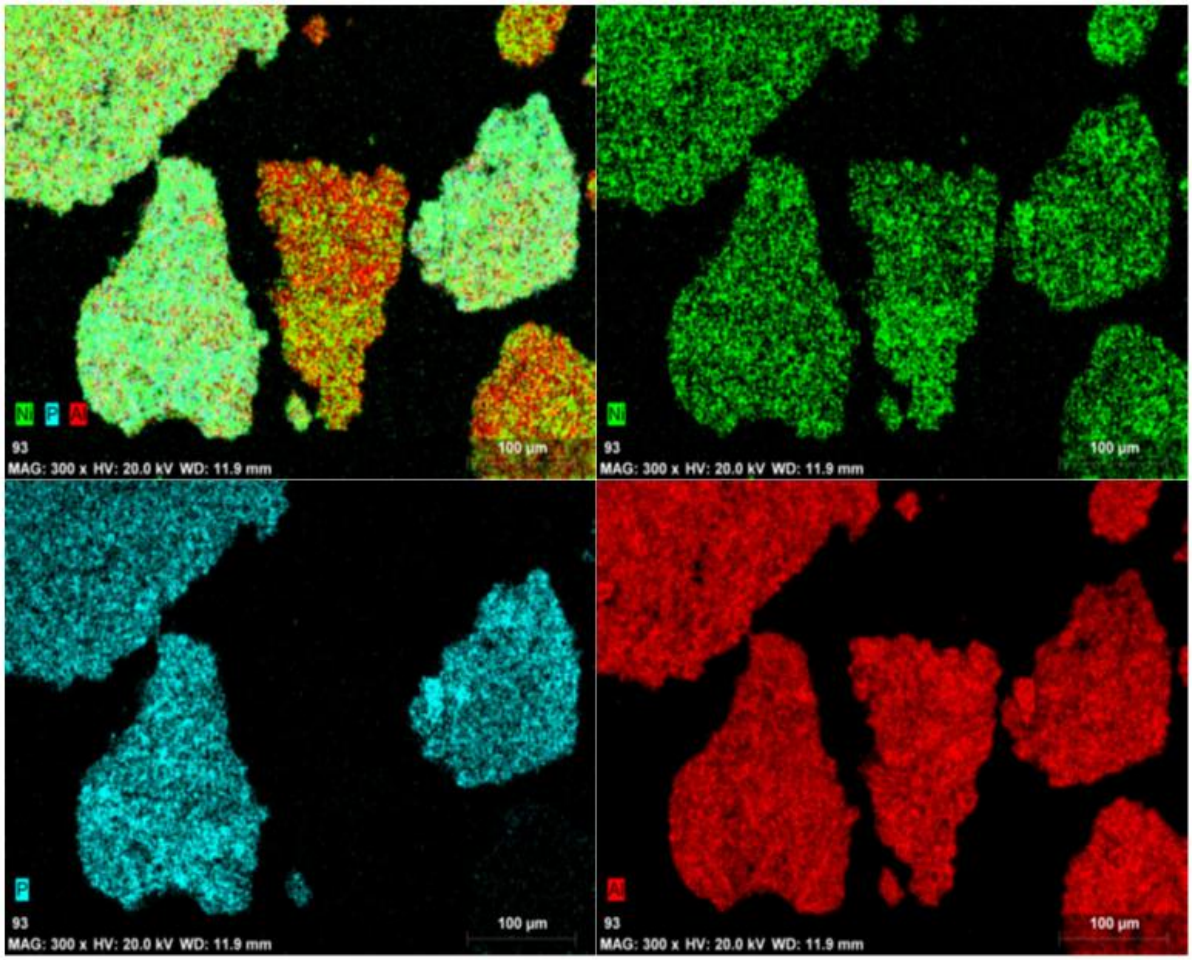

Figure A12: BSE-EDX maps showing the distribution of P, Ni on alumina for the 15 NiA catalyst that was regenerated with the hydrogen treatment, then removed from the reactor for characterisation purposes

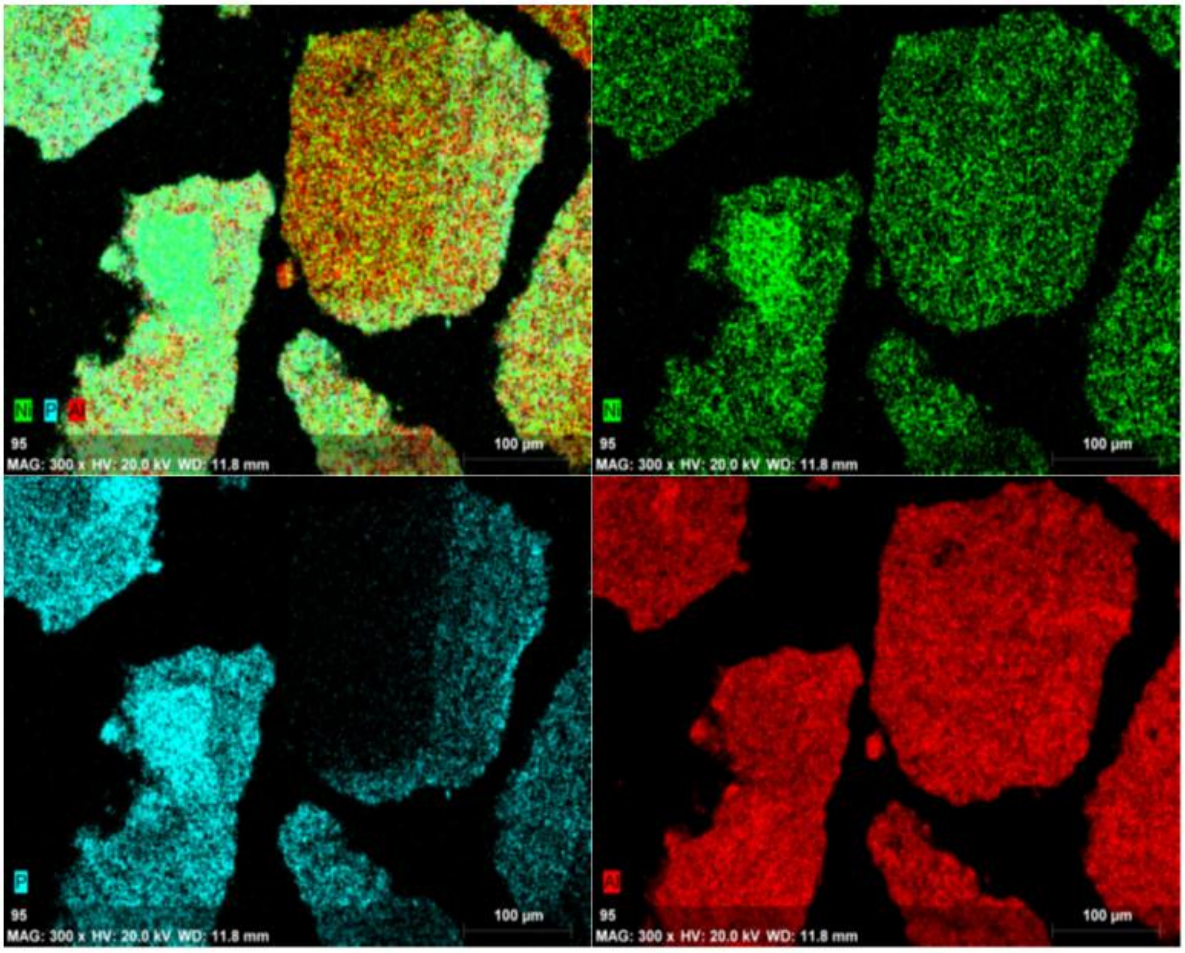

Figure A13: BSE-EDX maps showing the distribution of P, Ni on alumina for the 15 NiA catalyst that was regenerated with the combined regeneration, then removed from the reactor for characterisation purposes

Furthermore, STEM-EDX line scans were obtained for the 15 NiA catalyst samples that were removed after regeneration.

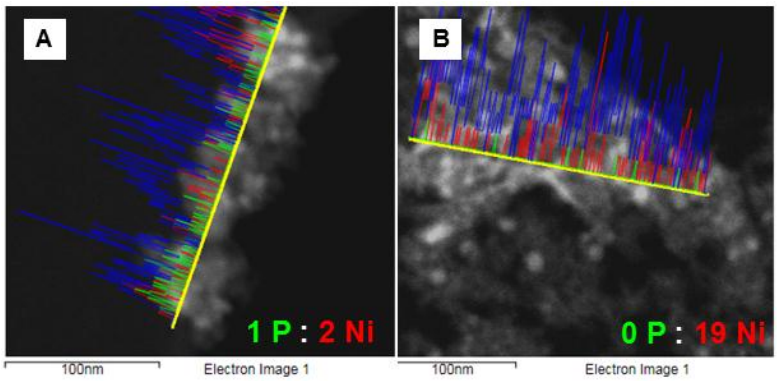

Figure A14: STEM-EDX showing the Ni and P distribution on (A) 15 NiA-H_R and (B) 15 NiA-SH_R

SEM-EDX maps were also obtained for the poisoned/regenerated 15 NiSi catalyst samples

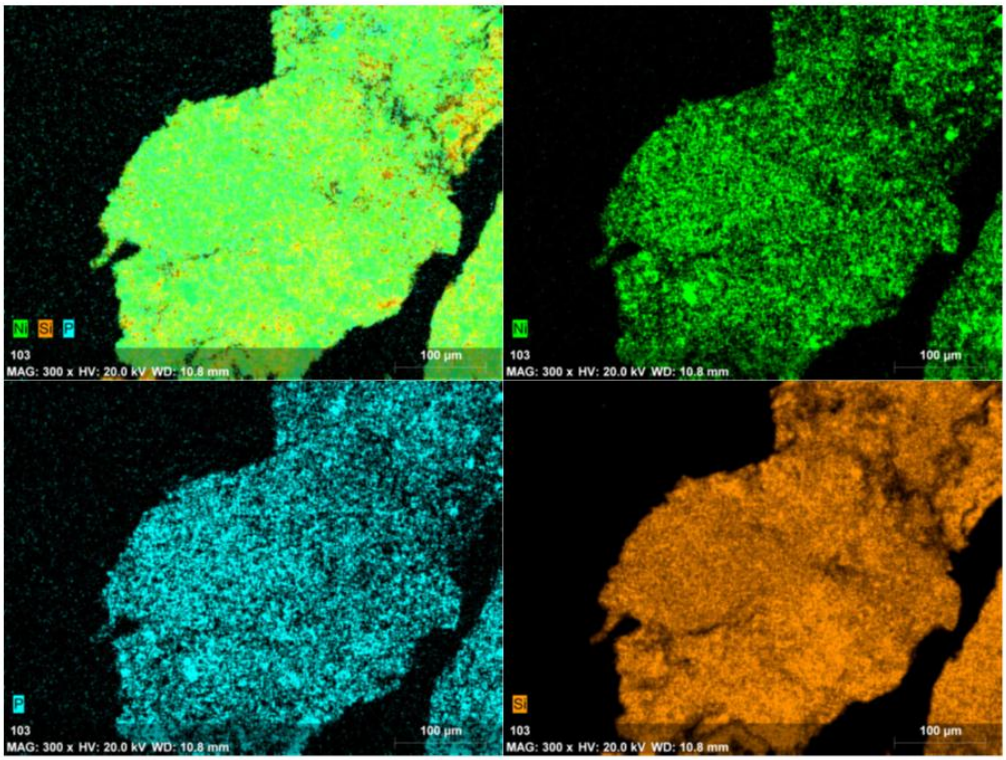

Figure A15: Combined and individual element maps for Ni, P, and Si on 15 NiSi-P

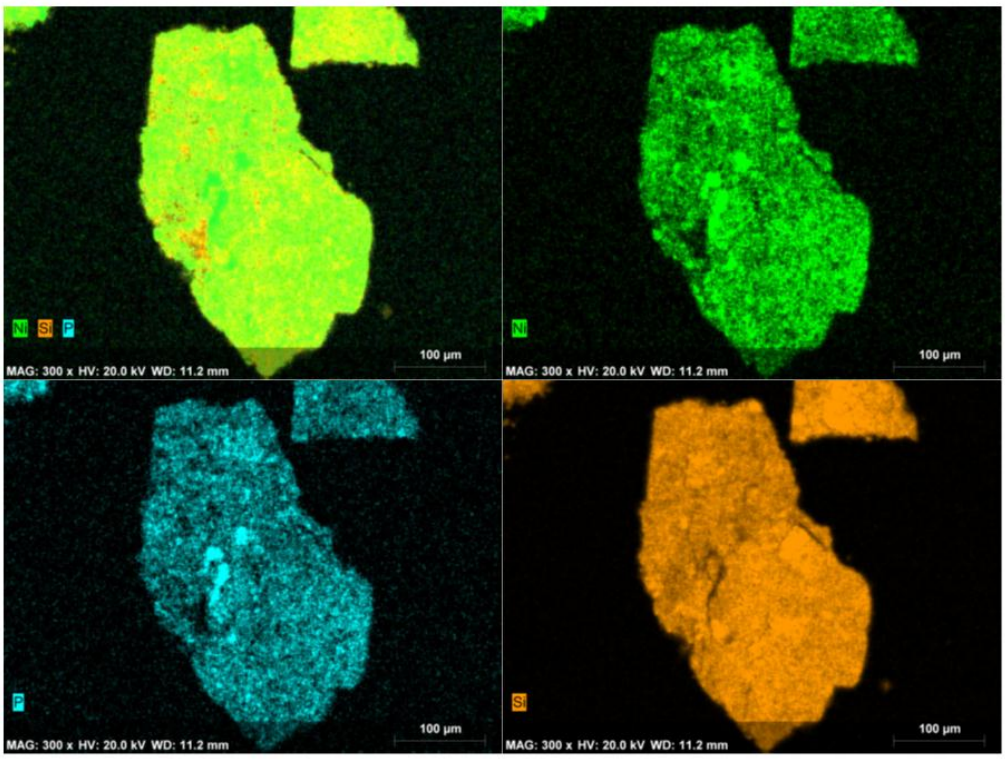

Figure A16: Combined and individual element maps for Ni, P, and Si on 15 NiSi-H

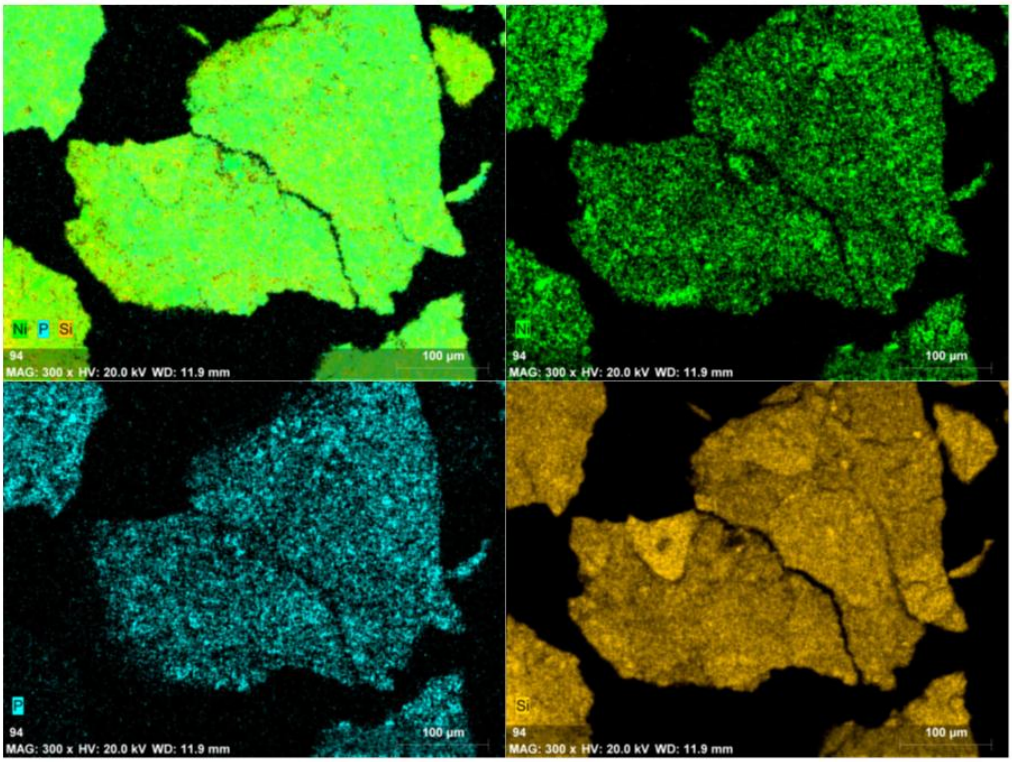

Figure A17: Combined and individual element maps for Ni, P, and Si on 15 NiSi-S

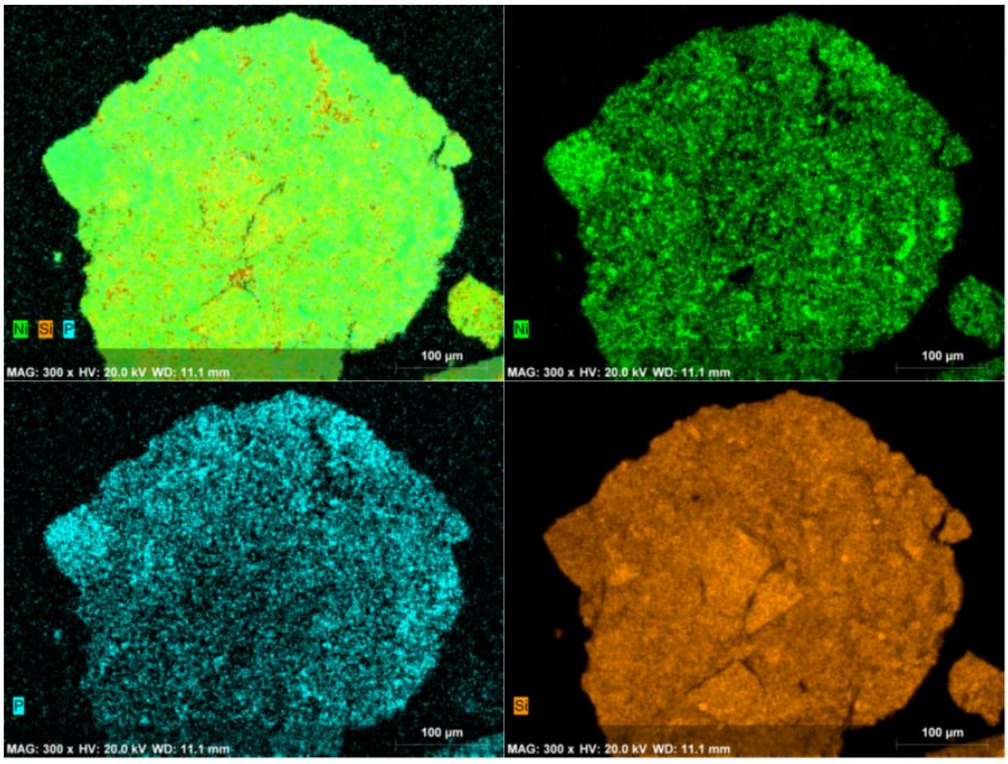

Figure A18: Combined and individual element maps for Ni, P, and Si on 15 NiSi-SH

A2.6: BET Pore size distribution

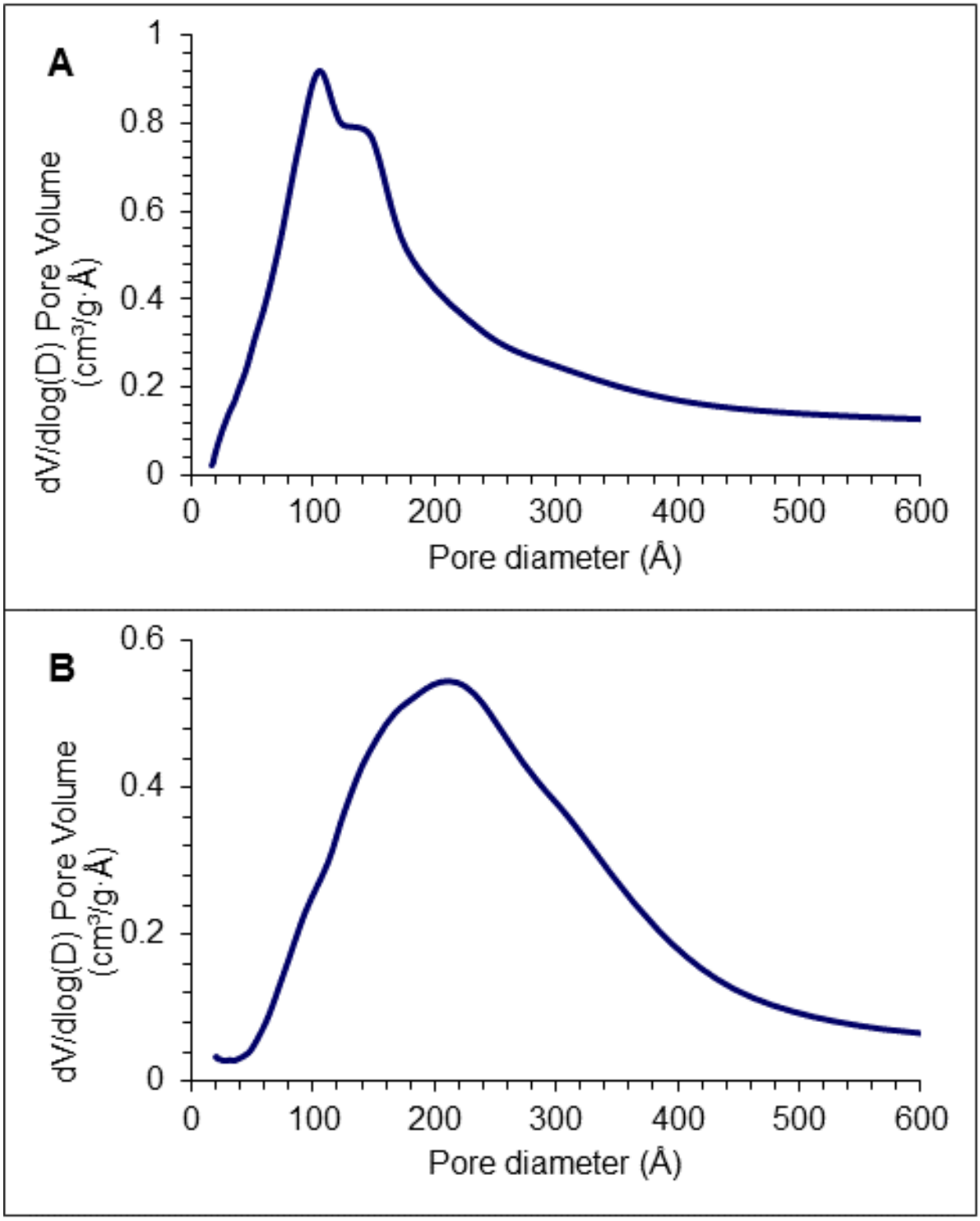

Figure A19: Pore size distribution of A) 15 NiA and B) 15 NiSi catalysts

A2.7: Attenuated total reflectance infrared spectroscopy to establish the transformation of TPP on the poisoned and regenerated catalysts

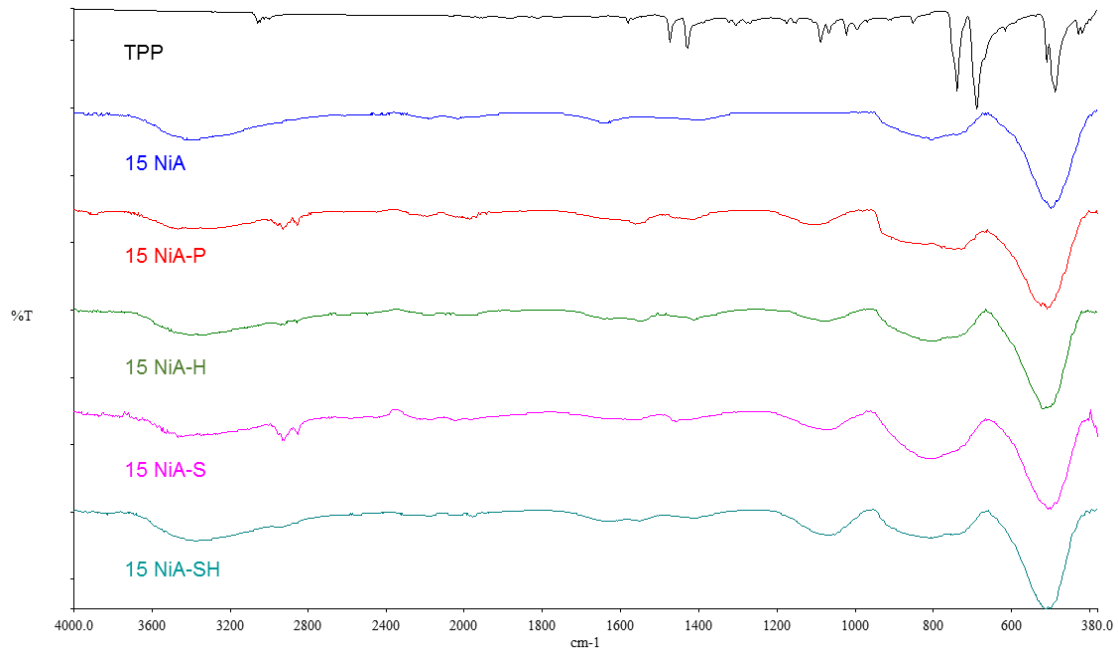

Figure A20: Attenuated total reflectance infrared spectra of the fresh, poisoned and regenerated 15 NiA catalyst samples

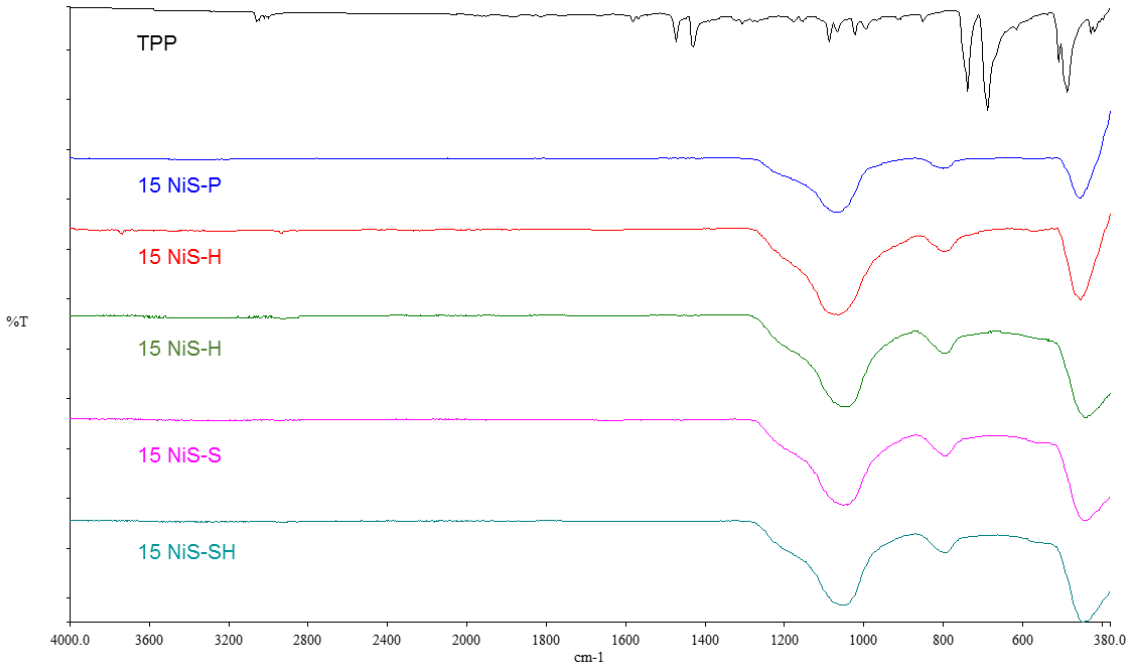

Figure A21: Attenuated total reflectance infrared spectra of the fresh, poisoned and regenerated 15 NiSi catalyst samples

Appendix 3: Tables

Table A1: Ni, P composition and amount of hydrogen desorbed for 15 NiA and regenerated 15 NiA catalyst samples

Sample	**Ni (wt.%)**	**P (wt.%)**	**H_2-TPD (mmol g^{-1})**
15 NiA	14.5	-	0.5149
15 NiA-H_R (regenerated with hydrogen treatment)	14.6	1.7	0.3898
15 Nia-SH_R (combined regeneration)	14.6	1.8	0.3395

Table A2: Quantity of hydrogen desorbed on the reduced and regenerated 15 NiSi catalyst samples during temperature programmed desorption of hydrogen

Sample	**H_2-TPD (mmol g^{-1})**
15 NiSi	0.1032
15 NiSi-H	0.5986
15 NiSi-SH	0.8736

Appendix 4: Product identification and quantitation

A4.1: GC-FID analysis of liquid products

Software Version	: 6.3.2.0646	Date	: 5/11/2016 5:05:39 AM
Sample Name	:	Data Acquisition Time	: 5/11/2016 2:58:26 AM
Instrument Name	: PEGC	Channel	: A
Rack/Vial	: 0/0	Operator	: manager
Sample Amount	: 1.000000	Dilution Factor	: 1.000000
Cycle	: 1		

Result File : C:\Vuyi\2016\15NiS\10052016\CFI\15NiS CFI H-Reg 140C LHSV18 s13,25hrs 11052016.rst
Sequence File : C:\PenExe\TcWS\Ver6.3.2\Examples\15NiS CFI H-Reg 140C LHSV18 s13,25hrs 11052016.seq

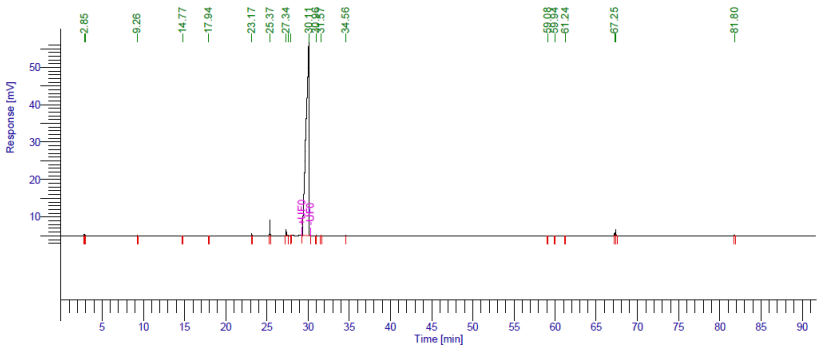

Samkelo

Peak #	Component Name	Time [min]	Area [uV*sec]	Area [%]
1		2.849	330.29	0.03
2		2.888	177.86	0.01
3		2.961	269.19	0.02
4		9.264	272.23	0.02
5		14.771	85.62	0.01
6		17.941	59.33	0.00
7		23.166	1245.92	0.10
8		25.375	12093.78	0.94
9		27.336	7708.67	0.60
10		27.541	392.26	0.03
11		27.930	944.62	0.07
12		30.105	1246645.08	97.33
13		30.958	139.60	0.01
14		31.572	170.82	0.01
15		34.560	261.50	0.02
16		59.080	157.38	0.01
17		59.941	155.01	0.01

5/11/2016 5:05:39 AM Result: C:\Vuyi\2016\15NiS\10052016\CFI\15NiS CFI H-Reg 140C LHSV18 s13,25hrs 11052016.rst

Peak #	Component Name	Time [min]	Area [uV*sec]	Area [%]
18		61.242	93.80	0.01
19		67.252	2725.40	0.21
20		67.415	6464.64	0.50
21		81.803	501.14	0.04
			1280894.15	100.00

Figure A22: GC-FID trace of the products from Step 1 (Figure 3.2, Chapter 3), using the 15 NiSi catalyst

Software Version	: 6.3.2.0648	Date	: 5/13/2016 7:13:03 AM
Sample Name	:	Data Acquisition Time	: 5/13/2016 5:06:55 AM
Instrument Name	: PEGC	Channel	: A
Rack/Vial	: 0/0	Operator	: manager
Sample Amount	: 1.000000	Dilution Factor	: 1.000000
Cycle	: 1		

Result File : C:\Vuyi\2016\15NiS\10052016\TPP\15NiS TPP H-Reg 140C LHSV18 s39,73hrs 13052016.rst
Sequence File : C:\PenExel\ToWS\Ver6.3.2\Examples\15NiS TPP H-Reg 140C LHSV18 s39,73hrs 13052016.seq

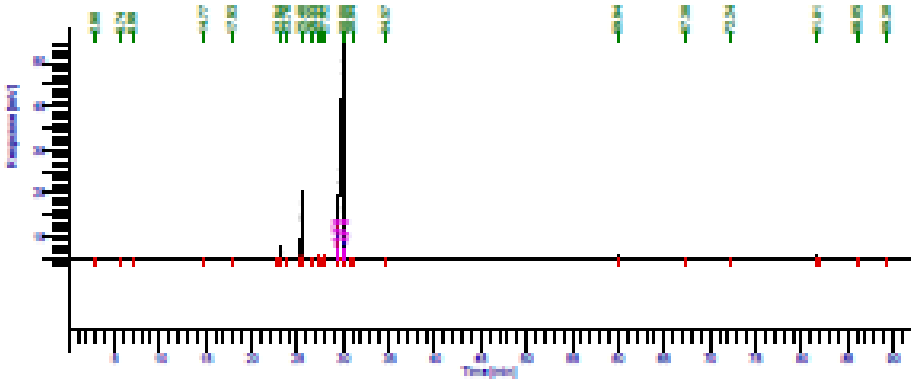

Samkelo

Peak #	Component Name	Time [min]	Area [uV*sec]	Area [%]
1		2.899	32.01	0.00
2		5.740	21.43	0.00
3		6.993	113.22	0.01
4		14.787	65.35	0.01
5		17.933	45.79	0.00
6		22.942	101.03	0.01
7		23.172	6504.59	0.51
8		23.783	132.94	0.01
9		25.479	87016.43	6.86
10		26.545	105.69	0.01
11		27.324	1595.32	0.13
12		27.545	279.09	0.02
13		27.924	388.23	0.03
14		30.077	1169241.97	92.21
15		30.939	54.80	0.00
16		34.574	455.02	0.04
17		59.939	754.64	0.06
18		67.381	100.57	0.01

5/13/2016 7:13:03 AM Result: C:\Vuyi\2016\15NiS\10052016\TPP\15NiS TPP H-Reg 140C LHSV18 s39,73hrs 13052016.rst

Peak #	Component Name	Time [min]	Area [uV*sec]	Area [%]
19		72.243	91.66	0.01
20		81.806	934.81	0.07
21		86.053	32.70	0.00
22		89.300	17.06	0.00
			1268062.36	100.00

TPP retention time

Figure A23: GC-FID trace of the products obtained during Step 2 (Figure 3.2, Chapter 3), using the 15 NiSi catalyst

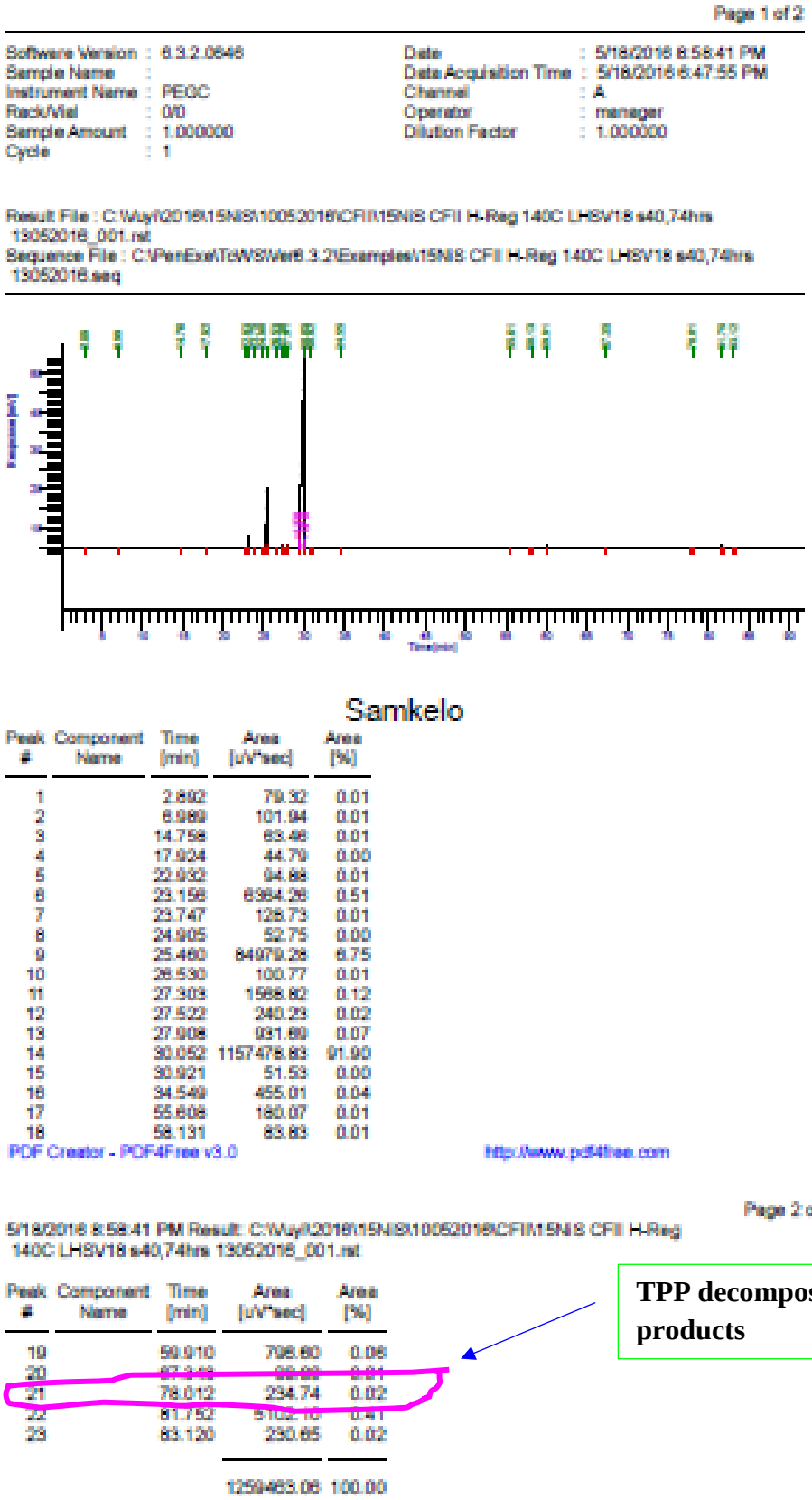

Page 1 of 2

Software Version	: 6.3.2.0646	Date	: 5/18/2016 8:58:41 PM
Sample Name	:	Data Acquisition Time	: 5/18/2016 8:47:55 PM
Instrument Name	: PEGC	Channel	: A
Rack/Vial	: 0/0	Operator	: manager
Sample Amount	: 1.000000	Dilution Factor	: 1.000000
Cycle	: 1		

Result File : C:\Wuyi\2016\15NiSi\10052016\CFII\15NiS CFII H-Reg 140C LHSV18 s40,74hrs 13052016_001.rst
Sequence File : C:\PenExel\ToWS\Ver6.3.2\Examples\15NiS CFII H-Reg 140C LHSV18 s40,74hrs 13052016.seq

Samkelo

Peak #	Component Name	Time [min]	Area [uV*sec]	Area [%]
1		2.802	79.32	0.01
2		6.969	101.94	0.01
3		14.758	63.46	0.01
4		17.924	44.79	0.00
5		22.932	94.88	0.01
6		23.156	6384.26	0.51
7		23.747	128.73	0.01
8		24.905	52.75	0.00
9		25.460	84979.28	6.75
10		26.530	100.77	0.01
11		27.303	1588.82	0.12
12		27.522	240.23	0.02
13		27.908	931.69	0.07
14		30.052	1157478.83	91.90
15		30.921	51.53	0.00
16		34.549	455.01	0.04
17		55.608	180.07	0.01
18		58.131	83.83	0.01

PDF Creator - PDF4Free v3.0 http://www.pdf4free.com

Page 2 of 2

5/18/2016 8:58:41 PM Result: C:\Wuyi\2016\15NiSi\10052016\CFII\15NiS CFII H-Reg 140C LHSV18 s40,74hrs 13052016_001.rst

Peak #	Component Name	Time [min]	Area [uV*sec]	Area [%]
19		59.910	708.60	0.06
20		[illegible]	[illegible]	[illegible]
21		78.012	234.74	0.02
22		81.752	[illegible]	[illegible]
23		83.120	230.65	0.02
			1259483.06	100.00

TPP decomposition products

Figure A24: GC-FID trace of the products obtained during Step 3 (Figure 3.2, Chapter 3), using the 15 NiSi catalyst

Software Version	: 6.3.2.0646	Date	: 3/3/2017 11:12:16 PM
Sample Name	:	Data Acquisition Time	: 5/29/2016 7:53:19 PM
Instrument Name	: PEGC	Channel	: A
Rack/Vial	: 0/0	Operator	: manager
Sample Amount	: 1.000000	Dilution Factor	: 1.000000
Cycle	: 1		

Result File : c:\vuyi\2016\15nis\25052016 ow\15nis octanol drain 1 ow-reg 28052016.rst
Sequence File : C:\PenExe\TcWS\Ver6.3.2\Examples\15NiS Octanol Drain 1 OW-Reg 28052016.seq

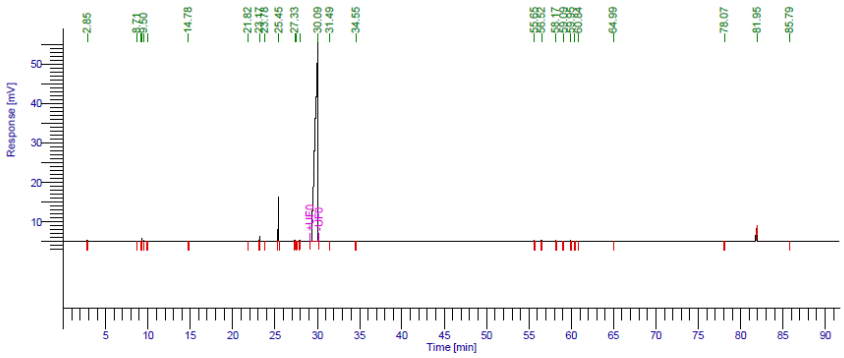

Samkelo

Peak #	Component Name	Time [min]	Area [uV*sec]	Area [%]
1		2.848	449.86	0.04
2		8.708	70.77	0.01
3		9.165	240.92	0.02
4		9.267	1428.98	0.11
5		9.498	345.21	0.03
6		9.913	142.67	0.01
7		14.776	102.66	0.01
8		21.820	27.97	0.00
9		23.174	2970.98	0.24
10		23.775	33.83	0.00
11		25.447	49417.46	3.94
12		27.335	1441.02	0.11
13		27.552	67.14	0.01
14		27.932	863.05	0.07
15		30.091	1193009.46	95.03
16		31.490	65.32	0.01
17		34.554	154.07	0.01
18		55.646	1071.84	0.09
19		56.524	693.84	0.06
20		58.171	649.44	0.05

3/3/2017 11:12:16 PM Result: c:\vuyi\2016\15nis\25052016 ow\15nis octanol drain 1 ow-reg 28052016.rst

Peak #	Component Name	Time [min]	Area [uV*sec]	Area [%]
21		59.086	298.90	0.02
22		59.946	638.00	0.05
23		60.392	241.50	0.02
24		60.837	15.68	0.00
25		64.994	41.47	0.00
26		78.071	322.60	0.03
27		81.953	526.88	0.04
28		85.789	21.78	0.00
			1255353.31	100.00

TPP decomposition products

Figure A25: GC-FID trace of the octanol washings obtained during regeneration of the 15 NiSi catalyst with the octanol wash (Figure 3.2, Step 4, Chapter 3)

Software Version	: 6.3.2.0848	Date	: 5/14/2016 6:07:01 PM
Sample Name	:	Data Acquisition Time	: 5/14/2016 4:09:50 PM
Instrument Name	: PEGC	Channel	: A
Rack/Vial	: 0/0	Operator	: manager
Sample Amount	: 1.000000	Dilution Factor	: 1.000000
Cycle	: 1		

Result File : C:\Wuyi\2016\15NiSi\10052016\CFIII\15NiS CFIII 140C LHSV18 s49,107hrs 14052016.rst
Sequence File : C:\PeriExe\ToWS\Wet6.3.2\Examples\15NiS CFIII 140C LHSV18 s49,107hrs 14052016.seq

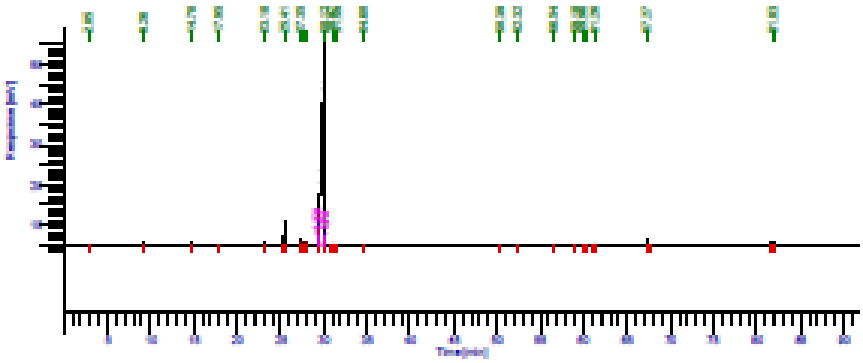

Samkelo

Peak #	Component Name	Time [min]	Area [uV*sec]	Area [%]
1		2.847	117.83	0.01
2		2.886	83.57	0.01
3		2.957	152.29	0.01
4		9.263	605.59	0.05
5		14.780	482.15	0.04
6		17.946	62.21	0.00
7		23.181	1611.88	0.13
8		25.409	19384.26	1.55
9		27.353	6666.58	0.53
10		27.559	44.62	0.00
11		27.945	957.66	0.08
12		30.116	1212122.23	96.76
13		30.971	122.67	0.01
14		31.590	94.73	0.01
15		34.602	459.16	0.04
16		50.387	139.16	0.01
17		52.317	138.85	0.01
18		56.536	488.40	0.04
19		59.100	331.11	0.03

5/14/2016 6:07:01 PM Result: C:\Wuyi\2016\15NiSi\10052016\CFIII\15NiS CFIII 140C LHSV18 s49,107hrs 14052016.rst

Peak #	Component Name	Time [min]	Area [uV*sec]	Area [%]
20		59.981	219.52	0.02
21		60.404	400.69	0.03
22		61.259	355.61	0.03
23		67.266	2344.80	0.19
24		67.420	3922.49	0.31
25		81.828	1376.62	0.11
			1252662.65	100.00

Figure A26: GC-FID trace of the products obtained during Step 5 (Figure 3.2, Chapter 3), using the 15 NiSi catalyst